

ASSESSMENT OF WIND ENERGY POTENTIAL IN
SOME LOCATIONS OF NORTH EASTERN
REGION OF INDIA AND CFD ANALYSIS OF
VERTICAL AXIS WIND TURBINE

Thesis submitted by
SYED MUJIBUR RAHMAN

Doctor of Philosophy (Engineering)

Department of Mechanical Engineering
Faculty Council of Engineering & Technology
Jadavpur University
Kolkata, India.

2021

JADAVPUR UNIVERSITY

KOLKATA-700032

INDEX NO. 226/18/E

1. **Title of the thesis:** **Assessment of Wind Energy Potential in some locations of North Eastern Region of India and CFD Analysis of Vertical Axis Wind Turbine**

2. **Name, Designation & Institution of the Supervisor/s:** Dr. Himadri Chattopadhyay
Professor
Department of Mechanical Engineering
Jadavpur University, Kolkata, India.

3. **List of publications:**
 - 1 **Rahman, S.M. and** Chattopadhyay, H. (2019). Statistical assessment of wind energy potential for power generation at Imphal, Manipur (India). *Energy Sources, Part A: Recovery, Utilization, and Environmental Effects*. DOI: 10.1080/15567036.2019.1675814
 - 2 **Rahman, S.M. and** Chattopadhyay, H. (2020). A new approach to estimate the Weibull parameters for wind energy assessment: Case studies with four cities from the Northeast and East India. *International Transactions on Electrical Energy Systems*. DOI: 10.1002/2050-7038.12574
 - 3 **Rahman, S.M.,** Chattopadhyay, H. and Romesh, L. (2020). Feasibility of Wind Energy as Power Generation Source at Shillong. *Advances in Mechanical Engineering, Lectures Notes in Mechanical Engineering*. DOI: 10.1007/978-981-15-0124-1_115
 - 4 **Rahman, S.M.,** Chattopadhyay, H. and Dutta, P. Computational Fluid Dynamics analysis on performance assessment of Darrieus type vertical axis wind turbine using NACA0016 and NACA0019 airfoil sections. *International Journal of Ambient Energy*. Under review

4. List of Patents:

Nil

5. List of Presentations in National / International :

1. **Rahman, S.M., Chattopadhyay, H. and Romesh, L. (2018).** Assessment of wind energy potential for power generation at Imphal, Manipur (India). **Conference Proceedings of 1st International Conference on Mechanical Engineering-2018 (INCOM18)**, January 4-6, 2018, Jadavpur university, Kolkata, India, pp. 593-596, ISBN 978-93-83660-38-4.
2. **Rahman, S.M., Chattopadhyay, H. and Romesh, L. (2018).** Feasibility of wind energy as power generation source at Shillong (Meghalaya). **International Conference on Recent Innovations and Developments in Mechanical Engineering, (IC-RIDME18)**, November 8–10, 2018, NIT Meghalaya, Shillong, India.
3. **Rahman, S.M. and Chattopadhyay, H. (2019).** Performance evaluation of four widely accepted numerical methods to estimate Weibull parameters for wind speed data of Kolkata, India. **International Conference on Recent Developments in Mechanical Engineering, (ICRDME2019)**, March 21-22, 2019, S.A. Engineering College, Chennai, India.
4. **Rahman, S.M., and Chattopadhyay, H. (2019).** A Statistical Assessment of Wind Energy Potential in East and Northeastern India. **International Conference on New and Renewable Energy Resources for Sustainable Future (ICONRER2019)**, November 07-09, 2019, Swami Keshvanand Institute of Technology, Jaipur, India.
5. **Rahman, S.M., Chattopadhyay, H. and Dutta, P. (2019).** Role of time step setting on the CFD result of Darrieus type Vertical Axis Wind Turbine. **Conference Proceedings of 5th International Conference on Advances in Mechanical Engineering Istanbul-2019**

(**ICAME2019**), December 17-19, 2019, Yıldız Technical University, Istanbul, Turkey, pp.117-122, ISBN 978-605-9546-16-4.

6. **Rahman**, S.M., Chattopadhyay, H. and Dutta, P. (2020). Two Dimensional Computational Fluid Dynamics study of H-type Darrieus Vertical Axis Wind Turbine with NACA0019 airfoil. **Conference Proceedings of International Conference on Advancements in Mechanical Engineering (ICAME2020)**, January 16-18, 2020, Aliah University, Kolkata, pp. 463-468, e-ISBN: 978-81-943641-6-0.
7. **Rahman**, S.M., Chattopadhyay H. and Romesh, L. (2020). A New Approach to Estimate the Weibull Parameters for the Assessment of Wind Energy Resources. **Conference Proceedings of International Conference on Energy and Sustainable Development (ICESD2020)**, February 14, 15, 2020, Jadavpur University, Kolkata, pp. 57-60, ISBN: 978-93-83660-56-8.
8. Karmakar, S.D., **Rahman**, S.M. and Chattopadhyay, H. (2020). Renewable Energy Sources for Power Generation: Recent Trend in India. **Conference Proceedings of International Conference on Energy and Sustainable Development (ICESD2020)**, February 14, 15, 2020, Jadavpur University, Kolkata, pp. 420-423, ISBN: 978-93-83660-56-8.

Statement of Originality

I *Syed Mujibur Rahman* registered on *13th April, 2018* do hereby declare that this thesis entitled “*Assessment of Wind Energy Potential in some locations of North Eastern Region of India and CFD Analysis of Vertical Axis Wind Turbine*” contains literature survey and original research work done by the undersigned candidate as part of Doctoral studies.

All information in this thesis have been obtained and presented in accordance with existing academic rules and ethical conduct. I declare that, as required by these rules and conduct, I have fully cited and referred all materials and results that are not original to this work.

I also declare that I have checked this thesis as per the “Policy on Anti Plagiarism, Jadavpur University, 2019”, and the level of similarity as checked by iThenticate software is 05 %.

Signature of the candidate:

Date:

Certified by the Supervisor:
(Signature with date, seal)

CERTIFICATE FROM THE SUPERVISOR

This is to certify that the thesis entitled “Assessment of Wind Energy Potential in some locations of North Eastern Region of India and CFD Analysis of Vertical Axis Wind Turbine” submitted by Shri Syed Mujibur Rahman who got his name registered on 13th April 2018 for the award of Ph.D. (Engg.) degree of Jadavpur University is absolutely based upon his own work under the supervision of Dr. Himadri Chattopadhyay, Professor, Department of Mechanical Engineering, Jadavpur University and that neither his thesis nor any part of the thesis has been submitted for any degree/ diploma or any other academic award anywhere before.

Signature of the Supervisor
and date with Office Seal

*Dedicated to
My family
&
My departed parents*

ACKNOWLEDGEMENT

At the very outset I would like to bow my head to the Almighty without whose blessings this work could not have been conceived.

First and foremost I would like to express my sincere respect, deepest gratitude and thank profusely to my guide Prof. (Dr.) Himadri Chattopadhyay, for his untiring efforts, valuable advice, heartfelt support, sincere guidance, tremendous help, total involvement, encouragement, meticulous surveillance and motivation throughout my research work, without whose help this work would have been incomplete nip in the bud. If I have succeeded to any extent it is due to his acute observation and deep perception of the subject. Any word of thankfulness will perhaps be a misnomer, I remain ever grateful to him that he agreed to supervise my research work. In fact no words are enough to express my indebtedness for his dedicated support.

I would like to thank my Ph.D committee members for their valuable advices and encouragement which helped in shaping up this work better.

I am very thankful to Head and the former Heads, faculty members, staff of Mechanical Engineering Department, Jadavpur University and fellow lab mates and my close friends namely Dr. Prasun Dutta, Romesh Laishram, etc., for their valuable support without which accomplishment of the present work could not happen.

I am also thankful to Prof. Subhasis Neogi, Professor, Mechanical Engineering Department, Alia University, Kolkata for his valuable suggestions and comments.

I am grateful to the Director, ICAR, Manipur, RMC Guwahati and RMC, Kolkata for providing me relevant wind data for Imphal, Guwahati, Shillong and Kolkata which are extensively used in wind power potential analysis part of the present work.

Above all, I am indebted to my family and my brothers and sisters, whose value to me only grows with age. And finally, I acknowledge my wife, who whole heartedly supported me in completing this herculean task.

Syed Mujibur Rahman

CONTENTS

	Page
Contents	viii
Abstract	xi
List of Figures	xiv
List of Tables	xix
Chapter 1: Introduction	
1.1 Background	1
1.2 Key Issues Led to Shift From Fossil Fuels to Renewable Source of Energy	2
1.3 Global and National Potential of Renewable Energy	6
1.4 Recent Trends in Renewable Energy	9
1.5 Future Role/ Forecast of Renewable Energy	11
1.6 Motivation	14
1.7 Horizontal Axis Wind Turbines (HAWT)	15
1.8 Vertical Axis Wind Turbines (VAWT)	16
1.9 Thesis organization	19
Chapter 2: Literature Review	
2.1 Literature review on wind energy potential assessment (WEPA)	21
2.1.1 Studies on WEPA of various locations	21
2.1.2 Studies on Statistical distribution models for WEPA	25
2.1.3 Studies on numerical estimation method for Weibull parameters	31
2.2 Literature review on Computational Fluid Dynamics of VAWT	36
2.2.1 The airfoils section	43
2.3 Objective of the Thesis	54

Chapter 3: Methodology on Assessment of Wind Energy Potential

3.1 Introduction	55
3.2 Statistical distribution models for the assessment of WEP	55
3.2.1 Two-parameter Weibull and Rayleigh distribution models	58
3.2.2 Vertical extrapolation of wind speed	59
3.2.3 Actual mean wind speed and standard deviation	60
3.2.4 Site specific wind speeds and coefficient of variation	61
3.3 Numerical models for the estimation of parameters	61
3.4 Development of a numerical estimation method: EVM	66
3.5 Wind power density (WPD)	66
3.6 Statistical performance evaluation criteria	67

Chapter 4: Results and Discussion on Wind Energy Potential Assessment

4.1 Introduction	68
4.2 Site Information and Data Source	69
4.3 Assessment of WEP of Imphal site	73
4.4 Assessment of WEP for Shillong site	77
4.5 Assessment of WEP of Guwahati site	80
4.6 Assessment of WEP for Kolkata site	83
4.7 Comparative analysis of WEP for all the selected sites	86
4.8 Performance comparison between Weibull and Rayleigh Distribution model	89
4.9 Validation and Performance comparison of the new estimation method	92
4.10 Comparison of PDF and CDF of all the selected methods	95
List of Symbols and Abbreviations	98

Chapter 5: CFD Analysis of VAWT

5.1 Introduction	102
5.2 Aerodynamics of H-rotor Darrieus VAWT and influencing parameters	103

5.3 Computational Model	107
5.4 Numerical implementation	115
5.5 Results and Discussion	120
List of Symbols and Abbreviations	133
Chapter 6: Conclusions and future scope	
6.1 Wind energy potential assessment of four sites	136
6.2 Performance comparison of Weibull and Rayleigh Distribution models	137
6.3 Development of a new numerical estimation method	138
6.4 CFD Analysis of VAWT	138
6.5 Future scope	139
References	141

ABSTRACT

In the application of wind energy conversion technology the kinetic energy of the wind is converted into useful electrical energy. However, as the wind energy is stochastic in nature, the analysis of wind characteristics and assessment of wind energy potential is vitally important for the selection or design of appropriate wind turbine of the concerned site before its installation. Therefore, this thesis is concerned with the assessment of wind power potential of some locations in Northeastern and Eastern regions of India and then CFD analysis of vertical axis wind turbine which can be deployed in such regions to assess the performance of rotors with some new airfoils section. Simultaneously, the present study also includes development of a new proposed estimation method namely, Energy Variance method (EVM) which can be effectively used in the assessment of wind energy potential.

For the assessment of wind energy potential four important locations namely, Imphal, Shillong, Guwahati and Kolkata the capital or the business capital of Manipur, Meghalaya, Assam and West Bengal respectively have been selected from the Northeastern and Eastern regions of India. Analysis of the wind characteristics and wind profiles of the all the selected sites reveal that all the sites fall in the low wind speed range and among them Kolkata provides the highest wind power potential followed by Guwahati site while Shillong provides the least wind power potential. Seasonal variations show that wind potential is higher during summer and lower during winter for all the sites. Even after extrapolating the data to twice the height of measurement, the available wind power of all the selected sites fall in the low wind power scale and in such situation deployment of vertical axis wind turbine is feasible.

Several previous studies showed that two-parameter Weibull distribution model associated with shape and scale parameters is an effective, simple, flexible and best statistical distribution method. However, from the earlier study it is also known that Weibull is properly unable to represent very low speeds in the set of wind speed data to be assessed. Therefore, an alternative model namely, Rayleigh distribution model is employed to assess the available data and the performance of both Weibull and Rayleigh models are compared. The results show that the overall performance of Weibull model is better than the same of the Rayleigh model except in case of Shillong site. It may be concluded that Weibull is still better for the assessment of low to higher wind speed range while Rayleigh model showed better result for the region having extremely low wind speed range.

Evaluating the exact and efficient parameters is imperative to get the best fit for the distribution for both Weibull and Rayleigh models. The Weibull parameters are estimated by utilizing four effective methods such as Moment method, Empirical method, Power Density method, and Maximum Likelihood method. Simultaneously, a new approach namely, Energy Variance method is developed which utilizes a non-iterative method to find out the Weibull distribution parameters effectively. Therefore, one of the objectives of the present work is to perform the comparative analysis of the proposed new method with four effective widely accepted estimation methods. The performance shows that the proposed Energy Variance method is a potential which provides the least error in case of Guwahati and Kolkata sites while the maximum likelihood method and moment method show the least error in case of Shillong and Imphal sites respectively. However, the overall performance shows that Energy Variance method is an effective and the most accurate method for estimating Weibull parameters followed by Maximum Likelihood method and Moment method for this region. Therefore, this new method may be considered as an improved, efficient and alternative estimation method for estimating Weibull parameters for wind energy applications.

Further, once the assessment of wind potential is completed, the next phase is to find suitable device to tap maximum possible energy from the stated energy source. A wind turbine is a device that can harness useful energy from wind energy source. Although there are two types of wind turbines: Horizontal Axis Wind Turbines and Vertical Axis Wind Turbine, the latter is more suited for the Northeastern and eastern regions as stated above. However, efficiency of vertical axis wind turbine is remarkably less than horizontal axis wind turbine and consequently the most important challenge of the former one is to enhance its aerodynamic performance. Earlier study showed that selection of efficient airfoil shape is an important criterion to enhance overall performance of wind turbine. Therefore, the last objective of the present work is to do two dimensional Computational Fluid Dynamics analysis of three bladed H-type Darrieus wind turbine having blade profile of NACA0019 and NACA0016 which are neither too thick nor too thin and the effectiveness of these profiles for harnessing wind energy are not reported till date. Prior to the Computational Fluid Dynamics simulation two dimensional mesh is generated using Ansys Meshing tool and then sliding mesh technique is used to simulate the rotational motion of the wind turbine. SST $k-\omega$ turbulence model is employed for the flow simulation. Initially both mesh and time step are optimized to reach independent solutions. Then the results from the simulation are compared with the pre-existing experimental result for the purpose of validation.

For this study several parameters such as lift coefficient, drag coefficient and torque coefficient are considered. The vortical structures at three different input wind speeds are also compared. Finally, the power coefficient curves at different speeds with respect to optimal value of tip speed ratio are compared. It is observed that power coefficient increases as the input wind speed increases.

Further, the performance of these two new airfoils are compared with an effective airfoil namely, NACA0015 which has been already accepted for excellent performance in wind turbine applications. The analysis reveals that the power coefficient of NACA0019 airfoils resulting from the CFD simulation is comparatively high and may be considered as one of the effective and alternative airfoil for the Darrieus VAWT which also provides better structural strength than thinner NACA 4 digit series like NACA0018, NACA0016 and NACA0015.

LIST OF FIGURES

Figure No.	Description of the figure	Page No.
Figure 1.1:	Sector wise GHGs emissions (IPCC, 2014)	3
Figure 1.2:	Country wise GHGs emissions (Colonbo,1992)	3
Figure 1.3:	Global employment in all sectors of renewable energy from 2012-2019 (ILO, 2011; IRENA, 2020)	5
Figure 1.4:	Employment of top countries in all sector of renewable energy in 2019 (ILO, 2011; IRENA, 2020)	5
Figure 1.5:	Global renewable energy potential in TW (Abas, 2015)	7
Figure 1.6:	Global renewable cumulative power installed capacity, 2004-2020 (Renewables 2021)	10
Figure 1.7:	Comparison of cumulative installed capacity of Renewable energy as on 30.11.2020 with available potential (Renewables 2021: MNRE 2020-21)	11
Figure 1.8:	Trends and forecasts of global energy consumption (Caineng, 2016)	12
Figure 1.9:	India's wind power forecasts for two scenarios (Singh, 2018)	13
Figure 1.10:	Past trend and future targets of wind energy in the EU (Kaldellis, 2011)	13
Figure 1.11:	Horizontal axis wind turbine with components (Mahmoud and Xia, 2012)	17
Figure 1.12:	(a) Darrieus vertical axis wind turbine (VAWT) (b) H-rotor Darrieus VAWT (c) Savonius VAWT ((Mahmoud and Xia, 2012)	17
Figure 1.13:	Power coefficient versus Tip speed ratio of different types of wind turbine (Hau/Springer, Germany, 2006)	19
Figure 2.1:	Yearly PDF and CDF of Hengchum site in Taiwan (Chang, 2011)	33
Figure 2.2:	Yearly PDF and CDF of Penghu site in Taiwan (Chang, 2011)	34
Figure 2.3:	Comparison of experiments and 2-D simulation (Bianchini et al., 2017)	37

Figure 2.4:	Two dimensional-Turbulence intensity contours at different angular positions at TSR=3.3 (Franchina et al., 2019)	38
Figure 2.5:	Two dimensional-Velocity magnitude contours at different angular positions at TSR=3.3 (Franchina et al., 2019)	38
Figure 2.6:	Two dimensional-Vorticity contours at different angular positions at TSR=3.3 (Franchina et al., 2019)	39
Figure 2.7:	Three dimensional-Turbulence intensity, vorticity and velocity contours on the symmetry, midspan and tip sections at $\Theta = 30^\circ$ and TSR=3.3 (Franchina et al., 2019)	39
Figure 2.8:	Effect of solidity in the performance of VAWT at inlet velocity =5.07 m/s and Reynolds = 35000 (Joo et al., 2015)	42
Figure 2.9:	Geometry of airfoil section	43
Figure 2.10:	Different symmetric and non-symmetric airfoils studied earlier (Hashem and Mohamed, 2018)	44
Figure 2.11:	Different symmetric NACA airfoils from 12% to 32% thickness and the last two digits in the airfoil series names provides the thickness percentage (Durrani et al., 2011)	44
Figure 2.12:	Performance of VAWT with Sixteen NACA 4- digital modified airfoils (Chen et al., 2016)	45
Figure 2.13:	Performance of H- rotor VAWT with NACA0015 and NACA0022 at Reynolds = 70000 (Chen and Lian, 2015)	46
Figure 2.14:	Performance of Darrieus turbines with two different airfoils at inlet velocity and solidity of 8 m/s and 0.75 respectively (Elkhoury et al., 2015)	47
Figure 2.15:	Power coefficient of H-rotor turbine with NACA 00XX and NACA 63-XXX-series airfoils at inlet velocity of 9 m/s (Hashem and Mohamed, 2018)	48
Figure 2.16:	Power coefficient of H-rotor turbine with S-series and SG60XX-series airfoils at inlet velocity of 9 m/s (Hashem and Mohamed, 2018)	48
Figure 2.17:	Power coefficient of H-rotor turbine with FX-series and LS-series airfoils at inlet velocity of 9 m/s (Hashem and Mohamed, 2018)	48

Figure 2.18:	Power coefficient of H-rotor turbine with DU-series and RISØ-A1-XX-series airfoils (Hashem and Mohamed, 2018)	49
Figure 2.17:	Power coefficients versus tip speed ratio of Darrieus turbine with 25 airfoils at inlet velocity and solidity 5 m/s and 0.1 respectively (Mohamed et al., 2015, 2019)	50
Figure 4.1:	Map of East and Northeastern India showing the study sites	68
Figure 4.2:	Comparison of wind data extrapolation by two approaches for Kol site	71
Figure 4.3:	Comparison of wind data extrapolation by two approaches for Imp site	72
Figure 4.4:	Frequency percentage for Twelve years (2012-16) wind speed of Imp site	73
Figure 4.5:	Twelve years (2005-16) monthly and whole year mean wind speed of Imp site	74
Figure 4.6:	Monthly mean COV of turbulence at 20 m and 40 m height for Imp site	76
Figure 4.7:	Seasonal variations for Five years (2012-16) mean wind speed of Shg site	77
Figure 4.8:	Frequency percentage of Five years wind speed of Shg site	78
Figure 4.9:	Five years (2012-16) monthly mean wind speed of Shg site	78
Figure 4.10:	Seasonal variations for Five years (2012-16) mean wind speed of Ghy site	80
Figure 4.11:	Frequency percentage for Five years (2012-16) wind speed of Ghy site	81
Figure 4.12:	Five years (2012-16) monthly mean wind speed of Ghy site	81
Figure 4.13:	Seasonal variations for Five years (2012-16) mean wind speed of Kol site	84
Figure 4.14:	Frequency percentage of Five years (2012-16) wind speed of Kol site	84
Figure 4.15:	Five years (2012-16) monthly mean wind speed of Kol site	85
Figure 4.16:	Yearly mean wind speed of four different sites	87
Figure 4.17:	Mean wind speed for Five years (2012-16) of four different sites	87
Figure 4.18:	Seasonal and annual wind power density of all the four different sites	88

Figure 4.19:	Wind power density of two different heights from the ground for Imp site	88
Figure 4.20:	Yearly Weibull PDF and CDF of Imp site	96
Figure 4.21:	Yearly Weibull PDF and CDF of Shg site	96
Figure 4.22:	Yearly Weibull PDF and CDF of Ghy site	97
Figure 4.23:	Yearly Weibull PDF and CDF of Kol site	97
Figure 5.1:	Three bladed H-type Darrieus VAWT	103
Figure 5.2:	Horizontal section of three bladed H-type Darrieus VAWT	104
Figure 5.3:	Airfoil aerodynamic	105
Figure 5.4:	Computational model with boundary conditions used in the study	109
Figure 5.5:	Details of mesh structure of the present study: (a) Whole computational domain (b) mesh around one blade (c) leading edge mesh view (d) trailing edge mesh view	110
Figure 5.6:	Validation of C_p of Darrieus turbine with the experimental and numerical results by Balduzzi et al. (2016b) and Castelli et al. (2011) as function of tip speed ratio (λ) at velocity 5 m/s, $Re= 10^5$	115
Figure 5.7:	Mesh independency study	116
Figure 5.8:	Influence of Time step size (TSS) at TSR=2.5	117
Figure 5.9:	Periodical torque coefficient over 8 Cycles at TSR=2.5	118
Figure 5.10:	Effect of NOTS on power coefficient at TSR=2.5	118
Figure 5.11:	Effect of blade airfoil types on instantaneous net torque coefficient at TSR=1.4 and inlet velocity of 5 m/s	121
Figure 5.12:	Effect of blade airfoil types on instantaneous net torque coefficient at TSR=1.7 and inlet velocity of 5 m/s	121

Figure 5.13:	Effect of blade airfoil types on instantaneous net torque coefficient at TSR=2.1 and inlet velocity of 5 m/s	122
Figure 5.14:	Effect of blade airfoil types on instantaneous net torque coefficient at TSR=2.5 and inlet velocity of 5 m/s	122
Figure 5.15:	Effect of blade airfoil types on instantaneous net torque coefficient at TSR=3.0 and inlet velocity of 5 m/s	123
Figure 5.16:	Effect of blade airfoil types on instantaneous net torque coefficient at TSR=3.5 and inlet velocity of 5 m/s	123
Figure 5.17:	Performance comparison of rotor with NACA0015, NACA0016 and NACA0019 at inlet velocity of 5 m/s	124
Figure 5.18:	Predicted total lift coefficient for rotor with NACA0019 at TSR=2.5	124
Figure 5.19:	Predicted total drag coefficient for rotor with NACA0019 at TSR=2.5	125
Figure 5.20:	Performance of rotor varying inlet velocity for rotor with NACA0019 at TSR=2.5	126
Figure 5.21:	Pressure contours at various azimuthal angle for NACA0019 at inlet velocity of 5 m/s and TSR=2.5	127
Figure 5.22:	Comparison of Pressure contours of three different airfoils at various azimuthal angle for NACA0019 at inlet velocity of 5 m/s and TSR=2.5	128
Figure 5.23:	Turbulent intensity for NACA0015 and NACA0019 @TSR=2.5	130
Figure 5.24:	Vorticity distributions at different angular positions for NACA0015, NACA0016 and NACA0019@TSR=2.5	131

LIST OF TABLES

Table No.	Description of the figure	Page No.
Table 1.1:	Global technical potential of Renewable Energy in TWh/yr (Hoogwijk,2008)	7
Table 1.2:	Renewable Energy Potential in India (in MW) (MNRE, 2020-21)	8
Table 1.3:	Total global cumulative installed/ rated capacity of renewable energy (Renewables, 2021)	10
Table 1.4:	Characteristics of horizontal and vertical axis wind turbines (Kragic, et al., 2018)	16
Table 1.5:	Comparison of Horizontal and vertical axis wind turbines	18
Table 2.1:	Peak wind potential of 11 years in Tehran (Keyhani et al., 2010)	22
Table 2.2:	Monthly average wind speed of all the eight sites in m/s (Mathew et al., 2002)	23
Table 2.3:	Summary of literature review on wind energy potential assessment	24
Table 2.4:	Previous studies on statistical distribution model associated with WEPA	27
Table 2.5:	Wind speed percentage of occurrence of all the sites (Wais 2017)	31
Table 2.6:	Previous studies on numerical estimation methods to determine Weibull parameters	35
Table 2.7:	Simulated airfoils with the corresponding peak power coefficient (Hashem and Mohamed 2018)	49
Table 2.8:	Simulated airfoils with the corresponding peak C_p (Mohamed, 2012)	51
Table 2.9:	Summary on airfoils type used during Numerical analysis of Darrieus VAWT	53
Table 3.1:	Statistical Distribution models (Uni-model)	56
Table 3.2:	Statistical Distribution models (Multi-model)	58
Table 3.3:	Value of power law exponent for different types of terrain	60

Table 4.1:	Geographical details of the selected sites	70
Table 4.2:	Month wise wind characteristics for Twelve years (2005-16) of Imp site	75
Table 4.3:	Monthly mean wind speed and standard deviation for 12 years of Imp site	76
Table 4.4:	Month wise wind characteristics for Five years of Shg site	79
Table 4.5:	Monthly mean wind speed and standard deviation for 5 years of Shg site	79
Table 4.6:	Month wise wind characteristics for Five years of Ghy site	82
Table 4.7:	Monthly mean wind speed and standard deviation for 5 years of Ghy site	82
Table 4.8:	Month wise wind characteristics for Five years of Kol site	85
Table 4.9:	Monthly mean wind speed and standard deviation for 5 years of Kol site	86
Table 4.10:	Comparison between Weibull and Rayleigh models for Imp site	89
Table 4.11:	Comparison between Weibull and Rayleigh models for Shg site	90
Table 4.12:	Comparison between Weibull and Rayleigh models for Ghy site	90
Table 4.13:	Comparison between Weibull and Rayleigh models for Kol site	91
Table 4.14:	Performance analysis of five numerical methods for Imp site	92
Table 4.15:	Performance analysis of five numerical methods for Shg site	93
Table 4.16:	Performance analysis of numerical methods for Ghy site	93
Table 4.17:	Performance analysis of numerical methods for Kol site	94
Table 4.18:	Shape parameter and corresponding RMSE values	95
Table 5.1:	Geometrical characteristics of the present model	108
Table 5.2:	Geometrical characteristics of the two similar models	108
Table 5.3:	Comparison of turbulence models at TSR=2.5	112
Table 5.4:	Boundary conditions used in the present study	114

1.1 Background

Energy is an essential item for improving wealth, social development and economic development of any country. Global energy demand is growing exponentially due to population increase, rapid urbanization and industrialization. All societies in all sectors of any country demand the services of energy to fulfill basic human needs such as foods, lighting, health, space comfort, transportation and connectivity.

Historically, it is the renewable energy which played essential role for the development during pre-industrial time. With technological advances in coal mining, coal became the prominent fuel for supplying energy and then from the late 1800s it became the fuel of choice. After 1945, oil expanded rapidly and superseded coal in the 1960s as energy demand for mobility increased (UNCTAD Note, 2010). Then all the fossil fuels became the dominant form of energy in all sectors of energy consumption till date. Looking at present scenario, the harvesting of conventional sources of energy has become too costly and environmentally damaging. Thus, increased energy prices owing to the continuous depletion of fossil fuels, rises in population, rises in energy consumption, increase in living standard and upcoming of important undesirable phenomena like climate changes, IPCC prediction on climate change, greenhouse effect and other environmental concerns led to shift from fossil fuels to renewable sources of energy (RE). According to IPCC report 2007 (Kalogirou, 2004), the earth's surface temperature has risen by about 0.6°C over the last century, and consequently sea level has risen by about 20 cm. It is also predicted that if the same trend of increase in atmospheric concentrations of greenhouse gasses is allowed to continue then the surface temperature of the earth may rise by another 2 to 4.5°C in the next century and corresponding sea level rise would be between 21 to 48 cm. As a result the soil erosion, flooding, shifting of fertile land toward higher latitudes and storm damage to some coastal settlements will follow. Consequently it will lead to an irrecoverable threat for the survival of living beings. Therefore, growing interest in renewable energy technologies to meet the scarcity of conventional energy resources and to minimize the environmental degradation rate is escalating day by day.

1.2 Key Issues that Led Shift from Fossil Fuels to Renewable Source of Energy

1.2.1 Increase in conventional fuel price

The prices of fossil fuels have been rising steadily and it can be unbearable in the near future. Meanwhile, the price of renewable energy is decreasing day by day and expected to be at par with fossil fuels in the very near future.

1.2.2 Energy Security

Energy security is considered to be one of the important factor for national security. In the past energy security issues were confined to the global oil prices, but now it is being recognized that energy security for most of the countries in the world as a part of national security. As far as our nation is concerned it has two role. The first is to provide better distribution of energy for people and effective utilization of available energy so that necessary commercial energy is available to every citizen of the country. The second is to meet the growing energy demand due to increase in living standards. The current trends in conventional fuels production indicate that most of the countries in the world face constraints in indigenous availability of conventional resources. This coupled with the widening of gap between demand and supply of energy. Such a trend obviously militates against energy security which ultimately affects the overall economy and national security of a country.

Fortunately, India and many countries in the world have abundant renewable energy resources. Hence the effective utilization of renewable energy would improve energy security and economic as well.

1.2.3 Growing Energy needs

Rise in world population and increase in living standard increase the growing energy needs which cannot be fulfilled by conventional sources of energy alone. Global energy demand is much faster than the population growth (Abas, 2015).

1.2.4 Climate change mitigation

At present the climate change due to greenhouse gas (GHG) emissions is considered as serious threat to mankind. In this regard, sector wise GHGs emission based on the global emissions in 2010 (IPCC, 2014) is presented in Figure 1.1 in which electricity and thermal production contributed highest percentage of GHGs emission. Further, some of the prominent

countries that contributed significant percentage of GHGs emission are clearly highlighted in Figure 1.2 (Colonbo, 1992). Due to present GHGs emission trend the global temperature have already increased by about 0.6°C over the last century (Kalogirou, 2004; Colonbo, 1992). If this trend continues in future, it is expected that there will be adverse effects in several areas of the world. Rise in sea-levels will eventually submerge coastal low-lying urban areas like Mumbai and Kolkata in India. In such situation the deployment of renewable energy source will mitigate the GHGs to large extent.

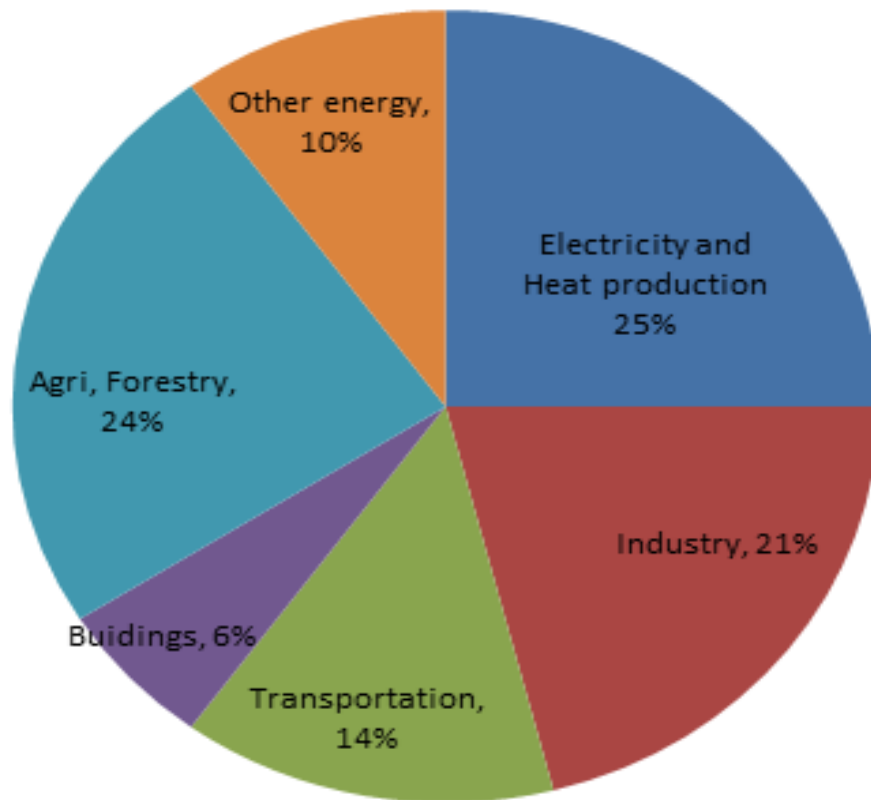


Figure 1.1 Sector wise GHGs emissions (IPCC, 2014)

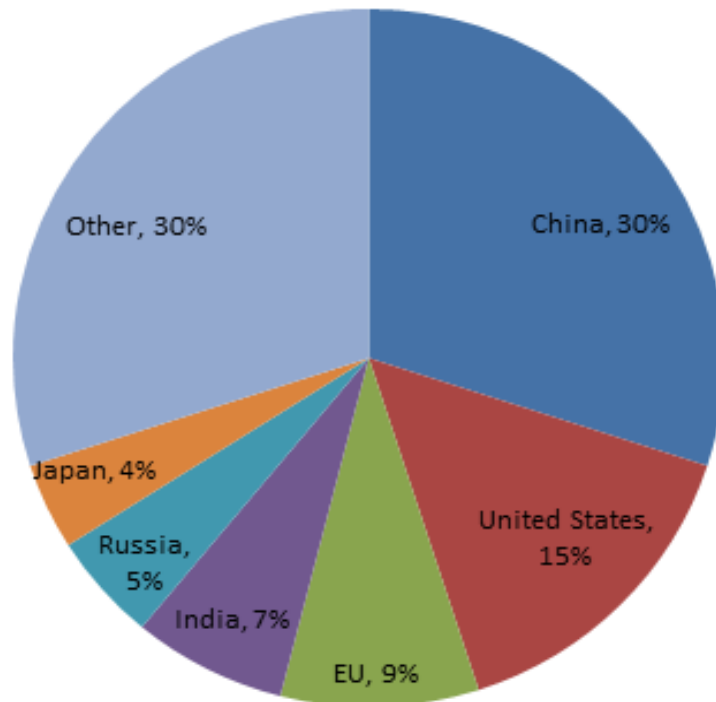


Figure 1.2 Country wise GHGs emissions (Colonbo, 1992)

1.2.5 Environmental pollution

Till late 1900s most of the environmental experts believed that environmental pollution is due to conventional pollutants such as SO₂, NO_x, CO and particulates. Now it is realised that there are several pollutants other than conventional pollutants such as carbon dioxide, micro pollutants or toxic chemical substances which are very much harmful in tiny quantity (Jacobson, 2011).

1.2.6 Depletion of conventional source of energy

As of now the conventional fuels such as coal, petroleum and natural gas meet the major share of the global energy demand. As the conventional source has limited availability if we continue to exploit at such alarming rates then these sources would exhaust in the very near future. Present scenarios shows that the reserves have got depleted to a great extent as these fuels were created over millions of years ago.

1.2.7 Economic development (Job creation)

As the exploitation of renewable energy is in developing stage it will not only helps in mitigating GHGs emission, reduction of environmental pollution but it will also offer considerable scope of generating employment opportunities. As per UNEP 2011 total number employments in all sectors of renewable energy was 2.416 million but it has reached 11.46

million in 2019 (ILO, 2011; IRENA, 2020). The detail employments in all types of renewable energy along with employment in top six countries are shown in Figure 1.3 and Figure 1.4 respectively. It reveals that solar and wind sectors provide employment of 33% and 10% respectively in 2019.

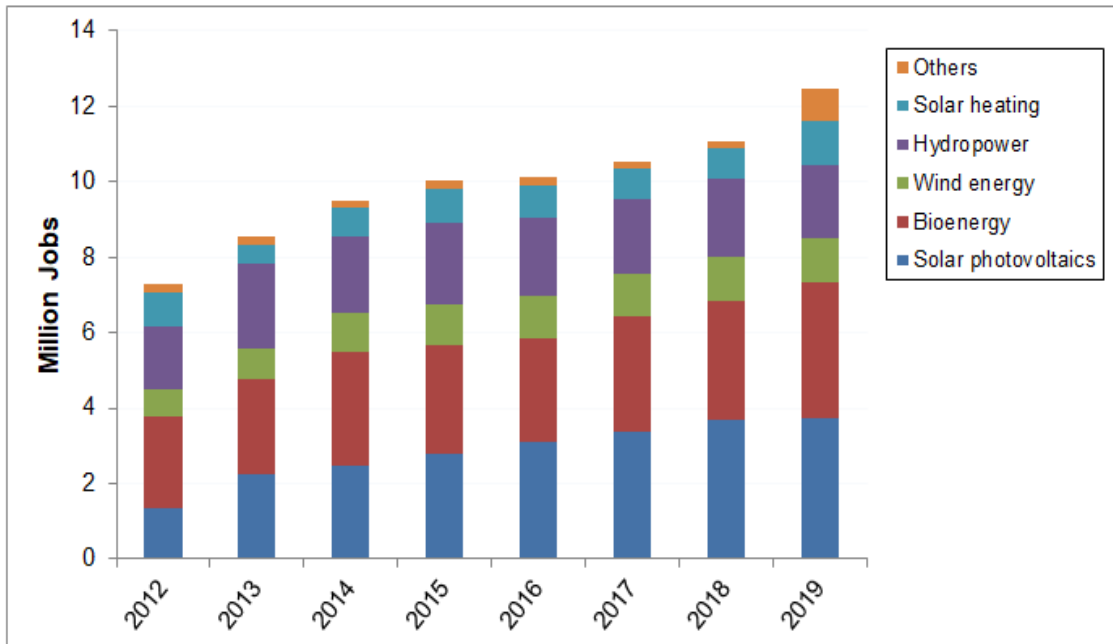


Figure 1.3 Global employment in all sectors of renewable energy from 2012-2019 (ILO, 2011; IRENA, 2020)

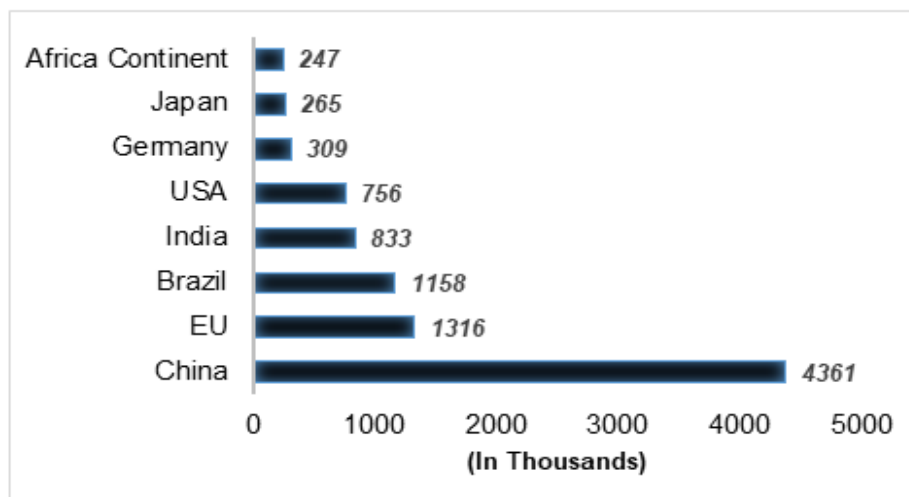


Figure 1.4 Employment of top countries in all sector of renewable energy in 2019(ILO, 2011; IRENA, 2020)

1.3 Global and National Potential of Renewable Energy

Effective exploitation of renewable energy can meet the present global energy demands (Kalogirou, 2004). Annual world power demand is hardly 17 TW that can be met by energy from sun or wind alone as the nature has given huge potential of 1700 TW of wind, 6500 TW of solar photovoltaic (PV), 5000TW of concentrating solar power (CSP) along with other renewable energy sources which are clearly shown in Figure 1.5 (Abas, 2015).

1.3.1 Solar energy

Sun is the source of solar energy which has energy output of 3.8×10^{20} MW and a fraction, 1.7×10^{11} MW is intercepted by the earth (Kalogirou, 2004; Abas, 2015). However, the solar power on the earth's surface is about 10^{10} MW which is about 1000 times the world's energy demand. Therefore, if we can tap the 5% of the available potential, it will be more than 50 times the global energy need. Detail global solar potential per year is given in the following Table 1.1.

As far as India context is concerned, with about 300 clear sunny days in a year, theoretically calculated India's solar energy potential is about 5000 trillion kWh/year which is equivalent to 750 GW (Ahmad, 2016; MNRE, 2020-21) and state wise detail potential is shown in the Table 1.2.

1.3.2 Wind energy

Although the wind power potential vary with the measuring altitude, it is estimated that globally about 580 trillion kWh of electrical power per year can be generated from wind energy resource or in other words the energy available in the wind over the earth's surface is estimated as 3.5×10^7 MW (Hoogwijk, 2008) approximately. As far as India's wind potential is concerned, it is estimated at 102.8 GW (@80m altitude) and 302.23 GW (@100m altitude) respectively.

1.3.3 Hydropower

Total global hydroelectric technical power potential per year is 14576 TWh, with an estimated total power potential of 3721 GW (Ahmad, 2016; Owusu, 2016) whereas India's total hydro potential is about 170 GW including the small hydro potential of 20 GW.

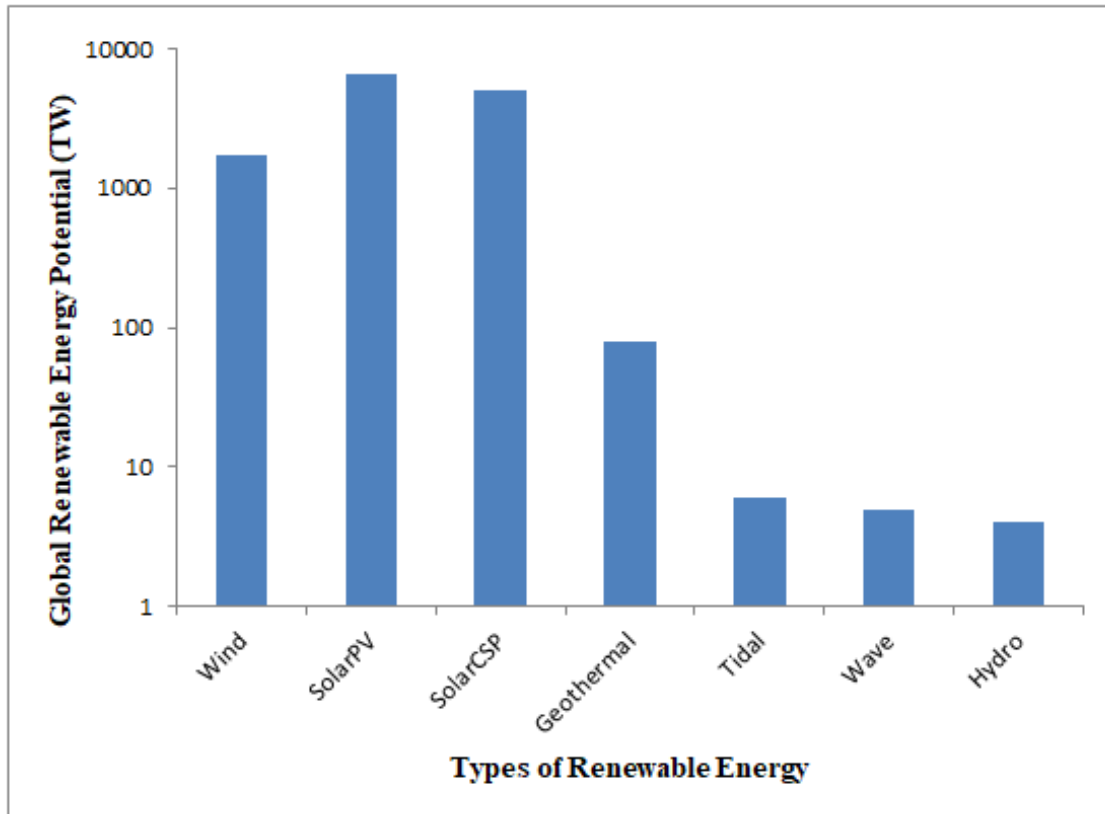


Figure 1.5 Global renewable energy potential in TW (Abas, 2015)

Table 1.1 Global technical potential of Renewable Energy in TWh/yr (Hoogwijk, 2008)

Region	Solar CSP	Solar PV	Hydro power	Wind power	Geothermal Power	Marine energy	Biomass power including thermal	Solar thermal	Geothermal Direct application
North America	5833	20000	1389	43889	1389	18889	20278	6389	173890
OECD Europe	139	3611	1944	5833	556	5556	6111	6389	56389
Non OECD Europe & FSU	6945	33334	1389	19722	1667	7500	9167	1667	185279
Middle East & Africa	188613	239724	2222	9445	1389	5278	6667	3333	338058
Asia	6111	70556	3889	3611	3333	28611	31945	12500	300002
Latin America	16389	36389	2778	12500	3056	8889	11944	3333	232224
Oceania	51945	66389	278	16666	1111	14167	15278	556	91112
World	275974	470004	13889	111668	12500	88890	101390	34167	1376955
Share (%)	11.10	18.91	0.56	4.50	0.50	3.60	4.08	1.37	55.40

Table 1.2 Renewable Energy Potential in India (in MW) (MNRE, 2020-21)

States/UTs	Wind Energy		Solar Energy	Small Hydro Power	Biomass Power	Bagasse Cogeneration	Waste to Energy	Total	
	@80m	@100m						Estimated Potential	Share (%)
Andhra Prad	14497	44228	38440	978	578	300	123	99144	8.27
Arunachal	236	-	8650	1341	8	-	-	10235	0.85
Assam	112	-	13760	239	212	-	8	14331	1.20
Bihar	144	-	11200	223	619	300	73	12559	1.05
Chhattisgarh	314	76	18270	1107	236	-	24	20027	1.67
Goa	-	1	880	7	26	-	-	914	0.08
Gujarat	35071	84432	35770	202	1221	350	112	157158	13.11
Haryana	93	-	4560	110	1333	350	24	6470	0.54
Himachal	64	-	33840	2398	142	-	2	36446	3.04
J&K	5685	-	111050	1431	43	-	-	118209	9.86
Jharkhand	91	-	18180	209	90	-	10	18580	1.55
Karnataka	13593	55857	24700	4141	1131	450	-	99872	8.33
Kerala	837	1700	6110	704	1044	-	36	10431	0.87
M.P.	2931	10484	61660	820	1364	-	78	77337	6.45
Maharashtra	5961	45394	64320	794	1887	1250	287	119893	10.00
Manipur	56	-	10630	109	13	-	2	10810	0.90
Meghalaya	82	-	5860	230	11	-	2	6185	0.52
Mizoram	-	-	9090	169	1	-	2	9262	0.77
Nagaland	16	-	7290	197	10	-	-	7513	0.63
Odisha	1384	3093	25780	295	246	-	22	30820	2.57
Punjab	-	-	2810	441	3172	300	45	6768	0.56
Rajasthan	5050	18758	142310	57	1039	-	62	167276	13.95
Sikkim	98	-	4940	267	2	-	-	5307	0.44
Tamil Nadu	14152	33799	17670	660	1070	450	151	67952	5.67
Telangana	-	4244	20410	-	-	-	-	24654	2.06
Tripura	-	-	2080	47	3	-	2	2132	0.18
UP	1260	-	22830	461	1617	1250	176	27594	2.30
Uttarakhand	534	-	16800	1708	24	-	5	19071	1.59
West Bengal	22	2	6260	396	396	-	148	7224	0.60
Others	505	167	2840	8	-	-	1162	4682	0.38
Total	102788	302235	748990	19749	17538	5000	2556	1198856	100.00
Share (%)	8.57	25.21	62.48	1.65	1.46	0.42	0.21	100.00	

1.3.6 Marine energy

There are three different energy sources in this sector namely OTEC, wave and tidal energy and its global total potential is about 28 million MW while the India's total potential is estimated as 50 GW from OTEC, 40 GW from wave energy and 8GW from tidal (Hoogwijk, 2008; Rai, 1997).

1.3.4 Bio energy

It is estimated that approximate total solar radiation absorbed by plants is 1.3×10^{19} kJ/year (Rai, 1997). Based on this data the global potential is about 101390 TWh/year (Hoogwijk, 2008). However, biomass energy potential for power generation is very small as compare to thermal application.

1.3.5 Geothermal energy

Potential of geothermal energy depends on the depth below the ground level. For a depth of 3 km, the total global potential is estimated as 8×10^{19} kJ and for a depth of 10 km it is about 4×10^{19} kJ (Rai, 1997). As far as global technical potential for power generation is concerned it is about 12500 TWh/year and detail is shown in the Table 1.1.

1.4 Recent Trends in Renewable Energy

Referring to Table 1.3 and Figure 1.6, since 2004 the amount of energy produced by renewable energy sources in global power sector has increased by 2028 GW, it means in the last 16 years more than 250% increase in the total cumulative installed capacity. Adding 256 GW in 2020 only global renewable energy generation capacity has reached 2,838 GW out of which 22% and 14% increase in solar PV and wind energy sector respectively (Renewables 2021). At present the total renewable energy accounts for about 19.9% of global energy consumption while in India it accounts for about 25% of total energy consumption (Renewables 2021; Patel, 2017).

Although China has topped in renewable energy capacity, India maintained 4th rank in both wind and hydro energy sector for the last few years. As far as comparison between the global and national available renewable energy potential and installed renewable energy capacity is concerned there is a huge gap which is clearly shown in Figure 1.7. Therefore, effective exploitation of renewable energy can easily meet the present global energy demand.

Table 1.3 Total global cumulative installed/ rated capacity of renewable energy (Renewables 2021)

POWER(GW)								
Types of RE	2004	2014	2015	2016	2017	2018	2019	2020
Hydropower	715	1018	1055	1095	1114	1132	1150	1170
Bio- Power	36	88	93	114	122	130	137	145
Geothermal power	8.9	12.1	12.8	12.1	12.8	13.3	14.0	14.1
Solar PV	2.6	138	177	303	402	505	621	760
Solar CSP	0.4	3.4	4.4	4.8	4.9	5.5	6.1	6.2
Wind Power	48	319	370	487	539	591	650	743
Marine Power	-	-	-	0.5	0.5	0.5	0.5	0.5
THERMAL (GW)								
Solar hot water	86	373	406	456	472	480		501
TRANSPORT (billion Litres)								
Ethanol	28.5	87.8	94	103	106	112	115	105
FAME Biodiesel	2.4	26.3	29.7	31	31	34	41	39
HVO	-	-	-	5.9	6.5	7.0	6.5	7.5

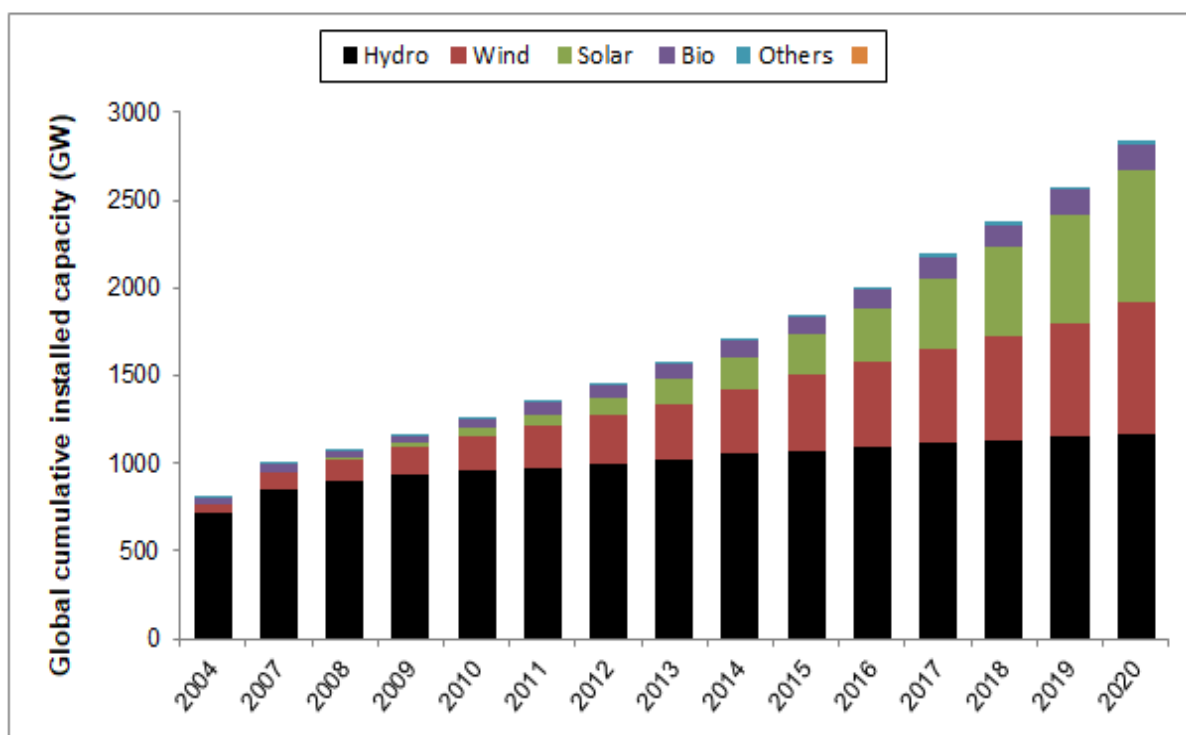


Figure 1.6 Global renewable cumulative power installed capacity, 2004-2020(Renewables 2021)

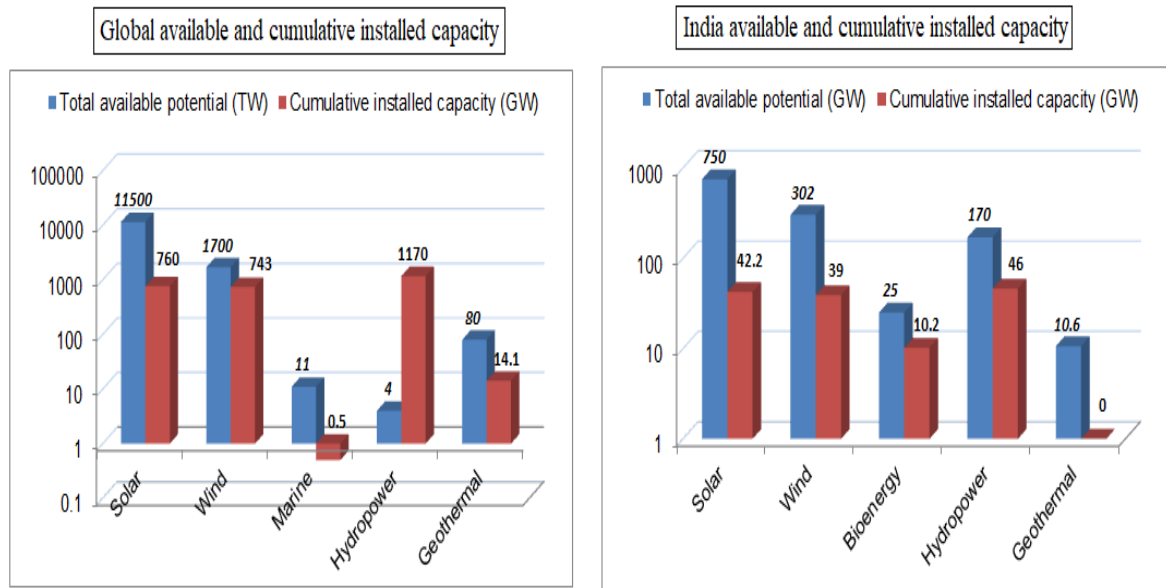


Figure 1.7 Comparison of cumulative installed capacity of Renewable energy as on 31.12.2020 with available potential (Renewables 2021; MNRE 2020-21)

1.5 Future Role/ Forecast of Renewable Energy

For the development of a country the gap between energy demand and energy supply is of immense importance. Without the enough energy supply as per the energy demand of a nation it will very difficult to have positive technology development, economic development and to have a desired level of energy security. On the other hand, increase in energy generation lead to more GHGs emission rate. Therefore, the most important objectives of future energy technologies are to match the energy supply with expected energy demand and secondly to mitigate the GHGs emissions while generating energy to fulfil the future energy demand.

In order to accomplish mentioned objectives, generation of more energy as per the need of stakeholders must rely on new energy sources which are also known as renewable energy sources. Based on the past and present trends of energy generation several agencies have predicted and forecasted future energy production model which are now discussed.

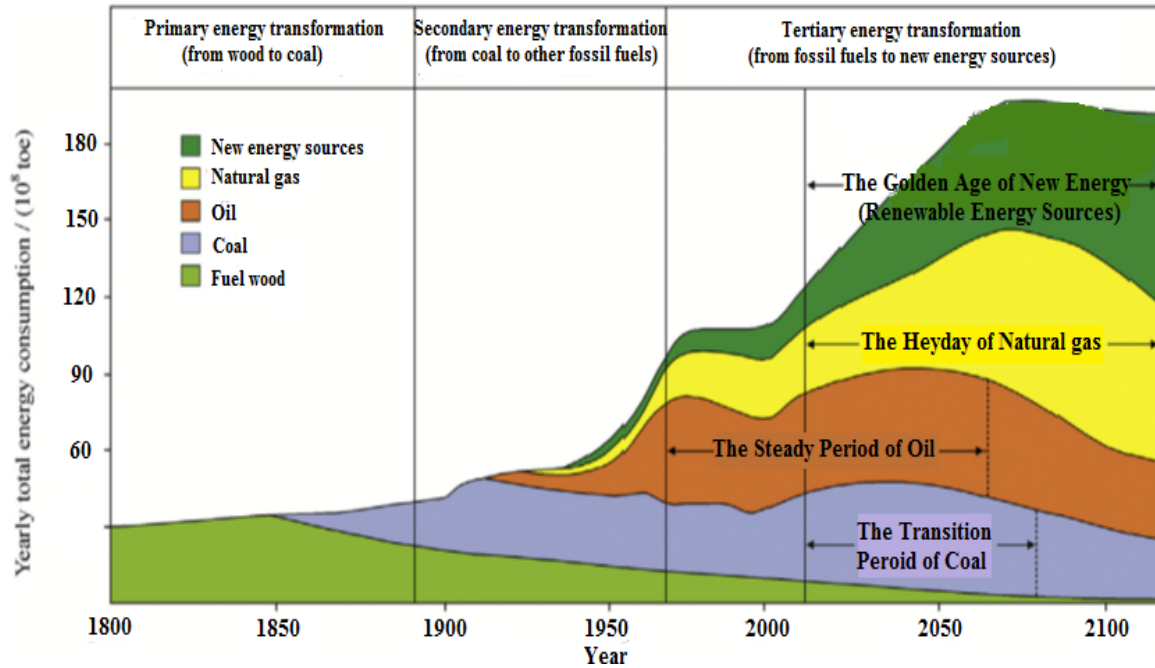


Figure 1.8 Trends and forecasts of global energy consumption (Caineng, 2016)

Figure 1.8 shows past and present trends in global energy consumption and thereby forecasts future model of energy production (Caineng, 2016). It is evident that use of traditional biomass will be almost out of picture by 2050. It is also observed that rate of consumption of conventional coal is already at declining rate and conventional coal will be replaced by clean form of coal which will continue during transition period. World oil extraction continues to grow steadily and based on present scenario it is expected that by 2040 the oil extraction will reach the peak and then rate of extraction will decrease. On the other hand, the cleanest fossil fuel, natural gas production will grow and will become transition phase fossil fuel to renewable energy. It is expected that annual natural gas production of the world will peak around 2060 and then gap of the energy demand will be compensated by renewable energy source. Entered renewable energy in the present scenario is in achieving the low carbon development in order to mitigate GHGs emission. As an example, India's wind power forecasts for two scenarios based on the present trend which shows that total cumulative wind power installed capacity may reach 80 GW or more by 2040 (Figure 1.9) (Singh, 2018).

To mitigate maximum possible GHGs emission several countries in the world including India set their own target for additional amount of renewable energy generation. For example, China set a target to achieve 26% share of electricity from renewable source by 2030 while India set a target of cumulative renewable energy capacity by 2030 is 450 GW. Similarly,

based on the past trend, EU has set a future target of 400 GW from both onshore and offshore wind power generation as shown in Figure 1.10 (Kaldellis, 2011).

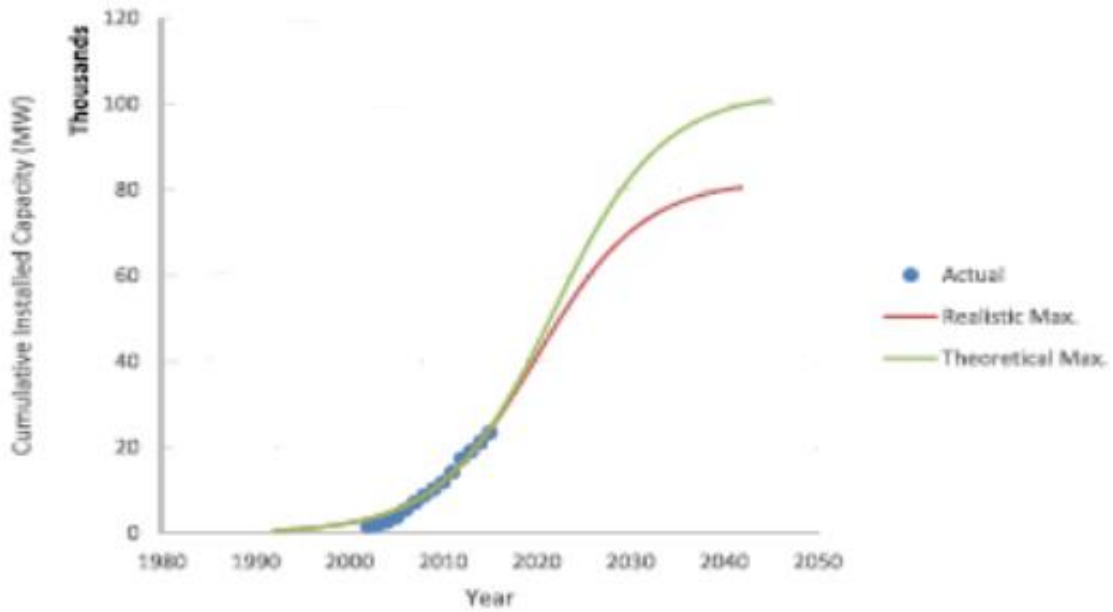


Figure 1.9 India's wind power forecasts for two scenarios (Singh, 2018)

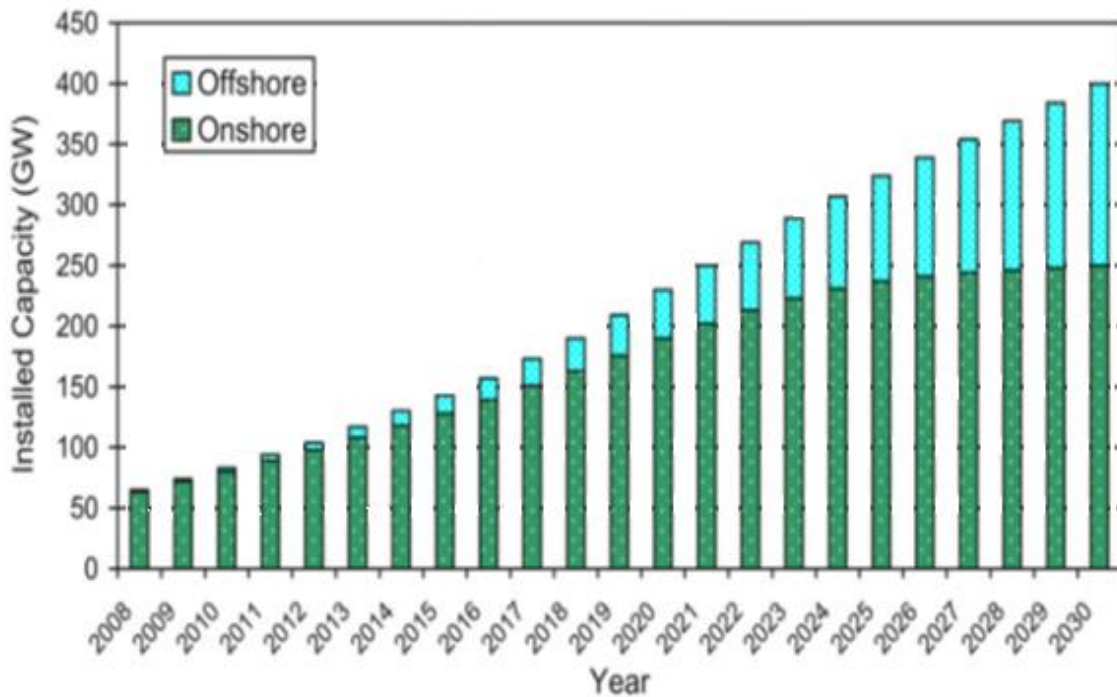


Figure 1.10 Past trend and future targets of wind energy in the EU (Kaldellis, 2011)

1.6 Motivation

From the above study it is realized that global renewable energy potential is about 13,295 TW comprising of solar energy (11500 TW), wind energy (1700 TW), geothermal energy (80 TW), marine energy (11 TW) and hydropower (4 TW). Whereas global total cumulative installed capacity are 743 GW of wind energy, 766.1 GW of solar energy, 14.1 GW of geothermal energy, 1170 GW of hydropower and 0.5 GW of marine energy. It shows that there is huge gap between the available renewable energy potential and total cumulative installed capacity. Therefore, the aim must be to reduce these gaps which will fulfill global energy demand while reducing the GHGs emissions. It will not only reduce GHGs emission by replacing conventional form of energy but will also generate millions of employments as record shows that till the end of 2019 about 11.6 million employments has been created in the renewable energy sector.

As far as India is concerned, the country ranked 4th in wind sector with cumulative installed capacity of 39 GW, 5th rank in solar PV with installed capacity of 39 GW, 4th rank in concentrated solar power with installed capacity of 3.2 GW and 7th rank in hydropower with capacity of 46 GW excluding small hydropower of 4.8 GW in the entire World. Therefore, at the end of 2020, the total cumulative installed capacity of renewable energy in India is 96 GW excluding 46 GW of large hydropower plant. Apart from this, India has also set a target of additional cumulative renewable capacity of 175 GW excluding large hydropower source to be achieved by 2022. However, India has huge potential of renewable energy of about 1199 GW. Out of which 302 GW of wind energy (at elevation of 100 m), 750 GW of solar energy, 20 GW of small hydro, 25 GW of bioenergy and 10.6 GW of geothermal energy. It shows that there is still huge energy gap between the available potential and installed capacity including the target to be achieved.

Present trend in renewable energy shows that the wind energy has emerged as the fastest growing energy not only in India but also globally. It is followed by solar energy source. As far as wind energy potential in India is concerned, some states like Gujarat (80.39 GW), Karnataka (52.98 GW), Andhra Pradesh (42.79 GW), Maharashtra (40.73 GW), Tamil Nadu (26.18 GW), Rajasthan (14.77 GW) & Madhya Pradesh (8.34 GW) have huge potential which accounts for about 88% of total wind energy potential in the country.

However, it must be borne in mind that wind is stochastic in nature and therefore, harnessing of wind energy involves three important phases: energy resource assessment, selection or

design of wind energy turbines and finally installation. Therefore, wind energy resource assessment is one of the most crucial phase in the wind energy conversion technology.

Further, once the assessment of wind potential is completed the next phase is to find suitable device to tap maximum possible energy from the stated energy source. A wind turbine is a device that can harness useful energy from wind energy source. Basically there are two types of wind turbines: Horizontal Axis Wind Turbines (HAWT) and Vertical Axis Wind Turbine (VAWT). Both types consist of essential parts such as tower, rotor, gearbox, generator and control system.

Although HAWT has better efficiency as compared to VAWT, the latter has several other advantages such as cost effectiveness, simple in structure, omni directional and can be deployed at low velocity region especially in the high rise building urban areas where there are many obstructions for HAWT. In order to maintain 90% of the performance of isolated HAWTs, the turbines in wind turbine farm must be spaced 3–5 turbine diameters apart in the cross-wind direction and 6–10 diameters apart in the downwind direction. Otherwise, overall efficiency of the wind farm will significantly decrease (Dabri, 2011). In contrast for the case of VAWT, the close arrangement of VAWTs in wind turbine farm improves their overall performance relative to the isolated. This encouraged many researchers to perform research work to improve and optimize the efficiency of VAWT.

Results and assessment data of India available till date shows that wind speed in the most places of India is of low scale which encourages the deployment of VAWT. However, it is realized from the earlier studies that there is still lack of detail assessment of wind energy potential in many places in India such as Eastern and North-Eastern regions of India which motivates to do wind energy resource assessment. Computational fluid dynamics analysis of suitable wind turbine for such low wind speed regions also need to be carried out.

1.7 Horizontal Axis Wind Turbines (HAWT)

A horizontal axis wind turbine is known as lift type wind turbine that has axis of rotor in parallel to the wind stream and ground. It may have either two or more blades connected to the hub of the rotor that will be connected to a hub assembly as shown in Figure 1.11. The hub is connected to gearbox through shaft and then to generator where mechanical energy is converted into electrical energy. Pitch system and yaw mechanisms are also incorporated to

adjust the blade angles and direct the rotor towards the wind direction respectively to optimize the performance.

1.8 Vertical Axis Wind Turbines (VAWT)

A vertical axis wind turbine may be either lift or drag type while the rotating shaft of the turbine is set vertically and other components are placed at the ground itself. It implies the gearbox and generator are placed at base of the tower which makes the system simple in structure. There are mainly two types of vertical axis wind turbine: Darrieus and Savonius VAWTs which are presented in Figure 1.12. Further, there are several Darrieus and Savonius VAWT out of which H-Type Darrieus VAWT (H-rotor Darrieus VAWT) is one of the prominent, simple in structure turbine which is shown in Figure 1.12(b). VAWT especially H-Rotor Darrieus drawn the interest of present researchers as the large scale turbine has been forced away from high energy demand population areas and moved towards remote areas or offshore sites where plenty of spaces are available. Moreover, VAWTs are capable of harnessing energy from high turbulent windy region and low wind speed sites as well. Characteristics of all the three major classification of wind turbines are presented in Table 1.4 and their merits and demerits are presented in Table 1.5.

Table 1.4 Characteristics of horizontal and vertical axis wind turbines (Kragic et al., 2018)

<i>Characteristics</i>	<i>HAWT</i>	<i>Darrieus VAWT</i>	<i>Savonius VAWT</i>
Power coefficient	0.45-0.5	0.35-0.4	0.15-0.2
Yaw system	Necessary	Not necessary	Not necessary
Pitch system	Required	Optional	No
High tower	Yes	No	No
Generator position	On top of tower	At the base	At the base
Power at low speed	impossible	possible	possible
Blade profile	Complicated	Simple/Complicated	Simple
Tip speed ratio	High	Moderate	Low
Overall structure	Complicated	Simple	Simple

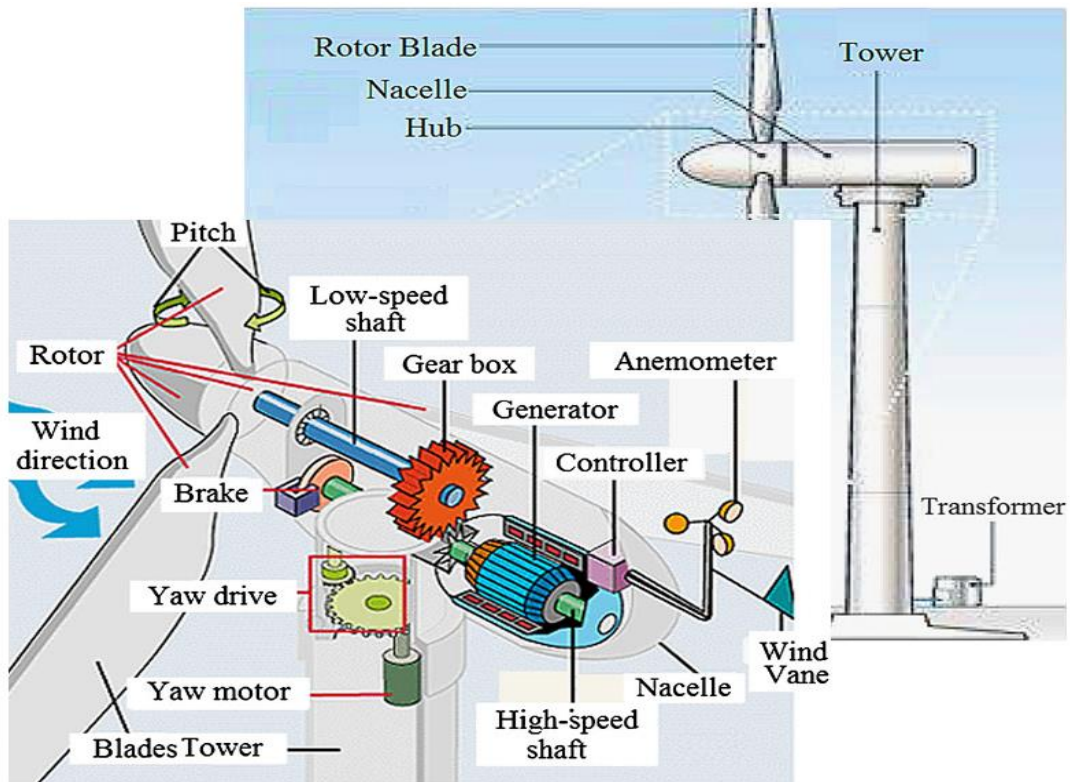


Figure 1.11 Horizontal axis wind turbine with components (Mahmoud and Xia, 2012)



Figure 1.12 (a) Darrieus vertical axis wind turbine (VAWT) (b) H-rotor Darrieus VAWT (c) Savonius VAWT (Mahmoud and Xia, 2012)

Table 1.5 Comparison of Horizontal and vertical axis wind turbines


Types 	Horizontal axis wind turbine	Darrieus vertical axis wind turbine
Advantages	<ul style="list-style-type: none"> • High efficiency and reliability • High power output and can be used for large scale wind power generation • High operational wind speed • Self-starting 	<ul style="list-style-type: none"> • Omnidirectional • Can be installed at low wind speed region and at high rise building area where mostly turbulent flow exists. • Strong support is not required as the nacelle can be mounted at ground level • Simplicity and ease of installation and service • Less space and Low maintenance cost
Disadvantages	<ul style="list-style-type: none"> • Difficult to transport and hence transportation cost is very high • Strong support is needed as nacelle at the top of the structure • Mechanism to control yaw and pitch is required • Create negative environmental impact such as noise, effect on wildlife, ecosystems • Large space is required • High maintenance cost • In case of downwind HAWTs' the regular turbulence produced leads to structural failure. 	<ul style="list-style-type: none"> • Rotors generally near ground where wind speed is poorer • Poor self-starting capabilities • Efficiency is significantly low as not all of the blades produce torque simultaneously. • Overall poor performance and reliability

Figure 1.13 shows the power coefficient (C_p) versus tip speed ratio of five different wind turbines. It is observed that the peak C_p of the one bladed rotor, two bladed rotors, the three bladed rotors and the Darrieus rotor are all above 30 %, while the American Multi-blade type, the Dutch windmills and the Savonius rotor peak at about 15 % to 30 %.

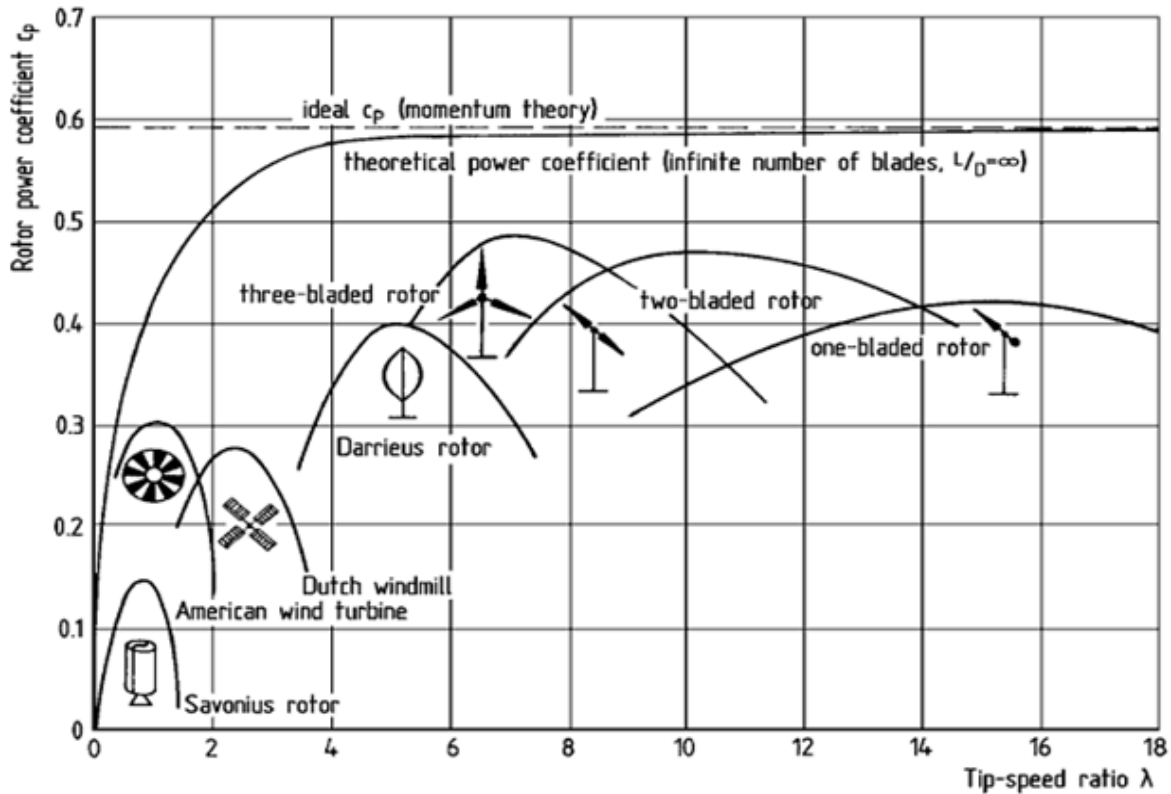


Figure 1.13 Power coefficients versus Tip speed ratio of different types of wind turbine (Hau/Springer, Germany, 2006)

1.9 Thesis Organisation

The present thesis contains six chapters. The content of the chapters are discussed below:

- In the first chapter, a brief introduction has been given on about the importance of wind energy in particular and renewable energy in general, then the global and national potential of renewable and wind energy as well. Also mentioned a brief about the phases of wind energy conversion technology, then the various techniques and devices to harness wind energy from wind resources are elaborately explained.

- Chapter two includes an extensive literature review of the entire thesis which has assisted the research methodically, technically and mathematically. It is divided into four parts so as to authorize to envision various aspects of the current investigation. These consist of literature survey of wind energy resource assessment, assessment methodology and numerical methods involve in it and then computational fluid dynamics (CFD) of vertical axis wind turbine (VAWT). Based on the literature survey objectives are itemized in the final part of this chapter.
- Chapter three deals with the wind energy potential assessment methodology and introduction of a new numerical method to estimate the parameters involve in the wind energy potential assessment (WEPA).
- In chapter four wind energy potential assessment in some locations in Northeastern and Eastern regions of India has been carried out. Then study the performance of the proposed numerical methods for the estimation of parameters involve in the Weibull distribution model for WEPA.
- Chapter five deals with methodology for the computational fluid dynamics (CFD) of vertical axis wind turbine (VAWT) and then modeling of computational model and validation. Finally, the results and discussion on CFD analysis of VAWT for assessing the performance of some airfoils such as NACA0016, NACA0019 airfoils for VAWT applications.
- Chapter six briefly describes the conclusions drawn from the analysis that is done in preceding chapters. Then the future scope of studies is also presented in this chapter.

CHAPTER 2

LITERATURE REVIEW

The importance of wind energy and the major phases required for harnessing useful energy from wind resources are clearly explained in the preceding chapter. In wind energy conversion technology (WECT) the most important phase is wind energy potential assessment and followed by the selection or design of wind turbine either horizontal axis or vertical axis wind turbine. In this chapter, a detailed state-of-art survey on assessment of wind energy potential, on statistical distribution and its numerical estimation methods and finally research and performance assessment of vertical axis wind turbine shall be reviewed.

2.1 Literature review on wind energy potential assessment (WEPA)

2.1.1 Studies on WEPA of various locations

In the application of wind energy conversion technology the kinetic energy of the wind is converted into useful electrical energy. As the wind energy is stochastic in nature, the analysis of wind characteristics and assessment of wind energy potential (WEP) is very important which is also considered as the basic input for the selection of wind turbine, the design of blade and then installation. Many earlier researchers have performed assessment of wind energy potential in different places of the world. For example Fagbenle et al. (2011) employed 21 years monthly average wind data to assess the WEP of Potiskum and Maiduguri, the two different sites in Nigeria. The data were measured using anemometer at a height of 10 m. They applied two parameter Weibull distribution model to analyse wind power potentials of the selected sites and found that 80% of wind data is of range 5.4 to 8.3 m/s and remaining is of range 3.6 to 5.4 m/s for Potiskum site. Similarly, 80% of data is of range 5.5 to 7.9 m/s and remaining is of range 4.5 to 6.8 m/s for the second site. Therefore, the corresponding wind power density based on the Weibull analysis came out to be 12.52 to 300.15 W/m² for Potiskum site and 114.77 to 360.04 W/m² for Maiduguri site which is not suitable for large scale power generation. Wind data collected during the year between 1995 and 2002 at five locations in Saudi Arabia were used to assess wind energy potential of the selected locations by Al-Abbadi (2005). The analysis revealed that Dhulum location provides highest average wind speed of 5.7 m/s followed by Arar with average wind speed of 5.4 m/s.

But the remaining three locations namely Dhahran, Yanbu and Gassim provide average wind speed of 5.3, 4.7 and 4.3 m/s respectively. Annual wind energy calculation shows that Dhulum, Arar, Dhahran, Yanbu and Gassim provide 990, 833, 730 and 454 MWh respectively at an altitude of 50 m. Similarly, Durak and Sen (2002) presented wind power potential of Akhisar site which is considered to be the most significant wind power potential availability site in Turkey. Performed the analysis collecting hourly wind speed data for one year (1997-98) and concluded that average wind power density of the site is 308 W/m² which can generate annual wind energy output between 31416 to 41560 MWh.

In another study eleven years wind speed data (1995-2005) of the capital of Iran, Tehran was used to find out the WEP of the country with the help Weibull distribution function by Keyhani et al. (2010). Analysis revealed that there was uniform wind speed throughout the data period; the whole year mean wind speed during cold and hot seasons are 4.338 and 4.067 m/s respectively. Therefore, the outcome of the analysis indicated that wind potential of the concerned site is not reliable for grid connection as it reported annual wind power density of 74.00-122.48 W/m² which are clearly shown in Table 2.1.

Table 2.1 Peak wind potential of 11 years in Tehran (Keyhani et al., 2010)

Year	Meteorological		Weibull	
	P/A (W/m ²)	E/A (kWh/m ² /year)	P/A (W/m ²)	E/A (kWh/m ² /year)
1995	103.25	904.47	98.44	862.33
1996	76.20	667.49	73.33	642.37
1997	88.85	778.32	82.15	719.63
1998	74.01	648.32	64.32	563.44
1999	93.55	819.54	84.04	736.19
2000	97.06	850.27	88.11	771.84
2001	94.63	828.97	88.95	779.20
2002	122.48	1072.96	108.95	954.66
2003	115.08	1008.14	101.92	884.76
2004	115.52	1011.98	103.88	909.98
2005	105.80	926.78	95.06	832.72
11 years	99.07	867.88	89.92	721.42

As far as India is concerned, several researchers studied wind energy potential assessment of a few places, for example Murthy and Rahi (2016) performed the assessment of wind energy potential for coastal site of Bheemunipatnam in Andhra Pradesh employing wind speed data of 32 years (1983-2014) collected at an anemometer height of 10 m while Nagababu et al. (2016) studied wind resources of entire coastal region of India by analysing the OSCAT

satellite data measured during 2012-2013 which will provide offshore wind power potential in India. In the first case, the peak, annual mean and mean wind speed were found in the range of 9.1-15.03 m/s, 4.41-5.6 m/s and 0.57-1.64 m/s respectively which falls wind power potential of class-1 (0 to 200 W/m²). Extrapolating the wind speed corresponding to 80 m or more, grid power can be generated from the available wind energy. But in the second case, the highest annual mean wind speed and corresponding wind power density of 6.6-13.4 m/s and 629.8-1632.5 W/m² was found at south-eastern coasts of India between Vizag and Tuticorin ports. India's average annual wind power from offshore wind resources excluding conflict area was found to be 1738.6 GW. However, if it is limited to 50 m depth, the average annual wind power will be 208.8 GW only.

As far as wind power assessment of onshore region of India is concerned Mathew et al. (2002) studied the analysis of WEP of eight sites (Trivandrum, Eranakulam, Aleppy, Calicut, Idukki, Palghat, Malapuram, Kasargod) of eight districts in Kerala, India using Rayleigh distribution method. Detail of the monthly mean speed of the 12 years wind speed data is reproduced in Table 2.2. When they compared the wind potential of selected sites, Palghat and Trivandrum provide the highest and lowest wind energy potential with annual average of 875 and 8.37 W/m² respectively. They also compared the performance of three wind turbine differing in their working velocity band for the said sites.

Table 2.2 Monthly average wind speed of all the eight sites in m/s (Mathew et al., 2002)

Month	Trivand	Eranak	Aleppy	Calicut	Idukki	Palghat	Malapu	Kasarg
Jan	1.39	2.33	2.64	2.2	6.2	9.14	5.68	3.06
Feb	1.54	2.52	2.8	2.55	5.4	8.3	4.57	3.54
Mar	1.7	2.75	3.15	2.77	3.42	7.38	2.5	3.78
Apr	1.8	2.58	3.15	2.74	2.74	7.29	2.38	3.62
May	2.28	2.97	3.33	2.99	3.89	10.06	2.62	3.58
Jun	2.41	2.44	3.17	2.18	4.73	11.07	3.18	3.89
Jul	2.58	2.61	3.07	2.15	4.49	11.44	3.06	4.09
Aug	2.76	2.66	2.93	1.95	4.61	11.07	4.57	4.17
Sep	2.48	2.49	2.96	2.13	2.46	10.33	2.82	3.10
Oct	1.8	2.19	2.56	1.95	3.3	7.11	2.38	2.78
Nov	1.29	1.99	2.24	1.83	4.13	6.74	2.62	3.02
Dec	1.24	2.05	2.77	1.85	4.89	8.58	6.0	3.38
Yearly	1.94	2.46	2.9	2.27	4.19	9.04	3.53	3.50

In another study, an effective simulation technique to generate wind power potential maps was presented by Tank et al. (2016). Using this technique wind power potential maps of all the 30 states were generated. Then identifying 4691 sites in entire India the wind power potential of all the sites were compared and results showed that highest wind power potential is available at some locations in Madhya Pradesh, Sikkim and Tamil Nadu. Next class of wind power potential were observed at some locations in Andhra, Gujarat, Jammu & Kashmir, Kerala, Maharashtra, Orissa, Rajasthan, Sikkim, Tamil Nadu and Madhya Pradesh. Last class of wind power potential is available in the rest of India.

In addition to above researchers many more researchers have analysed wind energy potential assessment which are summarized in Table 2.3. It shows that wind energy potential assessment have been studied globally, however, extensive assessment on wind energy potential of many places in India is still undergoing. To our knowledge wind energy potential assessment of eastern and north-eastern regions of India is still untouched.

Table 2.3 Summary of literature review on wind energy potential assessment

<i>Researchers</i>	<i>Country</i>	<i>Number of locations</i>	<i>Data period</i>	<i>Measurement height(m) Actual(A)/ Extrapolated(E)</i>	<i>Mean wind speed(M)/wind speed range (m/s)</i>
Ahmed (2010)	Egypt	Ras Benas	10 years	10 (A)	4.7 – 7.5
Akpinar & Akpinar (2005)	Turkey	4	1998-2003	10 (A)	5.72, 3.84, 3.11, 2.26
Albadi (2009)	Oman	Duqm	2003-07	10 (A)	2.93 -9.76
Aririguzo & Ekwe (2018)	Nigeria	Umudike	2006-15	30 (E)	6.23 -9.81
Bekele and Plam (2009)	Ethopia	4	2000-03	10 (A)	3.0 – 4.0
Carneiro et al. (2016)	Brazil	3	2012-13	80 (E)	5.63, 7.55, 6.71
Elnagger et al. (2017)	Palestine	Gaza	1991-2010	10(A)	2.0 - 6.0
Feretic et al. (1999)	Croatia	6	1966-74	35 (E)	3.14 - 7.16
Gaddada & Kodicherla (2016)	Ethopia	8	2002-14	10 (A)	1.04 – 3.49
He & Kammen (2014)	China	200	2001-10	100 (A)	4.0
Manwell et al. (2002)	USA	12	1975-98	60 (E)	7.0 – 8.4
Ngala et al. (2007)	Nigeria	Maiduguri	1995-2004	25 (E)	3.0 - 5.11

Table 2.3 (Continued)

Researchers	Country	Number of locations	Data period	Measurement height(m) Actual(A)/ Extrapolated(E)	Mean wind speed(M)/wind speed range (m/s)
Nhoud & Smairan (2015)	Jordan	Azraq	1991-2001	10 (A)	4.0 – 5.0
Nze-Esiaga & Okogbue (2014)	Nigeria	5	1961-2011	10 (A)	1.3 – 13.2
Optis et al. (2020)	USA	California	2000-19	100	8.6 – 9.8
Ozatpal et al. (2000)	Turkey	42	1990-95	50 (E)	1.7- 8.4
Pishgar-Komleh et al. (2015)	Iran	Firouzkooh	2001-10	10 (A)	4.83-8.60
Rehman et al. (2003)	Saudi Arabia	20	1972-82	5-10 (A)	
Rehman & Ahmad (2004)	Saudi Arabia	5	1970-83	10 (A)	3.8 – 6.2 (M)
Sengupta et al. (2016a)	India	Silcher	2008-11	25 (E)	1.0 – 1.69
Serdari et al. (2017)	Albania	Karaburun	1981-2014	50 (A)	5.96 – 6.98
Shata & Hanitsch (2006a)	Egypt	10	10 years	10 (A)	2.0 – 6.3
Shata & Hanitsch (2006b)	Egypt	7	5 & 10 years	10 (A)	3.0 – 7.3
Shu et al. (2015)	Hong Kong	3	2005-10		3.78 – 4.74
Soulouknga et al. (2017)	Sudan	3	1975-2010	10 (A)	2.3 -4.0
Tizgui et al. (2017)	Morocco	Agadir	2016	10 (A)	3.05 – 3.71
Ucar & Balo (2009)	Turkey	6	2000-06	10 (A)	4.4 -10.9
Weisser (2003)	West Indies	Grenada	1996		4.0 – 7.2

2.1.2 Studies on Statistical distribution models for WEPA

There are several statistical distribution models to assess wind energy potential such as Exponential (Exp), Weibull, Rayleigh, Gamma (Gam), Beta, Kappa, Normal, Lognormal (LN), Inverse Gaussian (IG), Log–Logistic (LL), Generalized extreme value (GEV), Erlang (Erl), Nakagami (Nak), etc. To select an appropriate and accurate distribution model is a crucial task as the accuracy of the assessment results depends on this distribution model. In this regards several authors have studied the performance comparison of various distribution models which are presented in this section of literature review.

Akpinar and Akpinar (2005) assessed the sessional variations of the wind characteristics and wind energy potential for four different sites in Turkey (Maden, Agin, Keban and Elazig)

employing wind speed for the period from 1998 to 2003. Weibull and Rayleigh distribution models were used for the analysis. The present set of wind speed data falls in the low scale wind speed range excepting Maden station and the seasonal mean wind speed ranges from 2.98-6.66 m/s, 2.45-4.75 m/s, 1.40-3.29 m/s and 1.19-2.48 m/s. It was observed that Maden site found to be the best location for wind power generation followed by Agin. Further, the results of the performance analysis showed that Weibull distribution provided the better results for all the stations and therefore, considered as the most accurate distribution method for wind power assessment.

A comparative analysis employing the wind speed data of five different stations in east and southeast parts of Iran was performed by Alavi et al. (2016) to obtain a suitable model from eight different statistical distribution models namely, Weibull, Exp, Gam, LN, IG, LL, GEV, and Nak. The wind speed range of the five locations are 4.82-15.20 m/s, 8.81-30.30 m/s, 4.87-22.30 m/s, 4.47-23.80 m/s and 5.66-32.00 m/s respectively. Among them Nak model was introduced for the first time and analysis revealed that performance of Nakagami function was as good as the performance of Weibull function. They observed that Weibull and Nak distribution models are two flexible and effective models for wind resource assessment and suggested to perform more comparative analysis using new set of wind speed data in future.

Performance of non-parametric and parametric distribution models was evaluated by Wang et al. (2016). Among parametric models the performance of six different statistical distributions namely, Normal, LN, Gam, LL, Weibull and Rayleigh distribution methods were compared through six statistical evaluation criteria namely, Mann-Whitney test, KS (Kolmogorov-Smirnov) test, Chi square error (Chi-SE), root mean square error (RMSE), correlation coefficient (CC). Simultaneously comparison of the effectiveness of five numerical estimation methods: Least Square method (LSM), Maximum Likelihood method (MLM), Moment method (MOM), Maximum entropy principle method (MEPM) and CS algorithm (CS) was also performed. For this 10 years wind speed data collected from four stations in central China was used and revealed that among the non- parametric: kernel density estimation was considered to be effective for data analysis and therefore, compared with parametric models and found that it performed better than the later one. But in case of parametric distribution models the Weibull distribution method outperformed all other methods. As far as numerical estimation methods are concerned CS algorithm provided optimum value of CC test while MOM provided the optimum value of KS test. Thus both the

CS algorithm and MOM showed almost equal effective performance in present analysis. . Similarly, Yilmaz and Celik (2008) compared the performance of both distribution models and Weibull parameter estimation methods employing wind speed of seven sites in Turkey. Mean wind speed of all the sites at 5 m anemometer are 5.8, 3.5, 6.2, 3.9, 2.6, 2.5 and 3.5 m/s. Statistical distribution models which were compared are Beta, Erl, Exp, Gam, LL, LN, Pearson V, Pearson VI, Uniform and Weibull distribution while the Weibull estimation methods were LSM, MLM and MOM. Applying three effective judgement criteria namely KS test, Chi-SE and Anderson Darling test (AD test) the results revealed that Beta and Weibull provided acceptable Chi- Square and KS test error while Weibull provided acceptable AD test error. Thus overall performance showed that Weibull distribution outperformed all other methods.

In another study (Garcia et al., 1998) the performance of Weibull and Lognormal distribution models employing wind speed of 20 sites in Navarre was analysed. Effectiveness of both the models was judged from the results of coefficient of determination with a linear regression for the Weibull and a nonlinear distribution for the later one. It was observed that later provided better fit for the wind speed less than 2 m/s and for other wind speed range Weibull provided better fit for distribution. In most cases percentage of wind speed is significantly higher than 0-2 m/s range and therefore, overall performance showed that Weibull model could be considered as the best distribution model for wind energy application.

Table 2.4 Previous studies on statistical distribution model associated with WEPA

<i>Study</i>	<i>Statistical distribution model (remark)</i>	<i>Mean wind speed/ Wind speed range (m/s)</i>	<i>Wind Data period</i>	<i>Height (m)</i>	<i>No. of sites & study area</i>
Acakpovi et al. (2017)	Weibull	3.77-8.24	2013-18	10	24 sites in Ghana
Ahmed (2010)	Weibull	4.7-7.5	10 years	10	Ras Benas in Egypt
Akdag & Dinler (2009)	Weibull	5.04, 3.78, 3.60, 5.95	1997-2006	10	4 sites in Turkey
Akpinar & Akpinar (2005)	Weibull (better) Rayleigh	2.98-6.66, 2.45-4.75, 1.40-3.29, 1.19-2.48	1998-2003	10	4 sites in Turkey
Akgul et al. (2016)	Weibull Inverse Weibull (same)	1.42-2.29, 1.34-1.95	2009	10	2 sites in Turkey
Alavi et al. (2016)	Weibull (best), Gam, LL, Exp, IG, LN, GEV, Nak (best)	4.8, 8.8, 4.8, 4.5, 5.7	1-3 years (2008-15)	10	5 sites in Iran

Table 2.4 (Continued)

Study	Statistical distribution model (remark)	Mean wind speed/ Wind speed range (m/s)	Wind Data period	Height (m)	No. of sites & study area
Albadi et al. (2009)	Weibull	2.93-9.76	2003-07	10	Duqm in Oman
Al-Buhairi (2006)	Weibull (better) Rayleigh	3.24-5.49	1999-2002	10	Taiz in Yemen
Andrade et al. (2014)	Weibull	0.5-8.5, 1-16	2005-10	10	2 sites in Brazil
Aririguzo & Ekwe (2018)	Weibull	6.23-9.81	2006-15	30	Umudike in Nigeria
Arslan et al. (2014)	Weibull	0.4-6.6	2008	10	Bilecik in Turkey
Aukitino et al. (2017)	Weibull	4-7	2012-13	34	2 sites in Kiribati
Azad et al. (2015)	Weibull	2.0-4.0, 2.28-8.34, 2.5-4.0	-	10	3 sites in Bangladesh
Bekele & Palm (2009)	Weibull	3.0-4.0	2000-03	10	4 sites in Ethiopia
Bidaoui et al. (2019)	Weibull (better) Rayleigh	3.8-5.3, 6.4-7.7	1 year	10	5 sites in Morocco
Bilir et al. (2015)	Weibull	2.986	2012-13	20	Atilim in Turkey
Carneiro et al. (2016)	Weibull	0.4-14.8, 0.4-16.8, 0.4-14.3	2012-13	80	3 sites in Brazil
Celik (2003)	Weibull (better) Rayleigh	0-2.00 (56%) 1.62-2.87	1996	10	Iskenderun in Turkey
Chang (2011)	Weibull	4.4-13.3, 5.3-10.0, 5.0-14.8	2006-07	64.7	3 sites in Taiwan
Chaurasiya et al. (2017)	Weibull	0.317-17.30		60	Kayathar, TN, India
Dorvlo (2000)	Weibull	0-2.0 (2.7%) 2.0-14.0	1986-98	10	4 sites in Oman
Fagbenle et al. (2011)	Weibull	3.6-8.3, 4.5-7.9	1987-2007	10	2 sites in Nigeria
Feretic et al. (1999)	Weibull	3.14-7.16	1966-74	35	6 sites in Croatia
Gaddada & Kodicherla (2016)	Weibull	1.04 – 3.49	2002-14	10	8sites in Ethiopia
Genc et al. (2005)	Weibull	1.41-1.77	1997-2001	10	Aksehir in Turkey
Gugliani (2020)	Weibull, Nak, RD, JD, GHD (best)	2.48-10.0, 2.86- 10.55, 2.21-9.72, 1.92-8.6, 2.4-10.0, 3.53-13.06	30 years	10	6 sites in India
Katinas et al. (2018)	2-Para Weibull (best), 3-Para Weibull Rayleigh	2.0-3.0 (lowest) 4.0-5.0 (highest)	1945-90 2014-16	10	18 sites in Lithuania
Keyhani et al. (2010)	Weibull	3.50-5.93	1995-2005	10	Tehran in Iran

Table 2.4 (continued)

Study	Statistical distribution model (remark)	Mean wind speed/ Wind speed range (m/s)	Wind Data period	Height(m)	No. of sites & study area
Kose (2004)	Weibull (better) Rayleigh	3.4-5.8	7/2001-2/2003	10	Dumlipinar in Turkey
Mathew et al. (2002)	Rayleigh	1.29-2.76 (lowest) 6.7-11.44 (highest)	12 years	10	8 sites in Kerala
Mohammadi et al. (2016)	Weibull	3.55, 3.67, 5.30, 5.27	2012-14	10	4 sites in Canada
Murthi & Rahi (2016)	Cubic factor method, Weibull (same)	4.42-5.41	1983-2014	10	Coastal site in Andhra
Nhoud & Smairan (2015)	Weibull	4.0-5.0	1991-2001	10	Azraq in Jordan
Nze-Esiaga & Okogbue (2014)	Weibull	1.3-13.2	1961-2011	10	5 sites in Nigeria
Ozay & Celiktas (2016)	Weibull (better) Rayleigh	0-2 (4%), 2-18	5.5 yrs	10	Izmir in Turkey
Pishgar-Komleh et al. (2015)	Weibull (little better) Rayleigh	4.83-8.60	2001-10	10	Firouzkooh in Iran
Rocha et al. (2012)	Weibull	6.67-10.65, 4.51-11.53	2004-06	10	2 sites in Brazil
Safari & Gasore (2010)	Weibull (better) Rayleigh	2.09, 2.07, 0.88, 2.75, 1.43	1974-93	10	5 sites in Rwanda
Saleh et al. (2012)	Weibull	3.8-12	1991-95	10	Zafarana in Egypt
Saxena & Rao (2015)	Weibull	3.2-8.6	2011-13	50	Soda in Rajasthan
Serban et al. (2020)	Weibull (better) Rayleigh	5.443, 5.414	2017-18	10	2 Galati in Romania
Shata & Hanitsch (2006a)	Weibull	2.4, 2.9, 4.4, 5, 5.3, 5.4, 4, 3.4, 4.6, 4.4	10 years	10	10 sites in Egypt
Soulouknga et al. (2017)	Weibull	2.69, 2.33, 1.91	1975-2010	10	3 sites in Chad
Sumair et al. (2020)	Weibull	1-8, 1-5, 1-12	2014-17	10	60 sites in Pakistan
Tizgui et al. (2017)	Weibull	1-6 m/s (92.7%), 0-1 (0.88%), >6 (6.4%)	2016	10	Agadir in Morocco
Ucar & Balo (2009)	Weibull	4.4-10.9	2000-06	10	6 sites in Turkey
Usta (2016)	Weibull	2.09-3.75, 1.45-2.33	2006-07	10	2 sites in Turkey

From the above literature on statistical distribution model for wind energy potential assessment (WEPA) and summary of it that presented in Table 2.4, it can be drawn that more

than 95% of the researchers claimed two-parameter Weibull distribution model is the most accurate and effective model for wind energy potential assessment. Although two-parameter Weibull distribution is most popular for providing the best fit comparing other available distribution models, Wais (2017), Weisser (2003) and Pishgar-Komleh et al. (2015) claimed that it does not reveal good conformity for low wind speed data and unable to represent the probabilities of null wind speeds. In such case sometimes few researchers suggested that Rayleigh distribution may be one of the alternative effective distribution models. Therefore, several studies have investigated to compare the performance of Weibull and Rayleigh distribution models. For example, Pishgar-Komleh et al. (2015) compared performance of Weibull and Rayleigh distribution models employing ten years (2001-2010) wind speed data collected at a height of 10 m and also estimated wind power potential of Firouzkooch located in Tehran. For better analysis they used the extrapolated wind speed using surface roughness value (α) of 0.143 in which 10% of wind speed data falls in the range of 0-2 m/s. The performance analysis revealed that correlation coefficient, RMSE, MPE and MAPE for Weibull were 0.976, 0.007, 41% and 55% respectively while corresponding value for Rayleigh model were 0.975, 0.008, 40%, and 55% respectively. Results indicated Weibull is still better than Rayleigh model.

Employing six years (2008-2014) wind speed data of Alacati region, Izmir collected at different height analysed the wind characteristics of the region and simultaneously performance of Weibull and Rayleigh distribution models was compared by Ozay and Celiktas (2016). In the given set of data the frequency of 0-1 m/s and 1-2 m/s wind speed range are 0.78% and 3.18% respectively and remaining are 2-18 m/s. For the comparison of Weibull and Rayleigh distribution models three effective performance criteria such as CC, Chi-SE, RMSE were used and the results revealed that Weibull distribution provided minimum error which ultimately better fit for the selected set of wind data. As far as wind potential is concerned mean wind speed of whole period is 8.11 m/s and highest wind speed was found in July with monthly mean speed of 9.10 m/s. Further, analysis revealed the most probable wind speed and wind speed carry the most energy as 6.61 m/s and 12.77 m/s respectively.

In another study (Bidaoui et al., 2019) employing the wind speed data of five locations (Tetuan, Tangier, Nador, Al-Hoceima and Larach) in Morocco compared the performance of Weibull and Rayleigh distribution models. Twelve months wind data collected at a height of 10 m has average wind speed range of 6.4-7.7 m/s for Tetuan and Tangier and 3.8-5.3 m/s for

the remaining three locations. For the comparative analysis four statistical performance criteria namely, coefficient correlation, RMSE, Chi-SE, Mean bias error (MBE) were applied and results showed that Rayleigh provided minimum value of MBE and Chi-SE error in Tetuan and Nador locations whereas Weibull provided optimum values of error in all other locations. Therefore, Weibull distribution function fitted the present set of data significantly better than Rayleigh model.

Another effective alternative model to two- parameter Weibull distribution may be three-parameter Weibull distribution model and therefore, Wais (2017) investigated the performance of three-parameter Weibull distribution model employing wind speed collected from three site in Poland and compared with former model. For the site 1 located in north-east, data were collected during 1971-2000, similarly for the site-2 and site-3 (located in south-east and north-west) data were collected during 1985-2000 and 1971-2000 respectively which has several 0, 1 and 2 m/s wind speed as shown in Table 2.5. Results revealed that two- parameter distribution model provide better fit when the frequency of zero/null velocity is insignificant but three-parameter distribution model is more effective when there is significant amount of null velocity and therefore, later may be considered as a useful alternative to former one.

Table 2.5 Wind speed percentage of occurrence of all the sites (Wais 2017)

<i>Wind speed (m/s)</i>	<i>Site 1</i>		<i>Site 2</i>		<i>Site 3</i>	
	<i>hour</i>	<i>% of Occurrence</i>	<i>(hour)</i>	<i>% of Occurrence</i>	<i>(hour)</i>	<i>% of Occurrence</i>
0	814	9.29	225	2.57	459	5.24
1	1126	12.85	912	10.41	1025	11.70
2	1590	18.15	1636	18.68	1817	20.74
3	1531	17.48	1707	19.49	1665	19.00
4	1242	14.18	1554	17.74	1353	15.44
5	981	11.20	1177	13.44	1002	11.44
6	638	7.28	667	7.61	599	6.84
87	432	4.93	434	4.95	463	5.28
98	262	2.99	216	2.47	207	2.36
9	144	1.64	118	1.35	108	1.23
10	0	0	69	0.79	38	0.43

2.1.3 Studies on numerical estimation method for Weibull parameters

Weibull parameters have significant effects on the success of Weibull distribution model. For a given set of wind data, several numerical methods can be used to estimate Weibull parameters. Selection of the best method is an important pre-requisite condition to obtain the

accurate value of Weibull parameters as the accurate and efficient parameters is very important to obtain the best fit for the distribution. Therefore, many earlier studies have compared the performance of several numerical methods which are presented in this section. Akdag and Dinler (2009) compared the performance of graphical method (GM), MLM, MOM and introduced a new method called power density method (PDM) which has simple non iterative formulation. Employed wind speed data of four sites collected at a height of 10 m in Turkey to perform the comparative analysis and results showed that PDM was an effective alternative method as it provided minimum errors.

The performance of seven numerical estimation methods namely, Empirical method (EM), PDM, GM, MOM, MLM, Modified MLM (MMLM) and Equivalent Energy method (EEM) was evaluated by Andrade et al. (2014) employing six years (January 2005-December 2010) wind speed data collected at two coastal regions (Camocim and Icapui) in Northeast region Brazil. To validate and compare the performance of all the selected numerical methods three effective statistical tests were applied: Chi-SE, RMSE, CC. Results of the analysis showed that EEM provided best ranking of performance with the data of Icapui site while PDM and GM provided best ranking of performance with the data of Camocin site. Overall performance showed that EEM was superior to all other methods. In the same way comparative analysis of seven numerical estimation methods namely, Median and quartiles method (MQM), MOM, LSM, MLM, MMLM, PDM and EEM was studied by Aukitino et al. (2017) while assessing the wind energy potential of two sites (Tarawa and Abaiang) in Kiribati which is located at the equator in the central Pacific Ocean. For the analysis wind speed at anemometer height of 20 m and 34 m were measured and it was observed that wind speed of Abaiang was slightly higher than other site, but both the sites have similar wind characteristics possessing wind speed range of 4-7 m/s at 20 m. For the performance analysis of the estimation methods effective statistical criteria such as, CC, RMSE, coefficient of efficiency (COE), mean absolute error (MSE) and mean absolute percentage error (MAPE) had been used. It was observed that MOM outperformed all other methods.

A new method called probability weighted moments based on the power density method (PWMBP) was developed for the first time by Usta (2016) for estimation of Weibull parameters and compared the performance with six conventional methods namely, MLM, MMLM, MOM, GM, PDM and PWMM (probability weighted moments method). For the analysis, two years (2006 and 2007) wind speed data collected at Cide and Keban of Turkey were used. To validate and analyse performance four important statistical criteria namely,

RMSE, CC, PDE and KS were considered. Results of the performance criteria showed that PWMBP provide more number of better performances followed by PWMM for both Cide and Keban stations. Again, Usta et al. (2018) introduced another new estimation method known as method of multi-objective moments (MUOM) and compared its performance with widely accepted numerical methods such as GM, MLM, MMLM, MOM and PDM. In this case wind speed data was collected at five sites in Turkey at a height of 10 m whose mean of the wind speed range are 2.30, 4.68, 3.33, 4.72, 2.30 m/s respectively. Applying five judgement criteria namely, Chi-SE, CC, RMSE, PDE and KS performance were compared and results revealed that MUOM significantly superior to other methods and followed by PDM.

Chang (2011) also studied the performance of six estimation methods (MOM, EM, GM, MLM, MMLM, PDM) employing wind speed data measured at Dayuan, Hengchun and Penghu of Taiwan. The collected wind speed data contains insignificant wind frequency 0-2 m/s wind speed range as the most of the monthly mean wind speed is greater than 4.4 m/s. Probability density function and cumulative distribution function along with histogram of actual wind speed data of Hengchun and Penghu are presented in Figure (2.1 and 2.2) which shows the accuracy of various estimation methods. Further for the performance analysis RMSE in pdf and max-error in cdf were compared and results showed that MLM provide least error in all three stations followed by MMLM; while EM and PDM provide similar performance. Least performance was reported by the GM.

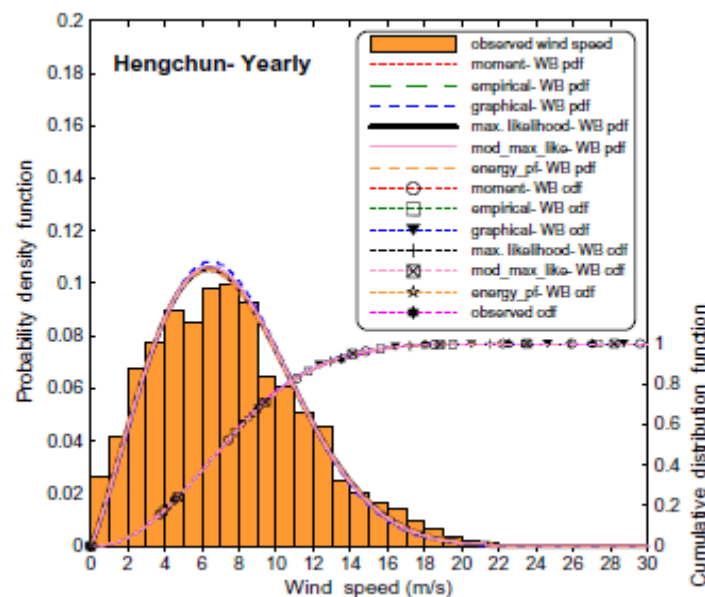


Figure 2.1 Yearly PDF and CDF of Hengchun site in Taiwan (Chang, 2011)

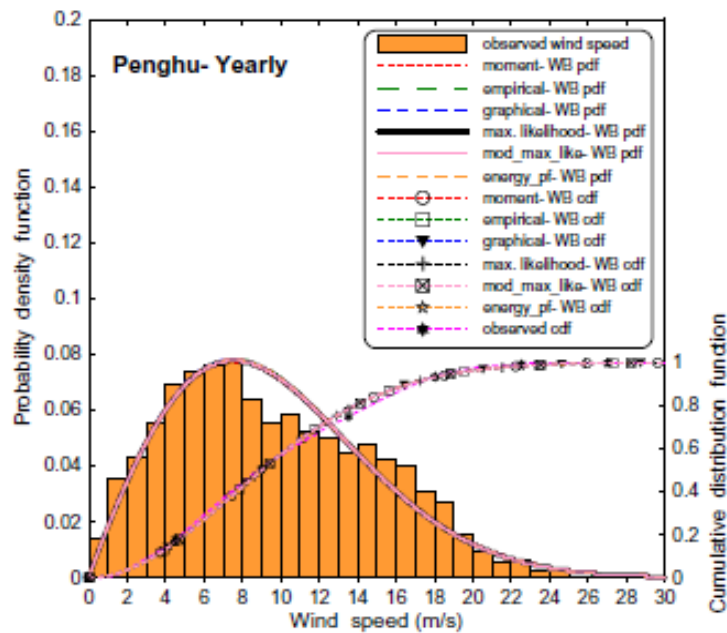


Figure 2.2 Yearly PDF and CDF of Penghu site in Taiwan (Chang, 2011)

In another similar study (Tizgui et al., 2017) comparative analysis of seven numerical estimation methods namely, GM, MLM, EM, Empirical method of Lysen (EML), PDM, MOM, Mabchour's method (MMab) was performed to select the most effective and accurate method. For the analysis, one year (2016) hourly wind speed data was collected at a height of 10 m at Agadir Airport, Morocco. Most of hourly wind speed falls in the range of 1-6 m/s as it has 0.88% of null speed and 6.4% of wind speed greater than 6 m/s only. For the performance analysis four effective judgement criteria namely, CC, Chi-SE, RMSE and PDE were considered and analysis revealed that MLM, PDM and MOM provided almost equal error percentage, further MLM provided minimum power density error. Therefore, overall performance showed that MLM is the most effective in estimating Weibull parameters for the current set of data. Similarly, performance of L- moment method was compared with the two of widely accepted numerical method namely, MOM and MLM by Arslan et al. (2004) employing wind speed collected at 10 m height at Bilecik Province in Turkey. Results revealed that L-moment provided better results for small sample size and otherwise MLM performed better result.

Moreover several other researchers have performed the comparative analysis of various numerical estimation methods to identify the effective estimation methods which are summarized in the following Table 2.6.

Table 2.6 Previous studies on numerical estimation methods to determine Weibull parameters

<i>Study</i>	<i>No of sites & study area</i>	<i>Numerical methods for Weibull parameters</i>	<i>Judgement criteria</i>	<i>Best method</i>
Azad et al. (2014a)	Hatiya Island in Bangladesh	GM, MOM, EM, EEM,	Chi-SE, RMSE, MPE, MAPE,	MOM
Azad et al. (2015)	3 sites in Bangladesh	PDM, LSM, MMLM	Chi- SE, CC, Relative percentage error (RPE)	LSM
Azad et al. (2014b)	3 sites in Bangladesh	GM, MOM, PDM, EM, MLM, EEM, MMLM,	RMSE, RPE, Chi-SE, CC, MPE, MAPE	MOM and MLM but PDM is effective for low altitude
Bilir et al. (2015)	Atilim University in Turkey	MLM, EM, PDM, MOM, GM	RMSE	EM and PDM
Carneiro et al. (2016)	3 sites in Brazil	PSO, MOM, EM, PDM, EEM, MLM	CC, RMSE, Relative bias (RB)	PSO followed by EEM
Chaurasiya et al. (2017)	Kayathar, Tamil Nadu, India	GM, MOM, EM, EML, PDM, MLM, MMLM, LSM, Alternative MLM	RMSE, CC, MAPE, Chi-SE	MLM followed by MMLM
Dorvlo (2002)	4 sites in Oman	MOM, LSM, Chi-square method	K-S test	Chi-square method
Genc et al. (2005)	Aksehir region in Turkey	MLM, LSM, MOM,	Monte-Carlo simulation	MLM followed by MOM
Katinas et al. (2018)	2 sites in Lithuania	MLM, MMLM, EEM	CC, RMSE, Chi-SE, PDE	MLM and EEM
Mohammadi et al. (2016)	4 sites Alberta province of Canada	GM, PDM, EM, EML, MLM, MMLM	MAPE, RMSE, RPE, RB, CC, Relative RMSE	EM followed by EML, PDM, MLM
Rocha et al. (2012)	3 sites in Brazil	GM, MLM, PDM, MOM, EM, MMLM, EEM	RMSE, Chi-SE, COV	EEM
Saleh et al. (2012)	Zafarna stations in Egypt	GM, EM, PDM, MLM, MMLM	RMSE	EM and MLM
Saxena & Rao (2015)	Thar desert in Rajasthan, India	GM, EM, MMLM, PDM	RMSE	MMLM followed by PDM
Seguro & Lambert (2000)	Sample data	MLM, MMLM, GM	Energy output error (%)	MLM
Sumair et al. (2020)	60 sites in Pakistan	Wind Energy Intensification Method (WEIM), MLM, MMLM	Wind energy error (WEE), RMSE, CC (R ²)	WEIM followed by MMLM
Werapun et al. (2015)	Phangan Island in Thailand	GM,EM, PDM, MLM, MMLM	KS test, CC, RMSE, PDE.	MLM followed by PDM

2.2 Literature review on Computational Fluid Dynamics of VAWT

Computational Fluid Dynamics (CFD) is considered to be one of the promising, cost effective and accurate methods for analyzing the complex, unsteady aerodynamics nature of VAWT and has ability to generate results as good as experimental results (Jin, 2015). Consequently CFD study of VAWT can check the possibility of improvement in the performance of VAWT and thereby its overall efficiency.

Several earlier researchers have tried to analyse the aerodynamic performance and then to improve the efficiency. For example, Bai et al. (2015) performed CFD analysis of H-Rotor type VAWT with modified NACA0015 airfoils section. A 2.5-dimensional model was also constructed and compared to a 2-dimensional model to examine the 3-dimensional effect using $k-\omega$ SST turbulence model. They discovered a small variation around 180° – 270° degrees of rotation, but the overall predictions indicated both were identical. The thrust values for the 2.5D model are greater at 180° – 224° and lower at 225° – 270° , indicating that the discrepancy is mostly due to the vortex structure. They also investigated the performance of VAWT with modified straight blades. The modified turbine blade's average and maximum thrusts were found to be 1–10% and 20–240 newton lower than the straight blade, respectively. With rising amplitudes and decreasing wavelengths, the overall values of the force were observed to decrease, owing to changes in the vortex structure. The major causes of this change in vortex structure were determined to be a decrease in vortex velocity magnitude and migration of the vortex toward the trailing edge of the blade.

In a different work, Balduzzi et al. (2016b) performed multivariate sensitivity analysis through two dimensional CFD simulations of Darrieus VAWT to determine the appropriate mesh and timestep sizes so as to obtain an accurate simulation. A Grid-Reduced version (GRV) of vorticity is recommended as the best indication for mesh refinement quality for this purpose. The necessity to accurately describe the vortices detaching from the blades in the upwind area makes the timing requirements much stringent for low TSRs. In order to accomplish so, the study emphasises suitable Courant Number thresholds. Finally, the integrated method provided in the study is considered to be capable of determining the mesh and timestep requirements in a Darrieus turbine CFD simulation. From the study, it is expected to make a significant contribution to numerical studies in the near future by establishing a standard for these simulations and concurrently lowering computing costs owing to preliminary sensitivity evaluations.

Accuracy of two dimensional CFD simulations was studied by Bianchini et al. (2017) comparing with the experimental result for Darrieus VAWT. For the simulation $k-\omega$ SST turbulence model was used and analysis revealed that two dimensional simulations can provide reasonably accurate estimates for both overall performance (Figure 2.3) and flow field description around rotor. In similar study Nobile et al. (2014) performed CFD investigation of augmented VAWT with NACA0018 airfoils. Although discrepancy factor of numerical and experimental data was observed, the overall numerical result was quite agreement with the experimental result.

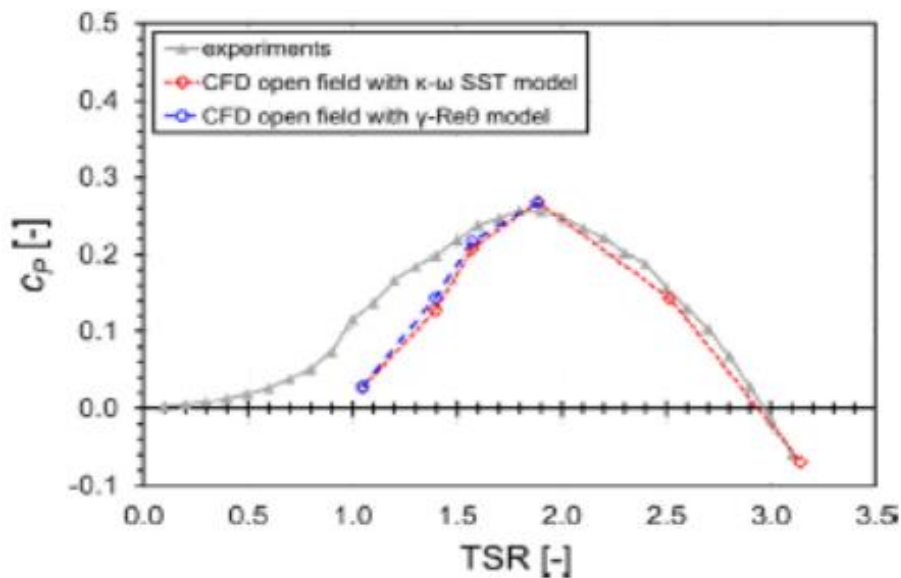


Figure 2.3 Comparison of experiments and 2D simulation (Bianchini et al., 2017)

Quantitative study of flow field past a VAWT under various operating parameters, using both 2D and 3D conditions was studied by Franchina et al. (2019). For this investigation, $k-\omega$ SST model was utilised, and a second experiment was undertaken to validate the numerical model. Details of the flow around rotor in 2D and 3D as well are presented in Figures 2.4 to Figure 2.7. The completely 3D character of the flow around VAWTs has been seen to have major effects on the flow distribution at midspan, resulting in a less restrictive condition in real 3D modelling than that predicted from 2D simulations. As a result, the evaluation study's principal finding is that results generated from 2D simulations are not supported by 3D computations. Based on 2D simulations, the presence of non-aerodynamic struts caused a considerable local loss generation, which lowered the turbine's performance by over a third. In addition, the complicated trailing vorticity released in the blade's tip area was examined. In

the downstream wake, the vortices formed by the blades towards wind direction are found to be the strongest and most persistent. As a whole the results of 3D simulation was quite consistent with experimental results.

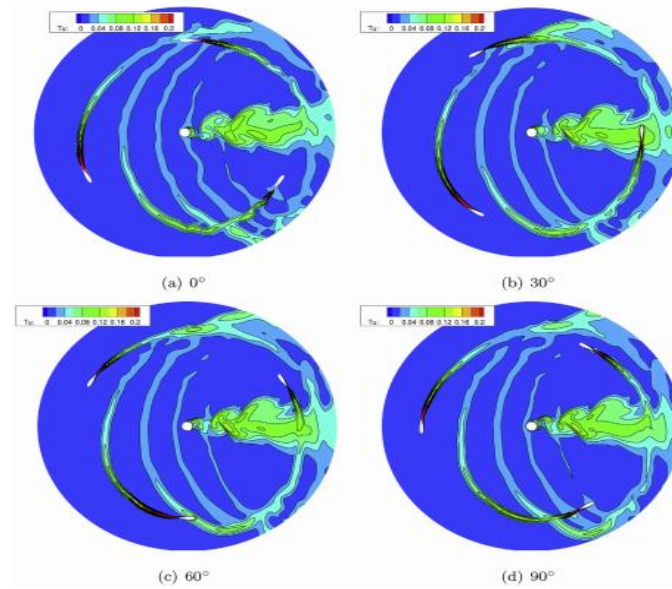


Figure 2.4 Two dimensional-Turbulence intensity contours at different angular positions at TSR=3.3 (Franchina et al., 2019)

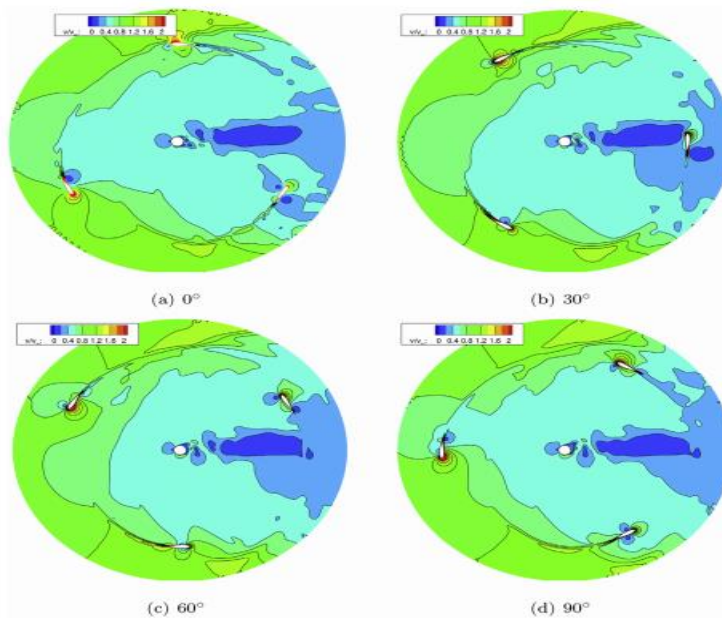


Figure 2.5 Two dimensional-Velocity magnitude contours at different angular positions at TSR=3.3 (Franchina et al., 2019)

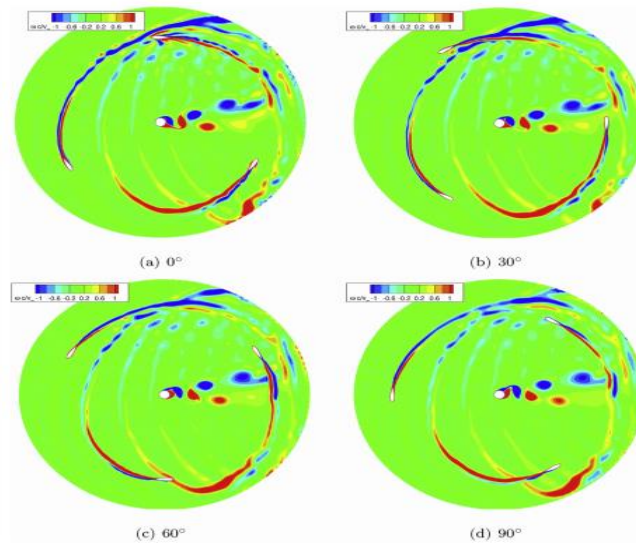


Figure 2.6 Two dimensional-Vorticity contours at different angular positions at TSR=3.3 (Franchina et al., 2019)

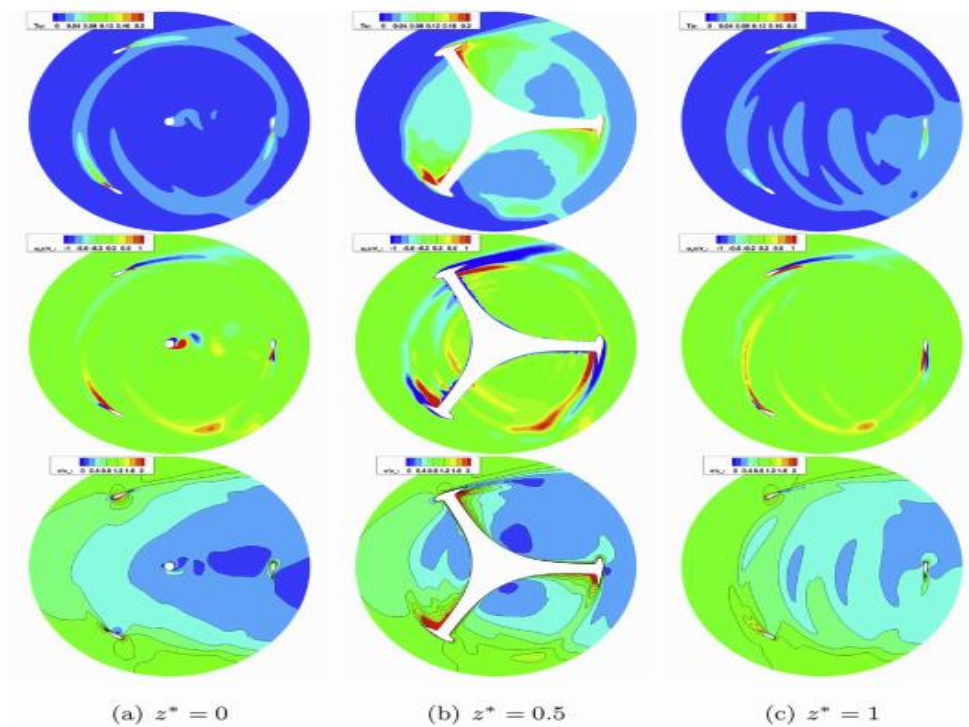


Figure 2.7 Three dimensional-Turbulence intensity, vorticity and velocity contours on the symmetry, midspan and tip sections at $\theta=30^\circ$ and TSR=3.3 (Fanchina et al., 2019)

A steady-state two-dimensional CFD study using Fluent 6.2 software was studied by Gupta and Biswas (2010) to model the flow across a twisted three-bladed H-Darrieus rotor. For this study, the conventional $k-\epsilon$ turbulence model was used. For two distinct wind velocities, aerodynamic coefficients such as lift, drag, and lift-to-drag coefficients were analysed with

regard to angle of attack. A new experimental method for determining aerodynamic coefficients was also emphasised. The correlation equations for lift and drag coefficients were developed for this purpose. The experimental and computational findings were compared, and the results indicated good agreement. Twist blades also found having positive lift at zero incidences, as opposed to symmetrical blades, which had zero lift at zero incidences.

A combined experimental and computational analysis of the aerodynamics and performance of a small-scale vertical axis wind turbine (VAWT) were presented by Howell et al. (2010). Wind tunnel experiments were conducted along with two and three dimensional unsteady computational fluid dynamics (CFD) to determine the overall performance of turbine. The surface roughness of the airfoils has a considerable influence on performance, according to the experimental investigation. Smooth rotor surface finishes reduce turbine performance below a certain wind speed (Reynolds number of 30,000), whereas smooth surface finishes improve turbine performance above it. Both two and three bladed rotors were examined, and the greater solidity rotors (three bladed rotors) showed a considerable increase in performance coefficient across the majority of the working range. The $k-\epsilon$ RNG turbulence model was employed for both 2D and 3D simulations in the numerical analysis. When small inaccuracies were taken into account, 3D results were quite agreement with experimental observations. The performance of the 2D results was much higher than that of the 3D, which was attributed to the existence of massive tip vortices in both the real turbine and the 3D models.

Pitch angle is one of the important geometrical parameters which affect the performance of VAWT and therefore, Bianchini et al. (2015) performed CFD simulation to investigate the effect of pitch angle on the performance of a Darrieus VAWT. Pitch modelling has been used to examine various pitch control techniques for this aim. The BEM code's prediction skills were first confirmed using sophisticated CFD simulations and then utilised to research pitch angle optimization. It has been discovered that optimising the pitch allows the aerofoil to better exploit the higher-lift sections of its polar during rotation. Their research also discovered a small sensitivity of optimum pitch angle to wind velocity. Three distinct optimization techniques were used to conduct an extensive sensitivity study of optimum pitch on turbine solidity and wind speed. They discovered that optimising pitch yielded some gains in terms of maximum power rate and yearly energy rate when utilising optimization techniques. It was also discovered that optimization techniques are a far more efficient and straightforward method of modifying pitch as a function of wind speed than a mechanical

actuator with more complicated control circuitry. According to their research a correctly determined pitch applied to blades, defined as a function of turbine geometry and operating circumstances, might give a cost-free boost in turbine performance.

In another study (Jiang et al., 2020) blade tip vortex was investigated to enhance overall performance VAWT employing the SST $k-\omega$ turbulence model. The influence ranges of tip vortex were determined by measuring the force and flow field at various levels of the blade. In their model, a bulkhead was also built to decrease blade tip vortex. The overall torque of the blade varied steadily when the bulkhead size rose to a certain level. Different heights of the supporting strut were taken into account separately in the calculations. It was discovered that when the strut's position changed spatially, overall power of the rotor increased. When the supporting strut was combined with the bulkhead at the blade tip, they discovered that it might lessen tip vortex. Furthermore, they compared the top supporting strut-bulkhead construction effect for different TSRs. They discovered that for low TSRs, torque of the entire structure was insignificant, but greatly enhanced with higher TSRs. Their research into the construction of this supporting strut-bulkhead structure offers a potential design and optimization alternative for big VAWT systems.

Solidity effect on the performance of VAWT cannot be ignored and therefore, many researchers have studied in this regard. For example, Joo et al. (2015) performed a three-dimensional CFD analysis to investigate the aerodynamic properties of two straight bladed VAWT. For the analysis realizable $k-\varepsilon$ model was used. Varying the solidities the aerodynamic performance of rotor with NACA0012 was investigated and the resulted performance (C_p) with respect to tip speed ratios (TSRs) is displayed in Figure 2.8. The results indicated that higher the solidity higher its optimum torque, but increasing solidity alone does not enhance the H-Darrieus' performance. It was also discovered that while lowering the solidity reduces the effect of blockage and contact, the self-starting properties via negative torque at low TSRs are lost. As a result, they came to the conclusion that a theoretical model like the DMST (double multiple stream tube) is ineffective in forecasting the performance of H-Darrieus with a high solidity. It was also observed that peak torque or power coefficient was seen at higher TSR for low solidity or vice versa. Similarly, Eboibi et al. (2016) performed experimental investigation of the influence of solidity on the performance of VAWT which revealed that larger overall power coefficient was observed in case of higher solidity rotor than that of lower solidity rotor.

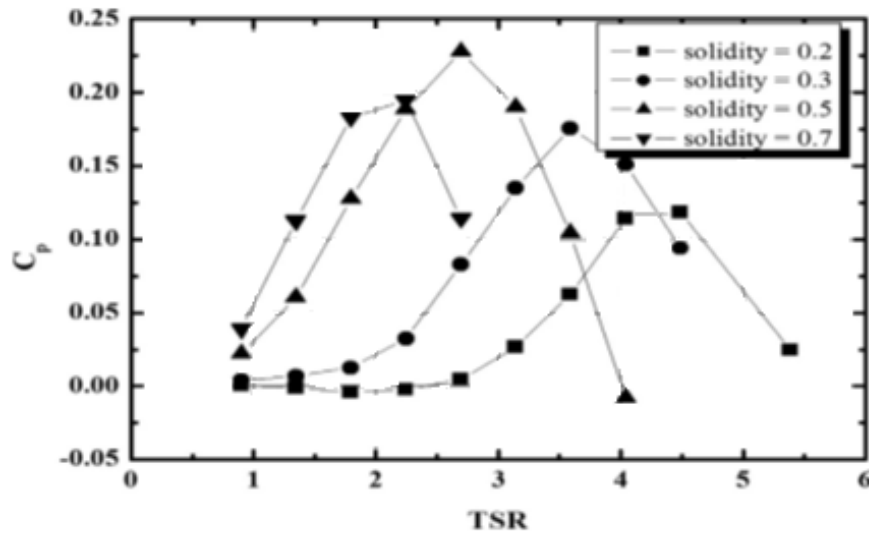


Figure 2.8 Effect of solidity in the performance of VAWT at inlet velocity=5.07 m/s and Reynolds= 35000 (Joo et al., 2015)

In another similar study, Giorgetta et al. (2015) evaluated the aerodynamic interactions of two moderate-solidity Darrieus rotors when they were placed near together. At various distances between rotor axes, the behaviour of counter-rotating and co-rotating systems is investigated. For turbulence closer, $k-\omega$ SST model was used. In comparison to the findings for the isolated turbine, the models reveal a 10% increase in power generation, regardless of the feeling of rotation. They discovered that medium and high solidities contribute to isolated turbines' poor power output, owing to wind obstruction caused by blades going upwind, which reduces the amount of kinetic energy available in the downwind route. When two rotors are close together, however, the wind barrier helps to accelerate the free-stream flow between them. As a result, the rotor wake may be shrunk and re-energised, and the available kinetic energy along the downwind route can be increased. The key finding is that enhanced free-stream flow between turbines is the primary driver of increased power extraction via turbine wake contraction and re-energization.

For the evaluation of energy performance and aerodynamic forces acting on a numerical model of a straight bladed Darrieus wind turbine with NACA0021 airfoils was presented by Castelli et al. (2011). The results of two dimensional CFD simulation revealed that decrease in blade relative angles of attack passing from lower to higher TSR values while optimum torque were developed during upwind motion of rotor. Also revealed that although average power coefficient is low, the instantaneous power coefficient crossed the Betz's limit in three

occasions per cycle may be due to sudden drop in pressure coefficient and therefore, suggested for further investigation.

Similarly, several authors (Almohammadi et al., 2013; Bedon et al., 2016; Cai et al., 2019; Chen et al., 2017; Lam and Peng, 2016; Li et al., 2016, 2018; Mohamed, 2013; Qin et al., 2011; Tai et al., 2013; Wekesa et al., 2016) have presented CFD simulations to study aerodynamic performance of VAWT so as to enhance its performance.

2.2.1 The aerofoils section

It is noticed that to improve the performance of the VAWT it is necessary to study and analyse the effects of several operating and geometrical parameters such as tip speed ratio (TSR), wind speed, number of blades, solidity, chord length, blade shapes, blade thickness, pitch angle, etc. Among them, blade shape cum blade thickness (airfoils section) is an important parameter as it is a critical element in the wind turbine and therefore, it influences on the performance of the wind turbine is generally quite significant. Geometry of the airfoil section is presented in Figure 2.9 where pitch angle (β) is the angle between the chord line of the blade and the plane of rotation. The angle between the chord line of the airfoil and the flight direction is called the angle of attack (γ). Many researchers have studied CFD analysis of VAWT with various types of airfoil shapes to assess the performance of blade shapes and review of some the selective earlier studies shall be presented below elaborately.

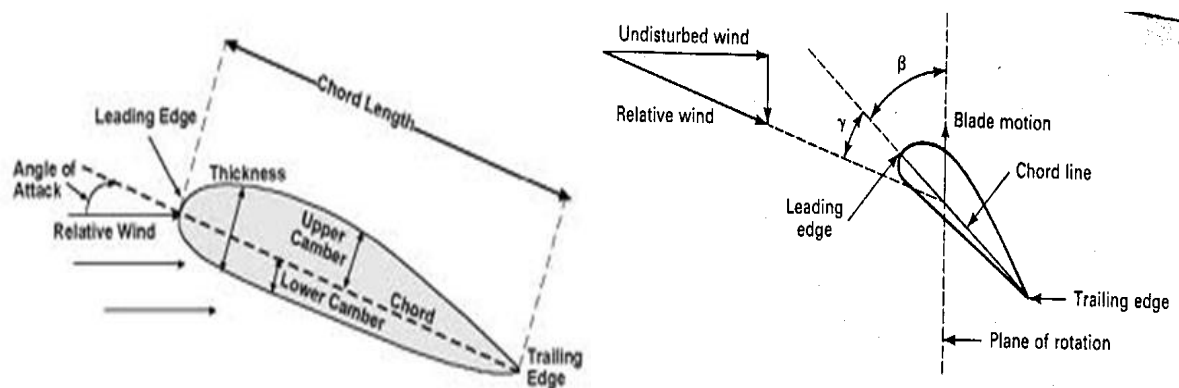


Figure 2.9 Geometry of airfoil section

Several airfoil sections have been studied by various researchers (Mohamed, 2012; Mohamed et al., 2015; Hashem and Mohamed, 2018) from which some of the airfoil sections are presented in Figure 2.10. It includes several series such as symmetrical and unsymmetrical NACA series, S- series, FX series, etc.

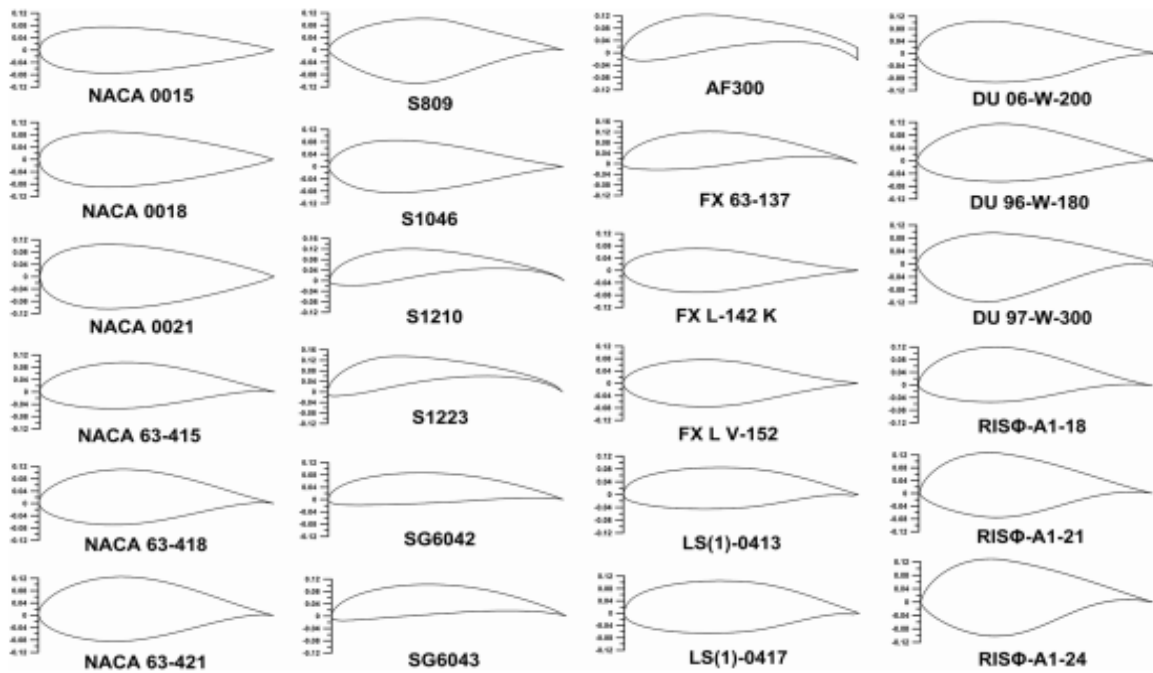


Figure 2.10 Different symmetric and non-symmetric airfoils studied earlier (Hashem and Mohamed, 2018)

Durrani et al. (2011) also investigated the performance of VAWT with different symmetric NACA 00XX series airfoils from 12 to 32 per cent thickness (Figure 2.11) through 2-D CFD analysis. The RNG k- ϵ model was used for turbulence closure. Analysis revealed that at low free stream velocity, the performance of rotor with NACA 0015 airfoil dominates all other selected airfoils but as the velocity increases performance of rotor with NACA 0022 overtakes others. Overall performance showed that NACA 0022 outperforms all other selected NACA series.

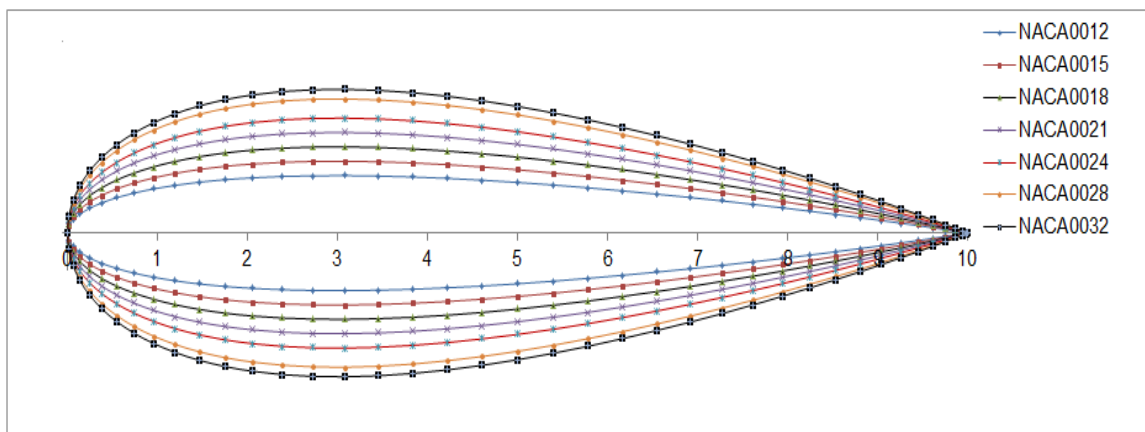


Figure 2.11 Different symmetric NACA airfoils from 12% to 32% thickness and the last two digits in the airfoils series names provides the thickness percentage (Durrani et al., 2011)

A loop algorithm with a genetic optimizer, a two-dimensional URANS CFD model, a fitness calculator, and an airfoil generator were used to produce a novel airfoil shape (WUP 1615) by Bedon et al. (2016) that might potentially improve the aerodynamic performance of a Darrieus wind turbine. The revised profile represents the best airfoil for increasing power performance throughout the turbine revolution, as determined by URANS CFD simulations that captured the rotor's dynamic characteristics. Despite the significant improvement in aerodynamic performance, estimating the cost of energy savings is difficult due to the lack of information on set up costs and energy prices in the literature. However, the new airfoil shape outperforms existing airfoils and may be carefully considered in future rotor designs.

Chen et al. (2016) also developed a methodology to effectively assess an airfoil family in a systematically manner by coupling automatic CFD analysis with orthogonal algorithm, secondly with OFAAT algorithm. The evaluated airfoil family was the NACA 4-digit modified airfoil family. Total 25 airfoils were accessed in this study out of which performance of 16 modified NACA 4 digits is presented in Figure 2.12. From the OFAAT algorithm analysis an optimal airfoil (NACA 0018-64) was found. The maximum power coefficient of rotor with NACA 0018-64 is 0.4585, which is about 15.5% higher than that of the rotor with NACA 0015. They also found that the optimal TSR of rotor varies with the design parameters of the airfoil. Thus, they concluded that the optimal TSR cannot be fixed at a constant TSR in the airfoil assessment research.

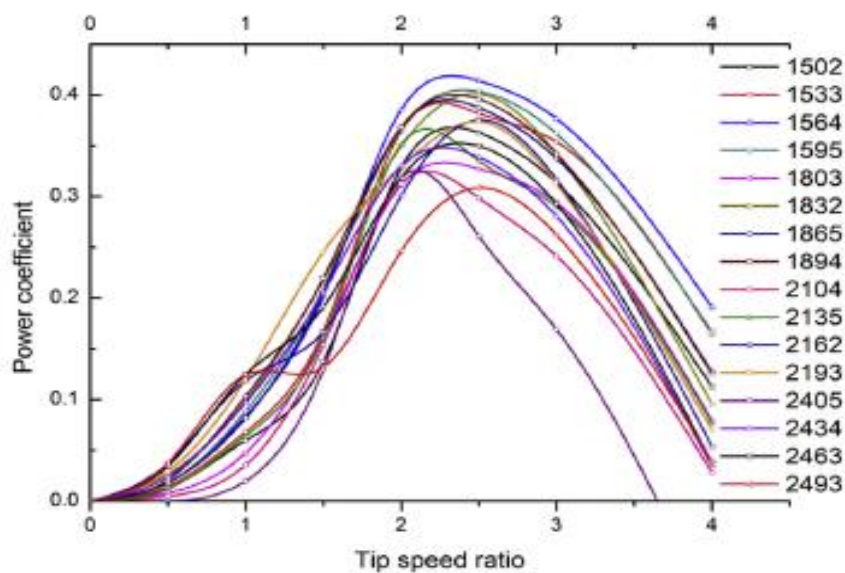


Figure 2.12 Performance of VAWT with sixteen NACA 4- digital modified airfoils (Chen et al., 2016)

In another study (Chen and Lian , 2015) it was observed a two dimensional numerical simulation of H-rotor VAWT using sliding mesh and employing k- ϵ turbulence model to analyse the effect of solidity, number of blades and importantly the blade profile (thickness) on the performance of VAWT. It was further observed that the vortex-blade interaction is found largely depending upon the solidity and TSR and therefore, the peak torque per blade was found decreased with the solidity. It also showed that power coefficient increases as the number blade increases until the number of blade reach three than decreases. They also found that there is significant change in performance due to blade thickness. Eventually, Figure 2.13 shows the comparison of NACA0015 and NACA0022 performance which reveals that increasing the blade thickness increases power performance of rotor at the low TSR or vice versa . However, for the thinner blade its peak power finds at higher TSR and its overall performance is better than thicker blade.

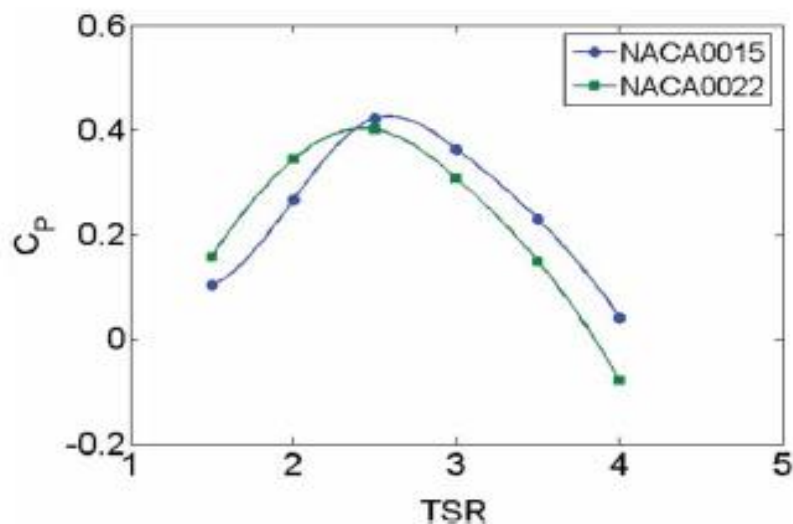


Figure 2.13 Performance of H-rotor VAWT with NACA0015 and NACA0022 at Reynolds = 70000 (Chen and Lian, 2015)

A combined experimental and 3-D numerical investigation has been carried out by Elkhoury et al. (2015) to study the performance of a micro VAWT with variable-pitch. They studied the effect of wind speed, turbulence intensity, airfoil shape, and strut mechanism with and without variable-pitch on the performance of the VAWT using large eddy simulation. They also included study of performance comparison of NACA0018, NACA0021 and NACA634-221 profiles. The findings revealed that NACA0021 (3% thicker than NACA0018) found in

better power performance than that obtained with the NACA0018 for all TSR probably due to the better stall characteristics with thicker airfoils inherit which is presented in Figure 2.14.

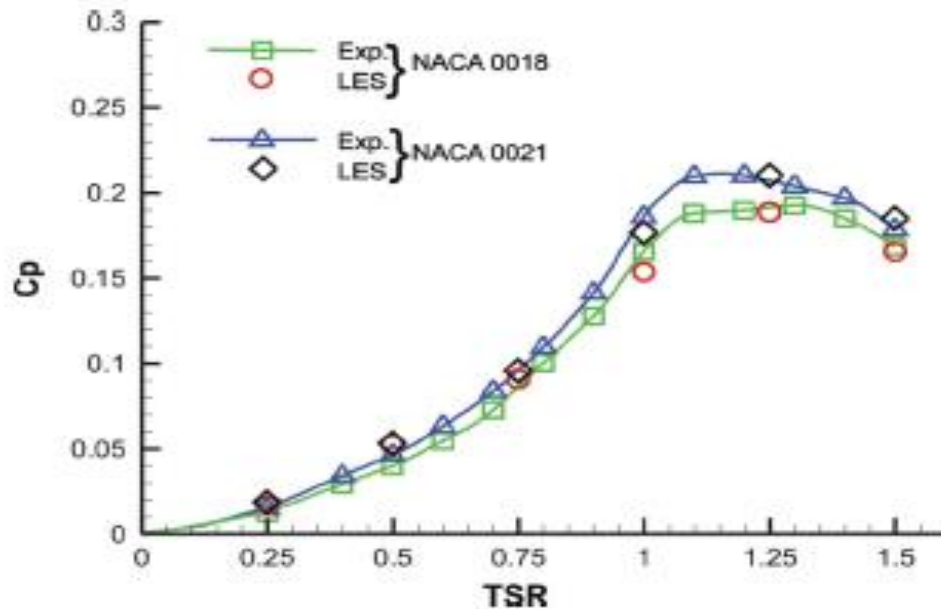


Figure 2.14 Performance of Darrieus turbines with two different airfoils at inlet velocity and solidity of 8 m/s and 0.75 respectively (Elkhoury et al., 2015)

Aerodynamic performance assessment of 24 novel airfoils was performed by Hashem and Mohamed (2018) to enhance the performance of H-rotor Darrieus turbine and performance of all the airfoils in terms power coefficient versus tip speed ratio operated at inlet velocity of 9 m/s and solidity of 0.1 are presented in Figures 2.15 to Figure 2.18. Two dimensional simulation focuses on eight series of novel airfoil designs for this purpose. The traditional $k-\epsilon$ realizable turbulence model was utilised in this investigation. Their findings pointed to certain novel forms that would be suited for the H-rotor Darrieus turbine and would boost performance significantly. For typical tip-speed ratios ranging from 2 to 7, the symmetric S1046 airfoil had been shown to be the highest performing airfoil and among NACA 00XX series NACA0015 shown the highest power coefficient (C_p). Table 2.7 shows the comparison of peak power coefficients of all the selected airfoils and among them S1046 airfoil provided greatest C_p with a value of 0.3463.

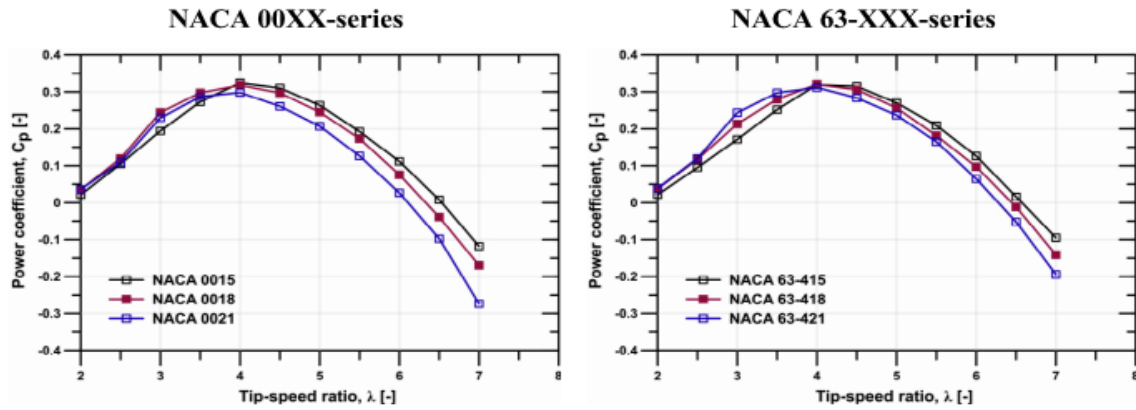


Figure 2.15 Power coefficient of H-rotor turbine with NACA 00XX and NACA 63-XXX-Series airfoils at inlet velocity of 9 m/s (Hashem and Mohamed, 2018)

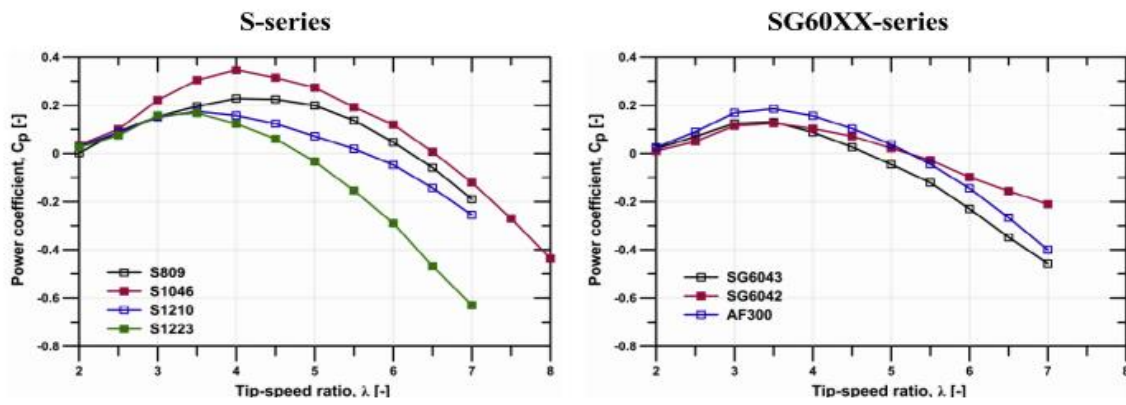


Figure 2.16 Power coefficient of H-rotor turbine with S-series and SG60XX-series airfoils at inlet velocity of 9 m/s (Hashem and Mohamed, 2018)

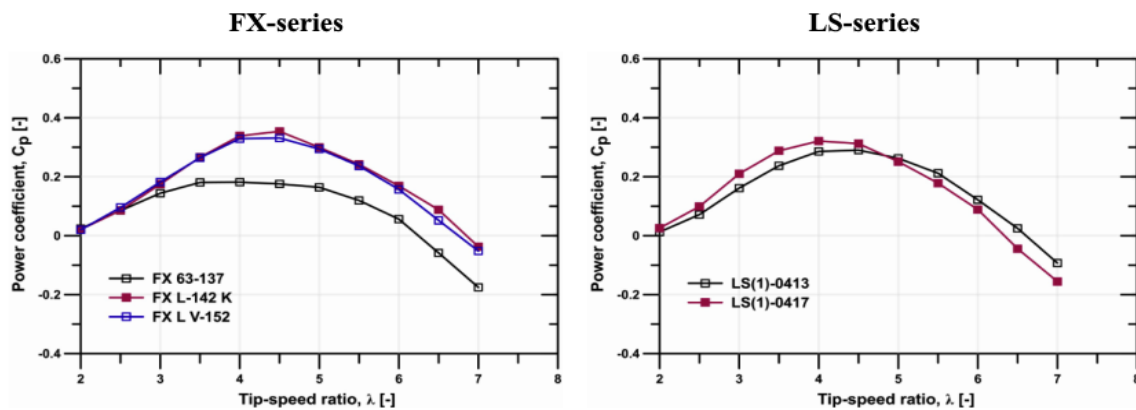


Figure 2.17 Power coefficient of H-rotor turbine with FX-series and LS-series airfoils at inlet velocity of 9 m/s (Hashem and Mohamed, 2018)

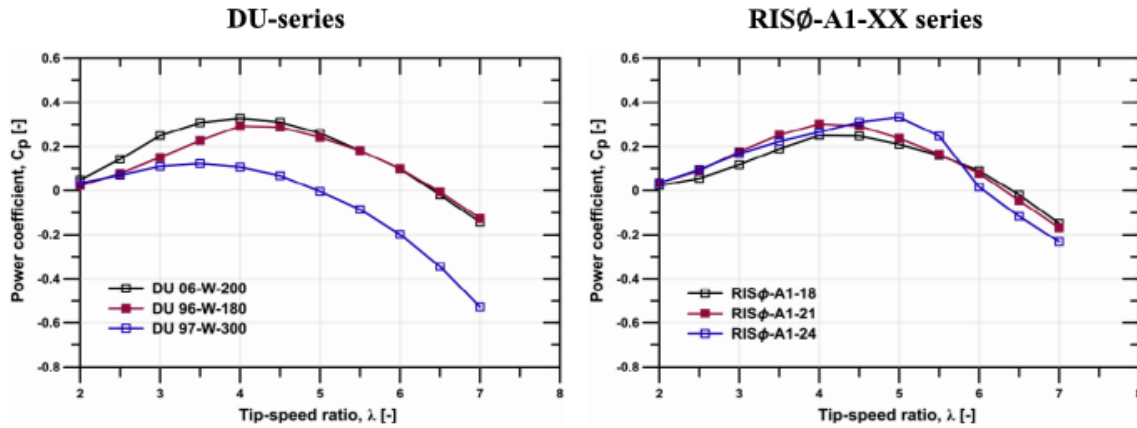


Figure 2.18 Power coefficient of H-rotor turbine with DU-series and RISØ-A1-XX-series airfoils (Hashem and Mohamed, 2018)

Table 2.7 Simulated airfoils with the corresponding peak power coefficient (Hashem and Mohamed, 2018)

Airfoil	Peak Cp	Airfoil	Peak Cp	Airfoil	Peak Cp
NACA 0015	0.3243	SG 6042	0.1147	FX63-137	0.1815
NACA 0018	0.3182	SG 6043	0.1251	FXL-142K	0.3385
NACA 0021	0.2980	AF 300	0.1693	FXL V-152	0.3289
NACA 63-415	0.3193	S-809	0.2280	RISo-A1-18	0.2497
NACA 63-418	0.3206	S-1046	0.3463	RISo-A1-21	0.3025
NACA 63-421	0.3119	S-1210	0.1580	RISo-A1-24	0.3324
DU 06-W-200	0.3277	S-1223	0.1577		
DU 96-W-180	0.2927	LS(1)-0413	0.2857		
DU 97-W-300	0.1098	LS(1)-0417	0.3210		

Numerical analysis of three bladed VAWT was performed by Mohamed et al. (2015, 2019) to assess the performance of 25 distinct airfoils profile consisting of 3 from NACA 4 digit family (symmetrical), 9 from NACA 5 digit family (non-symmetrical), 4 from S family, 2 from DU family, 3 from FFA family, 1 from FX family, 2 from LS (1) family and 1 A-airfoil. In both cases, the goal of the research was to optimise the power performance of the turbine. In addition to performance assessment of rotor with 25 airfoils the former investigate force analysis for the best airfoil while later investigates the effect of pitch angle. Based on finite volume analysis and CFD methods the flow field surrounding the turbine was solved and analysed using URANS equation. In both CFD work, the SST k- ω turbulence model was used. The analysis revealed that out of 25 shape airfoils Darrieus rotor with NACA 63-215, LS(1)-0413, NACA64-415, NACA 63-415 and NACA 0015 showed the dominant performance with peak power coefficient of 0.417, 0.415, 0.405, 0.404 and 0.401 respectively which is clearly displayed in Figure 2.17. Among the symmetrical NACA 4 digit family such

as NACA0015, NACA0018 and NACA0021, the first one provided the best performance followed by the NACA0018. However, in comparison to all other airfoils, NACA 63-415 has a larger operating range followed by NACA0015. The former paper also includes thorough force analysis for the turbine, which comprises of the airfoil (LS (1)-0413 and NACA 0021). Furthermore, the static torque coefficient, which reflects the turbine's self-starting capabilities, was evaluated. The turbine built by LS (1)-0413 had shown to be more self-starting than the usual design. As a result, the optimal Darrieus turbine design in their study, consisting of LS (1)-0413, looks to be extremely promising for WECT, particularly in rural and metropolitan settings. Similarly, in case of later paper using one of the best airfoils, the effect of pitch angle modification was explored from -10° to $+10^\circ$. It was found that as the pitch angle was increased or decreased from zero, performance began to deteriorate until it reaches rotation in the opposite direction across the whole working range at pitch angles of -10° and $+10^\circ$.

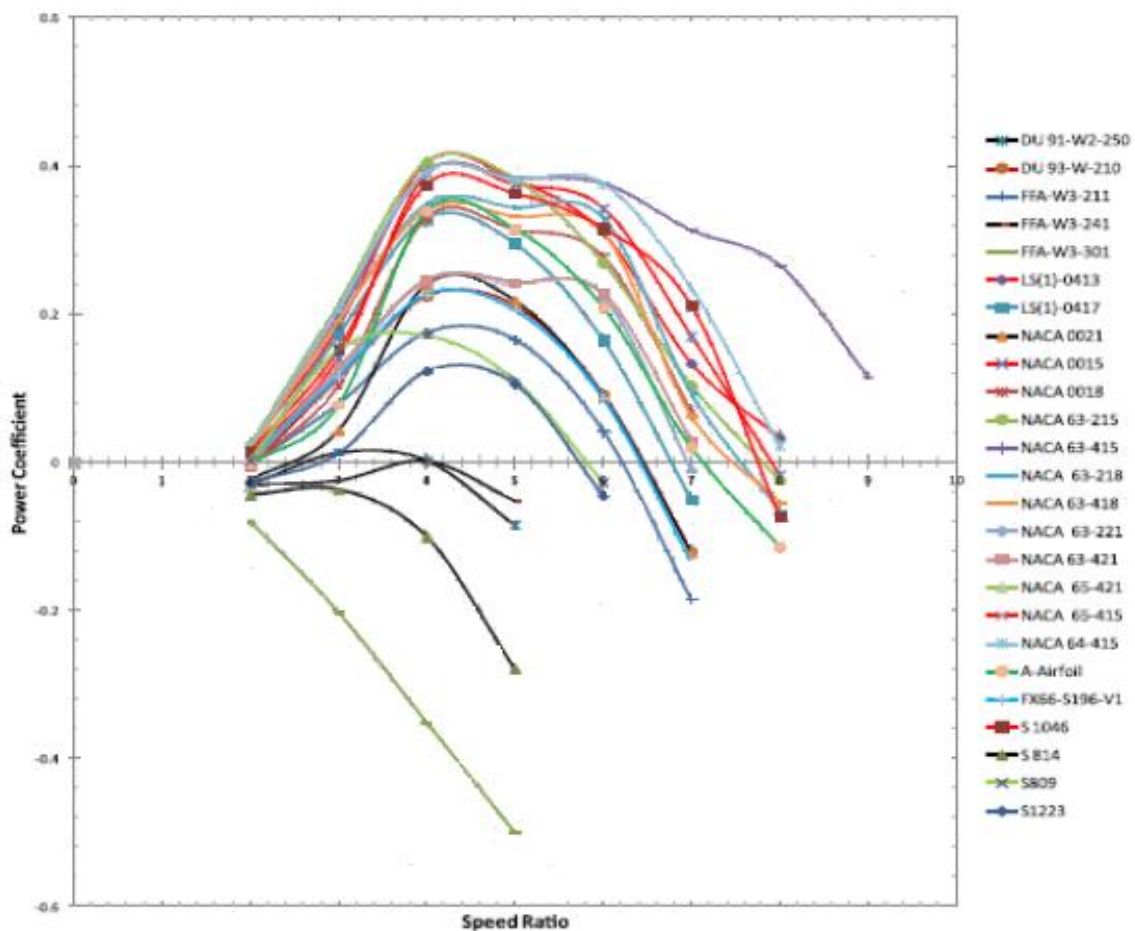


Figure 2.19 Power coefficients versus tip speed ratio of Darrieus turbine with 25 airfoils at inlet velocity and solidity of 5 m/s and 0.1 respectively (Mohamed et al., 2015, 2019)

Similarly, Mohamed (2012) also researched the Darrieus turbine airfoil shape in order to enhance the performance of H-rotor Darrieus turbine, resulting in a greater efficiency. Twenty distinct symmetric and non-symmetric airfoils were examined for this purpose. For the quantitative and qualitative examination of instability performance of the turbine, the realisable $k-\epsilon$ turbulence model was utilised. Due to the possible relevance of the airfoil form, a rigorous CFD approach was carried out while concurrently considering unsteadiness issues surrounding the Darrieus rotor during rotation. The power coefficient (C_p) was used to evaluate all turbines with various airfoil designs. The suggested CFD approach was proven to be capable of producing significantly superior airfoils than the traditional Darrieus turbine, with a relative gain in the C_p of 26.83% for the S-1046 airfoil when compared to the conventional NACA airfoils and performance comparisons of all the selected profiles are presented in Table 2.8. For a longer working range, the author recommended the low solidity for Darrieus turbine. As a result, the ideal Darrieus turbine layout including S-1046 looks to be highly promising for WECT, particularly in urban locations.

Table 2.8 Simulated airfoils with the corresponding peak C_p (Mohamed, 2012)

Airfoil	Peak C_p	Airfoil	Peak C_p	Airfoil	Peak C_p
NACA 0010	0.2345	AG18	0.01233	S-9000	0.1696
NACA 0015	0.2947	AH93W174	0.2469	FX66S196	0.2074
NACA 0018	0.2964	AH93W215	0.2541	FX77W256	0.1639
NACA 0021	0.2679	AH94W301	0.2130	FX71L150	0.2961
NACA 6312	0.1290	S-809	0.3428	FXL142	0.3311
NACA 63415	0.1711	S-1046	0.4051	FXLV152	0.3576
NACA 63418	0.2772	S-1014	0.2769		

Numerical simulations to compare the performance of the Joukowski airfoil with classical NACA airfoils (NACA0012, NACA4512 and NACA4312) were studied by Parakkal et al. (2019). The simulation had compensated for turbulence using the eddy viscosity model in conjunction with a typical wall function in the near-wall area for high enough Reynolds numbers (Re). Two transport equations for k and ω were used to express it. The Joukowski airfoil outperformed the standard NACA 0012 and cambered NACA 4312, according to the results. The lift coefficients were calculated using the panel technique, while the torque and power coefficients were calculated using computational fluid dynamics. At a greater TSR, the rotor delivers more uniform and homogenised torque, which was intuitively right. However,

the increased torque achieved by utilising Joukowski had a negative impact on the VAWT's capacity to self-start.

Two dimensional CFD analysis of small VAWT with NACA0018, NACA0021 and NACA0025 rotor was studied by Shukla et al. (2018). Analysis revealed that at lower TSR negative value of torque and power coefficient were observed but value of torque and power coefficient became positive when the TSR was greater than 3. Overall performance showed that NACA0025 provided the highest value of power coefficient.

As the selection of effective blade profile is an important criterion for the improvement of VAWT, the state of art discussed above revealed that several researchers tried to obtain best and most effective blade profile cum thickness and many more studies (Biswas and Gupta, 2014; Carrigan et al., 2012; Daroczy et al., 2018; Ismail and Vijayaraghavan, 2015; Jafaryar et al., 2016; Mazarbhuiya et al., 2018; Sengupta et al., 2016b; Sobhani et al., 2017) have also performed CFD analysis to fulfill the same objective. Based on the state of art discussed above, a summary of deployment of different airfoils with the purpose of the concerned study and the value of solidity is given in Table 2.9. The table shows that the most of the works attempted to increase the performance of Darrieus wind turbine consisting of conventional NACA 4-digit series with thickness ranging from 12% to 22% and the last two digits in the airfoil series names provides the thickness percentage which is clearly presented in Figure 2.11. In the literature survey several earlier studies claimed that VAWT with NACA0015 profile is the most effective NACA profile among the symmetrical NACA 4 digit series (Chen et al., 2015; Durrani et al., 2011; Hashem and Mohamed, 2018; Mohamed et al., 2019; Mohamed et al., 2015 and Subramanian et al., 2017) while Kavade and Ghanegaonkar (2018) and Mohamed (2012) claimed that NACA0018 as the most effective NACA profile among the 4 digit series. However, Elkhoury et al. (2015) reported NACA0021 airfoil having the best performance. It is also revealed that thicker airfoils is beneficial in terms of strength while the thinner airfoils like NACA0015 perform better when used with lower solidity at high TSR due to the amount of drag applied to thinner blade become relatively low (Lee and Lim, 2015; Elkhoury et al., 2015). In such situation performance analysis using CFD numerical simulation of H-type Darrieus VAWT with NACA0016 and NACA0019 airfoils (which are simple in structure and neither too thick nor too thin) will be quite benefited to the wind energy conversion system. To our knowledge, the effectiveness of these profiles for harnessing wind energy is not reported till date.

Table 2.9 Summary on airfoils type used during Numerical analysis of Darrieus VAWT

Author	Airfoil	Solidity	Model	Purpose
Almohammedi et al. (2013)	NACA0015	0.96	2D (SST Transition, RNG k- ϵ)	Obtained the appropriate mesh independency solution
Bai et al. (2015)	NACA0015	0.60	2D & 2.5D (SST k- ω)	Performance analysis of rotor blade with tubercle leading edge
Balduzzi et al. (2016a)	NACA0018	0.44	2D (SST k- ω)	Study of critical issues for an accurate 2D CFD simulation
Balduzzi et al. (2016b)	NACA0018	0.44	2D (SST Transition)	To obtain optimal mesh and time step sizes
Balduzzi et al. (2017)	NACA0021	0.17	3D (COSA code using SST k- ω)	Study of 3D flow effect on performance
Bedon et al. (2016)	NACA0018, WUP1615	0.10	2D (SST k- ω)	Performance checking of optimized airfoil
Bianchini et al. (2017)	NACA0020	0.84	Exp. & 2D (SST k- ω , Y-Re Θ)	To check the effectiveness 2D models
Li et al. (2018)	NACA0018	0.15, 0.3	2D (DES-SST)	Optimization of pitch angle
Bianchini et al. (2015)	NACA0018	0.2	BEM	
Beri & Yao (2011)	NACA2415	0.75	2D	Effect of camber airfoil
Biswas & Gupta (2014)	NACA0012	1.62	2D (SST k- ω)	CFD analysis of twisted bladed rotor
Castelli et al. (2011)	NACA0021	0.5	Exp. & 2D (CFD code with BE-M theory)	To compare the proposed model with experiment.
Chen et al. (2015)	NACA0015	0.25	2D (k- ϵ)	Numerical investigation to study influences of various parameters on VAWT
Chowdhury et al. (2016)	NACA0018	0.21	3D(SST k- ω)	To analyse performance of tilted rotor
Daróczy et al. (2018)	NACA0021, OPT1, OPT2	0.15	2D (SST k- ω)	Optimization of NACA0021 airfoil shape
Guo et al. (2019)	NACA0015	0.172	2D (SST k- ω)	Optimization of pitch angle
Howell et al. (2010)	NACA0022	0.67, 1	Exp., 2D&3D (RNG k- ϵ)	Comparison of 2D & 3D performance prediction with experiment.
Kavade & Ghanegaonkar (2018)	NACA0012, NACA0015, NACA0018, NACA0021	1.27	Single stream tube model	Performance enhancement by optimizing the blade pitch angle for different TSR
Lanzafame et al. (2014)	NACA0015, NACA4518	0.48, 0.5	Exp., SST k- ω , Transition SST	Comparison of CFD models
Lee & Lim (2015)	NACA0015, NACA0018, NACA0021	0.6, 0.8	Exp., & 3D (RNG k- ϵ)	Performance of H-type Darrieus turbine
Li et al. (2015)	NACA0021	0.53	Experiment(Field & Wind tunnel)	To analyse the effects some parameters and then performance analysis.

Table 2.9 (Continued)

<i>Author</i>	<i>Airfoil</i>	<i>Solidity</i>	<i>Model</i>	<i>Purpose</i>
Nobile et al. (2014)	NACA0018	0.73	2D (SST Turbulence)	To optimize the performance of rotor through augmentation
Qin et al. (2011)	NACA0022	0.48	2D&3D k- ϵ	Comparison of 2D &3D effects with experiment
Rezaeiha et al. (2019)	NACA0015 ^a , NACA0018 ^b , NACA0021 ^c	0.125a, 0.12b, 0.25c	2D(Seven turbulence models)	To select the method of choice in respect of turbulence model
Rezaeiha et al. (2017)	NACA0018	0.12	2D (SST transition)	Investigated the effect of domain size and azimuthal increment
Sengupta et al. (2016b)	NACA0018, S815, EN0005	0.46, 0.51, 0.56	Exp. & 2D (RNG k- ϵ)	To study flow physics and performance analysis of rotor with 3 different solidities
Subramanian et al. (2017)	NACA0012, NACA0015, NACA0030 AIR 001	0.33	2D(SST transition)	To study effect airfoil profile and solidity on the performance of VAWT

2.3 Objective of the Thesis

From the state of art survey as discussed above, it is realised that assessment of wind energy potential in the north-eastern and eastern regions of India is so far neglected. It is also realised that efficacy of numerical methods involve in the estimation of Weibull parameters depends on various factors such as wind characteristics, topographical parameters, etc. and therefore, search of effective alternative is still in progress. Last but not the least it is also realised that performance assessment of various geometrical and physical parameters of wind turbine to improve and optimise the overall performance of the turbine is still immature which provide huge scope of research in this area.

Therefore, from the above research gaps it is decided that the objective of the present research work is:

- 1) to assess the wind energy potential (WEP) in some locations of North-eastern region of India. As the need of effective alternative numerical method is noticed, an alternative numerical estimation method namely, “Energy Variance method (EVM)” is to be developed.
- 2) to go for computational fluid dynamics (CFD) analysis of vertical axis wind turbine (VAWT) for assessing performance of some airfoils for VAWT applications.

CHAPTER- 3

METHODOLOGY ON ASSESSMENT OF WIND ENERGY POTENTIAL

3.1 Introduction

Selection or the design of wind turbine depends on the wind resource assessment such as wind characteristics, nature of wind distribution and wind energy potential of the concerned site. Therefore, wind resource assessment is very first crucial stage in the WECT in order to develop successful wind energy conversion station.

Eventually this chapter describes the techniques with which the assessment of wind energy potential (WEP) is performed. In the preceding chapter, i.e., literature survey various effective statistical distribution models to study wind profile have been used by many earlier researchers which will be listed here. Then details about the model to be applied in the present study are described. Finally, a new approach for estimating parameters involved in statistical distribution models is developed. As a part of the analysis, validation of the new method shall be performed comparing with the performance of some widely accepted effective estimation methods.

3.2 Statistical distribution models for the assessment of WEP

From the literature survey presented in the preceding chapter we have come to know that there are several statistical distribution models for fitting the wind speed data for wind power assessment study and they may be classified as unimodel distribution models such as Weibull distribution, Rayleigh distribution, etc., and multimodal (mixture) distribution models such as Gamma-Weibull distribution, Weibull-Weibull distribution, etc. Some of the frequently used distribution models are presented in Table 3.1 and Table 3.2.

From the literature survey (sub-section 2.1.2 and Table 2.4) it is noticed that more than fifty studies have been performed related to the statistical distribution models in which about hundred times different distribution models have been applied for the wind energy potential assessment. Out of the different distribution models 51 times of Two-parameter Weibull

distribution models; 11 times of Rayleigh distribution models; 4 times of Lognormal; 3 times each of Gamma and Log-logistic models; 2 times each of Exponential, Nakagami and Three-parameter Weibull models; 1 time each of Inverse Gaussian, Generalised extreme value, Normal, Beta, Erlang, Pearson V, Pearson VI, Uniform, Rician, Johnson, Inverse Weibull, Cubic factor and Generalized hyperbolic distribution (GHD) models were employed for the assessment of WEP. Further Two-parameter Weibull model has been recommended as best model for 15 times while Rayleigh for 2 times and Lognormal, Three-parameter Weibull, GHD, Cubic factor, Inverse Weibull one time each. From this survey it is realised that Two-parameter Weibull distribution has been considered as effective, simple, flexible and best statistical distribution models and therefore, it is selected for the present wind energy potential assessment analysis.

Further, from the literature survey it has been noticed that two-parameter Weibull distribution is however unable to represent the probabilities of very low wind speeds in the set of wind speed data to be assessed (Weisser, 2003; Pishgar-Komleh et al., 2015; Wais, 2017a). In such cases, occasionally researchers suggested that Rayleigh distribution may be one of the alternative effective distribution model but some other researchers (Rehman and Abbadi, 2007; Rehman et al., 2015; Rahman and Chattopadhyay, 2019b) commented that effectiveness of distribution models depends on the wind characteristics and topographical data of the site to be assessed. Therefore, in the present analysis we will compare performance of Weibull and Rayleigh distribution as well.

Table 3.1 Statistical Distribution models (Uni-model)

Distribution	No of parameters	Equation
Weibull (Akpinar & Akpinar, 2005)	2	$f_w(v; c, k) = \left(\frac{kv}{c^k}\right)^{k-1} \exp\left(-\left(\frac{v}{c}\right)^k\right)$
Weibull (Wais, 2017)	3	$f(v; c, k, \gamma) = \frac{k}{c} \left(\frac{v-\gamma}{c}\right)^{k-1} \exp\left(-\left(\frac{v-\gamma}{c}\right)^k\right)$
Rayleigh (Akpinar, 2005)	1	$f(v; c) = \frac{2v}{c^2} \exp\left(-\left(\frac{v}{c}\right)^2\right)$
Normal (Wang et al., 2016)	2	$f_N(v; c, \gamma) = \frac{\exp\left[-\frac{1}{2}\left(\frac{v-\gamma}{c}\right)^2\right]}{c\sqrt{2\pi}}$
Exponential (Alavi et al., 2016)	1	$f(v; c) = c \exp(-cv)$

Table 3.1 (Continued)

Distribution	No of parameters	Equation
Erlang (Jung & Schindler, 2019)	2	$f(v; c, k) = \frac{v^{k-1}}{c^k \Gamma(k)} \exp\left(\frac{-v}{c}\right)$
Gamma (Alavi et al., 2016)	2	$f_G(v; c, k) = \frac{c^k v^{k-1}}{\Gamma(k)} \exp(-cv)$
Inverse Gamma (Jung & Schindler, 2019)	2	$f(v; c, k) = \frac{1}{c \Gamma(k) (v/c)^{k+1}} \exp(-c/v)$
Inverse Gaussian (Alavi et al., 2106)	2	$f(v; c, \gamma) = \sqrt{\frac{c}{2\pi v^3}} \exp\left[-\frac{c(v-\gamma)^2}{2v\gamma^2}\right]$
Log-logistic (Wang et al., 2016)	2	$f(v; c, k) = \frac{kv^{k-1}}{c^k} \sqrt{1+(v/c)^k}$
Lognormal (Alavi et al., 2016)	2	$f(v; c, k) = \frac{1}{vc\sqrt{2\pi}} \exp\left(-\frac{[\ln(v)-k]^2}{2c^2}\right)$
Nakagami (Alavi et al., 2016)	2	$f(v; c, k) = \frac{2k^k}{\Gamma(k)c^k} v^{2k-1} \exp\left(-\frac{k}{c}v^2\right)$
Beta (Jung & Schindler, 2019)	3	$f(v; k, m, bp) = \frac{1}{B(m, k)} \frac{(v-bp_1)^{m-1} (bp_2-v)^{k-1}}{(bp_2-bp_1)^{m+k-1}}$
Rician (Gugliani, 2020)	2	$f(v; c, n) = I_0\left(\frac{vn}{c^2}\right) \frac{v}{c^2} \exp\left(-\frac{(v^2+n^2)}{2c^2}\right)$
Generalized Extreme Value (Alavi et al., 2016)	3	$f_{GEV}(v; c, k, \gamma) = \frac{1}{c} \left[1 - \frac{k}{c}(v-\gamma)\right]^{\frac{1}{k}-1} \exp\left(-\left(1 - \frac{k}{c}(v-\gamma)\right)^{\frac{1}{k}}\right)$
GHD (Gugliani, 2020)	5	$f(v; c, k, s, \gamma, \sigma) = \frac{\sqrt{k(1-s^2)}^{0.5c-0.25}}{\sqrt{2\pi}\delta\sigma_c(k)} \left[\left(\frac{v-\gamma}{\delta\sigma}\right)^2 + 1\right]^{0.5c-0.25} I_c$ $\times \left[\frac{k}{\sqrt{1-s^2}} \sqrt{\left(\frac{v-\gamma}{\delta\sigma}\right)^2 + 1}\right] \times \exp\left[\frac{ks}{\sqrt{1-s^2}} \left(\frac{v-\gamma}{\delta\sigma}\right)\right]$
Generalized Gamma (Jung & Schindler, 2019)	4	$f(v; c, k, \gamma, m) = \frac{k(v-\gamma)^{km-1}}{c^{km}\Gamma(m)} \exp\left\{-\left[\frac{(v-\gamma)}{c}\right]^k\right\}$
Burr (Jung & Schindler, 2019)	3	$f_B(v; c, k, m) = \frac{mk(v/c)^{m-1}}{c(1+(v/c)^m)^{k+1}}$

Table 3.2 Statistical Distribution models (Multi-model)

Distribution (Multimodel) (Jung & Schindler, 2019)	No of parameters	Equation
G- mixture	5	$f(v; \omega, c_1, k_1, c_2, k_2) = \omega f_G(v; c_1, k_1) + (1 - \omega) f_G(v; c_2, k_2)$
G-W mixture	5	$f(v; \omega, c_1, k_1, c_2, k_2) = \omega f_G(v; c_1, k_1) + (1 - \omega) f_W(v; c_2, k_2)$
N-N mixture	5	$f(v; \omega, c_1, \gamma_1, c_2, \gamma_2) = \omega f_N(v; c_1, \gamma_1) + (1 - \omega) f_N(v; c_2, \gamma_2)$
N-W mixture	5	$f(v; \omega, c_1, \gamma, c_2, k) = \omega f_N(v; c_1, \gamma) + (1 - \omega) f_W(v; c_2, k)$
W-W mixture	5	$f(v; \omega, c_1, k_1, c_2, k_2) = \omega f_W(v; c_1, k_1) + (1 - \omega) f_W(v; c_2, k_2)$
GEV-W mixture	6	$f(v; \omega, c_1, k_1, \gamma, c_2, k_2) = \omega f_{GEV}(v; c_1, k_1, \gamma) + (1 - \omega) f_W(v; c_2, k_2)$
B-GEV mixture	7	$f(v; \omega, c_1, k_1, m, c_2, k_2, \gamma)$ $= \omega f_B(v; c_1, k_1, m) + (1 - \omega) f_{GEV}(v; c_2, k_2, \gamma)$

3.2.1 Two-parameter Weibull distribution and Rayleigh distribution models

Weibull distribution is one of the extreme-value distributions which was first proposed by W. Weibull who applied it during the analysis of material strength in tension and fatigue in the 1930s (Qin et al., 2012). It is defined by its probability density function $f(v)$ and cumulative distribution function $F(v)$. It involves three parameters known as shape parameter, k (dimensionless), scale parameter, c (m/s) and location parameter, b which has same unit with the input data such as wind speed, time, length, etc. The Weibull distribution involving three parameters is known as three-parameter Weibull and if the location parameter is neglected ($b = 0$) then Weibull distribution will become two-parameter Weibull distribution which is given by the following equation (3.1) (Rahman and Chattopadhyay, 2019a).

$$F(v) = 1 - \exp^{-\left(\frac{v}{c}\right)^k} \quad (3.1)$$

Where $F(v)$ is the cumulative distribution function (CDF) of wind speed (v). The shape parameter indicates the width of the wind distribution while the scale parameter indicates how windy the location is (Shu et al., 2015).

The corresponding probability density function (PDF) is given by the equation (3.2).

$$f(v) = \frac{dF(v)}{dv} = \left(\frac{kv^{k-1}}{c^k} \right) \exp^{-\left(\frac{v}{c}\right)^k} \quad (3.2)$$

Generally, the value of k ranges from 1.5-3.0 for most of the wind conditions (Akpinar and Akpinar, 2005). If the value k is fixed at 2 then Weibull distribution becomes a special type known as Rayleigh distribution model whose CDF and PDF are given by the following equations (3.3) and (3.4) respectively.

$$F(v) = 1 - \exp^{-\left(\frac{v}{c}\right)^2} \quad (3.3)$$

$$f(v) = \frac{dF(v)}{dv} = \left(\frac{2v}{c^2} \right) \exp^{-\left(\frac{v}{c}\right)^2} \quad (3.4)$$

3.2.2 Vertical extrapolation of wind speed

Wind speed collected from different sites is measured at different height. However, wind speed depends on the altitude and therefore, it is necessary to extrapolate the collected wind speed in order to compare the outcome of the analysis. For the present study we extrapolate the wind speed corresponding to 20 m so as to compare the wind potential of all the four sites. Therefore, vertical extrapolation of wind speed is necessary and it can be obtained by using the power law relation given in equation (3.5) (Akpinar and Akpinar, 2005; Pishgar-Komleh et al., 2015).

$$\frac{v}{v_o} = \left(\frac{h}{h_o} \right)^\alpha \quad (3.5)$$

Where, v_o (m/s) is the actual wind speed recorded at known height h_o (m) and v is the wind speed corresponding to standard height h (m). The power law exponent or friction coefficient or wind shear coefficient “ α ” depends on the surface roughness which ranges from 0.05 to 0.5 (Akpinar and Akpinar 2005). Effect of wind shear coefficient was investigated employing different sets of wind speed data and it was realized that although 1/7th power law provide the value of $\alpha = 0.143$ which can be considered as good approximation for wind profile in the stable atmospheric boundary layer, this value is not suitable for certain situations and locations as well (Farrugia, 2003; Werapun et al., 2017). Further, it was found that “ α ” is a dynamic parameter which varies with ground level height, time of day, surface temperature, season, surface roughness, and nature of terrain (Rehman and Abbadi, 2007; Rehman et al., 2015). Table 3.3 shows the value of wind shear coefficient for different types

of terrain (Faghani et al., 2018; Gualtieri and Secci, 2012; Khalfa et al., 2014; Lawan et al., 2013).

Table 3.3 Value of power law exponent for different types of terrain

Types of terrains	α, power law exponent
Water/ice surfaces/smooth hard ground	0.10
Grasslands (ground level)	0.15
Tall crops, hedges and shrubs	0.2
Heavily forested land	0.25
Small town with some trees and shrubs	0.30
City areas with high rise buildings	0.40

The power law exponent of any type of terrain or different climate or surface temperature may also be obtained from the following relation given in equation (3.6) (Acakpovi, 2017; Soulouknga, 2017; Soulouknga et al., 2018; Rahman and Chattopadhyay, 2020).

$$\alpha = \frac{0.37 - 0.088 \ln(v_0)}{1 - 0.088 \ln(h_o / h)} \quad (3.6)$$

3.2.3 Actual mean wind speed and standard deviation

Actual mean wind speed and standard deviation are given by the following equations (3.7) and (3.8) respectively.

$$\bar{v} = \frac{1}{n} \sum_{i=1}^n v_i \quad (3.7)$$

$$\sigma = \sqrt{\frac{1}{n-1} \sum_{i=1}^n (v_i - \bar{v})^2} \quad (3.8)$$

Where, v is the mean wind speed, σ is the standard deviation of the observed wind data, i is the measuring interval and n is the number of wind speeds.

The mean wind speed and standard deviation based on Weibull distribution may be expressed in terms of Weibull parameters as follows:

$$\bar{v}_w = c\Gamma\left(1 + \frac{1}{k}\right) \quad (3.9)$$

$$\sigma_w = \left[c^2 \left\{ \Gamma\left(1 + \frac{2}{k}\right) - \left(1 + \frac{1}{k}\right)^2 \right\} \right]^{1/2} \quad (3.10)$$

Where, \bar{v}_w and σ_w are the mean wind speed calculated based on Weibull distribution and Weibull standard deviation respectively and $\Gamma()$ is the Gamma function.

3.2.4 Site specific wind speeds and coefficient of variation

Once the values of shape and scale parameters are known, two important specific wind parameters like wind speed carrying maximum energy ($V_{\max E}$) and the most frequent wind speed (V_{mF}) can be obtained. The former represents the wind speed conveying the greatest wind energy while the later indicates the most frequent wind speed for a given wind probability distribution and is given in the following equations (Shu et al., 2015).

$$V_{\max E} = c\left(1 + \frac{2}{k}\right)^{1/k} \quad (3.11)$$

$$V_{mF} = c\left(1 - \frac{1}{k}\right)^{1/k} \quad (3.12)$$

Further, the coefficient of variation in percentage (COV) can be obtained as follows:

$$COV(\%) = \frac{\sigma}{\bar{v}} = \frac{\sqrt{\Gamma\left(1 + \frac{2}{k}\right) - \left(\Gamma\left(1 + \frac{1}{k}\right)\right)^2}}{\Gamma\left(1 + \frac{1}{k}\right)} \times 100\% \quad (3.13)$$

3.3 Numerical models for the estimation of parameters

As the accuracy and efficiency of statistical distribution depend on the parameters, the estimation of parameters is crucial important part in the assessment of wind power potential. The state of art discussed in the preceding chapter shows that for a given set of wind speed data several numerical methods can be employed to estimate the Weibull or Rayleigh parameters such as Graphical method (GM), Empirical method by Justus (EM), Empirical method by Lysen (EML), Moment method (MOM), Maximum Likelihood method (MLM),

Power Density method (PDM), Modified Maximum Likelihood method (MMLM), Equivalent Energy method (EEM), etc. The important numerical methods found in the literatures are briefly explained below:

3.3.1 Graphical method (GM)

The graphical methods have been used for some time because of their simplicity; however, they generate a bias because of the inaccuracy involved in plotting points. In this method the graph is constructed in such a way that the cumulative distribution of wind data becomes a straight line and it can be expressed by taking natural logarithms of equation (3.1) as follows:

$$\ln(-\ln(1 - F(v))) = k \ln(v) - k \ln(c) \quad (3.14)$$

Left term can be plotted as y-axis against $\ln(v)$ as x-axis, where k equals the slope and c can be obtained from intercept with y- axis (Seguro and Lambert, 2000; Werapun et al., 2015; Saleh et al., 2012).

3.3.2 Least Square method (LSM)

The least square method is widely used in estimating the parameters of a statistical distribution, but generally it is considered as effective method for large sample sizes. The expression for both k and c are given in equation (3.15) and (3.16) respectively (Azad et al., 2015).

$$k = \frac{n \sum_{i=1}^n \ln v \ln[-\ln\{1 - F(v)\}] - \sum_{i=1}^n \ln v \sum_{i=1}^n \ln[-\ln\{1 - F(v)\}]}{\sum_{i=1}^n \ln v^2 - \left(\sum_{i=1}^n \ln v\right)^2} \quad (3.15)$$

$$c = \exp \left\{ \frac{k \sum_{i=1}^n \ln v - \sum_{i=1}^n \ln[-\ln\{1 - F(v)\}]}{nk} \right\} \quad (3.16)$$

3.3.3 Maximum Likelihood method (MLM)

This method was proposed by Cohe and it was introduced by Stevens and Smulders in the field of wind energy application (Mohammadi et al., 2016; Rocha et al., 2012; Saleh et al., 2012). In this method extensive numerical iterations are required to obtain model parameters.

$$k = \left[\frac{\sum_{i=1}^n v_i^k \ln(v_i)}{\sum_{i=1}^n v_i^k} - \frac{\sum_{i=1}^n \ln(v_i)}{n} \right]^{-1} \quad (3.17)$$

Equation (3.17) provides shape parameter and corresponding scale parameters can be obtained as follows:

$$c = \left[\frac{\sum_{i=1}^n (v_i)^k}{n} \right]^{1/k} \quad (3.18)$$

3.3.4 Modified Maximum Likelihood method (MMLM)

It is a modification of MLM method in which frequency distribution is accounted for to estimate the parameters. This methodology is based on the idea of linearization of nonlinear terms in the maximum likelihood method using Taylor series expansion; otherwise it is similar to MLM (Mohammadi et al., 2016; Saleh et al., 2012). The shape parameter and scale parameter are obtained from the following relationships:

$$k = \left[\frac{\sum_{i=1}^n v_i^k \ln(v_i) f(v_i)}{\sum_{i=1}^n v_i^k f(v_i)} - \frac{\sum_{i=1}^n \ln(v_i) f(v_i)}{f(v \geq 0)} \right]^{-1} \quad (3.19)$$

$$c = \left[\frac{\sum_{i=1}^n (v_i)^k f(v_i)}{f(v \geq 0)} \right]^{1/k} \quad (3.20)$$

3.3.5 Empirical method (EM)

This method was suggested by Justus et al. (Mohammadi et al., 2016) which requires the mean wind speed (\bar{v}) and standard deviation (σ) of the wind speed data to estimate shape and scale parameters. The expressions are given below:

$$k = \left(\frac{\sigma}{\bar{v}}\right)^{-1.086} \quad (3.21)$$

$$c = \frac{\bar{v}}{\Gamma\left(1 + \frac{1}{k}\right)} \quad (3.22)$$

3.3.6 Empirical methods by Lysen (EML)

It is similar to empirical method by Justus where the difference is only in the expression for scale parameter which is estimated as follows (Mohammadi et al., 2016; Tizgui, 2017):

$$c = \bar{v} \left(0568 + \frac{0.433}{k} \right)^{1/k} \quad (3.23)$$

3.3.7 Moment method (MOM)

This method was suggested by Justus and Mikhail (Azad et al., 2014; Tizgui et al., 2017; Aukitino et al., 2017). Knowing the value of mean and standard deviation of wind speeds, the value of statistical parameters can easily be estimated as follows:

$$k = \left(\frac{0.9874}{\frac{\sigma}{\bar{v}}} \right)^{1.0983} \quad (3.24)$$

$$c = \frac{\bar{v}}{\Gamma\left(1 + \frac{1}{k}\right)} \quad (3.25)$$

3.3.8 Power Density method (PDM)

This was introduced by Akdag and Dinler (2009). Using a new term called energy pattern factor (E_p) the parameters are determined as follows:

$$k = 1 + \frac{3.69}{E_p^2} \quad (3.26)$$

$$\text{Where } E_p = \frac{\frac{1}{n} \sum_{i=1}^n v_i^3}{\left(\frac{1}{n} \sum_{i=1}^n v_i \right)^3} = \frac{\overline{v^3}}{(\bar{v})^3}$$

$$c = \frac{\bar{v}}{\Gamma\left(1 + \frac{1}{k}\right)} \quad (3.27)$$

3.3.9 Equivalent energy method (EEM)

In this method parameters are estimated as follows (Rocha et al., 2012; Azad et al., 2014):

$$\sum_{i=1}^n \left[W_{v_i} - \exp \left[- \frac{(v_i-1) \left\{ \Gamma(1+3/k) \right\}^{1/3}}{(\bar{v}^3)^{1/3}} \right]^k + \exp \left[- \frac{(v_i) \left\{ \Gamma(1+3/k) \right\}^{1/3}}{(\bar{v}^3)^{1/3}} \right]^k \right]^2 = \sum_{i=1}^n (\varepsilon_{v_i})^2 \quad (3.28)$$

$$c = \left[\frac{\bar{v}^3}{\Gamma(1+3/k)} \right]^{1/3} \quad (3.29)$$

Where, W_{v_i} and ε_{v_i} are the frequency of the measured wind speed and the error of the approximation respectively.

3.3.10 Probability weighted moments based on power density method (PWMBP)

Although this method had been applied to various engineering application, it was introduced by Usta to estimate parameters for the assessment wind energy resource (Usta, 2016) and it is expressed in the following equations (3.30) and (3.31).

$$k = \frac{\ln(2)}{\ln \left(\frac{\bar{v}}{(2/(n^2 - n)) \sum_{i=1}^n v_{(i)} (n - i)} \right)} \quad (3.30)$$

$$c = \left[\frac{\bar{v}^3}{\Gamma(1+3/k)} \right]^{1/3} \quad (3.31)$$

Where, $v_{(i)}$ is the i^{th} ascending ordered of ‘n’ number of measured wind speed data.

The state of art discussed in section 2.1.3 revealed that in the 39 earlier studies 23 different types of numerical methods were employed 147 times. Among the 23 different methods MLM, PDM, EM, MOM, GM, MMLM and EEM were used 24, 22, 19, 18, 16, 16 and 7 times respectively. As per the performance analysis studied earlier by several researchers the

MLM, MOM, PDM and EM were came out to be most effective methods and therefore, these numerical methods shall be applied in the present analysis.

3.4 Development of a new numerical estimation method: Energy Variance method (EVM)

Earlier studies showed that the accuracy and effectiveness of numerical methods for the Weibull parameter estimation depend on the set of data employed which again depend on the climatic status and nature of the surface such as roughness and orography of chosen location (Rahman and Chattopadhyay, 2019b; Rehman and Abbadi, 2007; Rehman et al., 2015). Therefore, with the aim to find the best alternative estimation method a new approach called “**Energy Variance method (EVM)**” is developed. The EVM considers the kinetic energy of wind which is proportional to the square of wind speed. The effectiveness of the method would be demonstrated by estimating Weibull parameters and comparing it with existing methods. According to new method parameters for shape and scale are calculated as follows:

$$k = \left[\frac{\sum_{i=1}^n v_i^2}{n\sigma^2} \right]^2 \quad (3.32)$$

Equation (3.32) shows the dimensionless distribution parameter known as shape parameter. The corresponding scale parameter described in Weibull parameters is shown below:

$$c = \frac{\bar{v}}{\Gamma(1 + 1/k)} \quad (3.33)$$

3.5 Wind power density (WPD)

The wind power density indicates the capacity of wind resources of a particular location. The WPD can be estimated based on actual wind power based on measured wind speed (P_v) and also using Weibull probability density function (P_w) which are given by the following equations (3.34) and (3.35) respectively (Shu et al., 2015; Akpınar and Akpınar, 2005; Keyhani et al.2010):

$$P_v = \frac{1}{2n} \rho \sum_{i=1}^n v_i^3 = \frac{1}{2} \rho \bar{v}^3 \quad (3.34)$$

$$P_w = \frac{1}{2} \rho \int_0^{\infty} v^3 f(v) dv = \frac{1}{2} \rho c^3 \Gamma\left(1 + \frac{3}{k}\right) \quad (3.35)$$

Where, ρ is the average air density. Earlier studies showed that difference between actual air density and standard air density is very insignificant even less than 5% (Shu et al., 2015; Safari and Gasore, 2010; Usta, 2016). Therefore, in the present study, the standard air density ($\rho=1.225 \text{ kg/m}^3$ for dry air at atmospheric pressure and 15°C) shall be used.

3.6 Statistical performance evaluation criteria

To validate and compare the performance of the proposed model with four widely used effective estimation methods, the following five effective statistical criteria were selected: the root mean square error (RMSE), mean square error percentage (MSEP), correlation coefficient (R^2), mean absolute bias error (MABE) and mean absolute percentage error (MAPE) (Mohammadi et al., 2016; Akdag and Dinler, 2009; Bekele and Palm, 2009; Pishgar-Komleh et al., 2015). The formulae are presented here:

$$RMSE = \left[\frac{1}{n} \sum_{i=1}^n (y_i - x_i)^2 \right]^{1/2} \quad (3.36)$$

$$MSEP = 100 \times \frac{1}{\bar{v}} \left[\frac{1}{n} \sum_{i=1}^n (y_i - x_i)^2 \right]^{1/2} \quad (3.37)$$

$$R^2 = 1 - \frac{\sum_{i=1}^n (y_i - x_i)^2}{\sum_{i=1}^n (y_i - z)^2} \quad (3.38)$$

Where, n , x_i , y_i , z are total numbers of observations, the frequency distribution calculated with Weibull distribution, frequency of the measured wind data and mean of the y_i values respectively. MABE and MAPE can be calculated as follows:

$$MABE = \frac{1}{n} \sum_{i=1}^n |P_{i,s} - P_{i,a}| \quad (3.39)$$

$$MAPE = \frac{1}{n} \sum_{i=1}^n \left| \frac{P_{i,s} - P_{i,a}}{P_{i,a}} \right| \times 100 \quad (3.40)$$

Where P_s and P_a are the power calculated using statistical parameter and actual power respectively.

CHAPTER- 4

RESULTS AND DISCUSSION ON WIND ENERGY POTENTIAL ASSESSMENT

4.1 Introduction

Important of assessment of wind energy potential (WEP) prior to the design and installation of wind turbine is clearly explained in the preceding chapter and in the state of art section by various earlier studies. From the assessment of wind energy potential of India, it is arrived that there is huge potential in wind energy in the country. However, there is lack of extensive local wind energy assessment in many places in the country especially the eastern and north-eastern region of India.

Therefore, this chapter presents analysis of results and discussion of wind energy potential of four important locations namely Imphal, Shillong, Guwahati and Kolkata in the eastern and north-eastern regions of India which are shown in Figure 4.1. Simultaneously a new simple numerical estimation method for the statistical distribution models for the assessment of wind energy potential is developed and its performance analysis is presented in this section.

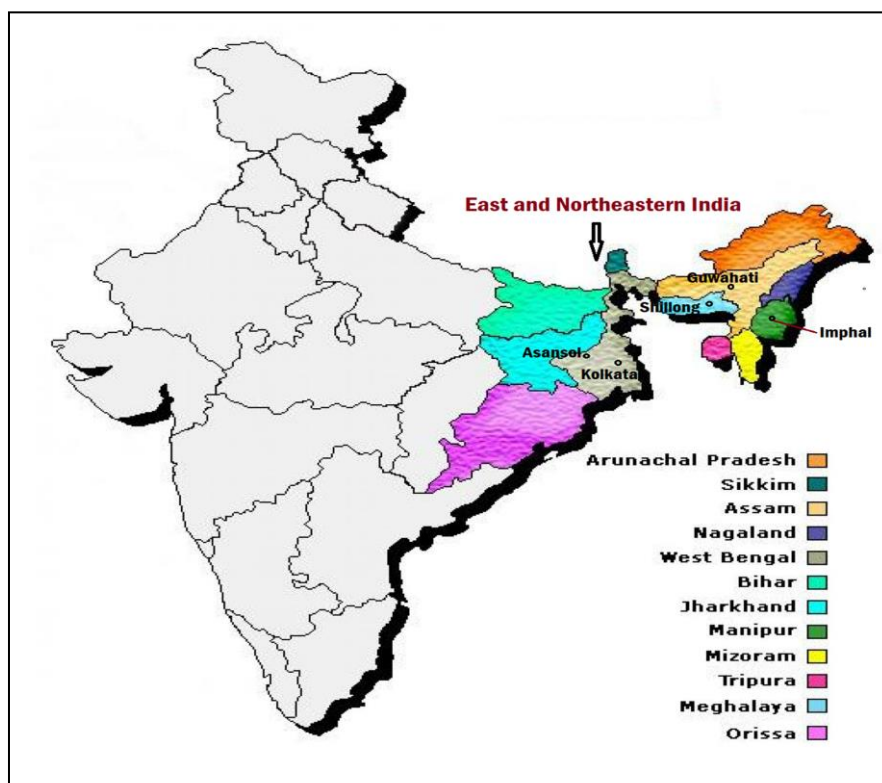


Figure 4.1 Map of East and Northeastern India showing the study sites

4.2 Site Information and Data Source

Geographically, Manipur is one of the Northeastern states of India covers an area of 22,327 square kilometers. The state lies at a latitude of 23°83' N – 25°68' N and longitude of 93°03'E - 94°78'E. There are several layers of hills from the surrounding to the central valley region. The Imphal is the capital of the state that lies in an oval-shaped valley surrounded by green hills. In between the hills and valley region some agricultural lands, rivers, lakes are also available. The climate in the Imphal region is normally cold to moderate hot which has annual minimum average and maximum average temperatures of 8°C and 31°C respectively. It has three different seasons namely winter, summer and rainy. Twelve years (2005–2016) daily mean wind speed data collected at 3 m height from the ground level for Imphal region are employed in this study. The data are collected from the Meteorological center, ICAR Research Complex, Lamphelpat, Imphal, Manipur (India). The site of the data collection is a small space adjacent to some layers of hills to the north, several double and some multistoried buildings and hills to the west; play grounds, double and multistoried buildings to the east and multistoried buildings, markets to the south. It falls within small town known as Imphal. The available data from the concerned site are especially for agricultural purposes and therefore, no other data are available at the greater anemometer height.

Meghalaya is a small hilly and mountainous state in the north-eastern region of India whose area is about 22429 square km of which 98.74% in rural areas. Shillong is a hill station and the capital of the Meghalaya and situated at an elevation of 1520 m within the urban areas having about 1.5 lakh population. Shillong lies at a latitude and longitude of 25.57°N and 91.88°E respectively. The city lies in the centre of the plateau and is surrounded by hills. The climate in the Shillong station is normally cold to warm which has annual minimum average and maximum average temperatures of 4°C and 24°C respectively. Five years (2012 - 2016) daily mean wind speed of Shillong station has been collected from Regional Meteorological Centre (RMC), Guwahati for the study. However, measuring site of the Shillong location is situated in the heart of Shillong hill station which is surrounded by medium to large trees on the east and south, small trees and low height buildings on the remaining sides.

Guwahati is the 5th fastest growing city of India where the capital (Dispur) of Assam: a north-eastern state is situated. The latitude and longitude of Guwahati is 26.17°N and 91.75°E respectively and it lies between the banks of Brahmaputra River and the foothills of the Shillong plateau. For Guwahati station five years (2012-2016) wind speed data were collected from the Regional Meteorological Centre, Guwahati where measuring anemometer

is installed and it is located near LGB International Airport. Beside adjacent to Airport towards west the measuring station is surrounded by large number of trees and multi-storied buildings in all sides. The climate in Guwahati station is normally very cold to hot which has annual minimum average and maximum average temperatures of 0°C and 40°C respectively.

Kolkata is the oldest Metropolitan city in India and capital of West Bengal situated in the eastern region of India. It has an area of 1886.67 square kilometer and spread linearly along the banks of Hooghly River. Five years (2012-2016) wind speed data were collected from the Regional Meteorological Centre, Kolkata: situated in the South 24 Parganus Kolkata District of West Bengal which is surrounded by small trees and multi-storied buildings.

Climatically both the Northeast and East India lie in the humid subtropical zone and experiences mild/hot humid summers from March to May, severe monsoons from June to October/November and mild to snowy winter in the remaining months. Therefore, the whole 12 months is divided into three different seasons namely winter (December, January, and February), summer (March-May) and rainy (June-November). Details of these four different sites of these two regions are presented in Table 4.1.

Table 4.1 Geographical details of the selected sites

Sl. No.	Station	Latitude (N)	Longitude (E)	Altitude (m)	Anemometer Height (m)
1	Imphal (Imp)	24°45'	93°54'	774	3
2	Shillong (Shg)	25°34'	91°53'	1600	11.6
3	Guwahati (Ghy)	26°06'	91°35'	54	6.6
4	Kolkata (Kol)	22°32'	88°20'	6.4	17.01

Measuring height of all the four sites are unequal and therefore, comparison of wind speed and wind power potential among different sites is possible by adjusting the height of the turbine to a standard height. For the present analysis we considered to extrapolate wind data of all the sites corresponding to 20 m height and in this regard a relation is already presented in equation (3.5) where the value of power law exponent (α) has to be either selected from the Table 3.2 or found out using relation given in the equation (3.6).

To check find more reliable value of “ α ” we shall compare the extrapolated wind data of two familiar sites, i.e., Kolkata and Imphal using both the equation (3.6) and value from Table

3.2. Referring to this table, we have selected $\alpha=0.40$ for Kolkata site as the location falls within the city areas with high rise buildings and $\alpha=0.30$ for Imphal site as the location is more or less small town with some trees and shrubs.

Figure 4.2 shows the comparison of extrapolated wind speed data by two approaches for Kolkata site which reveals that extrapolated data using $\alpha=0.4$ and the extrapolated data using equation (3.6) are almost equal. Similarly, Figure 4.3 shows the variation of extrapolated wind speed data by two approaches for Imphal site which reveals that the extrapolated wind speed by taking $\alpha=0.3$ is insignificantly lower than the extrapolated data using the equation (3.6). Therefore, for the assessment analysis equation (3.6) shall be used to extrapolate the wind data of all the selected sites so as to maintain the uniformity in all sites.

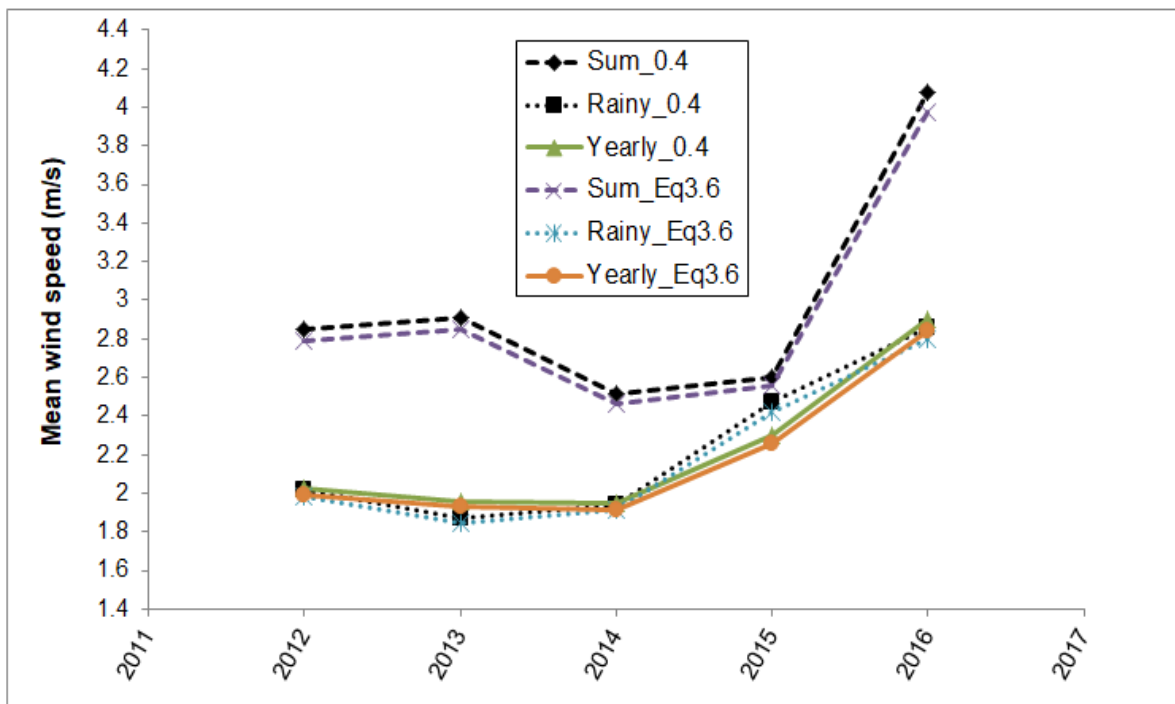


Figure 4.2 Comparison of wind data extrapolation by two approaches for Kol site

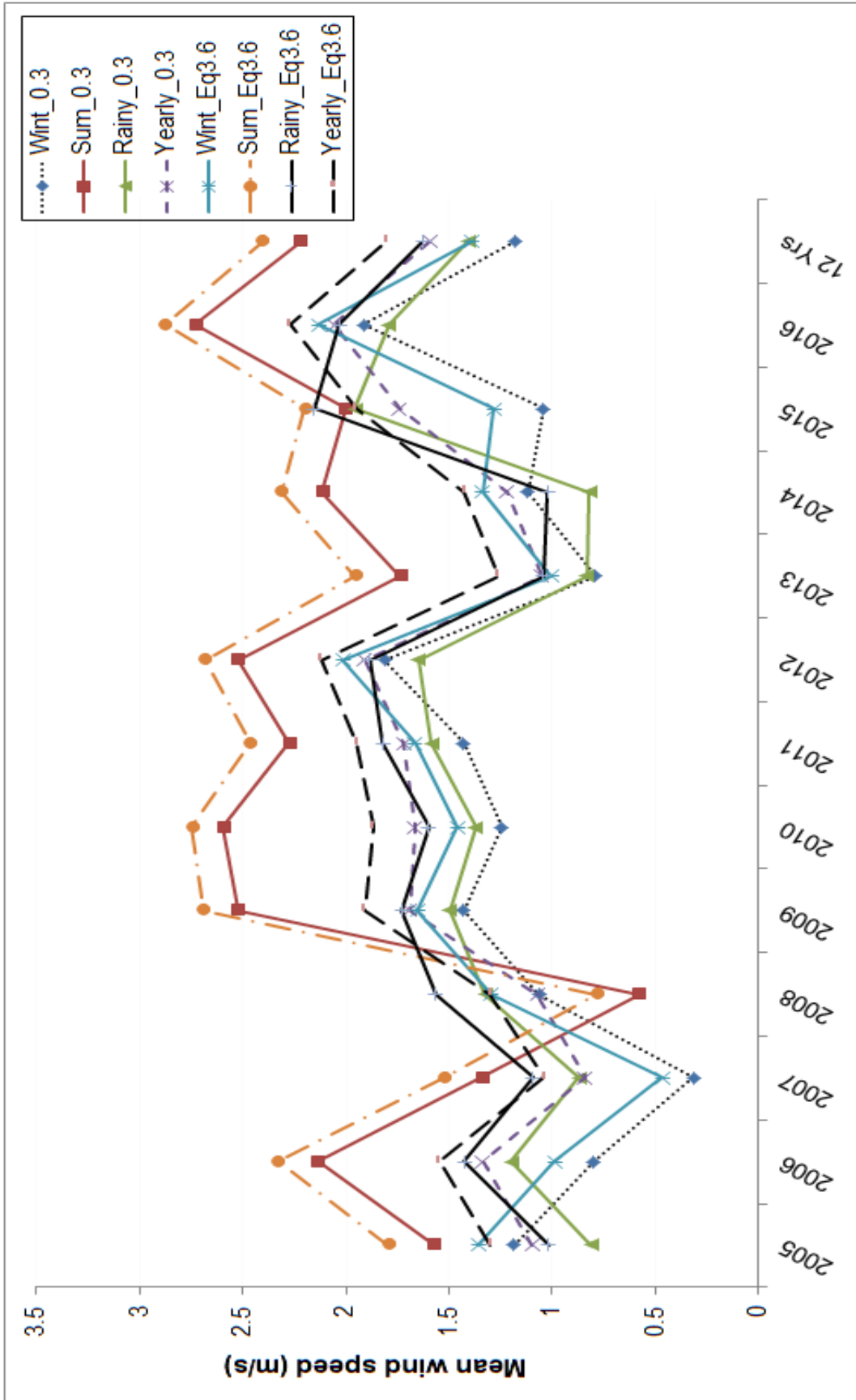


Figure 4.3 Comparison of wind data extrapolation by two approaches for Imp site

4.3 Assessment of WEP of Imphal site

4.3.1 Wind characteristics of the site

Figure 4.2 shows seasonal variation of mean wind speed for 12 years (2005-2016) of Imphal site which reveals that summer season have higher wind speed range lays between 0.79 m/s and 2.88 m/s while winter got the lowest mean speed range lays between 0.47 m/s and 2.13 m/s. Consequently yearly mean wind speed falls within the range of 1.04 m/s and 2.30 m/s. As far as year wise comparison from 2005 to 2016 is concerned, the lowest mean wind speed is seen during the year 2007 and 2013-14 while highest mean speed range is observed during the year 2009-12 and 2016.

The frequency (percentage) of wind speed values of Imphal site is calculated and presented in Figure 4.4. The result shows that wind speed at 1, 1.5 and 2-3 m/s has approximately 19.5%, 23.5% and 41% respectively.

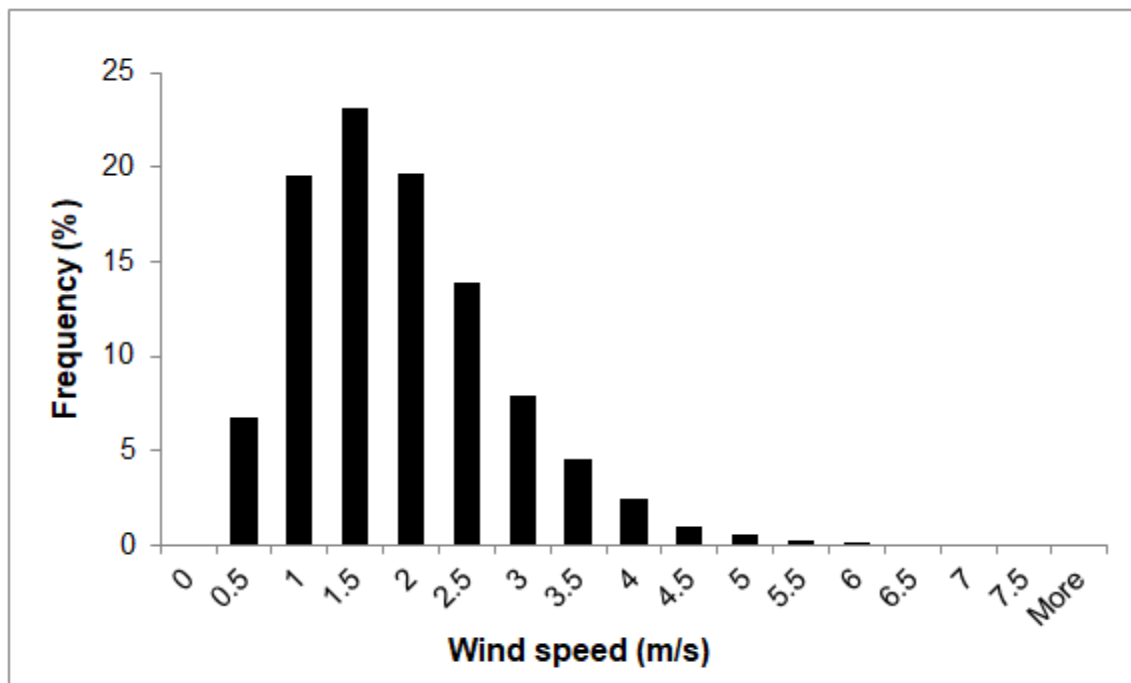


Figure 4.4 Frequency percentages for Twelve years (2005-16) wind speed of Imp site

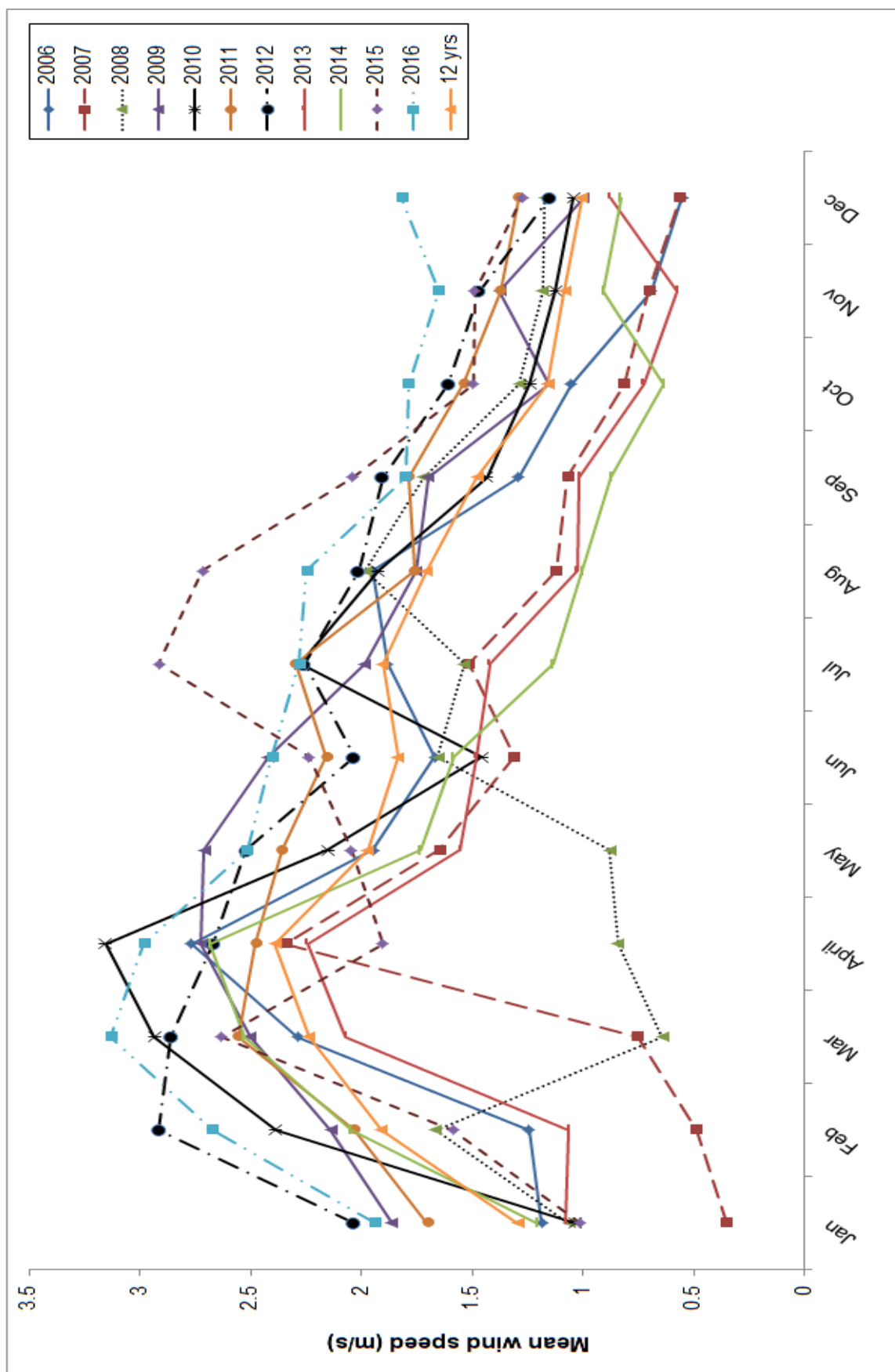


Figure 4.5 Twelve years (2005-16) monthly and whole year mean wind speed of Imp site

Figure 4.5 shows the comparisons of month wise mean wind speed for 12 years (2005-2016) of Imphal site and reveals that March and April provides highest mean speed in 3 and 6 years respectively while February, May, July and Aug provides highest mean speed in one year each. Further, overall variation shows that the highest and lowest mean wind speed range is available during February- June and September- December during which highest and lowest wind energy potential is available respectively.

Table 4.2 shows monthly maximum speed, minimum speed, standard deviation and coefficient of variation (percentage) at 20 m and 40 m. It reveals that minimum speed is in the range of 0.18-2.33 m/s while maximum speed is in the range of 2.67-12.55 m/s. Further, the comparison of COV (%) at 20 m and 40 m is reproduced in Figure 4.6 which shows that the variation of COV (%) is more at low altitude (20 m) with the value of 41-61, whereas at higher altitude those variations are decreased and found to be in the range of 38-56. The reason is that instability due to obstacles, turbulence effect on the wind's motion decreases at higher altitude.

Table 4.2 Month wise wind characteristics for Twelve years (2005-16) of Imp site

Wind	Jan	Feb	Mar	Apr	May	Jun	Jul	Aug	Sep	Oct	Nov	Dec
n	372	338	348	353	372	338	371	367	360	371	359	370
V_{\min}	0.182	2.332	0.182	0.323	0.255	0.357	0.182	0.102	0.182	0.102	0.102	0.182
V_{\max}	4.532	6.180	5.424	12.551	4.504	4.568	7.045	4.973	3.973	3.301	3.594	2.662
σ	0.787	1.060	1.121	1.187	0.823	0.760	0.965	0.850	0.630	0.535	0.538	0.473
COV (%) at 20 m	60.72	55.45	50.08	49.64	41.73	41.28	50.63	49.74	42.54	46.12	49.41	47.01
COV (%) at 40 m	56.36	51.87	47.04	45.62	38.91	38.32	46.83	46.37	39.64	43.02	46.05	43.60

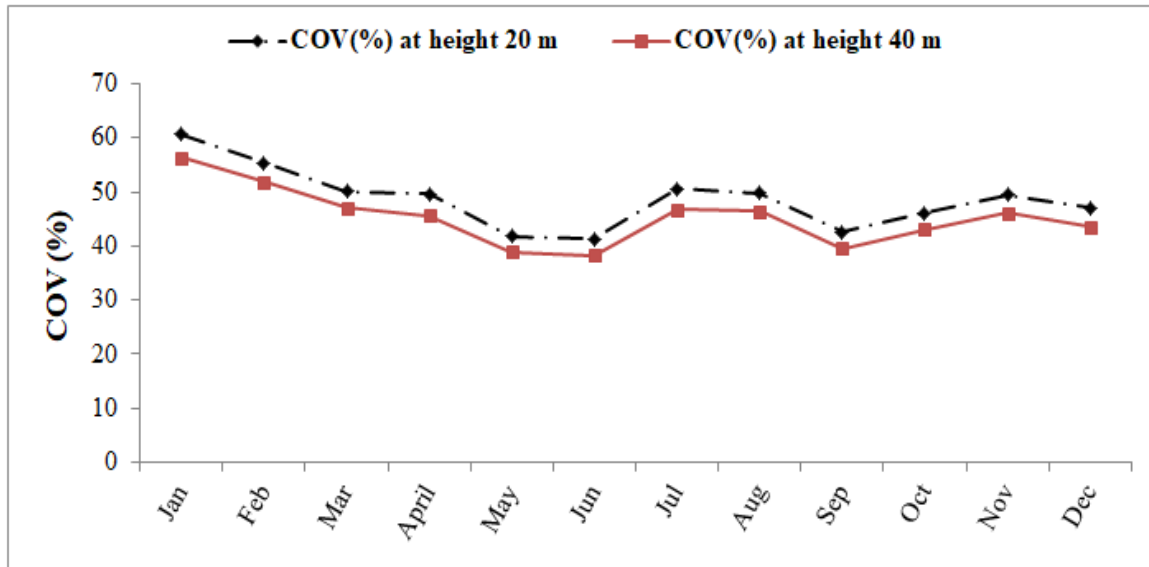


Figure 4.6 Monthly mean COV of turbulence at 20 m and 40 m height for Imp site

Table 4.3 Monthly mean wind speed and standard deviation for 12 years of Imp site

Month	Para	2005	2006	2007	2008	2009	2010	2011	2012	2013	2014	2015	2016	12 Yrs
Jan	\bar{v}	1.059	1.188	0.355	1.067	1.866	1.036	1.704	2.036	1.079	1.210	1.016	1.941	1.296
	σ	0.764	1.082	0.172	0.676	0.837	0.401	0.607	0.773	0.531	0.559	0.280	0.413	0.787
Feb	\bar{v}	2.674	1.245	0.490	1.667	2.139	2.388	2.036	2.918	1.064	2.049	1.589	2.676	1.911
	σ	1.093	0.758	0.291	0.710	0.822	0.959	0.842	0.848	0.773	0.808	0.595	0.932	1.060
Mar	\bar{v}	1.933	2.290	0.758	0.644	2.504	2.938	2.558	2.861	2.072	2.533	2.632	3.133	2.238
	σ	1.064	0.581	0.319	0.264	0.429	0.670	1.056	0.901	0.925	0.806	1.115	0.803	1.121
Apr	\bar{v}	1.886	2.771	2.345	0.843	2.726	3.159	2.481	2.670	2.247	2.684	1.907	2.985	2.392
	σ	0.672	1.154	2.360	0.255	0.781	1.292	0.616	1.129	0.799	0.617	0.876	0.946	1.187
May	\bar{v}	1.574	1.951	1.651	0.883	2.713	2.155	2.362	2.523	1.556	1.737	2.047	2.519	1.972
	σ	0.605	0.603	0.663	0.285	0.830	0.655	0.645	0.843	0.580	0.808	0.690	0.546	0.823
Jun	\bar{v}	1.628	1.671	1.313	1.659	2.422	1.459	2.160	2.036	1.482	1.587	2.240	2.405	1.839
	σ	0.630	0.326	0.547	0.758	0.699	0.490	0.712	0.537	0.487	0.882	1.079	0.418	0.759
Jul	\bar{v}	1.351	1.885	1.519	1.538	1.986	2.276	2.301	2.260	1.422	1.1386	2.916	2.283	1.906
	σ	0.687	0.691	0.349	0.581	0.672	1.184	0.968	0.725	0.830	1.079	1.310	0.351	0.965
Aug	\bar{v}	0.983	1.948	1.125	1.986	1.757	1.925	1.763	2.015	1.029	1.005	2.717	2.250	1.709
	σ	0.463	0.735	0.494	0.734	0.669	0.798	0.637	0.568	0.758	0.660	0.776	0.638	0.850
Sep	\bar{v}	1.116	1.294	1.073	1.721	1.702	1.435	1.790	1.906	1.017	0.875	2.040	1.805	1.481
	σ	0.614	0.639	0.564	0.410	0.500	0.597	0.326	0.532	0.366	0.336	0.722	0.315	0.630
Oct	\bar{v}	0.551	1.054	0.818	1.290	1.157	1.241	1.541	1.609	0.729	0.638	1.497	1.789	1.159
	σ	0.256	0.381	0.374	0.426	0.343	0.390	0.322	0.536	0.411	0.199	0.418	0.256	0.535
Nov	\bar{v}	0.482	0.695	0.705	1.184	1.378	1.126	1.376	1.472	0.576	0.910	1.492	1.654	1.087
	σ	0.127	0.377	0.374	0.383	0.701	0.424	0.158	0.410	0.359	0.226	0.397	0.306	0.537
Dec	\bar{v}	0.471	0.554	0.567	1.174	1.002	1.046	1.293	1.155	0.880	0.830	1.278	1.822	1.006
	σ	0.184	0.205	0.187	0.295	0.220	0.492	0.344	0.179	0.265	0.277	0.467	0.314	0.473
Yrly	\bar{v}	1.301	1.547	1.039	1.302	1.909	1.869	1.946	2.119	1.264	1.427	1.951	2.270	1.661
	σ	0.910	0.923	0.885	0.644	0.862	1.046	0.769	0.874	0.788	0.927	0.970	0.732	0.945

Table 4.3 shows the actual monthly mean wind speed and corresponding standard deviation based on actual mean wind speed for 12 years (2005-2016). It reveals that monthly mean wind speed range from 0.47 to 3.16 m/s while its standard deviation ranges from 0.13 to 2.36 m/s respectively. From this table, it is realized that seasonal consistency in the wind profile is not found while there is good consistency in the yearly wind profile.

4.4 Assessment of WEP for Shillong site

Figure 4.7 shows seasonal mean wind speed variations for five years (2012-2016) which reveals that summer provide the highest wind speed range while winter provides the lowest wind speed range. However, yearly mean wind speed is almost equal to mean wind speed of rainy season except in 2016. Seasonal variations also show that in all years mean wind speed of all the seasons fall within the range of 1 to 2.3 m/s.

The frequency (percentage) of wind speed values of Shillong site is presented in Figure 4.8 and it shows that wind speed 1-3 m/s has approximately 91% out of which wind speed of 1.5 m/s has the maximum share with 40% approximately.

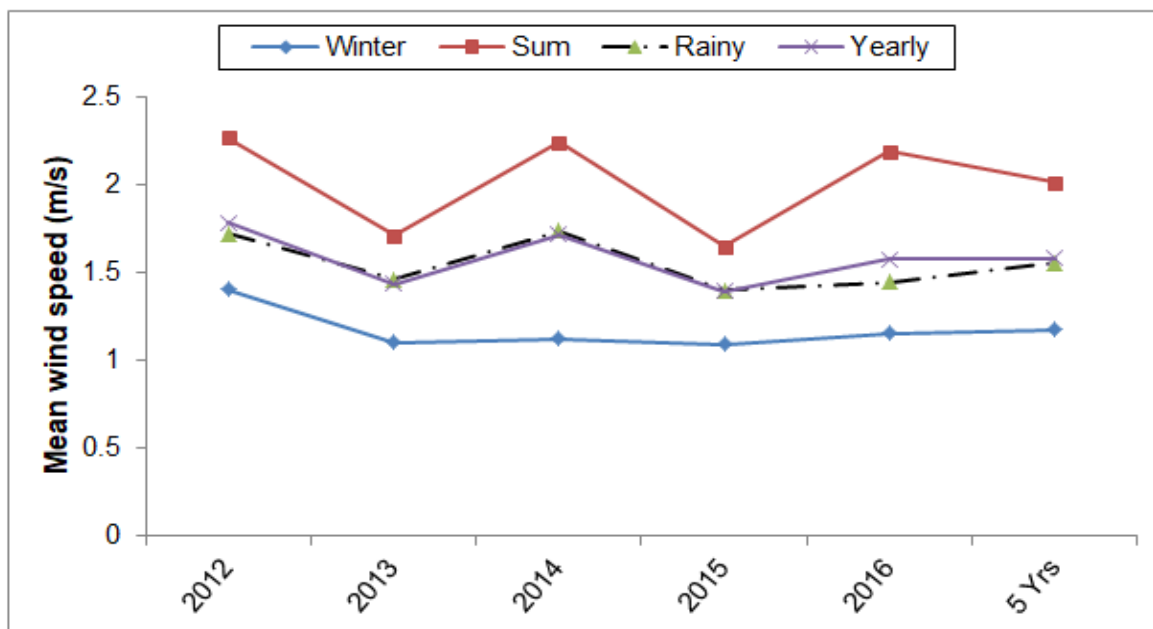


Figure 4.7 Seasonal variations for Five years (2012-16) mean wind speed of Shg site

Month wise mean wind speed for each year and whole five years of Shillong site are compared in Figure 4.9. It reveals that monthly mean wind speed of 2012, 2014 and 2016 is

found to be highest during April. While the mean wind speed of 2013 and 2015 is found to be highest in the month of May and June respectively. However, the monthly variation of mean wind speed of all five individual year and whole years are more or less consistent in nature providing the highest mean wind speed during March-June and the lowest mean wind speed during September- January.

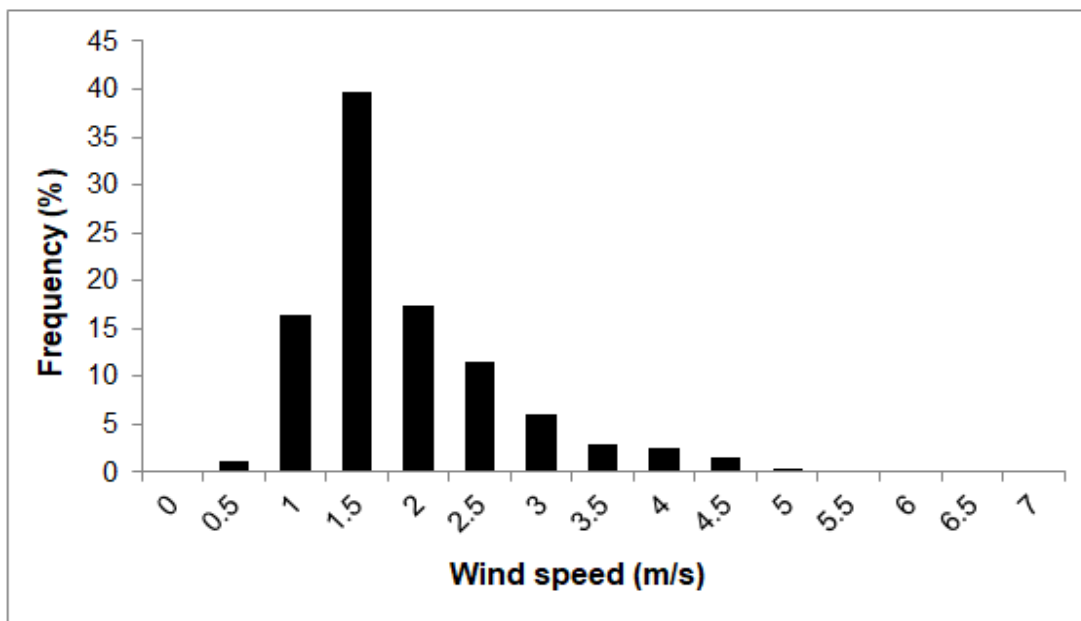


Figure 4.8 Frequency percentages for Five years (2012-16) wind speed of Shg site

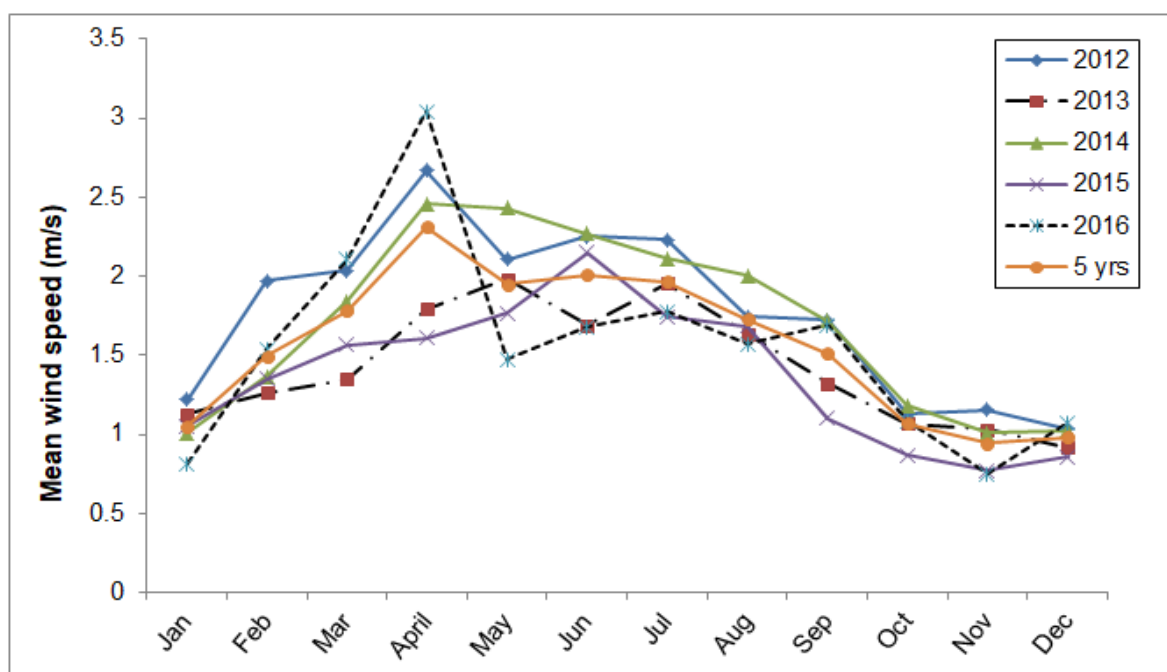


Figure 4.9 Five years (2012-16) monthly mean wind speed of Shg site

Table 4.4 Month wise wind characteristics for Five years of Shg site

Wind	Jan	Feb	Mar	Apr	May	Jun	Jul	Aug	Sep	Oct	Nov	Dec
n	146	138	155	149	155	148	155	154	144	143	137	139
V_{\min}	0.361	0.361	0.361	0.699	0.699	0.632	0.187	0.632	0.361	0.361	0.361	0.361
V_{\max}	4.760	4.911	4.760	6.557	5.062	6.260	4.306	4.002	12.110	3.236	3.849	3.236
σ	0.507	0.878	1.015	1.199	0.875	0.957	0.709	0.627	1.139	0.367	0.384	0.479
COV(%) at 20 m	48.19	58.70	57.04	51.81	44.85	47.65	36.14	36.28	75.40	34.48	40.45	48.82

Table 4.5 Monthly mean wind speed and standard deviation for 5 years of Shg site

Month	Para	2012	2013	2014	2015	2016	5 Yrs
Jan	\bar{v}	1.219	1.127	1.007	1.050	0.816	1.0524
	σ	0.411	0.432	0.215	0.460	0.820	0.507
Feb	\bar{v}	1.968	1.261	1.363	1.349	1.537	1.496
	σ	1.302	0.435	0.520	0.790	0.907	0.878
Mar	\bar{v}	2.035	1.350	1.841	1.564	2.108	1.780
	σ	1.109	0.813	0.979	0.958	1.049	1.015
Apr	\bar{v}	2.669	1.791	2.459	1.608	3.040	2.314
	σ	1.257	0.770	0.827	0.981	1.451	1.199
May	\bar{v}	2.107	1.982	2.429	1.767	1.471	1.951
	σ	1.000	0.691	0.860	0.882	0.633	0.875
Jun	\bar{v}	2.253	1.689	2.268	2.150	1.680	2.008
	σ	1.140	0.620	1.151	0.831	0.787	0.957
Jul	\bar{v}	2.230	1.955	2.112	1.743	1.778	1.963
	σ	0.627	0.494	0.826	0.823	0.637	0.709
Aug	\bar{v}	1.745	1.633	2.005	1.682	1.572	1.728
	σ	0.496	0.529	0.705	0.677	0.643	0.627
Sep	\bar{v}	1.720	1.324	1.719	1.101	1.689	1.511
	σ	0.847	0.691	0.570	0.642	2.134	1.139
Oct	\bar{v}	1.127	1.068	1.179	0.868	1.085	1.065
	σ	0.238	0.293	0.335	0.321	0.550	0.367
Nov	\bar{v}	1.190	1.028	1.010	0.773	0.750	0.950
	σ	0.623	0.215	0.305	0.195	0.237	0.384
Dec	\bar{v}	1.034	0.914	1.025	0.858	1.074	0.981
	σ	0.292	0.249	0.383	0.577	0.751	0.479
Yrly	\bar{v}	1.787	1.436	1.716	1.391	1.574	1.581
	σ	0.987	0.655	0.881	0.828	1.150	0.924

Table 4.4 shows monthly maximum speed, minimum speed, standard deviation and coefficient of variation (percentage) at 20 m. It reveals that minimum speed is in the range of 0.19-0.70 m/s while maximum speed is in the range of 3.24-2.11 m/s. COV percentage of all the months is in the range of 36-58 but in case of September the value is 75.

Further, Table 4.5 shows the actual monthly mean wind speed and corresponding standard deviation based on actual mean wind speed for 5 years (2012-2016). It reveals that monthly mean speed range from 0.75 to 3.04 m/s while standard deviation ranges from 0.19 to 1.30 m/s respectively. From this table, it is realized that seasonal consistency in the wind profile is not found while there is good consistency in the yearly wind profile.

4.5 Assessment of WEP for Guwahati site

Figure 4.10 shows seasonal variations for five years (2012-2016) which reveals that summer provide the highest wind speed range followed by wind speed range of rainy season while winter provides the lowest wind speed range. Although yearly mean wind speed is significantly less than the same of summer season but a little better than rainy season. Seasonal variations also show that in all years mean wind speed of all the seasons fall within the range of 2 to 3 m/s.

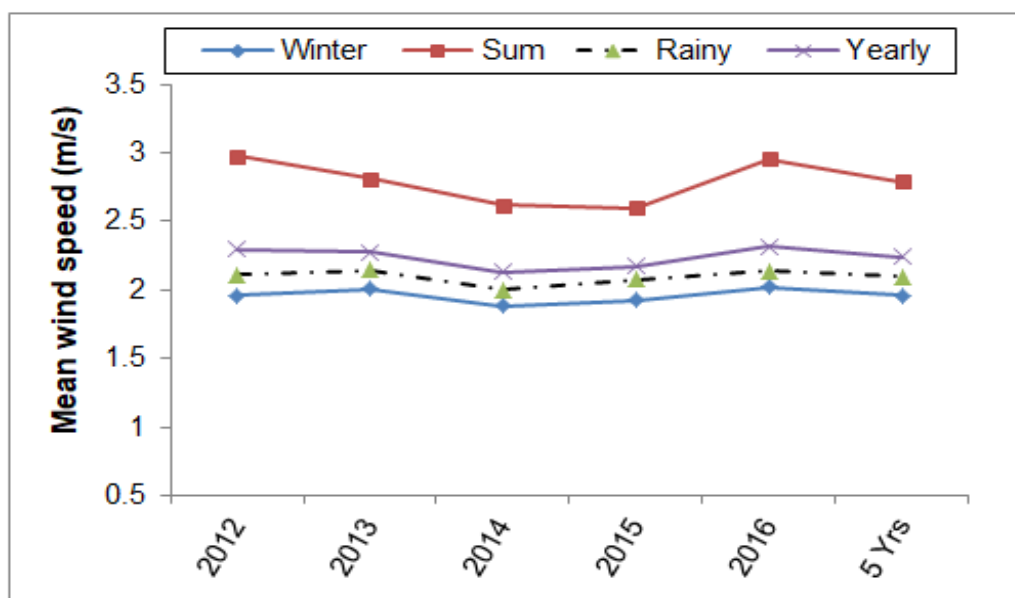


Figure 4.10 Seasonal variations for Five years (2012-16) mean wind speed of Ghy site

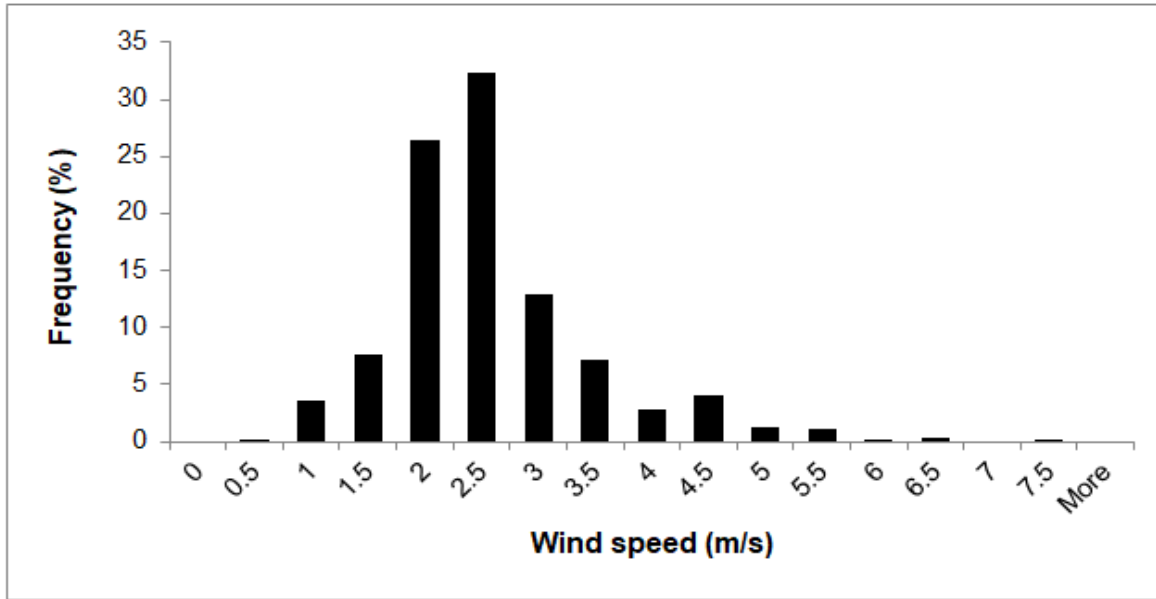


Figure 4.11 Frequency percentages for Five years (2012-16) wind speed of Ghy site

Figure 4.11 shows the frequency (percentage) of wind speed values of Guwahati site which reveals that wind speed 1.5-3.5 m/s has approximately 87% out of which wind speed of 2.5 m/s has the maximum share with 33% approximately.

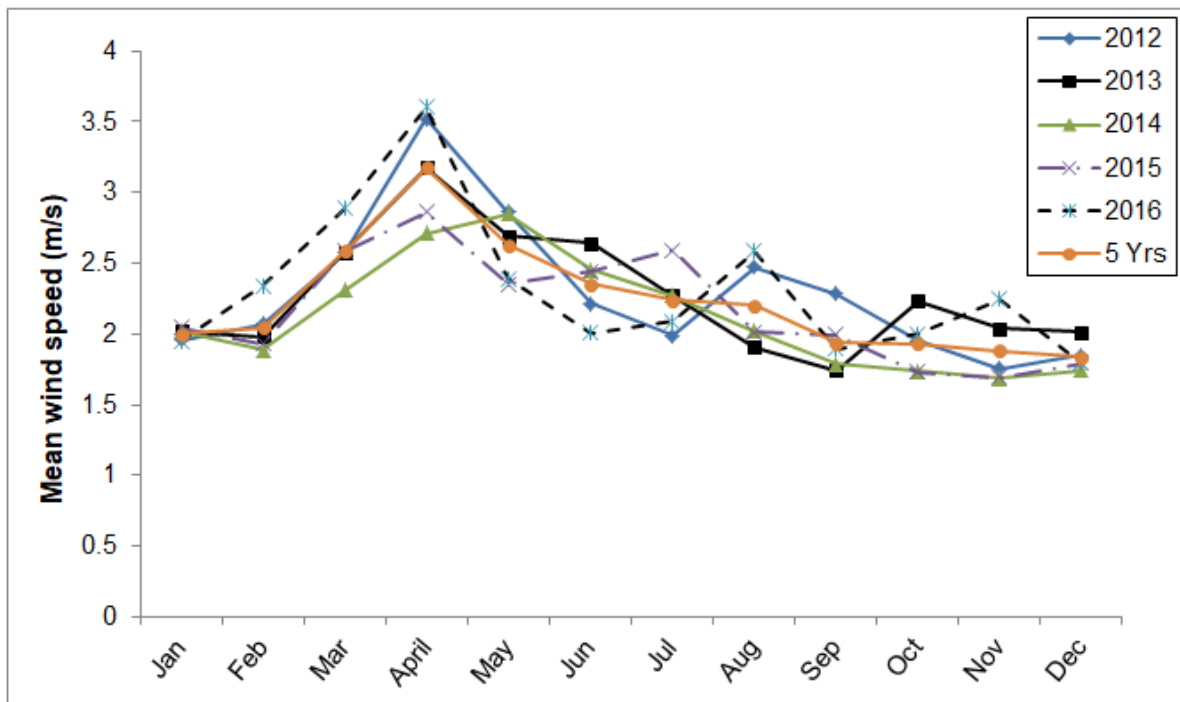


Figure 4.12 Five years (2012-16) monthly mean wind speed of Ghy site

Table 4.6 Month wise wind characteristics for Five years of Ghy site

Wind	Jan	Feb	Mar	Apr	May	Jun	Jul	Aug	Sep	Oct	Nov	Dec
n	150	139	153	149	151	149	155	154	146	150	146	149
V_{\min}	0.887	0.887	0.887	1.278	0.887	0.887	0.887	0.474	0.887	0.474	0.887	0.887
V_{\max}	3.446	3.446	6.117	6.441	5.463	7.083	5.463	4.47	4.467	5.463	5.627	3.098
σ	0.572	0.558	1.067	1.221	1.005	1.101	1.026	0.900	0.787	0.691	0.646	0.471
COV(%) at 20 m	28.66	27.34	41.26	38.47	38.21	46.82	45.79	40.93	40.60	35.82	34.30	25.60

Table 4.7 Monthly mean wind speed and standard deviation for 5 years of Ghy site

Month	Para	2012	2013	2014	2015	2016	5 Yrs
Jan	\bar{v}	1.958	2.018	2.021	2.043	1.947	1.997
	σ	0.559	0.517	0.495	0.761	0.511	0.572
Feb	\bar{v}	2.068	1.984	1.884	1.930	2.342	2.042
	σ	0.419	0.574	0.402	0.632	0.632	0.558
Mar	\bar{v}	2.570	2.579	2.310	2.586	2.888	2.587
	σ	0.794	1.250	1.049	1.162	1.025	1.067
Apr	\bar{v}	3.520	3.173	2.710	2.862	3.601	3.173
	σ	1.196	1.105	1.071	1.190	1.339	1.221
May	\bar{v}	2.859	2.691	2.850	2.351	2.393	2.629
	σ	0.956	1.278	0.987	0.882	0.804	1.005
Jun	\bar{v}	2.215	2.643	2.451	2.443	2.004	2.351
	σ	1.033	1.228	1.414	0.956	0.691	1.101
Jul	\bar{v}	1.989	2.271	2.270	2.594	2.086	2.242
	σ	0.843	1.072	1.057	1.274	0.767	1.026
Aug	\bar{v}	2.471	1.908	2.021	2.010	2.582	2.199
	σ	0.907	0.836	0.883	0.779	0.928	0.900
Sep	\bar{v}	2.285	1.742	1.783	1.996	1.892	1.940
	σ	1.023	0.626	0.623	0.748	0.781	0.787
Oct	\bar{v}	1.951	2.232	1.735	1.731	2.002	1.930
	σ	0.525	1.012	0.414	0.540	0.691	0.691
Nov	\bar{v}	1.754	2.040	1.685	1.692	2.245	1.883
	σ	0.406	0.681	0.449	0.453	0.923	0.646
Dec	\bar{v}	1.850	2.011	1.743	1.796	1.792	1.838
	σ	0.388	0.478	0.595	0.443	0.400	0.471
Yrly	\bar{v}	2.296	2.277	2.129	2.171	2.316	2.238
	σ	0.928	1.006	0.923	0.928	0.951	0.949

Month wise mean wind speed for each year and whole five years are compared in Figure 4.12. It reveals that monthly mean wind speed of all the years except 2014 is found to be highest during April. However, monthly variation of mean wind speed of all five individual year and whole years are more or less consistent in nature providing the highest mean wind speed during March-June and the lowest mean wind speed during September- December.

Table 4.6 shows monthly maximum speed, minimum speed, standard deviation and coefficient of variation (%) at 20 m. It reveals that minimum speed is in the range of 0.47-1.28 m/s while maximum speed is in the range of 3.10-6.44 m/s. COV (%) of all the months is consistent in nature whose values is between 26-47.

Table 4.7 shows the actual monthly mean wind speed and corresponding standard deviation based on actual mean wind speed for 5 years (2012-2016). It reveals that monthly mean speed range from 1.68 to 3.60 m/s while standard deviation ranges from 0.39 to 1.41 m/s respectively. From this table, it is realized that there is good consistency in the seasonal and yearly wind profile as well.

4.6 Assessment of WEP for Kolkata site

Figure 4.13 shows seasonal variations for five years (2012-2016) which reveals that summer provide the highest wind speed range while winter provides the lowest wind speed range. However, yearly mean wind speed is almost equal to mean wind speed of rainy season. Seasonal variations also show that in all years mean wind speed of all the seasons fall within the range of 1.2 to 4 m/s.

Figure 4.14 shows the frequency (percentage) of wind speed values of Kolkata site which reveals that wind speed 1.0-4.5 m/s has approximately 92% out of which wind speed of 1.5 and 2.5 m/s have the maximum share with 21% and 17% respectively.

Month wise mean wind speed for each year and whole five years are compared in Figure 4.15. It reveals that monthly mean wind speed of all the years except 2015 is found to be highest during April and May. However, the monthly variation of mean wind speed of all five individual year and whole years except 2015 are more or less consistent in nature providing the highest mean wind speed during March-August and the lowest mean wind speed during October- December and January.

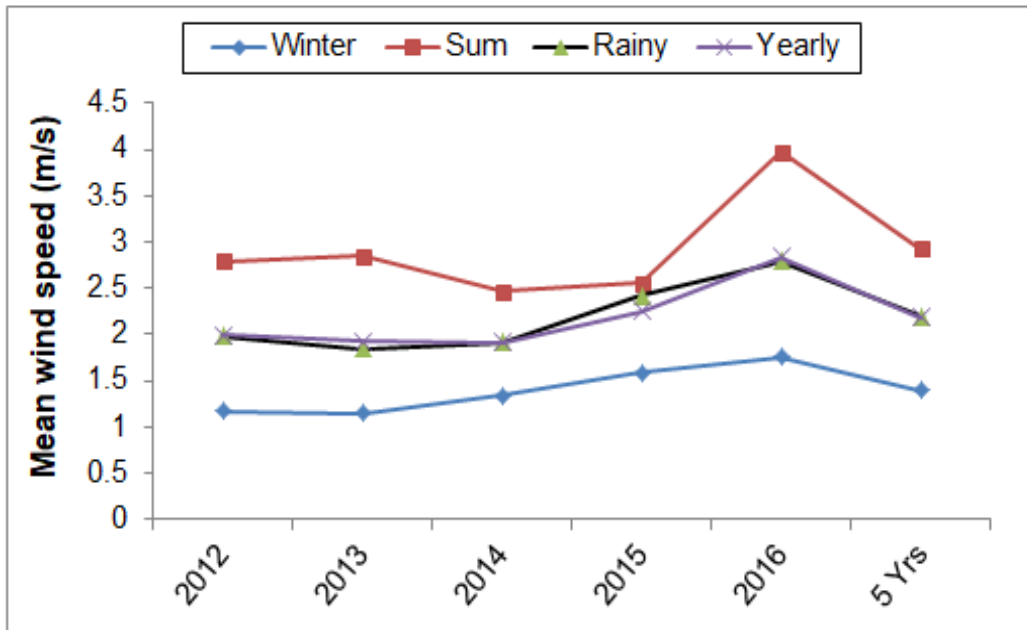


Figure 4.13 Seasonal variations for Five years (2012-16) mean wind speed of Kol site

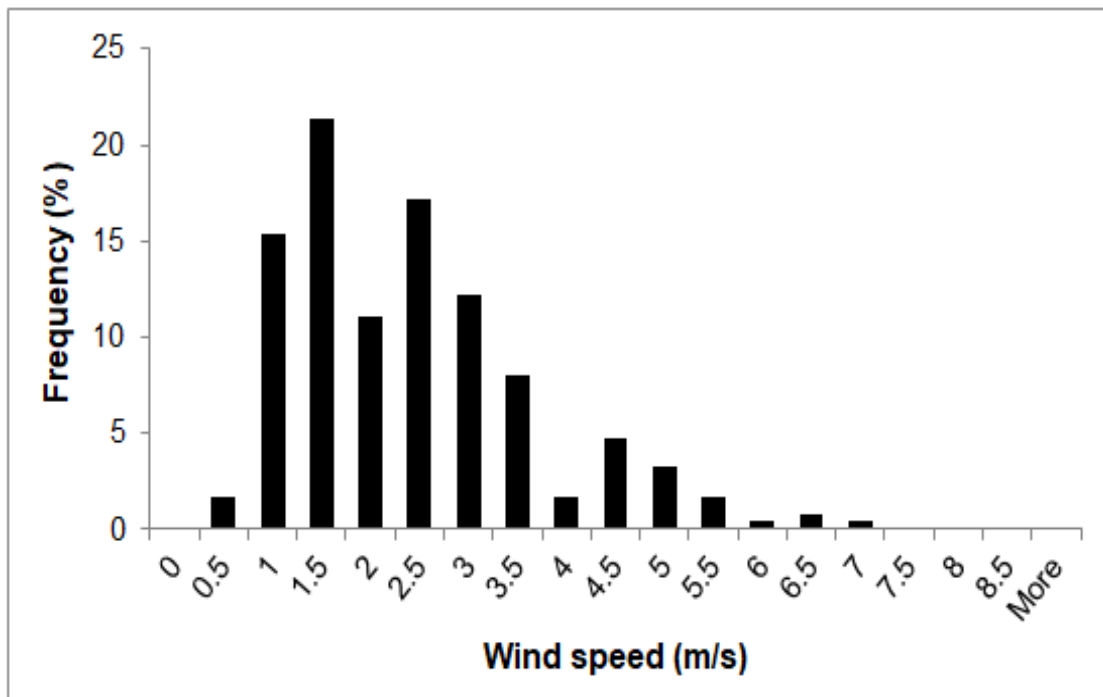


Figure 4.14 Frequency percentages for Five years (2012-16) wind speed of Kol site

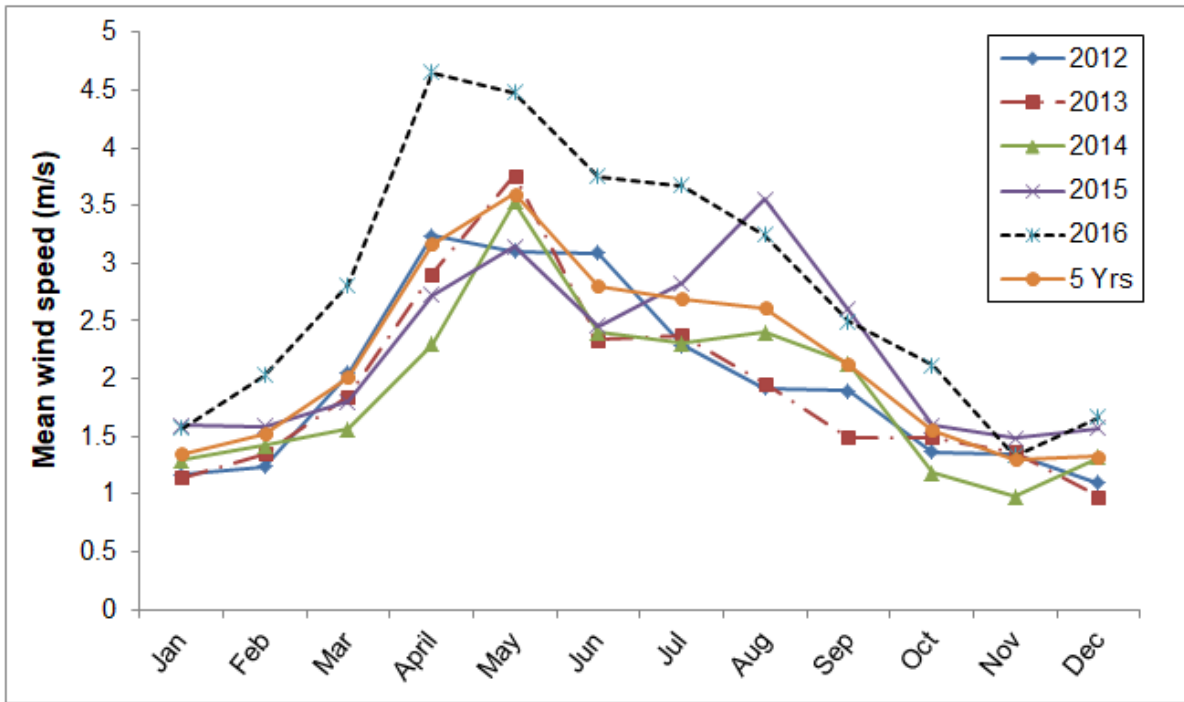


Figure 4.15 Five years (2012-16) monthly mean wind speed of Kol site

Table 4.8 Month wise wind characteristics for Five years of Kol site

Wind	Jan	Feb	Mar	Apr	May	Jun	Jul	Aug	Sep	Oct	Nov	Dec
n	152	141	154	150	155	148	154	154	148	152	143	146
V_{min}	0.300	0.300	0.595	1.178	0.595	0.595	0.595	0.887	0.595	0.300	0.300	0.300
V_{max}	4.050	4.050	6.890	6.890	8.020	6.890	6.323	7.455	4.620	4.904	6.890	4.050
σ	0.705	0.756	1.017	1.296	1.300	1.266	1.051	1.227	0.944	0.864	0.847	0.763
COV(%) at 20 m	52.12	49.54	50.54	40.95	36.06	45.10	39.02	46.89	44.51	55.66	65.08	57.64

Table 4.8 shows monthly maximum speed, minimum speed, standard deviation and coefficient of variation (percentage) at 20 m. It reveals that minimum speed is in the range of 0.30-1.18 m/s while maximum speed is in the range of 4.05-8.02 m/s. COV percentage of all the months is consistent in nature whose values is between 36-58.

Table 4.9 shows the actual monthly mean wind speed and corresponding standard deviation based on actual mean wind speed for 5 years (2012-2016). It reveals that monthly mean speed range from 0.98 to 4.66 m/s while standard deviation ranges from 0.46 to 1.57 m/s respectively. Further, table shows that there is good consistency in the seasonal and yearly wind profile as well.

Table 4.9 Monthly mean wind speed and standard deviation for 5 years of Kol site

Month	Para	2012	2013	2014	2015	2016	5 Yrs
Jan	\bar{v}	1.167	1.146	1.298	1.592	1.569	1.353
	σ	0.527	0.649	0.528	0.586	1.028	0.705
Feb	\bar{v}	1.235	1.348	1.424	1.589	2.033	1.526
	σ	0.737	0.581	0.628	0.779	0.799	0.756
Mar	\bar{v}	2.043	1.852	1.559	1.801	2.809	2.013
	σ	0.766	0.593	0.6036	0.763	1.570	1.017
Apr	\bar{v}	3.239	2.904	2.302	2.722	4.655	3.164
	σ	0.887	0.938	0.767	1.162	1.295	1.296
May	\bar{v}	3.106	3.760	3.532	3.145	4.479	3.604
	σ	1.192	1.442	0.988	0.888	1.453	1.300
Jun	\bar{v}	3.091	2.341	2.398	2.453	3.752	2.807
	σ	1.172	0.727	1.219	1.256	1.315	1.266
Jul	\bar{v}	2.294	2.378	2.303	2.827	3.671	2.695
	σ	0.532	0.482	0.845	1.473	0.907	1.051
Aug	\bar{v}	1.918	1.960	2.405	3.558	3.245	2.617
	σ	0.688	0.702	0.892	1.440	1.249	1.227
Sep	\bar{v}	1.894	1.496	2.130	2.597	2.493	2.122
	σ	0.753	0.634	0.709	1.178	0.937	0.945
Oct	\bar{v}	1.369	1.491	1.186	1.596	2.117	1.552
	σ	0.763	1.155	0.484	0.713	0.816	0.864
Nov	\bar{v}	1.341	1.369	0.979	1.482	1.336	1.301
	σ	0.720	0.638	0.536	1.282	0.796	0.847
Dec	\bar{v}	1.095	0.979	1.315	1.568	1.664	1.324
	σ	0.656	0.465	0.717	0.845	0.887	0.763
Yrly	\bar{v}	1.989	1.929	1.915	2.256	2.842	2.186
	σ	1.104	1.113	1.038	1.266	1.549	1.276

4.7 Comparative analysis of WEP for all the selected sites

Figure 4.16 shows the comparison of yearly wind profile in which the mean wind speed of Guwahati site is almost the same in all five years and it is higher than the remaining three

sites except in 2015-16. Although the wind speeds of Kolkata site is slightly lower than Guwahati site it overtakes the later from 2015 onwards. The mean wind speed range of Imphal site is slightly higher than that of Shillong site except in 2013 and 2014.

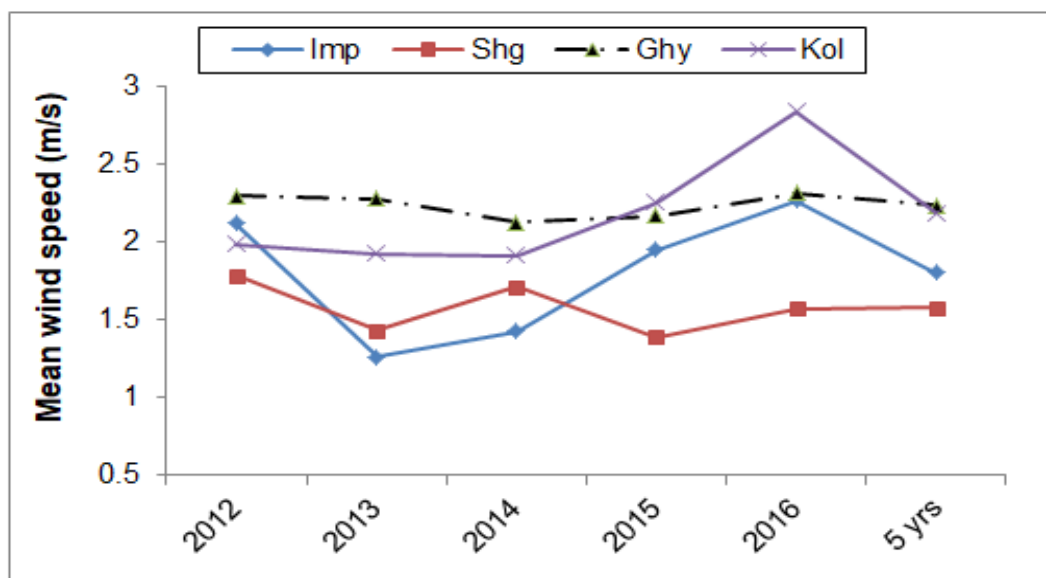


Figure 4.16 Yearly mean wind speed of four different sites

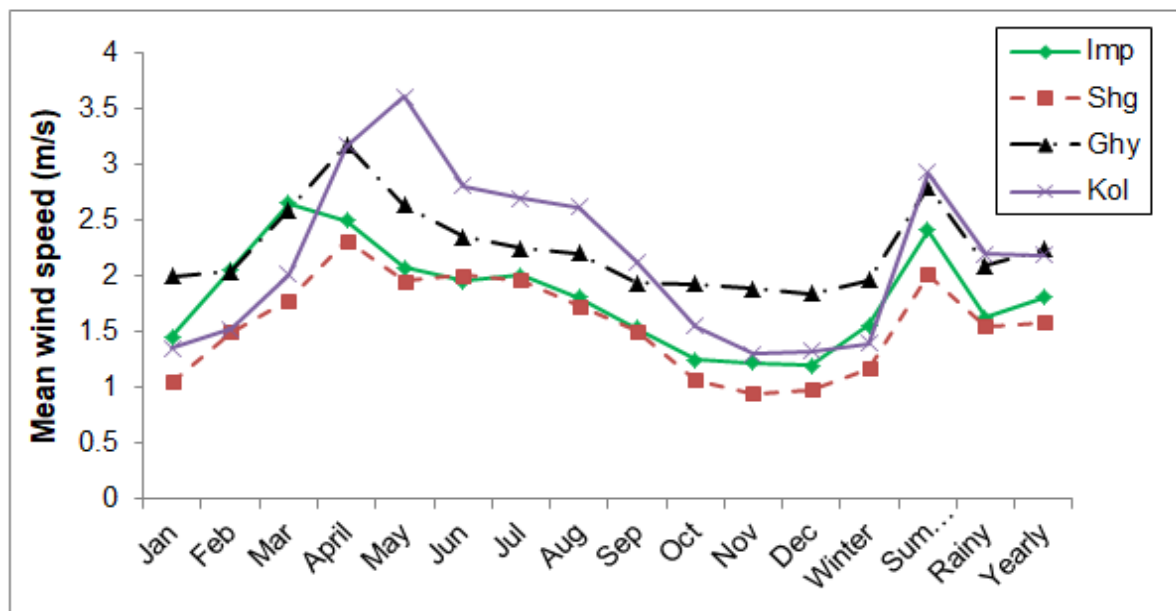


Figure 4.17 Mean wind speed for Five years (2012-16) of four different sites

The graphical representation of the mean wind speed of selected sites in the east and northeastern region of India is shown in Figure 4.17. The mean wind speed of Kolkata site is highest in all months except during the winter season followed by that of Guwahati site. The

wind profile for the Shillong and Imphal sites is almost the same except during winter season during which Imphal has higher wind speed range.

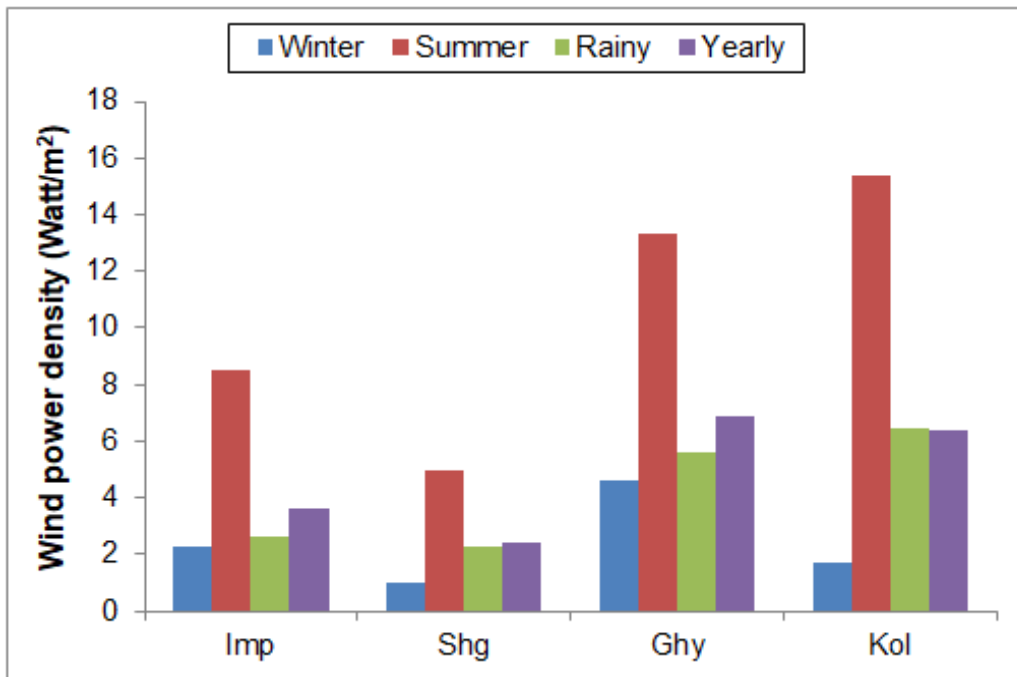


Figure 4.18 Seasonal and annual wind power density of all the four different sites

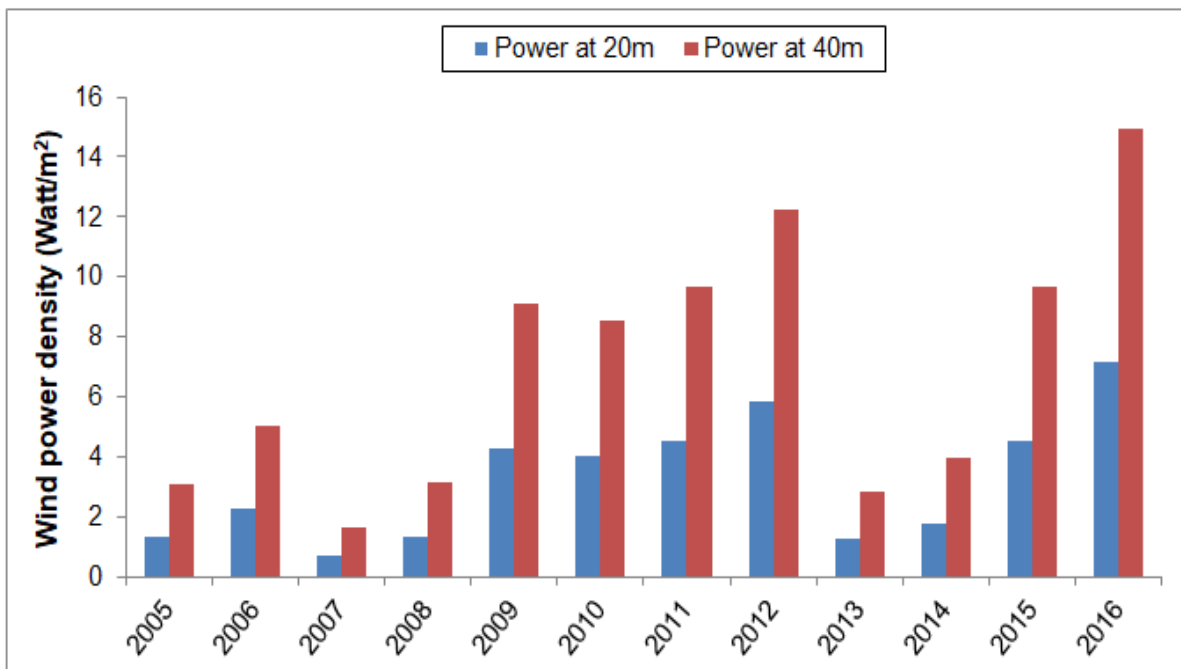


Figure 4.19 Wind power density of two different heights from the ground for Imp site

Figure 4.18 shows the seasonal and annual wind power density (WPD) based on actual mean wind speed of all the selected sites and it reveals that summer provides highest WPD while winter provides the least WPD in all stations. Among the sites Kolkata provides highest WPD during summer but in case annual WPD Guwahati provides little higher than the value of Kolkata and least WPD is available at Shillong site.

In the high-rise building area, the base of the wind turbine may not be sufficient by 20 m height; in such situation the wind power density at 40 m or more height may be needed. So the comparison of wind power density of two different heights: 20 m and 40 m for Imphal site is shown in Figure 4.19. It shows that wind power density at 40 m height increased by about 110-140% which ultimately can tap more energy from the wind resource.

4.8 Performance comparison between Weibull and Rayleigh Distribution model

Table 4.10 Comparison between Weibull and Rayleigh models for Imp site

Season	Model	Estimation method	Parameters		Statistical Evaluation		
			k	c (m/s)	R ²	RMSE	MABE
Winter	Weibull	MOM	1.93155	1.75490	0.96118	0.02056	0.60
		EM	1.94394	1.75520	0.96090	0.02059	0.59
		PDM	3.37970	1.73305	0.88863	0.02932	0.06
	Rayleigh	MOM/EM/PDM	2.00000	1.75628	0.95927	0.02072	0.53
Summer	Weibull	MOM	2.76210	2.70344	0.97979	0.01824	1.92
		EM	2.76871	2.70320	0.97973	0.01827	1.91
		PDM	4.29715	2.64362	0.94997	0.02672	0.92
	Rayleigh	MOM/EM/PDM	2.00000	2.71494	0.97061	0.01632	3.49
Rainy	Weibull	MOM	1.96946	1.83594	0.97252	0.01445	0.34
		EM	1.98167	1.83620	0.97273	0.01449	0.33
		PDM	3.30231	1.81436	0.92289	0.02103	0.01
	Rayleigh	MOM/EM/PDM	2.00000	1.83651	0.97298	0.01454	0.32
Yearly	Weibull	MOM	2.00379	2.03806	0.97392	0.00954	0.25
		EM	2.01582	2.03827	0.97394	0.00956	0.24
		PDM	3.84302	1.99714	0.90414	0.01585	0.01
	Rayleigh	MOM/EM/PDM	2.00000	2.03799	0.97394	0.00954	0.25

Table 4.11 Comparison between Weibull and Rayleigh models for Shg site

Season	Model	Estimation method	Parameters		Statistical Evaluation		
			k	c (m/s)	R ²	RMSE	MABE
Winter	Weibull	MOM	1.78961	1.31906	0.84623	0.02979	0.12
		EM	1.80264	1.31953	0.84703	0.02977	0.11
		PDM	4.47505	1.28618	0.84189	0.03969	0.31
	Rayleigh	MOM/EM/PDM	2.00000	1.32399	0.85680	0.02949	0.01
Summer	Weibull	MOM	1.99812	2.26763	0.96594	0.01872	1.37
		EM	2.01019	2.26787	0.96568	0.01874	1.35
		PDM	4.31749	2.20749	0.87758	0.03178	0.16
	Rayleigh	MOM/EM/PDM	2.00000	2.26766	0.96590	0.01873	1.37
Rainy	Weibull	MOM	1.89780	1.74177	0.96244	0.01619	0.17
		EM	1.91036	1.74213	0.96269	0.01618	0.16
		PDM	4.44057	1.69502	0.90734	0.02476	0.25
	Rayleigh	MOM/EM/PDM	2.00000	1.74407	0.96388	0.01616	0.11
Yearly	Weibull	MOM	1.78024	1.77566	0.97099	0.01117	0.13
		EM	1.79331	1.77632	0.97096	0.01116	0.13
		PDM	4.49303	1.73146	0.91146	0.01753	0.20
	Rayleigh	MOM/EM/PDM	2.00000	1.78278	0.96825	0.01111	0.06

Table 4.12 Comparison between Weibull and Rayleigh models for Ghy site

Season	Model	Estimation method	Parameters		Statistical Evaluation		
			k	c (m/s)	R ²	RMSE	MABE
Winter	Weibull	MOM	4.04958	2.15979	0.97689	0.03050	0.53
		EM	4.04192	2.16002	0.97705	0.03045	0.53
		PDM	4.67489	2.14194	0.96021	0.03428	0.42
	Rayleigh	MOM/EM/PDM	2.00000	2.17310	0.93265	0.02521	1.96
Summer	Weibull	MOM	2.66361	3.14143	0.97853	0.01733	3.29
		EM	2.67107	3.14115	0.97845	0.01735	3.28
		PDM	4.61858	3.05525	0.94692	0.02594	1.35
	Rayleigh	MOM/EM/PDM	2.00000	3.15080	0.97499	0.01653	5.55
Rainy	Weibull	MOM	2.51640	2.35968	0.97081	0.01448	0.54
		EM	2.52506	2.35947	0.97073	0.01449	0.53
		PDM	4.67608	2.28950	0.94539	0.02011	0.05
	Rayleigh	MOM/EM/PDM	2.00000	2.36283	0.96977	0.01452	0.96
Yearly	Weibull	MOM	2.52881	2.52136	0.97126	0.00975	0.36
		EM	2.53737	2.52114	0.97120	0.00976	0.36
		PDM	4.66590	2.44700	0.95004	0.01364	0.06
	Rayleigh	MOM/EM/PDM	2.00000	2.52505	0.96938	0.00978	0.62

Table 4.13 Comparison between Weibull and Rayleigh models for Kol site

Season	Model	Estimation method	Parameters		Statistical Evaluation		
			k	c (m/s)	R ²	RMSE	MABE
Winter	Weibull	MOM	1.96975	1.57824	0.95961	0.02284	0.44
		EM	1.98195	1.57845	0.95936	0.02287	0.43
		PDM	4.12235	1.54093	0.81811	0.03785	0.11
	Rayleigh	MOM/EM/PDM	2.00000	1.57873	0.95891	0.02292	0.42
Summer	Weibull	MOM	2.24552	3.30446	0.98323	0.01569	4.50
		EM	2.25612	3.30434	0.98318	0.01574	4.45
		PDM	3.98988	3.22951	0.95141	0.02570	1.28
	Rayleigh	MOM/EM/PDM	2.00000	3.30256	0.98218	0.01484	5.75
Rainy	Weibull	MOM	1.92303	2.47181	0.97068	0.01235	1.04
		EM	1.93547	2.47225	0.97066	0.01237	1.03
		PDM	4.13192	2.41452	0.93552	0.02233	0.06
	Rayleigh	MOM/EM/PDM	2.00000	2.47407	0.97033	0.01252	0.93
Yearly	Weibull	MOM	1.78148	2.45719	0.96591	0.00850	0.57
		EM	1.79454	2.45810	0.96587	0.00852	0.55
		PDM	4.15390	2.40684	0.90758	0.01634	0.10
	Rayleigh	MOM/EM/PDM	2.00000	2.46695	0.96214	0.00888	0.39

It is realized from the section 2.1.2 of literature survey that Weibull distribution models outperforms in the most of studies, however, it has an important weakness that it may not be suitable for low wind speed data (Pishgar-Komleh et al., 2015) and in such cases other reliable alternative models like Rayleigh model may be applied. With this objective Table 4.10, 4.11, 4.12 and 4.13 shows the performance comparison of Weibull and Rayleigh distribution model employing wind speed data of Imphal, Shillong, Guwahati and Kolkata sites respectively. For the estimation of shape and scale parameters three effective numerical methods: MOM, EM and PDM were employed. Results reveal that Weibull model provides optimum value of statistical evaluation test such as correlation coefficient (R²), root mean square error (RMSE), mean absolute bias error (MABE) in most of the seasonal and yearly performance analysis of Imphal, Guwahati and Kolkata sites. However, Rayleigh model significantly performed better in case of Shillong site providing 8 numbers of 1st ranking in performance while Weibull provided 4 numbers of 1st ranking.

As far as value of parameters are concerned the value of *k* range from 1.77 to 4.68, while *c* ranges from 1.29 to 3.31 m/s irrespective of sites and it indicates that wind characteristics in East and Northeastern regions are almost uniform with low to medium wind power potential.

4.9 Validation and Performance comparison of the new estimation method

Concluding remarks of section 2.1.3 of literature survey stated that success of Weibull distribution model depends on the effectiveness of estimation method. Studies revealed that several numerical methods have been applied to estimate the parameters, among them MOM, EM, PDM, MLM were considered to be most effective and most frequently used methods. However, some studies reveals that effectiveness of estimation methods also depends on the on the set of data employed which again depend on the climatic status and nature of the surface such as roughness and orography of the chosen location (Rahman and Chattopadhyay, 2019b; Rehman and Abbadi, 2007; Rehman et al., 2015; Saxena and Rao, 2015). Therefore, with the aim to find the best alternative estimation method a new approach called “Energy variance method (EVM)” is developed in the present study and its performance is compared with MOM, EM, PDM and MLM.

Table 4.14 Performance analysis of five numerical methods for Imp site

Season	Method	V_{mF}	V_{maxE}	Statistical evaluation				Ranking			
				R^2	RMSE	MSEP	MAPE	a	b	c	d
				a	b	c	d	a	b	c	d
Winter	MOM	1.203	2.535	0.96118	0.02056	3.96107	0.09450	1	2	1	5
	EM	1.210	2.526	0.96090	0.02059	3.97337	0.09239	2	3	2	3
	PDM	1.562	1.989	0.88863	0.02932	5.01226	0.01020	5	5	5	1
	MLM	1.237	2.517	0.95815	0.02050	3.99534	0.09300	4	1	3	4
	EVM	1.243	2.482	0.95917	0.02072	4.02712	0.08300	3	4	4	2
	MOM	2.297	3.293	0.97979	0.01824	1.98373	0.11759	3	3	3	3
Summer	EM	2.299	3.290	0.97973	0.01827	1.98498	0.11709	4	4	4	2
	PDM	2.485	2.889	0.94997	0.02672	2.35886	0.05630	5	5	5	1
	MLM	2.288	3.310	0.97999	0.01808	1.97649	0.12067	2	2	2	4
	EVM	2.247	3.374	0.98073	0.01757	1.95997	0.13126	1	1	1	5
	MOM	1.281	2.621	0.97252	0.01445	2.99337	0.20386	3	2	2	4
Rainy	EM	1.288	2.611	0.97273	0.01449	2.99603	0.20190	2	3	3	3
	PDM	1.627	2.094	0.92289	0.02103	3.20718	0.10646	5	5	5	1
	MLM	1.280	2.624	0.97227	0.01443	2.99282	0.20482	4	1	1	5
	EVM	1.300	2.595	0.97301	0.01455	3.00048	0.19854	1	4	4	2
	MOM	1.443	2.879	0.97392	0.00954	1.27983	0.02651	2	2	1	4
Yearly	EM	1.451	2.869	0.97394	0.00956	1.28186	0.02601	1	3	3	3
	PDM	1.846	2.227	0.90414	0.01585	1.73321	0.00137	5	5	5	1
	MLM	1.451	2.878	0.97340	0.00953	1.28080	0.02665	4	1	2	5
	EVM	1.463	2.852	0.97389	0.00961	1.28517	0.02519	3	4	4	2

Table 4.15 Performance analysis of five numerical methods for Shg site

Season	Method	V_{mF}	$V_{\max E}$	Statistical evaluation				Ranking			
				R^2	RMSE	MSEP	MAPE	a	b	c	d
				a	b	c	d				
Winter	MOM	0.835	2.006	0.84623	0.02979	4.66395	0.03329	2	3	3	3
	EM	0.842	1.996	0.84703	0.02977	4.65315	0.03103	1	2	2	2
	PDM	1.215	1.397	0.84189	0.03969	5.42146	0.08528	5	5	5	5
	MLM	0.884	1.963	0.84586	0.02942	4.57913	0.02543	3	1	1	1
	EVM	0.824	2.020	0.84507	0.02982	4.67847	0.03656	4	4	4	4
Summer	MOM	1.602	3.209	0.96594	0.01872	2.30787	0.10806	2	3	2	4
	EM	1.610	3.198	0.96568	0.01874	2.31315	0.10612	3	4	3	2
	PDM	2.077	2.411	0.87758	0.03178	3.17519	0.01271	5	5	5	1
	MLM	1.637	3.188	0.96401	0.01870	2.31748	0.10648	4	2	4	3
	EVM	1.571	3.250	0.96667	0.01869	2.29588	0.11528	1	1	1	5
Rainy	MOM	1.174	2.545	0.96244	0.01619	2.1196	0.02300	2	3	2	3
	EM	1.182	2.535	0.96269	0.01618	2.12348	0.02204	1	2	3	1
	PDM	1.600	1.843	0.90734	0.02476	3.10732	0.03273	5	5	5	5
	MLM	1.202	2.530	0.96184	0.01606	2.12978	0.02255	4	1	4	2
	EVM	1.164	2.559	0.96208	0.01620	2.11429	0.02428	3	4	1	4
Yearly	MOM	1.117	2.711	0.97099	0.01117	1.45670	0.01695	1	3	1	5
	EM	1.127	2.697	0.97096	0.01116	1.46071	0.01634	2	2	3	3
	PDM	1.637	1.879	0.91146	0.01753	2.11658	0.01541	4	4	5	2
	MLM	1.174	2.660	0.96945	0.01106	1.47895	0.01512	3	1	4	1
	EVM	1.121	2.705	0.97099	0.01116	1.45881	0.01669	1	2	2	4

Table 4.16 Performance analysis of five numerical methods for Ghy site

Season	Method	V_{mF}	$V_{\max E}$	Statistical evaluation				Ranking			
				R^2	RMSE	MSEP	MAPE	a	b	c	d
				a	b	c	d				
Winter	MOM	2.014	2.385	0.97689	0.03050	2.69644	0.05917	4	4	4	2
	EM	2.013	2.386	0.97705	0.03045	2.69207	0.05936	3	3	3	3
	PDM	2.034	2.311	0.96021	0.03428	3.00056	0.04655	5	5	5	1
	MLM	2.001	2.408	0.98037	0.02960	2.60002	0.06272	2	2	2	4
	EVM	1.988	2.453	0.98417	0.02826	2.48952	0.07146	1	1	1	5
Summer	MOM	2.633	3.877	0.97853	0.01733	1.72845	0.12997	2	3	3	3
	EM	2.635	3.872	0.97845	0.01735	1.72983	0.12932	3	4	4	2
	PDM	2.898	3.303	0.94692	0.02594	2.22285	0.05317	5	5	5	1
	MLM	2.631	3.901	0.97841	0.01721	1.72154	0.13482	4	2	2	4
	EVM	2.564	3.984	0.97984	0.01690	1.70006	0.14612	1	1	1	5
Rainy	MOM	1.929	2.977	0.97081	0.01448	1.68398	0.04219	3	3	3	3
	EM	1.932	2.973	0.97073	0.01449	1.68591	0.04182	4	4	4	2
	PDM	2.175	2.471	0.94539	0.02011	2.03027	0.00361	5	5	5	1
	MLM	1.910	3.017	0.97094	0.01440	1.66674	0.04599	2	2	2	4
	EVM	1.872	3.062	0.97187	0.01439	1.64408	0.04957	1	1	1	5
Yearly	MOM	2.066	3.175	0.97126	0.00975	1.10925	0.02390	2	3	3	3
	EM	2.069	3.170	0.97120	0.00976	1.11106	0.02370	4	4	4	2
	PDM	2.324	2.641	0.95004	0.01363	1.34179	0.00408	5	5	5	1
	MLM	2.047	3.215	0.97125	0.00970	1.09377	0.02577	3	2	2	4
	EVM	2.015	3.251	0.97198	0.00969	1.08040	0.02713	1	1	1	5

Table 4.17 Performance analysis of five numerical methods for Kol site

Season	Method	V_{mF}	$V_{max E}$	Statistical evaluation				Ranking			
				R^2	RMSE	MSEP	MAPE	a	b	c	d
				a	b	c	d	a	b	c	d
Winter	MOM	1.101	2.252	0.95961	0.02284	3.33151	0.09609	2	3	2	4
	EM	1.107	2.244	0.95936	0.02287	3.34216	0.09406	3	4	3	2
	PDM	1.440	1.696	0.81811	0.03785	4.88223	0.02384	5	5	5	1
	MLM	1.119	2.240	0.95824	0.02283	3.35040	0.09418	4	2	4	3
	EVM	1.072	2.292	0.96019	0.02271	3.30076	0.10602	1	1	1	5
Summer	MOM	2.543	4.388	0.98323	0.01569	1.60789	0.14039	2	2	2	3
	EM	2.549	4.378	0.98318	0.01574	1.61007	0.13897	3	4	4	2
	PDM	3.004	3.576	0.95141	0.02570	2.17931	0.04005	5	5	5	1
	MLM	2.564	4.382	0.98276	0.01573	1.60995	0.14109	4	3	3	4
	EVM	2.519	4.420	0.98332	0.01556	1.60105	0.14479	1	1	1	5
Rainy	MOM	1.687	3.581	0.97068	0.01235	1.51135	0.06421	1	1	1	5
	EM	1.698	3.567	0.97066	0.01237	1.51492	0.06303	2	2	3	2
	PDM	2.258	2.656	0.93552	0.02233	2.04935	0.00356	4	3	5	1
	MLM	1.715	3.567	0.96983	0.01235	1.51603	0.06388	3	1	4	4
	EVM	1.695	3.571	0.97068	0.01237	1.51388	0.06337	1	2	2	3
Yearly	MOM	1.547	3.749	0.96591	0.00850	1.05901	0.03256	1	1	1	5
	EM	1.561	3.731	0.96588	0.00852	1.06105	0.03183	2	3	2	4
	PDM	2.252	2.646	0.90758	0.01634	1.53816	0.00591	5	5	5	1
	MLM	1.592	3.716	0.96474	0.00851	1.06408	0.03171	4	2	3	3
	EVM	1.607	3.671	0.96552	0.00858	1.06757	0.02945	3	4	4	2

The values of two important specific wind speeds V_{mF} and $V_{max E}$ reveals that the minimum value of both the terms occurs during the winter season while the maximum occurs during the summer season in all selected sites. Performance comparison of the numerical methods for Imphal site is indicated in Table 4.14. It reveals that PDM, MLM and EVM provide four times each 1st ranking in performance followed by MOM with three times 1st ranking. Overall performance shows that MOM and MLM give better performance followed by EVM for Imphal site.

As for Shillong site shown in Table 4.15, MLM, EVM and EM provide six, five and three times 1st ranking respectively and overall performance shows that MLM significantly better other numerical methods followed by EVM and EM.

As far as Guwahati site is concerned, EVM and PDM provide twelve and four times 1st ranking in performance respectively which is clearly shown in Table 4.16. Overall performance of the site reveals that EVM outperforms all other methods followed by MLM.

Similarly, performance analysis of the numerical methods employing wind data of Kolkata site is shown in Table 4.17 which reveals that EVM and MOM provide seven and six numbers of 1st ranking in performance. Overall performance of the site reveals that EVM provided least error in performance followed by MOM.

However, overall performance of the all the selected site shows that EVM outperforms all other method followed by MLM and MOM.

Further, the maximum shape parameter and the minimum RMSE values of different existing methods are provided in Table 4.18 which also shows that newly developed (EVM) method provides least error in performance.

Therefore, the performance analysis shows that the proposed Energy Variance method may be considered as an effective and accurate alternative for estimating Weibull parameters in the wind energy resource assessment.

Table 4.18 Shape parameter and corresponding RMSE values

Methods	Shape parameter (k)	Root Mean Square Error (RMSE)
EVM (Newly developed)	4.42	0.0085
EEM (Shaban et al., 2020)	2.55	0.018
EM (Shaban et al., 2020)	2.04	0.019
MMLM (Shaban et al., 2020)	1.87	0.0204
MLM (Katinas et al., 2017)	2.122	0.0221
EM (Katinas et al., 2017)	2.00	0.0245

4.10 Comparison of PDF and CDF of all the selected methods

Weibull PDFs and CDFs of Imphal site are shown in Figure 4.20 and reveals that PDFs and CDFs of all the methods except the same of PDM method are much closure to the actual data.

Weibull PDFs and CDFs of Shillong site are shown in Figure 4.21 and reveals that PDFs and CDFs of all the methods except the same of PDM and MOM methods are in good agreement with the actual wind speed profile.

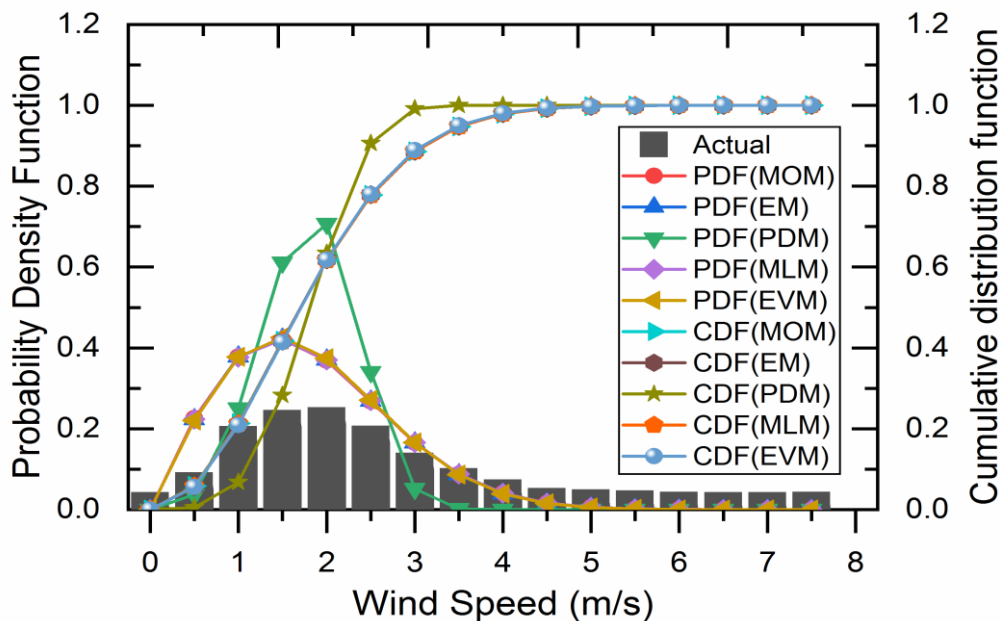


Figure 4.20 Yearly Weibull PDF and CDF of Imp site

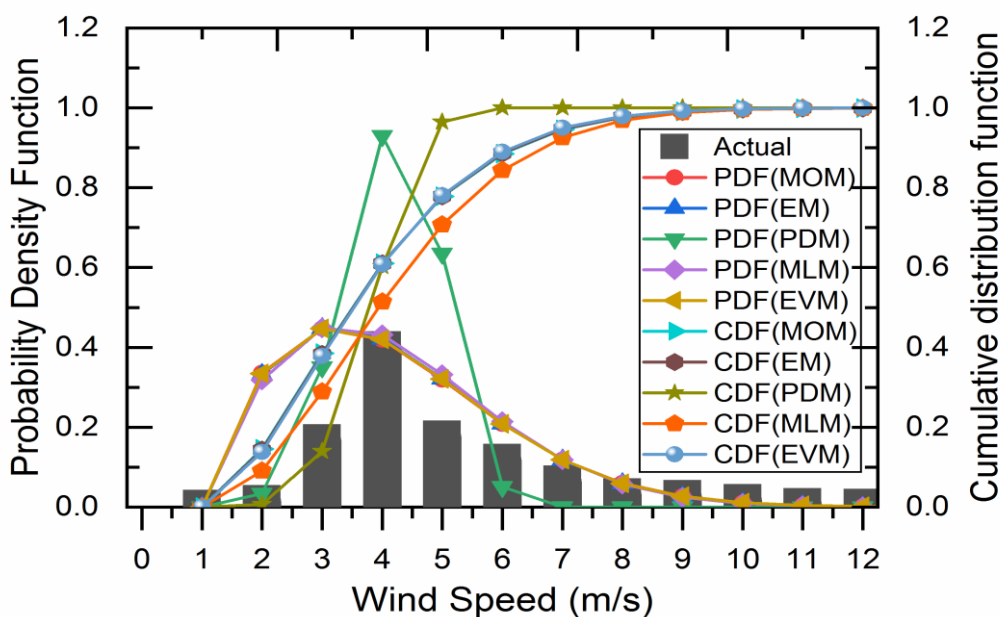


Figure 4.21 Yearly Weibull PDF and CDF of Shg site

Similarly PDFs and CDFs of Guwahati site are presented in Figure 4.22 and reveals that PDFs and CDFs of all the methods excepting PDM method are in good agreement with actual wind profile.

Finally, Weibull PDFs and CDFs of Kolkata site are indicated in Figure 4.23. It reveals that PDFs and CDFs corresponding to all the methods except PDM are more or less quite close to actual distribution of data.

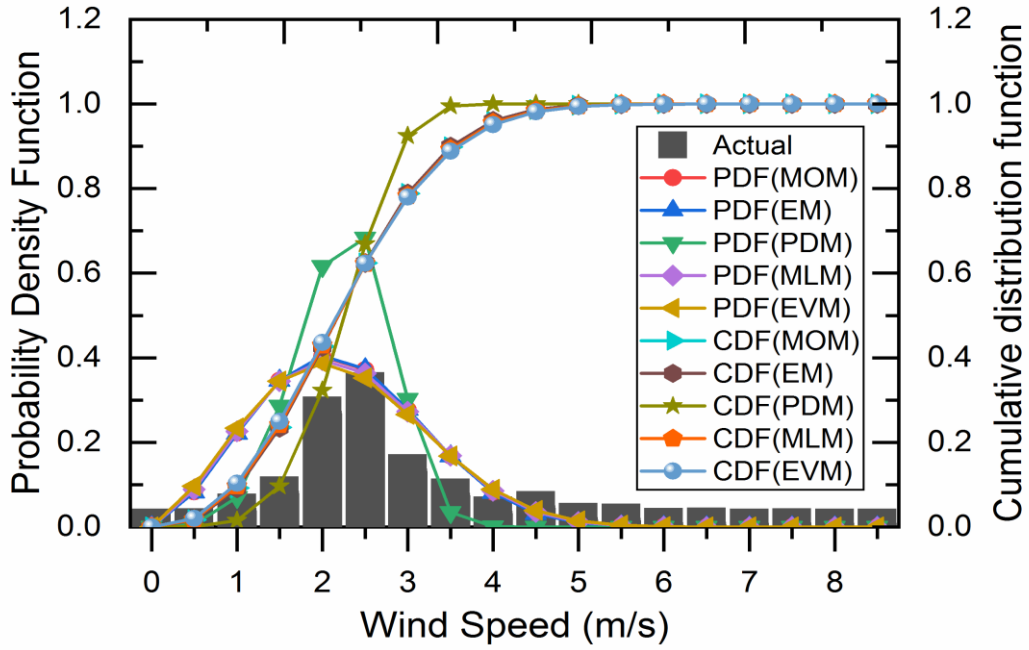


Figure 4.22 Yearly Weibull PDF and CDF of Ghy site

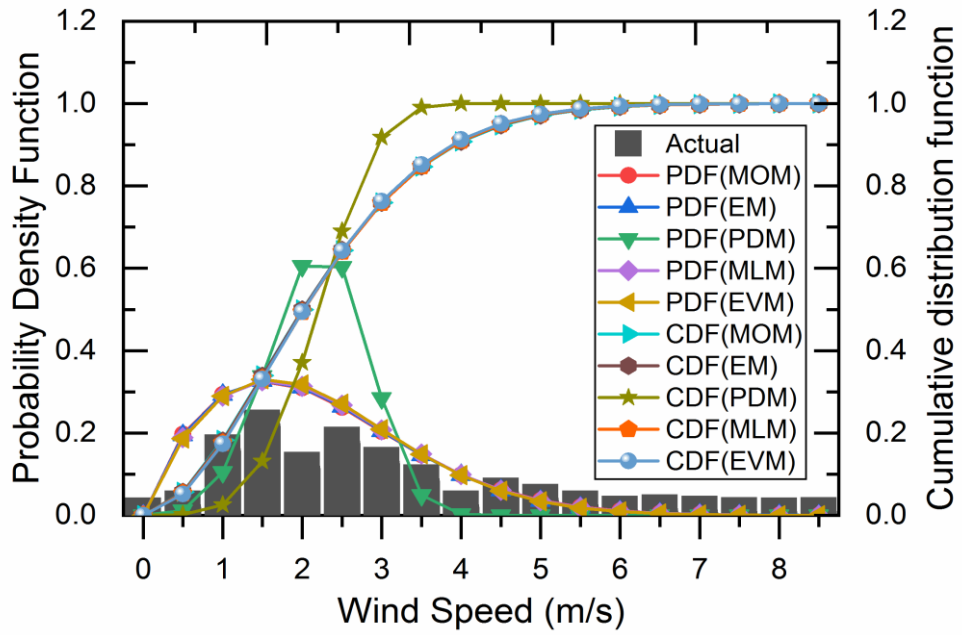


Figure 4.23 Yearly Weibull PDF and CDF of Kol site

LIST OF SYMBOLS AND ABBREVIATIONS

Roman Letters

b	Location parameter
$B - GEV$	Burr-Generalized extreme value
c	Scale parameter
C_p	Power coefficient
E_p	Energy pattern factor
E / A	Energy density per unit area
$f(v)$	Probability density function
$F(v)$	Cumulative distribution function
G	Gamma
$G - W$	Gamma-Weibull
$GEV - W$	Generalized extreme value-Weibull
h	Anemometer height
k	Shape parameter
n	Number of observation
$N - N$	Normal-Normal
$N - W$	Normal-Weibull
R^2	Correlation coefficient
P_v	WPD based on measured wind speed
P_w	WPD based on Weibull PDF
P / A	Power density per unit area
R_e	Reynolds number
V_{\max}	Maximum wind speed

V_{\min}	Minimum wind speed
$V_{\max E}$	Wind speed carrying maximum energy
V_{mF}	Most frequent wind speed
v	Wind speed
\bar{v}	Mean wind speed
\bar{v}_w	Mean wind speed based on Weibull
$W - W$	Weibull-Weibull

Greek Letters

α	Power law exponent
β	Pitch angle
γ	Angle of attack
Γ	Gamma function
λ	Tip speed ratio
μ	Dynamic viscosity
ρ	Density
σ	Standard deviation
σ_w	Standard deviation based on Weibull
θ	Azimuth angle

Abbreviations

Bio	Bio energy
CC	Correlation coefficient
CFD	Computational fluid dynamics

CDF	Cumulative Distribution Function
Chi-SE	Chi square error
COV	Coefficient of variation
DMST	Double multiple stream tube model
EEM	Equivalent energy method
EM	Empirical method of Justus
EML	Empirical method of Lysen
Erl	Erlang distribution
EVM	Energy variance method
Exp	Exponential distribution
FAME	Fatty acid methyl esters
Gam	Gamma distribution
GEV	Generalized extreme value
GHG	Greenhouse gases
Ghy	Guwahati
GM	Graphical method
GW	Giga Watt
HAWT	Horizontal-axis wind turbine
HVO	Hydro treated vegetable oil
IG	Inverse gaussian
Imp	Imphal
Kol	Kolkata
LL	Log-logistic
LN	Log normal
LSM	Least square method
MABE	Mean absolute bias error
MAPE	Mean absolute percentage error

MLM	Maximum likelihood method
MMLM	Modified MLM
MOM	Moment method
MSEP	Mean square error percentage
MW	Mega Watt
NACA	National Advisory Committee for Aeronautics
Nak	Nakagami distribution
Para	Parameter
PDE	Power density error
PDF	Probability density function
PDM	Power density method
PWMBP	Probability weighted moments based on power density method
PWMM	Probability weighted moment's method
RANS	Reynolds Averaged Navier-Stokes simulations
RE	Renewable energy
SB-VAWT	Straight-bladed VAWT
Shg	Shillong
SST	Shear stress transport
TSR	Tip speed ratio
TW	Tetra Watt
URANS	Unsteady RANS
VAWT	Vertical-axis wind turbine
WECT	Wind energy conversion technology
WEP	Wind energy potential
WEPA	Wind energy potential assessment
WPD	Wind power density

In the preceding part, a new methodology for assessment of wind energy potential is presented and compared with existing methods. Wind energy assessment at different locations in North-eastern and eastern regions of India is presented. In this section numerical studies of vertical axis wind turbine (VAWT) shall be presented.

5.1 Introduction

Once the selection of site and assessment of wind energy potential is completed the next or the last phase of WECT is to design or select appropriate wind turbine. Outcome of the assessment of wind energy potential in the eastern and north-eastern regions of India reveals that low wind speed range is available in these regions and in such region deployment of VAWT is feasible. Moreover, in spite of having low efficiency quality the VAWT especially H-Rotor Darrieus gain the interest of present researchers as the large scale turbine has been forced away from high energy demand population areas and moved towards remote areas or offshore sites where plenty of spaces are available. Many researchers have already started extensive research in the field of VAWT using analytical, experimental and numerical methods to improve its performance.

In this regard Computational Fluid Dynamics (CFD) is considered to be one of the promising, cost effective and accurate methods for analyzing and understanding the complex flow physics, unsteady inducing nature of aerodynamics for vertical axis wind turbine (VAWT) and has ability to generate results as good as experimental results (Jin, 2015). Consequently CFD study of VAWT can suggest the possibility of improvement in the performance of VAWT and thereby its overall efficiency. Therefore, in this section detail operation of H-type VAWT will be discussed and then procedural steps of CFD simulation, computational model and mathematical model of the present study will be discussed. Finally, the model is used to assess the performance of VAWT having rotor with new airfoils and then to provide more insightful understanding of flow physics.

5.2 Aerodynamics of H-type Darrieus VAWT and influencing parameters

Concept of vertical axis wind turbine (VAWT) was proposed by Darrieus in 1931 and development in this area is still of interest and in progress. Figure 5.1 shows a three bladed H-type Darrieus VAWT whose blades are similar identical in shape with height of H and chord length of c . The turbine rotates when encounter with free stream wind speed, v and corresponding rotational speed of the turbine would be ω . Turbine rotates in one direction covering an area of radius R and therefore, projected area of the turbine will be $2HR$ or HD (Diameter, $D = 2R$).

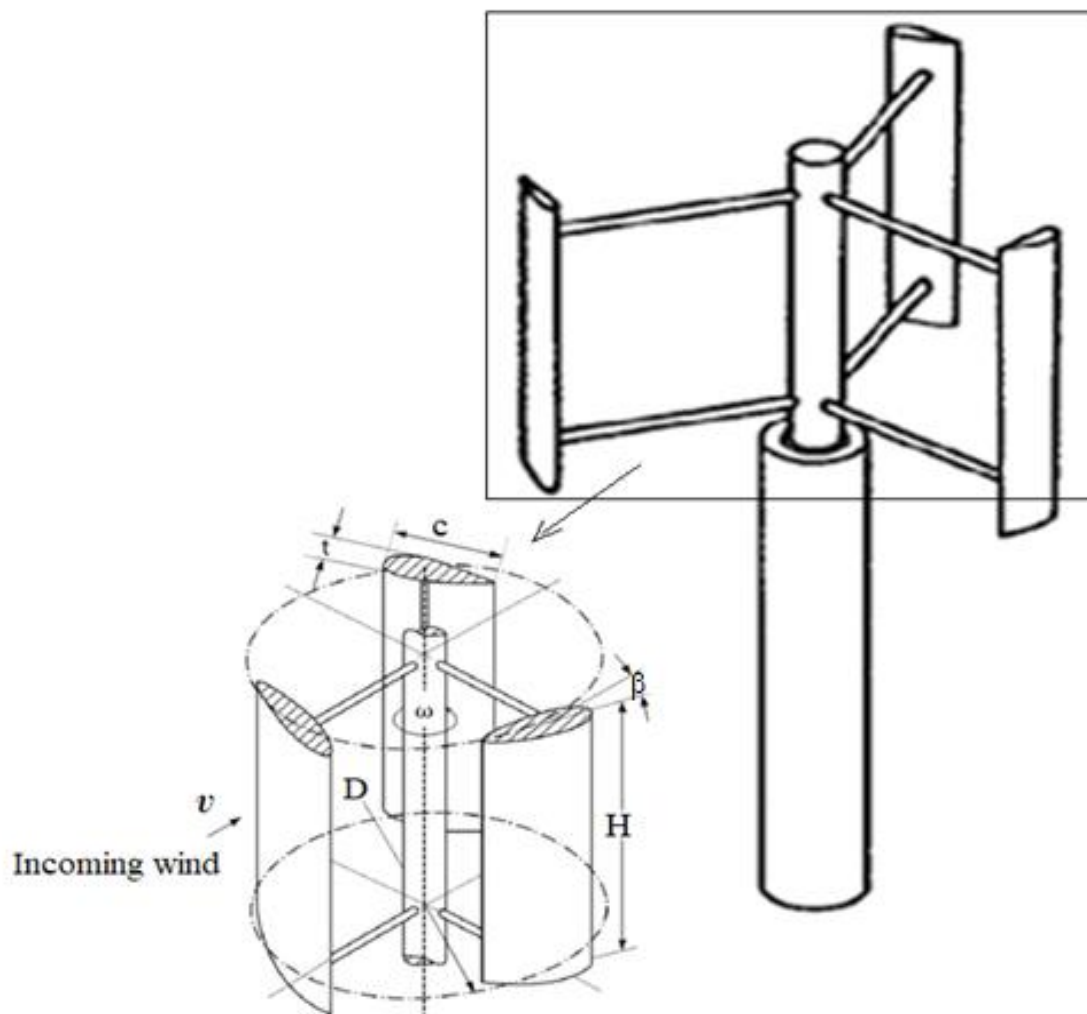


Figure 5.1 Three bladed H-type Darrieus VAWT

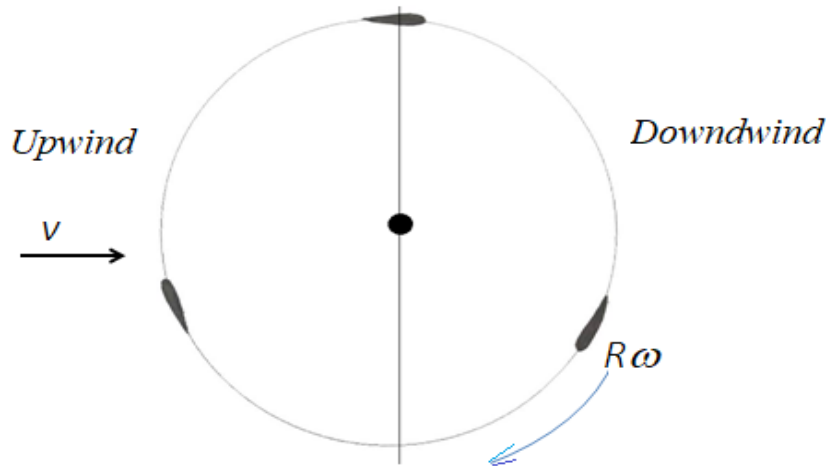


Figure 5.2 Horizontal section of three bladed H-type Darrieus VAWT

Figure 5.1 and 5.2 show the working of a three bladed H- rotor turbine in which blades are rotated with an angular speed ω around an axis with a radius R . As the lift force zeroing at the right side ($\theta=0^\circ$) and left side ($\theta=180^\circ$) where one of the airfoils moves parallel to the incoming wind direction, torque changes from positive to negative chord length of c . If the same blade moves by 180° towards left side lift increases and lift component become much higher than drag component when the blade reaches near front ($\theta=90^\circ$). Consequently the total torque per cycle will be positive.

Parameters of interest which shall be evaluated from CFD analysis are introduced now.

Tip speed ratio (TSR)

The free stream wind speed and rotational speed of the turbine can generate an important influencing non dimensional parameter known as tip speed ratio (TSR) which is given in equation (5.1).

$$TSR(\lambda) = \frac{R\omega}{v} \quad (5.1)$$

The TSR dictates the operating condition of a turbine and it influences a number of flow parameters and thereby the performance of turbine. For the present study, the range of TSR will be considered from 1 to 4.

Solidity

The solidity (σ) of a wind turbine is another important non dimensional parameter which is defined as suggested by Strickland (1975) in the following equation (5.2).

$$\sigma = \frac{Nc}{R} \tag{5.2}$$

Where N is the number of blades incorporated in the turbine. The solidity measures how much of the swept area is occupied by the turbine blades. Value of the solidity along with other geometrical characteristics of the present model used in this study is listed in Table 5.1.

Lift Coefficient and Drag coefficient

From Figure 5.3 it is realized the motion of an airfoil into the wind creates a force (F_n) having two components: lift force or simply lift (F_l) in the normal direction and drag force or drag (F_d) in the tangential direction which are expressed as follows:

$$F_l = \frac{1}{2} C_l \rho v^2 c \tag{5.3}$$

$$F_d = \frac{1}{2} C_d \rho v^2 c \tag{5.4}$$

Where C_l and C_d are Lift and drag coefficients which define the characteristics of an airfoil.

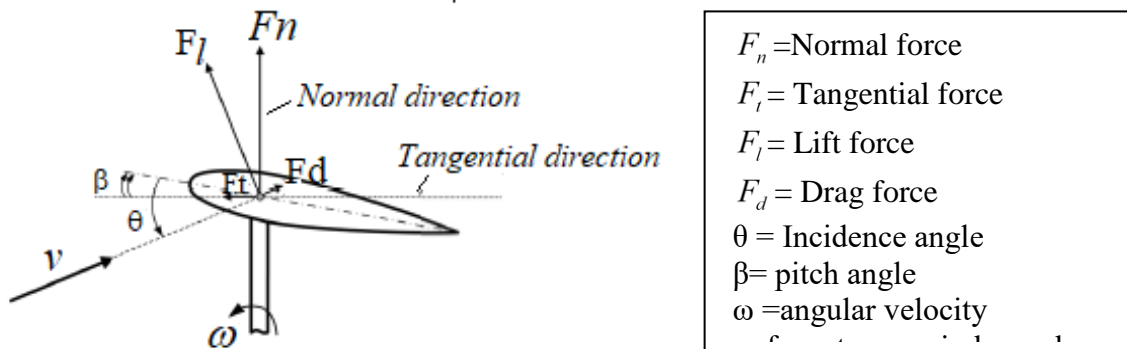


Figure 5.3 Airfoil aerodynamic

Power coefficient and Torque coefficient

The kinetic energy of air per unit kg of m (mass) flowing at wind speed of v can be expressed as

$$KE = \frac{1}{2}v^2 \quad (5.5)$$

If air passes through an area of A m² at the velocity v , then the volume (Q) of air passing through it can be expressed as follows:

$$Q = Av \quad (5.6)$$

Then mass flow rate of air (\hat{m}) with the air density, ρ kg/m³ is given as:

$$\hat{m} = \rho Q = \rho Av \quad (5.7)$$

Equation (5.5) and (5.7) finally provides the power available in the wind (P_o) due to kinetic energy of wind as follows:

$$P_o = \frac{1}{2}\rho Av^3 \quad (5.8)$$

However, if we extract entire power available in the wind, the flow would be arrested; it means certain part of the kinetic energy cannot be captured. To measure the usable power fraction an important non-dimensional term was developed which is known as power coefficient (C_p). Therefore power coefficient is one of the most important parameter for evaluating the performance of turbine and it is the ratio of actual power generated by turbine to the power available in the wind which is given as follows:

$$C_p = \frac{P}{P_o} = \frac{P}{\frac{1}{2}\rho Av^3} \quad (5.9)$$

According to Betz, C_p can never exceed the value of $16/27 \approx 0.59$ which is known as Betz limit. Similarly if T is the actual torque generated by the turbine then the torque coefficient (Moment coefficient) can be expressed as follows:

$$C_m = \frac{T}{\frac{1}{2}\rho Av^2 R} \quad (5.10)$$

Now power and torque can be related as follows:

$$P = T\omega \quad (5.11)$$

From equations (5.7) and (5.9) the following relation can be finally obtained as follows:

$$C_p = C_m \left(\frac{\omega R}{v} \right) = C_m \times TSR \quad (5.12)$$

5.3 Computational Model

Summary of the literature survey as presented in section 2.2 reveals that either NACA0015 or NACA0018 or NACA0021 as the effective NACA profiles for VAWT application among the NACA four digit series. However, most of studies claimed that NACA0015 as the most effective profile among NACA four digit series and even better than many NACA five digit series. In such situation, the performance analysis of H-type Darrieus VAWT with alternative airfoils like NACA0016 and NACA0019 which are simple in structure and neither too thick nor too thin will create an opportunity to find better airfoils. To our knowledge the performance assessment of Darrieus turbine with NACA0016 and NACA0019 airfoils has not yet reported. Therefore, aim of this part of the work is to numerically analyze the performance of a H-type Darrieus VAWT with NACA0016 and NACA0019 airfoils through the CFD model, the simulation was carried out using commercial CFD software ANSYS Fluent (version 16.2). In this work, we consider straight bladed configuration with adequately long shape of H-type Darrieus VAWT. Section 2.2 of Literature survey also reveals that 3-D effects are neglected in such environment as the results from 2-D CFD reasonable agree with experimental data (Hashem and Mohamed, 2018; Bianchini et al., 2017). A major advantage in such situations is the number of elements is significantly less as compared to the 3-D counterpart, which ultimately leads to significant reduction in computational time and thereby the overall computational cost. Therefore, in the present work we went ahead with 2-dimensional CFD simulation. The detail geometrical characteristics of the present model are provided in the Table 5.1. Further two similar models

studied by Balduzzi et al. (2016b) and Castelli et al. (2011) were selected to validate analysis of the present model and its details geometrical characteristics are provided in Table 5.2.

Table 5.1 Geometrical characteristics of the present model

Characteristics	Value
Type of airfoils	NACA0015, NACA0016, NACA0019
No of blades	3
Diameter of rotor (D)	0.7 m
Chord of the blade (c)	0.1 m
Swept area, A	0.7 m ²
Solidity, σ	0.425

Table 5.2 Geometrical characteristics of the two similar models

Characteristics	Balduzzi et al. (2016b)	Castelli et al. (2011)
Type of airfoils	NACA0018	NACA0021
No of blades	3	3
Diameter of rotor (D)	1.7 m	1.03 m
Chord of the blade (c)	0.246 m	0.0858 m
Aspect ratio of blades	12	1.46
Solidity, σ	0.44	0.5

5.3.1 Computational procedure

Improper selection of computational domain size may result in the overestimation of the performance during the CFD analysis. An earlier study of effect of domain size revealed that when the inlet distance from the centre of rotor and outlet distance from the centre rotor of the turbine are less than 7.5D and 10D respectively, there was significant amount of overestimation in the performance (Rezaeiha et al., 2017). As far as width of the domain is concerned when the blockage ratio (D/W) is 5% and 10%, the power coefficient is over predicted by about 0.2% and 3.8% respectively. Further, in most of the earlier studies aspect ratio of the stationary region (outgoing boundary distance from the rotor centre/ incoming boundary distance from the rotor centre) is kept as 2 (Balduzzi et al., 2016a). Therefore, as shown in Figure 5.4, the computational domain of the present work, the incoming boundary, the outgoing boundary and the horizontal boundaries are located at a distance of 7.5D, 15D and 7.5D from the rotor center, where D is the rotor diameter. Thus the domain of the CFD analysis has a size of 22.5D x 7.5D. The geometry is divided in two regions, namely rotating

region for rotor bounded within the circular interface and a rectangular stationary region beyond the interface in order to use the unsteady sliding mesh model. The two regions are connected with each other across the sliding interface so as to allow the continuity of the absolute incoming velocity and then to provide the correct neighbor velocities values for the rotating region.

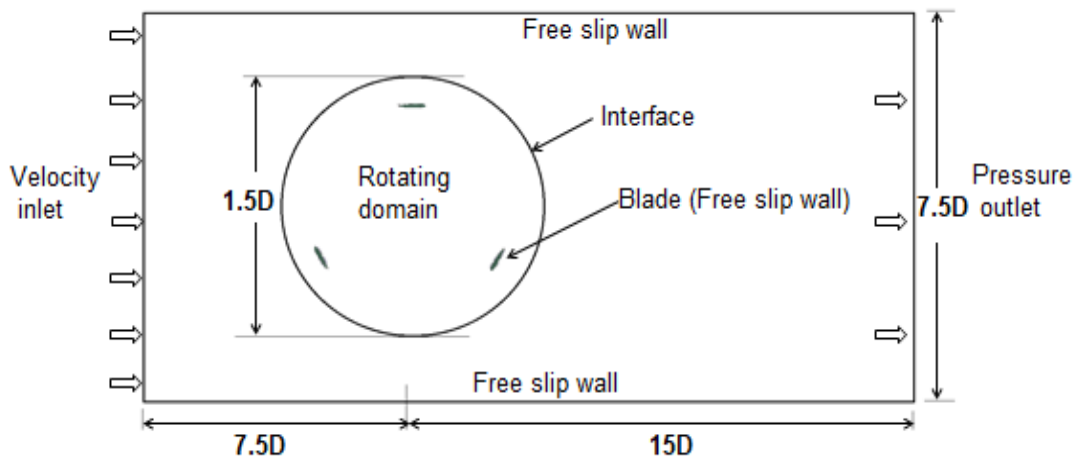


Figure 5.4 Computational model with boundary conditions used in the study

5.3.2 Mesh generation

After the geometrical modeling of domain is completed the next step is to discretize the complete computational domain which is known as mesh generation. High quality mesh can be used to capture flow physics accurately. However, due to complex geometry the flow may be difficult to predict with the onset of turbulence and separation. For the present analysis the Quad dominant mesh type was selected for the entire computational domain and the mesh was generated using Ansys meshing tool. But near the airfoils walls mesh was refined with purely quadrilateral mesh whose maximum skewness was always less than 0.86 in order to reduce the computational time consumption and increasing accuracy of the simulation result. In order to capture the aerodynamic phenomena occurring in the boundary layer which is critical for understanding the VAWT aerodynamics the mesh size was carefully controlled near all wall boundaries. The criterion used was to refine the mesh for a thickness equivalent to $y^+=1.3$. The mesh on both sides of the interface has matching grid sizes to provide faster convergence. The growth rate parameter for meshing has been fixed at 1.2 so as to change the mesh density gradually from airfoils wall to stationary domain. Figure 5.5 represents mesh structure of the present study.

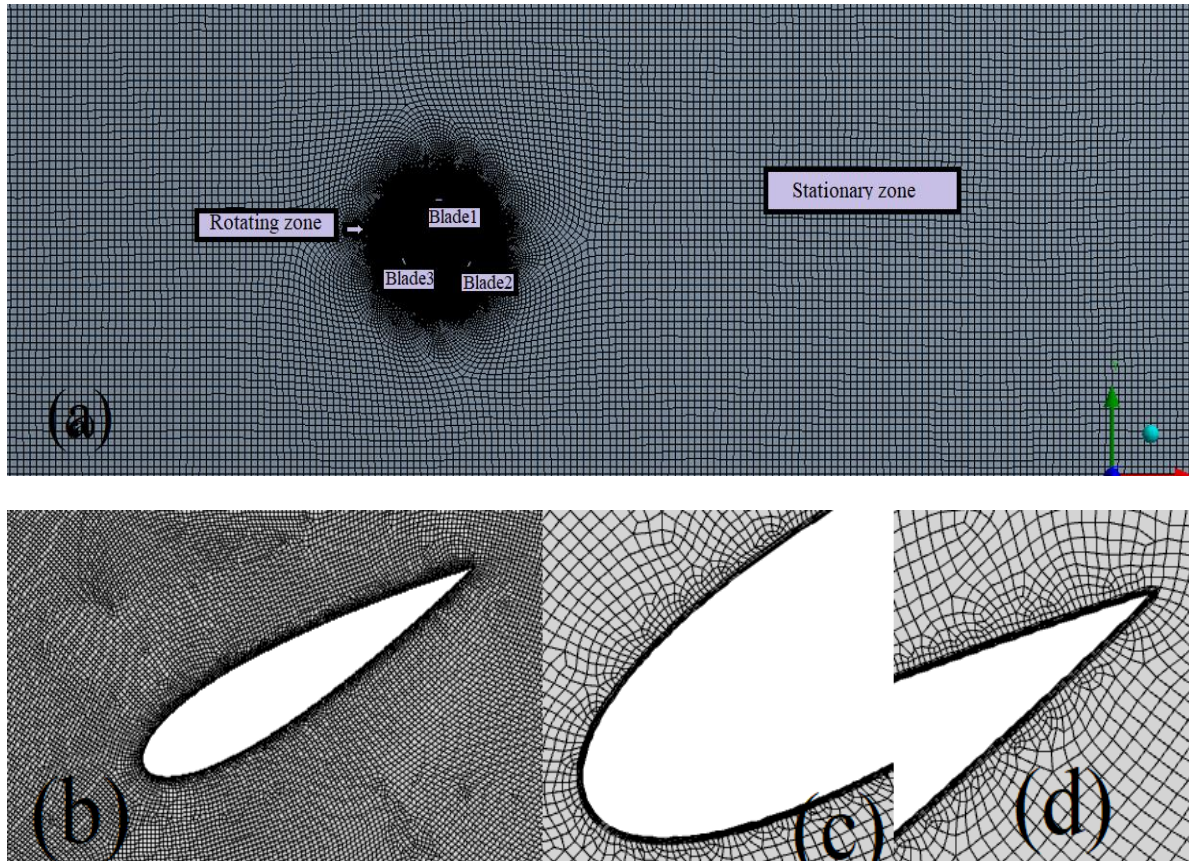


Figure 5.5 Details of mesh structure of the present study: (a) Whole computational domain (b) mesh around one blade (c) leading edge mesh view (d) trailing edge mesh view

5.3.3 Governing equations, turbulence closure and boundary conditions

From the literature review it has come to know that CFD based numerical study of VAWT have been widely used in the earlier studies due to several advantages such as faster in process, low cost, capable of full size analysis whether time dependent or independent. Since the flow field is predominantly turbulent, it is necessary to go for Unsteady Reynolds-averaged Navier-Stokes (URANS) equations to predict the velocity and pressure at each element of the computational domain. The continuity equation for unsteady, incompressible flow can be calculated as:

$$\frac{\partial \bar{u}_i}{\partial t} + \frac{\partial \bar{u}_i}{\partial x_i} = 0 \quad (5.13)$$

and the momentum equations can be written as:

$$\frac{\rho \partial \bar{u}_i}{\partial t} + \rho \bar{u}_i \frac{\partial \bar{u}_j}{\partial x_i} = \frac{\partial}{\partial x_i} \left[-\bar{p} \delta_{ij} + \mu \left(\frac{\partial \bar{u}_i}{\partial x_j} + \frac{\partial \bar{u}_j}{\partial x_i} \right) - \tau_{ij} \right] \quad (5.14)$$

Where, i and j are the subscripts of velocity, \bar{u}_i and \bar{u}_j are the mean and fluctuating parts of the velocity component, \bar{p} is the mean pressure, ρ is the density, μ is the fluid dynamic viscosity, δ_{ij} is the Kronecker function and the term $(\tau'_{ij} = -\rho \overline{u'_i u'_j})$ is referred as Reynolds shear stress tensor which unclosed the problem. The Boussinesq assumption can be used to calculate τ'_{ij} and is given as (Mohamed et al., 2015):

$$\tau'_{ij} = \mu_t \left(\frac{\partial \bar{u}_i}{\partial x_j} + \frac{\partial \bar{u}_j}{\partial x_i} \right) - \frac{2}{3} \rho k \delta_{ij} \quad (5.15)$$

Where, μ_t is the turbulent viscosity and k is turbulent kinetic energy which will be obtained by using turbulence model.

For closure of turbulent field, selection of proper turbulence model is a big challenge in the field of CFD study as it affects the computational resources, time, result accuracy and ultimately overall cost. In RANS type formulations mean flow field is resolved but the effect of fluctuating scales is calculated through turbulent closures which provide a turbulent viscosity.

In the literature survey section 2.2 it has been come across that there are several turbulence models such as one equation model(SAS), k-epsilon, RNG k-epsilon, SST k- ω , Transition SST (TSST), etc. Finding of effective and appropriate turbulence models is crucial task. Several earlier studies analysed the effectiveness and suitability of various turbulence models deals with CFD simulation of VAWT. For example, Balduzzi et al. (2016a) stated that for wind turbine applications, one –equation models of turbulent closure are generally not considered due to its inaccurate prediction in largely separated flows and free shear flows. They also concluded that out of three turbulence models from two-equation family, namely Standard k- ϵ , RNG k- ϵ and SST k- ω , the last one provided better performance and results were quite agreement with the experimental data. Daroczy et al. (2015) presented the comparative analysis of nine turbulence models for CFD simulation of H-rotor wind turbine using four different validation techniques and revealed that k- ϵ model provide the best result followed by SST k- ω model. It was further stated that SST k- ω model can provide better characteristic curve for the low TSR domain where dynamic stall is present. Lanzafame et al. (2014) studied performance comparison of SST k- ω and TSST models for the 2D CFD simulation of H-Darrieus turbine and the later one provided the closer results to the experimental data. Rezaeiha et al. (2019) performed comparative analysis of 7 turbulence

models (Inviscid, SAS, RNG k- ϵ , Realizable k- ϵ , SST k- ω , SST k- ω with intermittency, k-kl- ω transition, TSST) for CFD simulations using VAWT with three different airfoils and revealed that SST models predictions were well matched with three different experimental data considered during the analysis. For the study aerodynamics performance of straight bladed rotor Rogowski et al. (2018) compared the accuracy of four turbulence models: standard k- ϵ ; RNG k- ϵ ; Realizable k- ϵ ; and SST k- ω . Results indicated that SST k- ω turbulence model better predicts drag coefficients at angles of attack up to the critical angle of attack and both SST k- ω and the k- ϵ family models produce adequate lift coefficients. Saghairichi et al. (2018) compared the performance of three numerical models namely RNG k- ϵ , SST k- ω and TSST with experimental results. Result of the SST k- ω well matched with the experimental results. Moreover, in many earlier studies (Daroczy et al., 2015; Chowdhury et al., 2016; Arab et al., 2017), either SST k- ω or TSST was selected as a method of choice for CFD simulation of VAWT due to its high reliability of the results and its flexibility in the wall boundary treatment compared to other RANS models and therefore, comparative study of both Transition SST and SST k- ω shall be performed and then the best method among them shall be selected for the present CFD analysis of Darrieus VAWT.

Table 5.3 shows the comparison of power coefficient between two models and it reveals that there is significant difference of power coefficient value up to 5th NOR which may be due to instability of the simulation result, but 6th NOR onwards both the models agree well with each other. As a result, any one of these two models may be used for tackling the present problem. We have finally used SST k- ω for all cases and for few cases additional runs were performed using transition SST with the aim of comparing the performance of these two models.

Table 5.3 Comparison of turbulence models at TSR=2.5

<i>Model</i> \ <i>NOR</i>	<i>3rd</i>	<i>4th</i>	<i>5th</i>	<i>6th</i>	<i>7th</i>	<i>8th</i>
<i>SST transition</i>	0.49592	0.47263	0.43795	0.42199	0.41236	0.40674
<i>SST k-ω</i>	0.48635	0.46517	0.43927	0.42121	0.41117	0.40446

The transport equations for turbulent kinetic energy (k) and turbulent specific dissipation (ω) in the SST k- ω are expressed in Equations (5.16 and 5.17) (Abraham et al., 2009).

$$\frac{\partial(\rho k)}{\partial t} + \frac{\partial(\rho k u_i)}{\partial x_i} = \frac{\partial}{\partial x_i} \left[\left(\mu + \frac{\mu_t}{\sigma_k} \right) \frac{\partial k}{\partial x_i} \right] + \gamma G_k - \beta_1 \rho k \omega \quad (5.16)$$

$$\frac{\partial(\rho\omega)}{\partial t} + \frac{\partial(\rho\omega u_i)}{\partial x_i} = A\rho S^2 - \beta_2\rho\omega + \frac{\partial}{\partial x_i} \left[\left(\mu + \frac{\mu_t}{\sigma_\omega} \right) \frac{\partial\omega}{\partial x_i} \right] + 2(1-F_1)\rho \frac{\rho}{\omega\sigma_{\omega_2}} \frac{\partial k}{\partial x_i} \frac{\partial\omega}{\partial x_i} \quad (5.17)$$

Where G_k is the generation of turbulent kinetic energy k , and the terms σ_k , σ_ω and σ_{ω_2} are Prandtl number like parameters for the transport k and ω . F_1 is a blending function that simplifies the combination of the standard $k-\epsilon$ model and the Wilcox $k-\omega$ model (Wilcox, 1993; Suzen and Haung, 2000). S represents the absolute value of the shear strain rate and β_1 , β_2 are the model constants. The term γ is used in Equation (5.16) to reduce the rate of turbulence production in flows that are not fully turbulent and it ranges from 0 to 1.

Similarly, the four equations transition SST turbulence model is expressed based on the SST $k-\omega$ equations coupled with two additional transport equations: the transport equations for intermittency (γ) and intermittency adjunct function (Π) which are given in equations (5.18 and 5.19) (Abraham et al., 2009).

$$\frac{\partial(\rho\gamma)}{\partial t} + \frac{\partial(\rho\gamma u_i)}{\partial x_i} = \frac{\partial}{\partial x_i} \left[\left(\mu + \frac{\mu_t}{\sigma_\gamma} \right) \frac{\partial\gamma}{\partial x_i} \right] + G_{k,1} - E_{\gamma,1} + G_{\gamma,2} - E_{\gamma,2} \quad (5.18)$$

$$\frac{\partial(\rho\Pi)}{\partial t} + \frac{\partial(\rho\Pi u_i)}{\partial x_i} = G_{\Pi,t} + \frac{\partial}{\partial x_i} \left[\sigma_{\Pi,t} (\mu + \mu_t) \frac{\partial\Pi}{\partial x_i} \right] + 2(1-F_1)\rho \frac{\rho}{\omega\sigma_{\omega_2}} \frac{\partial k}{\partial x_i} \frac{\partial\omega}{\partial x_i} \quad (5.19)$$

Here, G denotes production of the respective dependent variables, and the E terms refer to destruction processes. The solution of Equations (5.16) and (5.17) produces the values of k and ω while Equations (5.18) and (5.19) yields the values of γ and Π which are then used to evaluate the turbulent viscosity (μ_t) from Equation (5.8) as follows:

$$\mu_t = \frac{a\rho k}{\max(a\omega, SF_2)} \quad (5.20)$$

In which F_2 is a function that limits the values of the turbulent viscosity in the near wall region and a is a constant.

The free stream velocity at the inlet boundary condition are 3, 4, 5 m/s and corresponding Reynolds numbers are 21,116, 28,155 and 35,184 respectively. At the outlet, as the domain is flushed with ambient, a zero gauge pressure is used. On the other surfaces, free slip condition is considered. Details of the boundary conditions are presented in Table 5.4.

Table 5.4 Boundary conditions used in the present study

Zone	Type
Inlet	Velocity inlet
Outlet	Pressure outlet
Wall of rotating domain	Interface
Airfoils	Free slip wall
Upper wall and lower wall	Symmetry (Zero velocity and pressure)

5.3.4 Validation of the model

In order to validate the present CFD simulation result, experimental data of Balduzzi et al. (2016b) and Castelli et al. (2011) were chosen, which have almost similar rotor characteristics. Comparison of the present simulation and experimental data and numerical results of above two models is presented in Figure 5.6. Power coefficient increases rapidly as the TSR increases till it reaches peak value than decreases slowly. Pattern of the curve of the present result is more closure to data of former model probably due to more similarity in solidity value. The comparison between the simulation and experimental results is qualitative rather than the quantitative as the computational simulation does not count the effects of blade tip, airfoil shape, connector and rotating shaft. Validation shows that present numerical result is slightly higher than the numerical result of Balduzzi et al. (2016b) but, both of them are in a good agreement with experimental results. It is quite acceptable for wide range of operating TSR and closer to experimental data as compared to CFD result of Castelli et al. (2011). The highest deviation in power coefficient was around 35% at TSR=2.5. The present work shows the peak power coefficient value at TSR=2.5 while Balduzzi and Castelli show at TSR = 2.35 and 2.65 respectively.

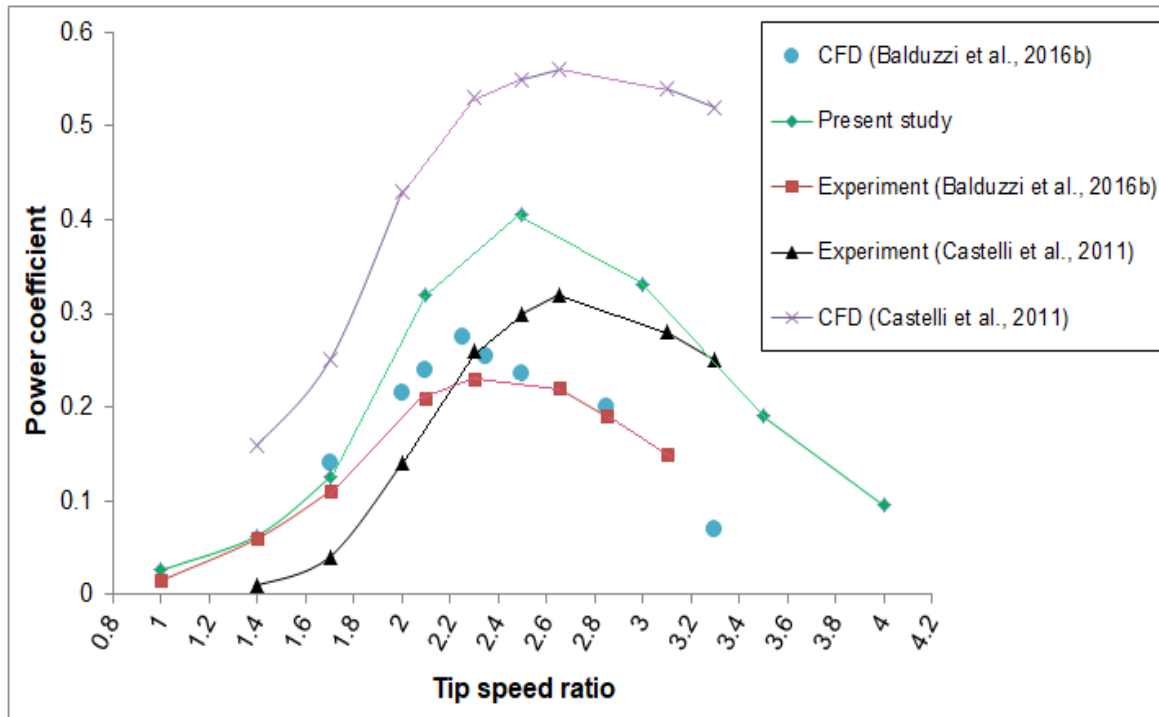


Figure 5.6 Validation of C_p of Darrieus turbine with the experimental and numerical results by Balduzzi et al. (2016b) and Castelli et al. (2011) as function of tip speed ratio (λ) at velocity 5 m/s, $Re = 10^5$

5.4 Numerical Implementation

In this section, results shall be presented which is preceded by mesh independence study and other implementation details.

5.4.1 Mesh independency

A number of simulations were carried out using eight different levels of mesh with element sizes of 331807, 397130, 412099, 537378, 606857, 789071, 811957 and 908244 employing SST $k-\omega$ turbulence model at TSR of 1.4 with a constant inlet velocity of 5 m/s in order to get an appropriate mesh that can provide optimal result during the simulation. Practically, the coarsest mesh itself contains a large number of elements as the complexity of the flow field is too demanding. Figure 5.7 shows the comparison of power coefficient obtained for eight different mesh element sizes and observed that the calculated power coefficient reached a plateau of stable value from sixth mesh size onwards. Results for a grid independent value from extrapolation of last three levels agree with the value from seventh mesh size within

2%. Therefore, the seventh mesh size which has mesh element of 8,11,957 was considered for the present analysis.

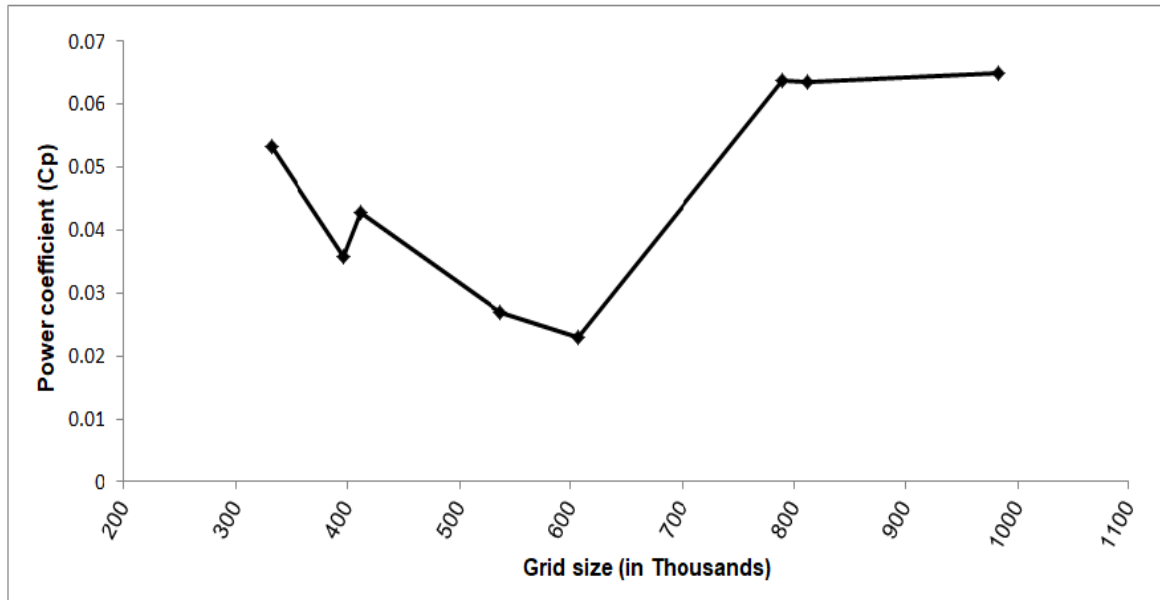


Figure 5.7 Mesh independency study

5.4.2 Time step independence

Transient analysis for wind turbine involves two important variables and they are time step size (TSS) and number of time steps (NOTS). Qin et al. (2011) pointed out that time step size for each simulation need to be selected properly to achieve good convergence in the final result. In many earlier studies the time step size (TSS) was decided based on the CFL condition (Bianchini et al., 2017; Biswas and Gupta, 2014; Carrigan et al., 2012; Franchina et al., 2019) which may not be the optimum time step size. From numeric point, it is obvious that the smaller the TSS, the greater the accuracy of the simulation results. However, the smaller TSS results in higher the computational cost. Therefore, the researchers usually performed the TSS sensitivity test to obtain the optimal value of TSS (Balduzzi et al., 2016b; Elkhoury et al., 2015; Kragic et al., 2018; Lanzafame et al., 2014; Siddiqui et al., 2015; Hashem and Mohamed, 2018; Qin et al., 2011). To obtain the optimal value of TSS for the present study we have selected six TSS and they are 0.082, 0.0123, 0.164, 0.205, 0.245 and 0.41 degree, out of which first three fulfilled the CFL condition and remaining three, are greater than the CFL threshold level. Figure 5.8 shows the influence of TSS on the result of

simulation at TSR=2.5 and it revealed that all the TSS value within the threshold level provide almost same result while the TSS value greater than threshold level (CFL=1) provide the deviated results. The TSS of 0.164 degree shall be the optimum TSS, as the power coefficient up to this value is stable and therefore, the corresponding TSS value shall be used in the present CFD simulation.

At the initial stage of simulation, the periodic flow field took some time to be established and an example of such behaviour is shown in Figure 5.9. It shows that several revolutions had to be simulated before converged periodical solution. Therefore, in respect of NOTS the decision is taken based on the stability condition of the performance curve such as torque or power coefficient with respect to flow time or azimuth angle. NOTS may be expressed in terms of number of revolution (NOR) of the rotor. More the number of NOTS or number of revolution (NOR) the more the result will stable and computational time as well. In order to compromise the stability of the result and computational time we need to obtain an optimum NOTS or NOR. As an example, the Figure 5.10 shows the influence of NOTS in terms of NOR vs power coefficient at TSR =2.5. It shows that from the 6th revolution onwards the result is quite stable. Therefore, the NOTS corresponding to 6th revolution is the optimum size which provides a stable solution with relatively less computational time. For this reason, all of the data presented herein is considered from the 6th or more revolution of the rotor.

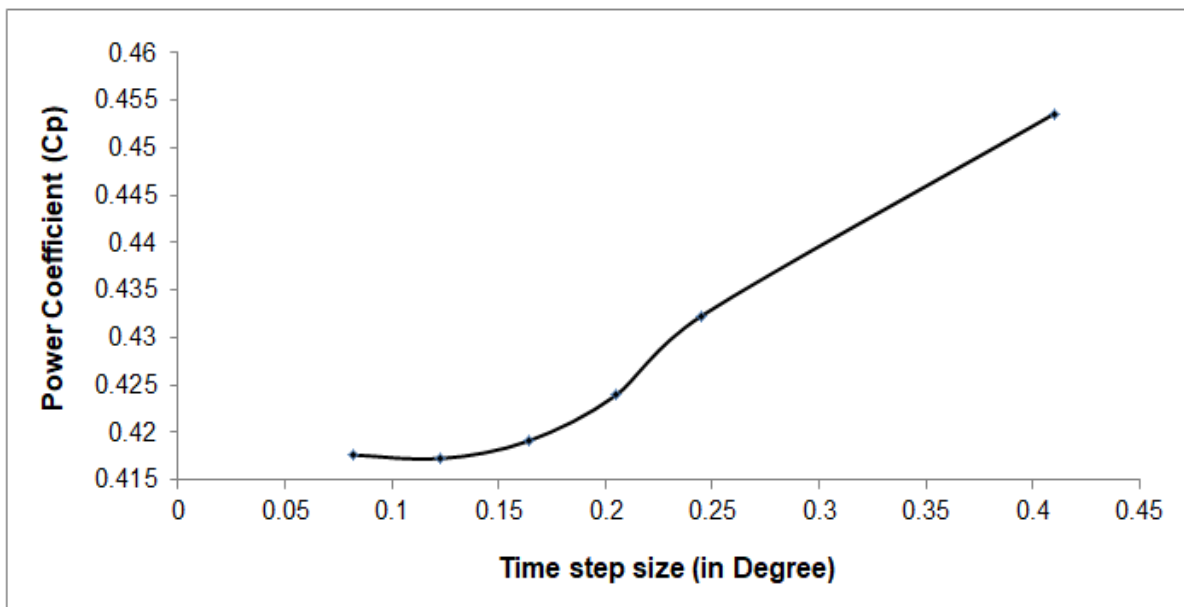


Figure 5.8 Influence of Time step size (TSS) at TSR=2.5

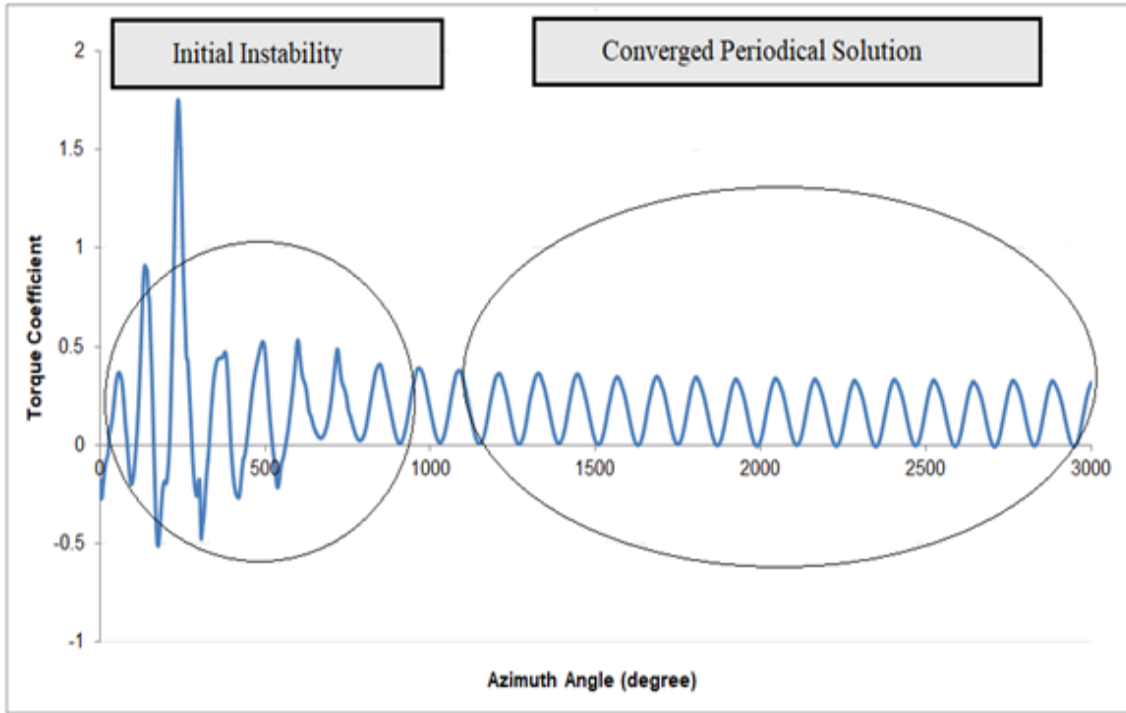


Figure 5.9 Periodical torque coefficient over 8 Cycles at TSR=2.5

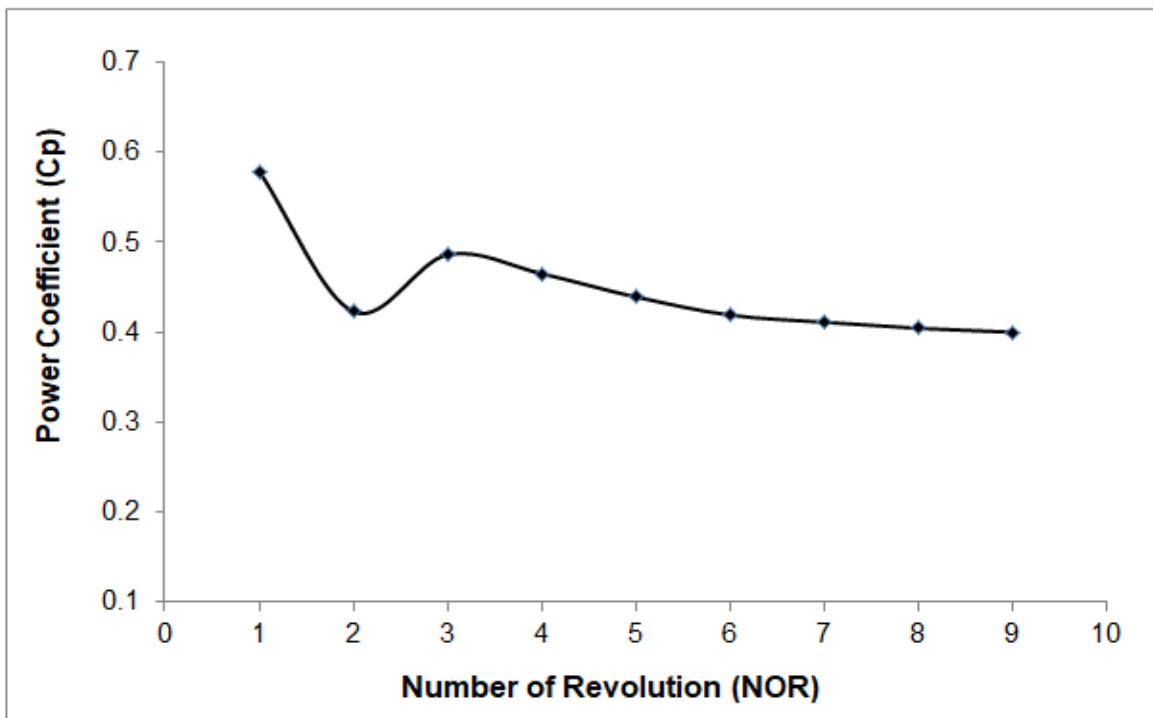


Figure 5.10 Effects of NOTS on power coefficient at TSR=2.5

5.4.3 Solver setting

For the numerical analysis of complex flow field in fluid machineries like wind turbines, the solver setting is very crucial to achieve meaningful result. To study dynamic stall and interactions between the motions of blades and wake, it is necessary to resolve the flow transients. For the simulation the solver was set as pressure based with Semi-Implicit Method for Pressure-Linkage Equations (SIMPLE) algorithm for pressure–velocity coupling (Patankar, 1980). Second order discretization schemes were employed for the governing flow equations. Of gradients spatial discretization Green-Gauss node based method was chosen. The second order upwind scheme and second order implicit scheme were applied for all spatial discretization and for transient formulation respectively. The sliding mesh model was selected to compute the relative motion between rotating zone and static zone with constant rotational speed for TSR. The convergence criterion was set at 10^{-5} at each time steps. Under-relaxation parameters for continuity, momentum and Reynolds closure equations were within 0.8.

5.5 Results and Discussion

Numerical results shall be discussed elaborately in this section. The change of drag and lift coefficient along with time is the very first characteristics. Then instantaneous torque coefficient with respect to azimuthal angle, the overall power coefficient are discussed. The pressure contours, vorticity and turbulent intensity at different azimuthal angles are also discussed. Further, the effect of inlet wind speed on the overall power coefficient is also included in the present analysis.

5.5.1 Numerical results

The computational model having three NACA0015, NACA0016 and NACA0019 blades has been simulated for TSR range from 1.0 to 4.0. The simulation results show that optimum power coefficient is found at TSR=2.5 as evident from Figure 5.5. Therefore, the effect of blade profile on instantaneous net torque coefficient at various TSR values for at least one complete revolution at inlet velocity 5 m/s is presented in the Figure 5.11 to Figure 5.16. It shows that torque coefficient of NACA0019 is slightly greater than that of NACA0015 and NACA0016 at TSR 1.4, 1.7 and 2.1, whereas torque coefficient of NACA0019 and NACA0015 are almost equal but much greater than that of NACA0016 at TSR 2.5, 3 and 3.5. However, overall torque coefficient of NACA0019 is slightly greater than NACA0015 and significantly greater than NACA0016 which is presented in Figure 5.17 in the form of average power coefficient (C_p) versus TSR where the value of TSR ranges from 1 to 4. Further, it reveals that at lower TSR the average C_p value of rotor with NACA0015 and NACA0016 are almost equal but slightly less than that of NACA0019. As the TSR increases beyond 2, the value of average power coefficient (C_p) of rotor with NACA0019 and NACA0015 are almost equal but greater than that of NACA0016. Thus, overall performance shows that NACA0019 provides the highest average C_p value, followed by NACA0015. The peak C_p of rotor with NACA0019, NACA0015 and NACA0016 are obtained at TSR=2.5 with the values of 0.405, 0.40 and 0.35, respectively for incoming wind velocity of 5 m/s.

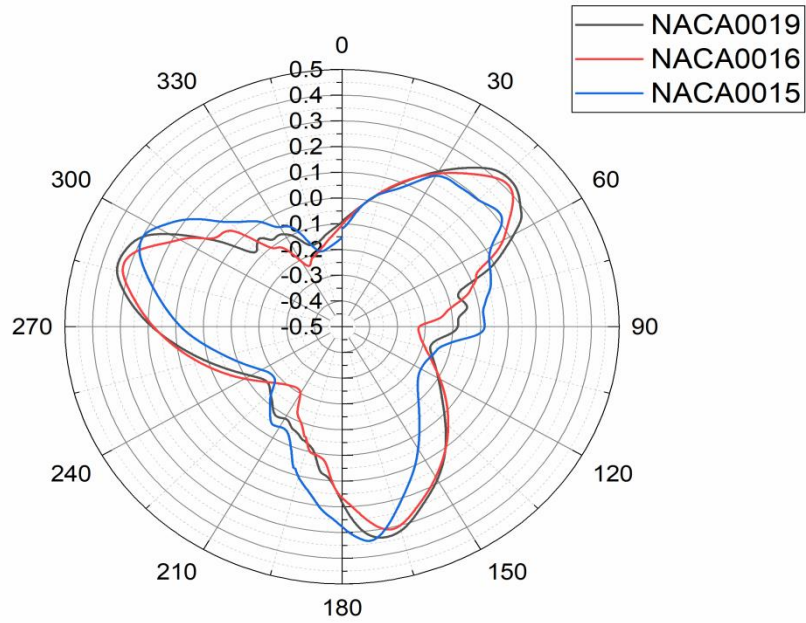


Figure 5.11 Effect of blade airfoil types on instantaneous net torque coefficient at TSR=1.4 and inlet velocity of 5 m/s

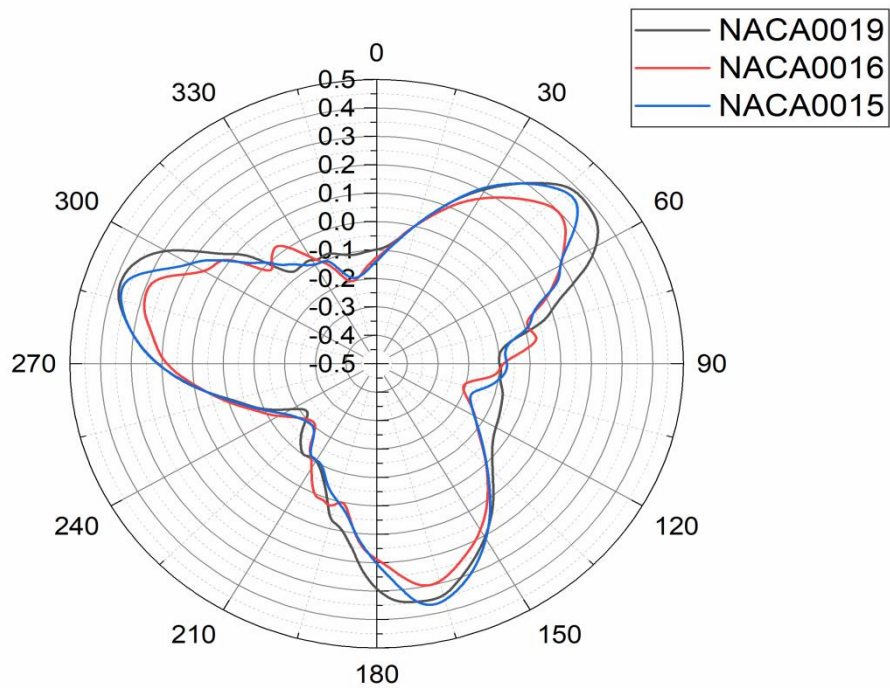


Figure 5.12 Effect of blade airfoil types on instantaneous net torque coefficient at TSR=1.7 and inlet velocity of 5 m/s

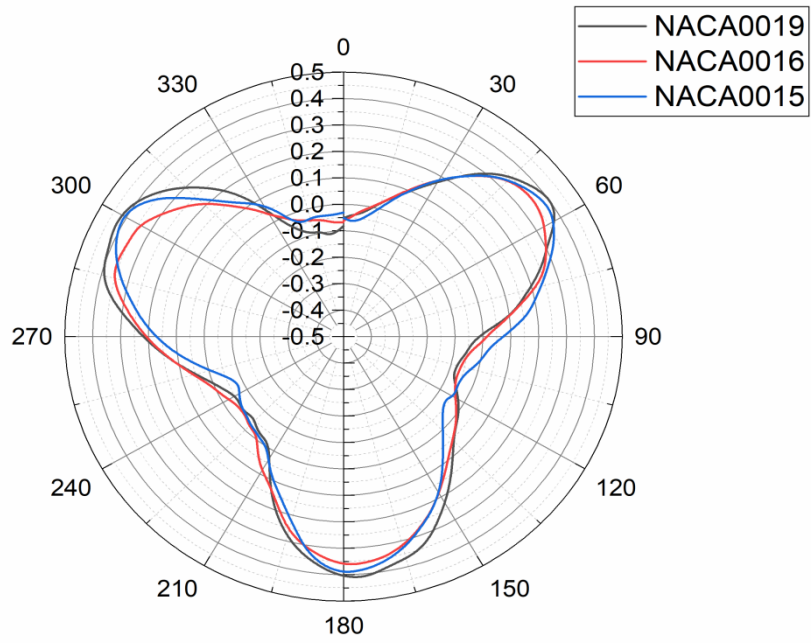


Figure 5.13 Effect of blade airfoil types on instantaneous net torque coefficient at TSR=2.1 and inlet velocity of 5 m/s

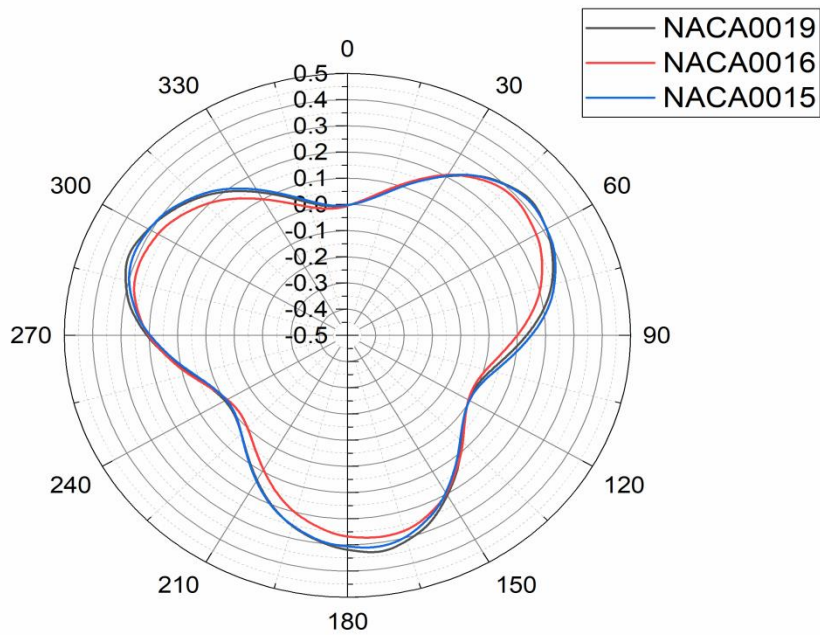


Figure 5.14 Effect of blade airfoil types on instantaneous net torque coefficient at TSR=2.5 and inlet velocity of 5 m/s

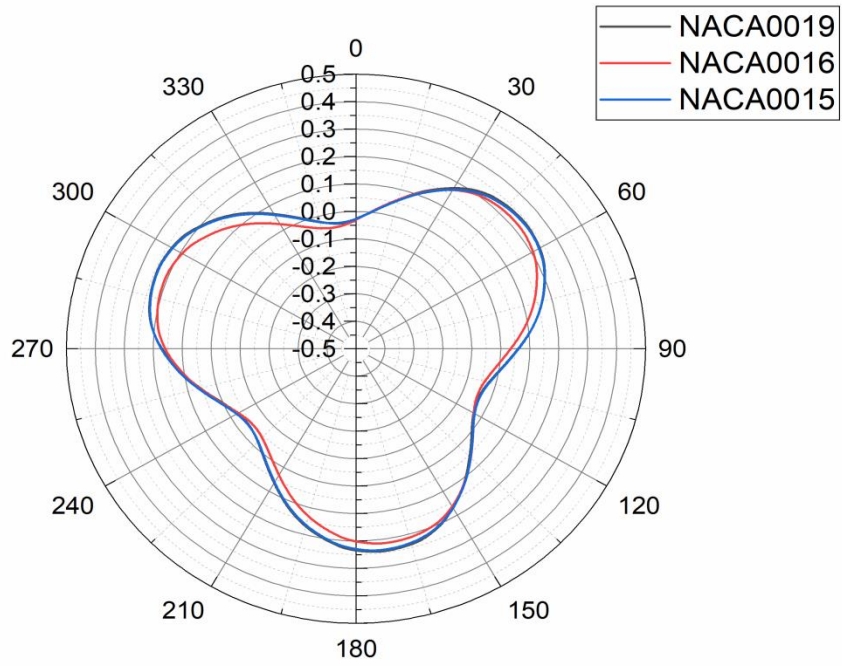


Figure 5.15 Effect of blade airfoil types on instantaneous net torque coefficient at TSR=3.0 and inlet velocity of 5 m/s

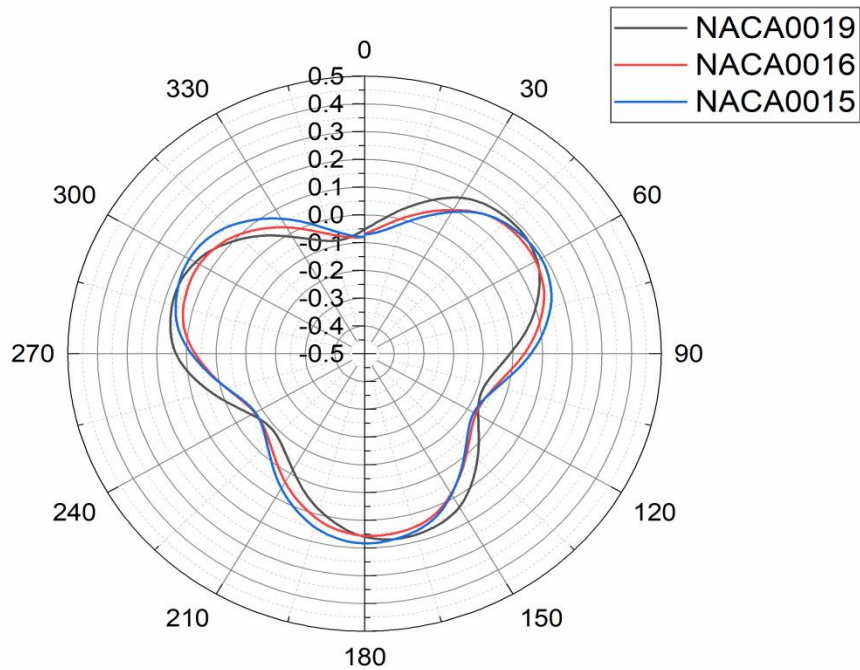


Figure 5.16 Effect of blade airfoil types on instantaneous net torque coefficient at TSR=3.5 and inlet velocity of 5 m/s

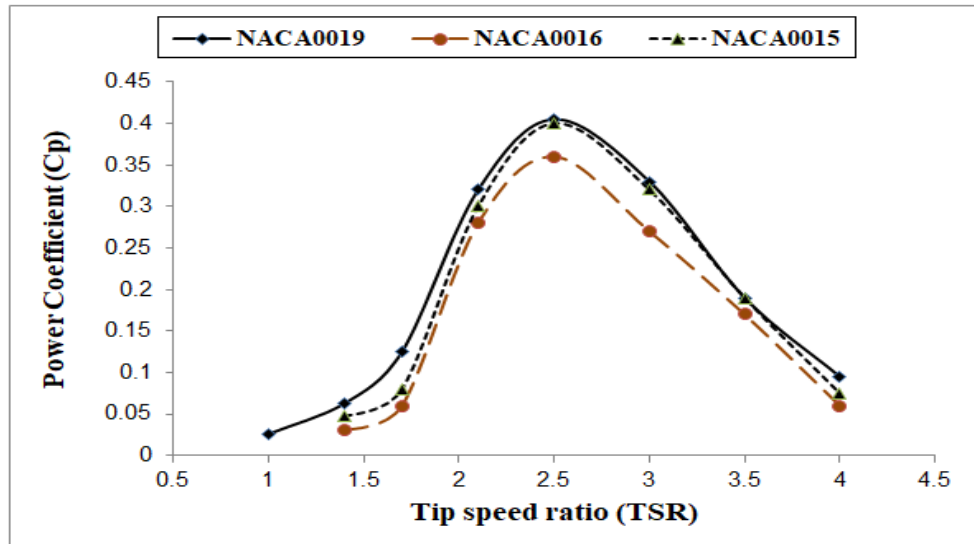


Figure 5.17 Performance comparison of rotor with NACA0015, NACA0016 and NACA0019 at inlet velocity of 5 m/s

Above discussion shows that Darrieus rotor with NACA0019 provides better power performance compared to that of NACA0015 and NACA0016. Therefore, the effect of incoming wind velocity on instantaneous net lift at $TSR=2.5$ for at least one complete revolution is presented in the Figure 5.18. It shows that negative lift is less in case of higher velocity which will generate more useful torque.

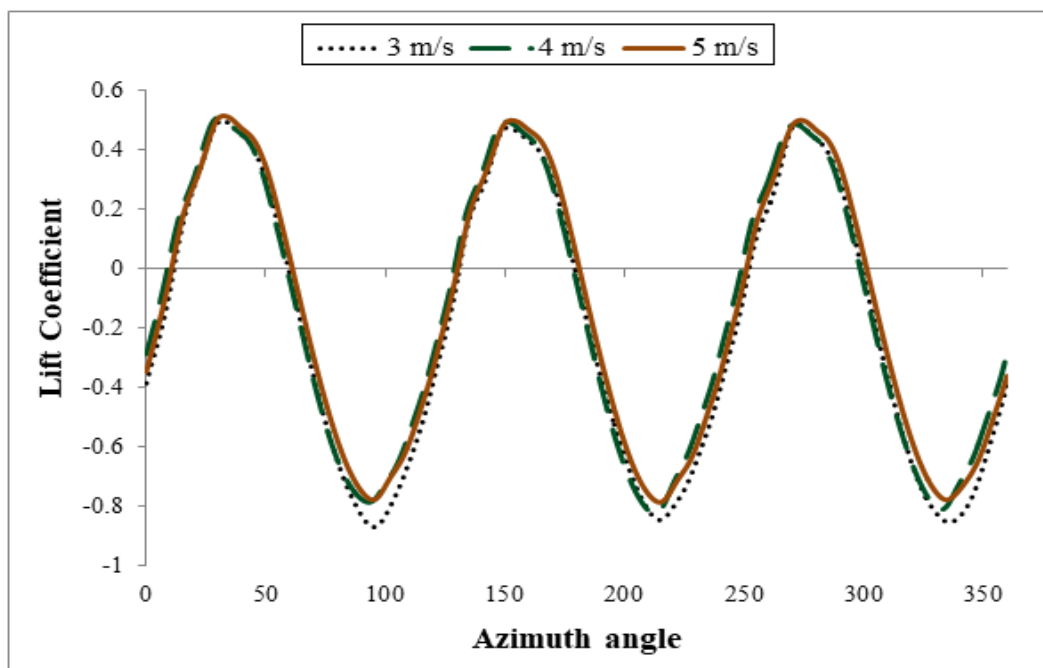


Figure 5.18 Predicted total lift coefficient for rotor with NACA0019 at $TSR=2.5$

Similarly, the effect of incoming wind velocity on instantaneous net drag coefficient at TSR=2.5 for at least one complete revolution is presented in Figure 5.19 and result shows that there is insignificant differences in the total average drag coefficient of all the three different incoming velocity.

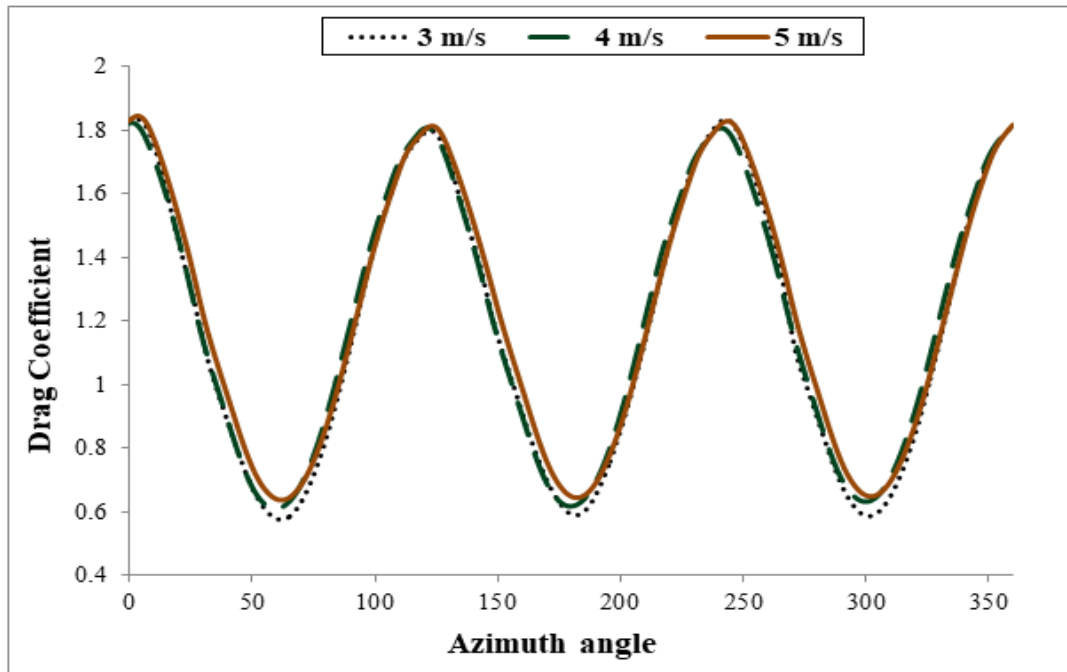


Figure 5.19 Predicted total drag coefficient for rotor with NACA0019 at TSR=2.5

Figure 5.20 shows the effect of wind velocity on power coefficient as the Reynolds number is also depends on free stream inlet velocity. Three different inlet velocities are considered at values of 3, 4, and 5 m/s. It may be emphasized here that the VAWT turbine is envisaged to be deployed for harnessing energy at locations with lower velocity. The figure reveals that the decrease in Reynolds number with decrease in inlet velocity which reduces the wind flux to the domain and as a consequence overall performance is expected to decrease. The values of peak power coefficients are small for low wind velocity and it increases with increase in velocity and peak power coefficients are 0.35, 0.38 and 0.405 for velocities of 3 m/s, 4 m/s and 5m/s respectively. Thus, the value of C_p increases by 8.6 % and 6.6 % as the wind velocity changes by an amount of 1 m/s respectively.

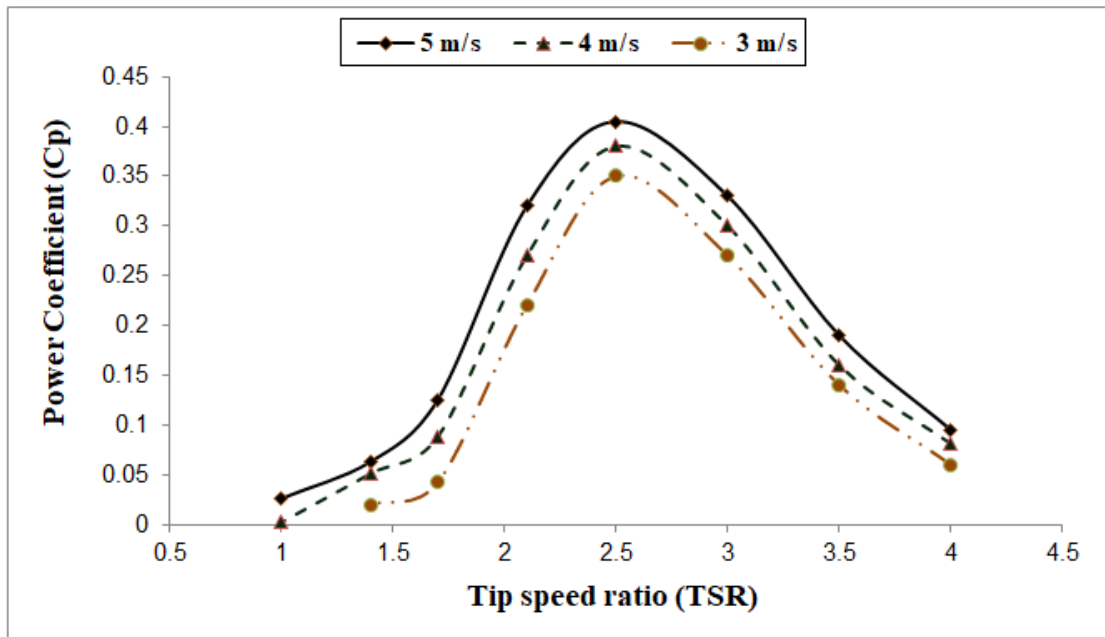


Figure 5.20 Performance of rotor varying inlet velocity for rotor with NACA0019 at TSR=2.5

The fluctuation in the torque curve for a particular TSR can also be explained through instantaneous pressure contours which are plotted in Figure 5.21. The contour levels are set at the same level to compare pressure intensity at azimuthal angles (θ) of 0° , 60° , 120° , 180° , 240° , 270° , 300° and 330° . It is observed that the pressure intensity is higher from $\theta = 210^\circ$ to 300° than 0° to 180° . Moreover flow separation region, the inner side of the airfoil has negative pressure from $\theta = 180^\circ$ to 300° out of which more negative pressure at $\theta = 240^\circ$ and 270° which corresponds to highest pressure difference leading to more torque generation.

Further instantaneous torque contours of all the three NACA airfoils are presented at Figure 5.22 at various azimuthal angles with same contours levels. Results reveal that the largest pressure difference is obtained in the upwind part of rotor and a clear vortex is formed at the inner side of the airfoil. Larger pressure differences are observed in cases of both NACA0019 and NACA0015 compared to that of NACA0016 airfoil which leads to more torque generation in case of rotor with the former two airfoils.

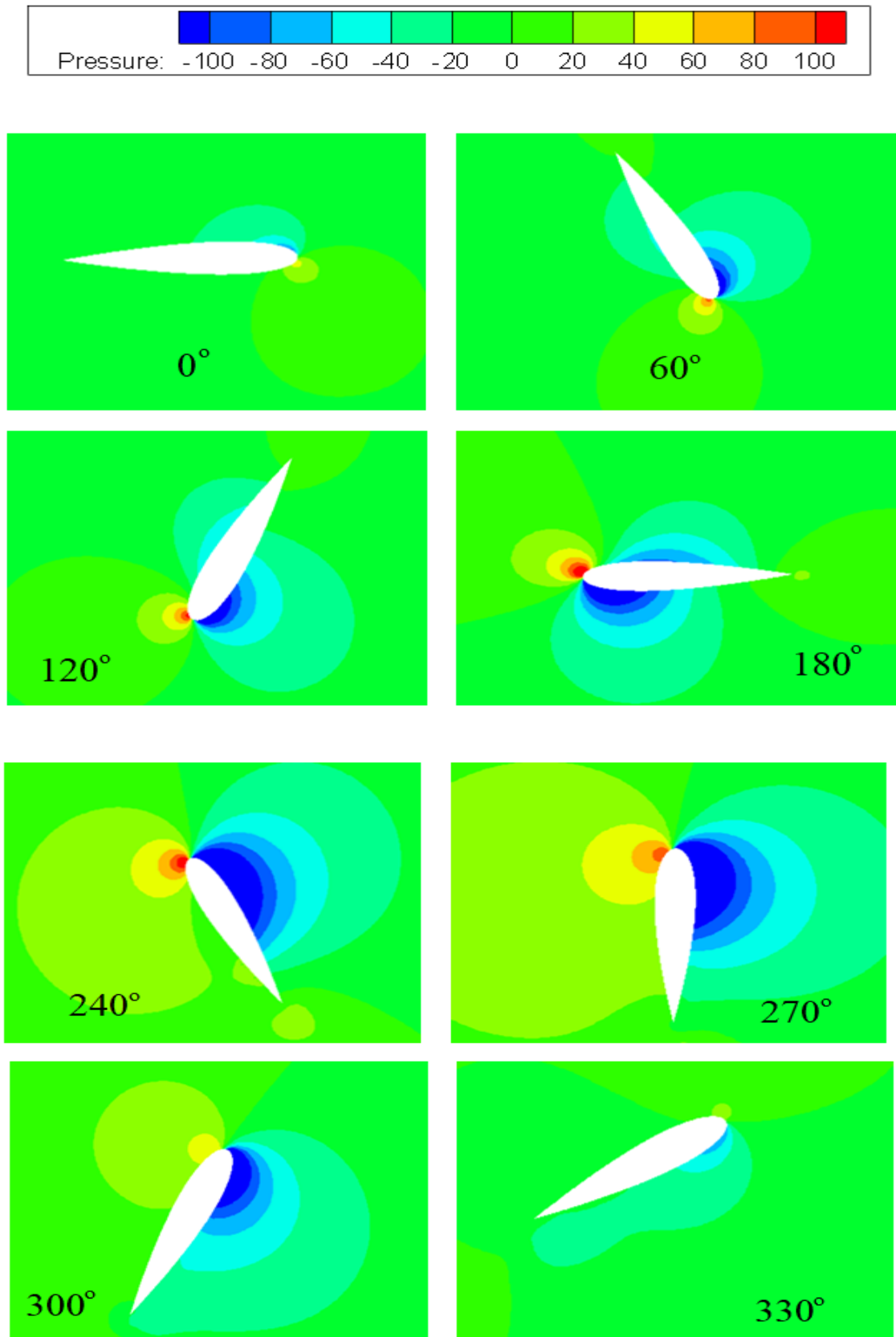


Figure 5.21 Pressure contours at various azimuthal angle for NACA0019 at inlet velocity of 5 m/s and TSR=2.5

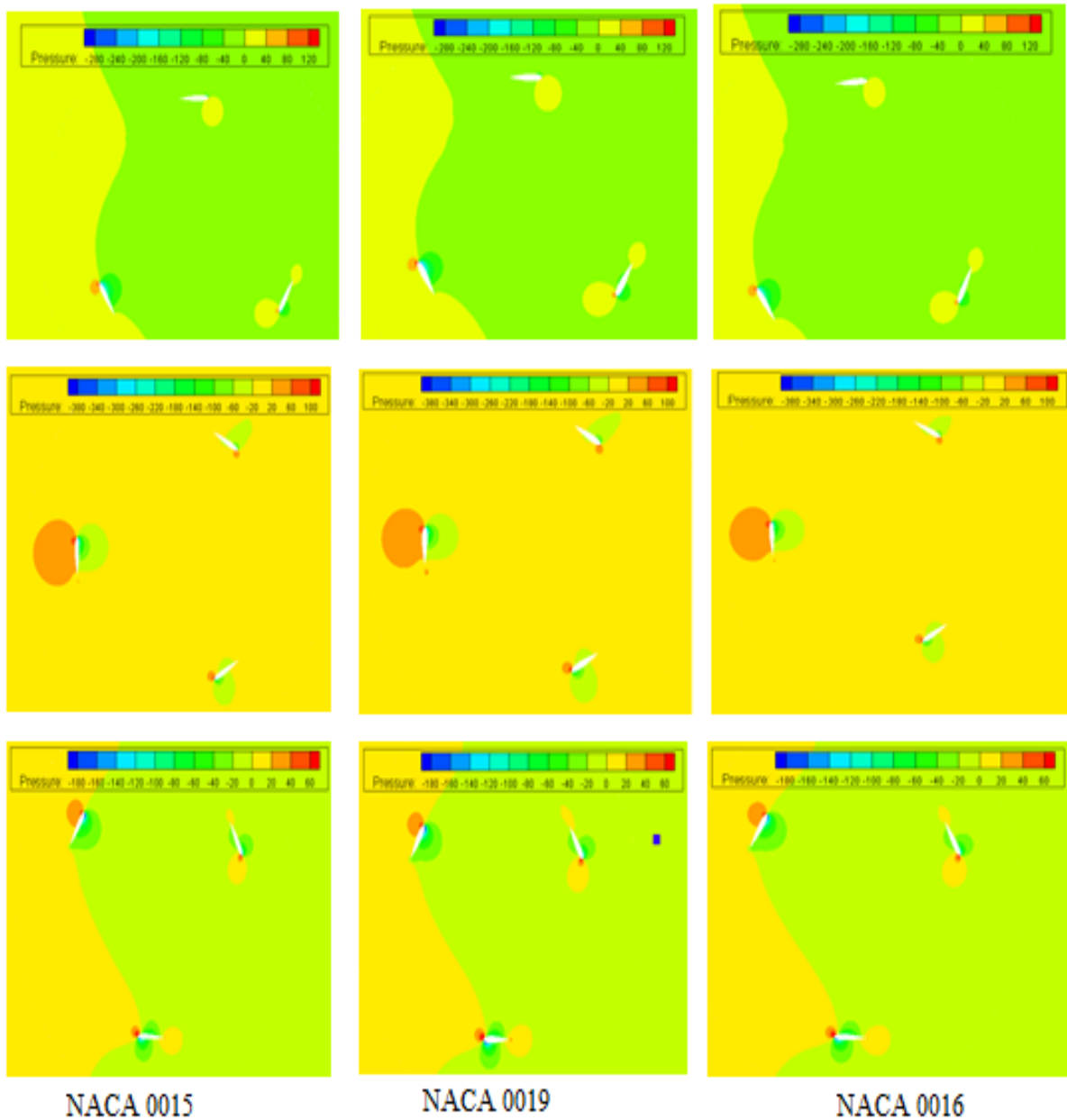


Figure 5.22 Comparison of Pressure contours of three different airfoils at various azimuthal angle for NACA0019 at inlet velocity of 5 m/s and TSR=2.5

To gain more insightful understanding of flow description, snapshots of the instantaneous flow structures obtained at azimuth angle of 0° , 90° , 180° and 270° at TSR=2.5, for a wind velocity of 5 m/s are reported in Figures 5.23 and 5.24 showing the contours of turbulence intensity and vorticity of the three bladed rotors. Turbulent intensity signifies the strength of fluctuating part to the mean velocity component. In Figure 5.23, the effect of turbulent

intensity is visualized for different NACA airfoils. It is noticed that at the beginning of a cycle the leading edge of the blade is disturbed by the turbulent vortices structures released by preceding blade which ultimately affects the performance of the rotor. However, in the later part of the cycle blades are undisturbed by the vortices where more useful torque is generated, as already observed from Figure 5.11 to 5.16. Further, the nature of turbulent wake development is more or less similar for both NACA0015 and NACA0019, but greater separation of the wake is noticed in case of TSST model as compared that for SST k- ω model.

Figure 5.24 reports the comparison of predicted vorticity distribution around the rotor at TSR =2.5 for different NACA airfoils using SST k- ω model and TSST model. It is noticed that remarkable differences between NACA0019 and NACA0016 but insignificant differences of wake development in case of NACA0019 and NACA0015. It is also noticed that there are insignificant differences of wake development due to vortices between SST k- ω model and TSST model but more separation is observed in case of TSST model. Results therefore demonstrate the capability of the closure models.

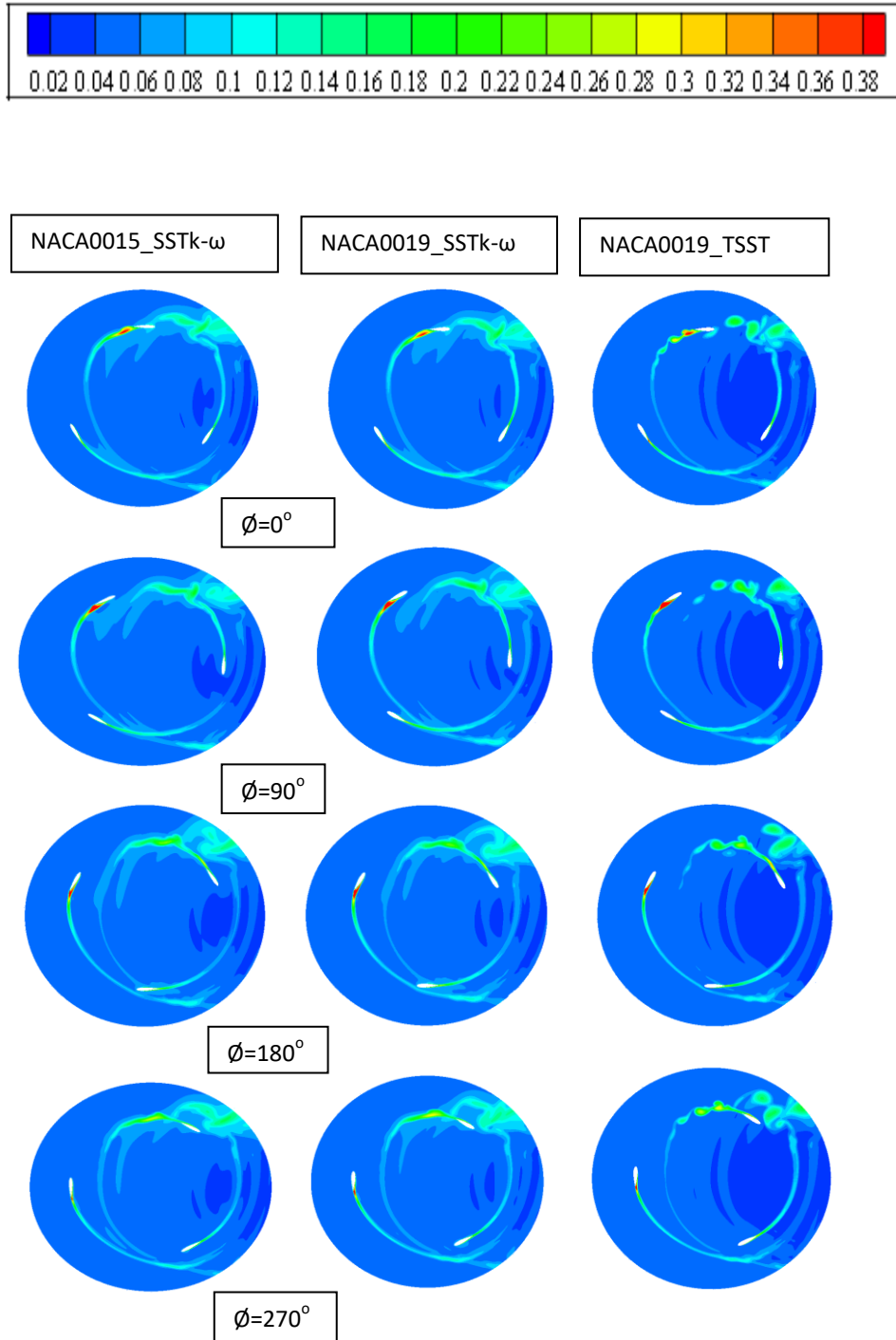


Figure 5.23 Turbulent intensity for NACA0015 and NACA0019 @TSR=2.5

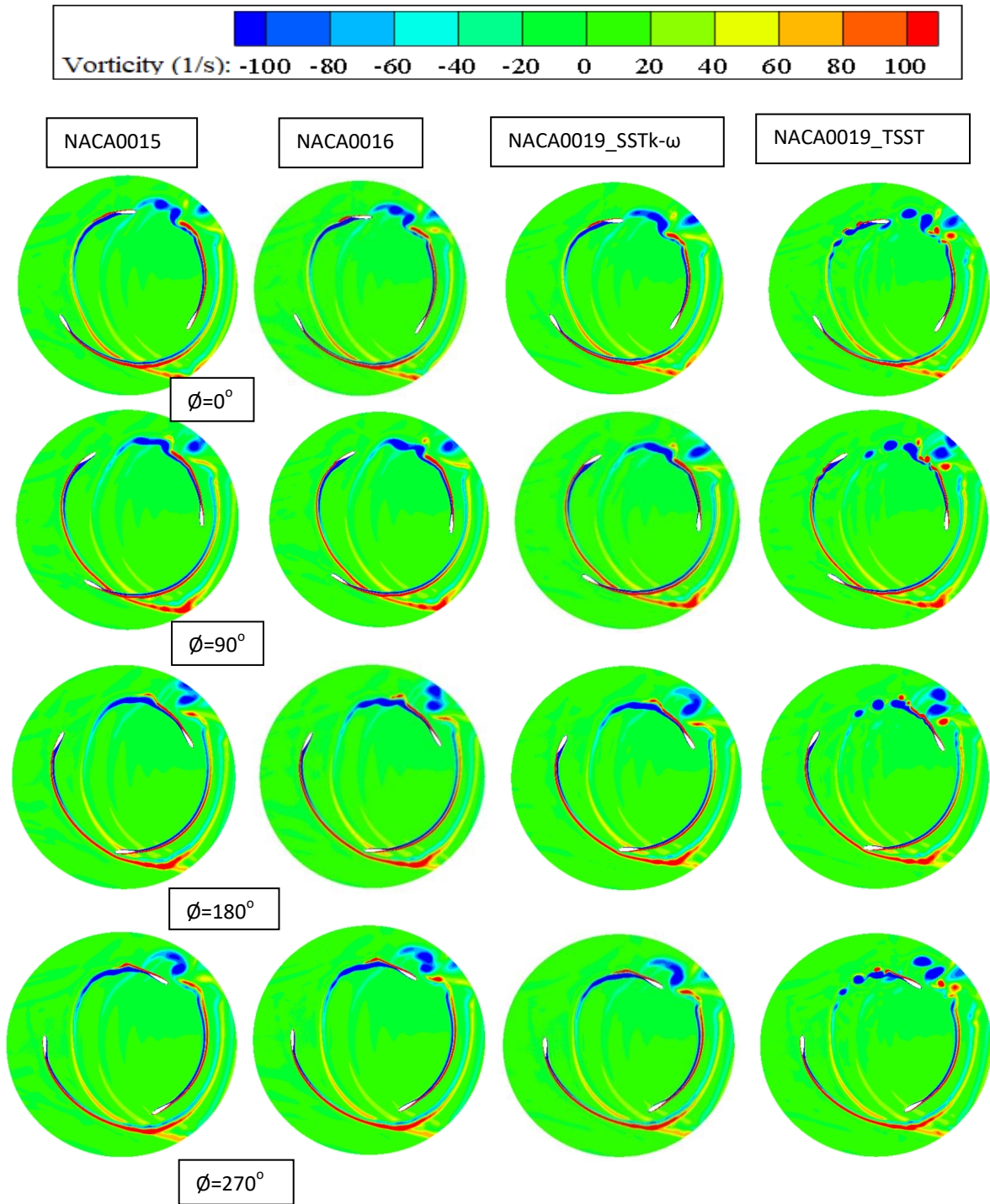


Figure 5.24 Vorticity distributions at different angular positions for NACA0015, NACA0016 and NACA0019@TSR=2.5

5.5.2 Concluding remarks

In this section performance assessment of Darrieus wind turbine with two new NACA airfoils namely, NACA0019 and NACA0016 airfoils was studied and their performance are compared with the established effective rotor with NACA0015. First of all, the instantaneous torque variation with azimuthal angle is presented which shows that torque characteristic of NACA0019 and NACA0015 are almost similar while significantly differ from the torque characteristics of NACA0016. Eventually, the overall power coefficient with respect to tip speed ratio revealed that average power coefficient of NACA0019 is almost equal to that of NACA0015 but significantly greater than the average power coefficient of rotor with NACA0016.

Further, to gain more insightful of understanding of flow characteristics pressure contours, vorticity distributions and turbulent intensity obtained at different azimuthal angles are reported. From the present analysis, it is realized that the rotor with NACA0019 in spite of having more thickness than the established rotor with NACA0015, the former rotor provides almost equal performance to the latter one, but significantly better than NACA0016. Therefore, NACA0019 shows dominant quality than the NACA0015 providing better power performance and greater structural strength as well.

LIST OF SYMBOLS AND ABBREVIATIONS

Roman letters

A	Swept area of rotor
C_d	Drag coefficient
C_l	Lift coefficient
C_m	Torque coefficient
C_p	Power coefficient
C_t	Tangential force coefficient
c	Blade chord
D	Diameter
F_d	Drag force
F_l	Lift force
F_n	Normal force
F_t	Tangential force
H	Rotor height
k	Turbulence kinetic energy
N	Number of blades
\hat{m}	Mass flow rate
P	Actual power generated by turbine
P_o	Power available in the wind
Q	Volume of air passing
R	Rotor radius
R_e	Reynolds number
T	Torque generated

t	Blade thickness
u	Velocity

Greek letters

α	Angle of attack
β	Pitch angle
λ	Tip speed ratio
μ	Dynamic viscosity
μ_t	Turbulent dynamic viscosity
ω	Angular speed
ϕ	Azimuth Angle
ρ	Density
σ	Solidity
θ	Incidence angle

Abbreviations

CFD	Computational fluid dynamics
CFL	Courant Friedrichs Lewy
KE	Kinetic energy
NACA	National Advisory Committee for Aeronautics
NOR	Number of revolution
NOTS	Number of time steps
RANS	Reynolds Averaged Navier-Stokes simulations
RPM	Revolutions per minute
SB-VAWT	Straight bladed VAWT
SST	Shear stress transport

TSST	Transition SST
TSS	Time step size
TSR	Tip speed ratio
URANS	Unsteady RANS
VAWT	Vertical axis wind turbine

CONCLUSIONS AND FUTURE SCOPE

Wind energy conversion technology (WECT) has three major phases: wind energy resource assessment to select feasible site for wind power generation, selection or design of wind energy harnessing device (wind turbine) and installation of the wind turbine. For the first phase wind energy potential assessment of four important sites in North-eastern and Eastern regions of India has been performed. The sites are Imphal, Shillong, Guwahati and Kolkata , the capital or business capital of Manipur, Meghalaya, Assam and West Bengal respectively. Wind energy potential assessment (WEPA) has been carried out by adopting Weibull and Rayleigh distribution models which are considered to be effective statistical distribution models and using four widely accepted efficient numerical estimation methods namely, empirical method (EM), moment method (MOM), power density method (PDM) and maximum likelihood method (MLM). We also performed assessment analysis using a new alternative estimation method known as energy variance method (EVM) whose performance is validated with the performance of existing efficient methods. Finally, for the second phase of WECT, the computational fluid dynamics of H-type Darrieus VAWT to assess performance of rotor with NACA0016 and NACA0019 airfoils. Therefore, the thesis embodies the above tasks in six chapters combining WEPA of selected sites and CFD studies of VAWT, the suitable for low speed wind regions.

6.1 Wind energy potential assessment of four sites

Analysis on the assessment of wind energy potential of Imphal, Shillong, Guwahati and Kolkata has been presented in the Chapter 4 of this thesis from which the following conclusions are drawn:

- From the frequency of the wind speed analysis of Imphal site it has come to know that wind speed at 1, 1.5 and 2-3 m/s has approximately 19.5%, 23.5% and 41% respectively. For Shillong site wind speed of 1-3 m/s has approximately 91% out of which 1.5 m/s has the maximum share with 40% approximately. For Guwahati site wind speed of 1.5-3.5 m/s has approximately 87% out of which wind speed of 2.5 m/s has the maximum share with 33% approximately. Similarly, for Kolkata site wind

speed of 1-4.5 m/s has approximately 92% out of which wind speed of 1.5 and 2.5 m/s have the maximum share with 21% and 17% respectively.

- Seasonal variation analysis shows that summer and winter provide highest and lowest wind speed range respectively for all four sites. However, yearly mean wind speed range for Imphal, Shillong, Guwahati and Kolkata sites are 1.04-2.30 m/s, 1.4-1.79 m/s, 2.13-2.3 m/s and 1.91-2.84 m/s respectively and corresponding standard deviations are 0.64-1.05 m/s, 0.65-1.15 m/s, 0.92-1.0 m/s and 1.1-1.55 m/s respectively.
- The month wise comparison shows that highest mean wind speed range for Imphal, Shillong, Guwahati and Kolkata sites are available during February-June, March-June, March-June and March-August respectively. Corresponding monthly maximum mean wind speed range are 2.67-12.55 m/s, 3.24-12.11 m/s, 3.1-6.44 m/s and 4.05-8.02 m/s respectively. Overall comparison shows that mean wind speed of Kolkata site is the highest in all months except during the winter season followed by that of Guwahati site. The wind profiles for Shillong and Imphal sites are almost same but during winter season Imphal has higher wind speed range.
- Seasonal and annual wind power density (WPD) based on actual mean wind speed at hub height of 20 m shows that Guwahati provide highest annual mean WPD followed by Kolkata and least is available at Shillong. But during summer season Kolkata provides highest mean WPD with 15.4 W/m^2 followed by Guwahati with 13.33 W/m^2 while lesser Mean WPD is found at Imphal and Shillong sites with 8.53 W/m^2 and 4.97 W/m^2 respectively. However, extrapolating wind data corresponding to 40 m the WPD can be increased more than 100%. Still the available wind power of all the selected regions falls in the low wind power scale and in such situation deployment of vertical axis wind turbine is feasible.

6.2 Performance comparison of Weibull and Rayleigh Distribution models

Studied performance comparison of Weibull and Rayleigh distribution models employing wind speed data of Imphal, Shillong, Guwahati and Kolkata sites. For the estimation of shape and scale parameters three effective numerical methods: MOM, EM and PDM are employed. Results reveal that Weibull model provides optimum value of statistical evaluation test in most of the seasonal and yearly performance analysis of Imphal, Guwahati and Kolkata sites.

However, Rayleigh model significantly performs better in case of Shillong site than Weibull model. It is concluded that Weibull is better for the assessment of low to higher wind speed range while Rayleigh model shows better result for the region having extremely low wind speed range.

6.3 Development of a new numerical estimation method

As a part of the wind energy potential assessment a new estimation method (EVM) is developed for the first time and its performance has been compared with MOM, EM, PDM and MLM for Weibull parameters employing wind speed data of all the selected four sites. From the analysis it can be summarized as:

- In case of Imphal site overall performance shows that MOM and MLM equally give better performance followed by EVM.
- As for Shillong site MLM shows significantly better performance than other numerical methods followed by EVM and EM.
- Analysis of Guwahati site reveals that EVM outperforms all other methods followed by MLM.
- Similarly, performance analysis of the numerical methods employing wind data of Kolkata site reveals that EVM and MOM provide seven and six numbers of 1st ranking in performance.
- Moreover, the PDFs and CDFs show that PDFs of all the methods except for power density method are more or less quite close to the distribution of actual wind data.
- Finally, the overall performance shows that EVM is an effective and the most accurate method for estimating Weibull parameters followed by MLM and MOM for these regions. Therefore, this new method may be considered as an improved, efficient and alternative estimation method for estimating Weibull parameters for wind energy applications.

6.4 CFD Analysis of VAWT

This act of work focuses on the performance of vertical axis wind turbines using NACA0016 and NACA0019 airfoils. First of all computational model is developed and unsteady RANS bases simulations are performed to resolve the flow field of three bladed H-type VAWT. The

turbulence closure is effectively provided by SST $k-\omega$ model and transition SST model. From the analysis the following conclusions are drawn:

- Present model is validated with two different experimental data, the maximum power coefficient of the three bladed H-type present model is found at tip speed ratio, $\lambda=2.5$. The two dimensional results of the present model is in qualitatively good agreement with both the experimental results and quantitatively better than CFD result of one of it.
- Further, results show that the power coefficient of NACA0019 airfoils resulting from the CFD simulation is comparable to established rotor profiles like NACA0015. The dependence of power coefficient on tip speed ratio follows similar pattern as for NACA0015. The advantage of using NACA0019 comes from the fact that it provides better structural strength than thinner NACA four digit series like NACA0018, NACA0016, or NACA0015.

6.5 Future Scope

The present work analyzed the assessment of wind energy potential of four important sites in Northeastern and Eastern regions of India and performed computational fluid dynamics analysis of VAWT to assess the performance of rotor with two new airfoils section namely, NACA0016 and NACA0019 as the VAWT has low efficiency and is the only type which can be deployed in such low wind potential regions. Therefore, the scope for the future work may be noted down as follows:

- Extensive wind potential assessment of various sites in the entire Northeastern and Eastern regions of India by employing wind data to be measured continuously at two or more anemometer height for each site may be studied in future.
- In case of CFD analysis of VAWT, the present study may be extended with additional symmetric and asymmetric airfoil sections both NACA families and other families as well with or without modification of blades.
- For better understanding of the physics additional physical and geometrical parameters such as effect of pitch angle, solidity, chord length, diameter, shaft effect and connector may be studied.

- While this study is limited by two dimensional studies, three-dimensional CFD analysis can be carried out with validation from experimental data.
- Finally, in order to enhance the overall performance of the turbine, augmentation strategies may be deployed which ask for additional analysis.

REFERENCES

- Acakpovi, A., Issah, M.B., Fifatin, F.X. and Michael, M.B. (2017). Wind velocity extrapolation in Ghana by Weibull probability density function. *Wind Engineering*, 1-13.
- Abas, N., Kalair, A. and Khan, N. (2015). Review of fossil fuels and future energy technologies. *Futures*, 69, 31–49.
- Abraham, J.P., Sparrow, E.M. and Tong, J.C.K. (2009). Heat transfer in all pipe flow regimes: laminar, transitional/intermittent, and turbulent. *Int. J. Heat Mass Transf.*, 52, 557–563.
- Ahmad, M., Kumar, N. and Roy, L.B. (2016). Current Trends in Renewable Energy: An Overview. *Renewable and Sustainable Energy: An International Journal (RSEJ)*, 1(1), 1-17.
- Ahmed, A.S. (2010). Wind energy as a potential generation source at Ras Benas, Egypt. *Renewable and Sustainable Energy Reviews*, 14, 2167–2173.
- Akdag, S.A. and Dinler, A. (2009). A new method to estimate Weibull parameters for wind energy applications. *Energy Conversion and Management*, 50, 1761–1766.
- Akgül, F.G., Senoglu, B. and Arslan, T. (2016). An alternative distribution to Weibull for modeling the wind speed data: Inverse Weibull distribution. *Energy Conversion and Management*, 114, 234–240.
- Akpınar, E.K. and Akpınar, S. (2005). An assessment on seasonal analysis of wind energy characteristics and wind turbine characteristics. *Energy Conversion and Management*, 46, 1848–1867.
- Alavi, O., Mohammadi and K., Mostafaeipour, A. (2016). Evaluating the suitability of wind speed probability distribution models: A case of study of east and southeast parts of Iran. *Energy Conversion and Management*, 119, 101–108.
- Al-Abbadi, N.M. (2005). Wind energy resource assessment for five locations in Saudi Arabia. *Renewable Energy*, 30, 1489–1499.
- Albadi, M.H., El-Saadany, E.F. and Albadi, H.A. (2009). Wind to power a new city in Oman. *Energy*, 34, 1579–1586.
- Al Buhairi, M.H. (2006). A Statistical Analysis of Wind Speed Data and an Assessment of Wind Energy Potential in Taiz-Yemen. *Ass. Univ. Bull. Environ. Res.*, 9(2), 21-31.
- Almohammadi, K.M., Ingham, D.B., Maa, L. and Pourkashan, M. (2013). Computational fluid dynamics (CFD) mesh independency techniques for a straight blade vertical axis wind turbine. *Energy*, 58, 483-493.

- Andrade, C.F., Neto, H.F.M., Rocha, P.A.C. and Silva, M.E.V. (2014). An efficiency comparison of numerical methods for determining Weibull parameters for wind energy applications: A new approach applied to the northeast region of Brazil. *Energy Conversion and Management*, 86, 801–808.
- Arab, A., Javadi, M., Anbarsooz, M. and Moghiman, M. (2017). A numerical study on the aerodynamic performance and the self-starting characteristics of a Darrieus wind turbine considering its moment of inertia. *Renewable Energy*, 107, 298-311.
- Aririguzo, J.C. and Ekwe, E.B. (2018). Weibull distribution analysis of wind energy prospect for Umudike, Nigeria for power generation. *Robotics and Computer-Integrated Manufacturing*, 1-4.
- Arslan, T., Bulut, Y.M. and Yavuz, A.A. (2014). Comparative study of numerical methods for determining Weibull parameters for wind energy potential. *Renewable and Sustainable Energy Reviews*, 40, 820–825.
- Aukitino, T., Khan, M.G.M. and Ahmed, M.R. (2017). Wind energy resource assessment for Kiribati with a comparison of different methods of determining Weibull parameters. *Energy Conversion and Management*, 151, 641–660.
- Azad, A.K., Rasul, M.G., Alam, M.M., Uddin, S.M.A. and Mondal, S.K., (2014a). Analysis of wind energy conversion system using Weibull Distribution. *Procedia Engineering*, 90, 725 – 732.
- Azad, A.K., Rasul, M.G. and Yusaf, T. (2014b). Statistical Diagnosis of the Best Weibull Methods for Wind Power Assessment for Agricultural Applications. *Energies*, 7, 3056-3085.
- Azad, A.K., Rasul, M.G., Islam, R. and Shishir, I.R. (2015). Analysis of wind energy prospect for power generation by three Weibull distribution methods. *Energy Procedia*, 75, 722 – 727.
- Bai, C.-J., Lin, Y.-Y., Lin, S.-Y. and Wang, W.-C. (2015). Computational fluid dynamics analysis of the vertical axis wind turbine blade with tubercle leading edge. *Journal of Renewable and Sustainable Energy*, 7(033124), 1-15. doi: 10.1063/1.4922192
- Balduzzi, F., Bianchini, A., Riccardo, Maleci, R., Ferrara, G. and Ferrari, L. (2016a). Critical issues in the CFD simulation of Darrieus wind turbines. *Renewable Energy*, 85, 419-435.
- Balduzzi, F., Bianchini, A., Riccardo, Maleci, R., Ferrara, G. and Ferrari, L. (2016b). Dimensionless numbers for the assessment of mesh and time step requirements in CFD simulations of Darrieus wind turbines. *Energy*, 97, 246-261.

- Balduzzi, F., Drofelnik, J., Bianchini, A., Ferrara, G., Ferrari, L. and Campobasso, M.S. (2017). Darrieus wind turbine blade unsteady aerodynamics: a three-dimensional Navier-Stokes CFD assessment. *Energy*, 128, 550-563.
- Bedon, G., Betta, S.D. and Benini, E. (2016). Performance-optimized airfoil for Darrieus wind turbines. *Renewable Energy*, 94, 328-340.
- Bekele, G. and Palm, B. (2009). Wind energy potential assessment at four typical locations in Ethiopia. *Applied Energy*, 86, 388-396.
- Beri, H. and Yao, Y. (2011). Effect of Camber Airfoil on Self Starting of Vertical Axis Wind Turbine. *Journal of Environmental Science and Technology*, 4(3), 302-312.
- Bianchini, A., Balduzzi, F., Bachant, P., Ferrara, G. and Ferrari, L. (2017). Effectiveness of two-dimensional CFD simulations for Darrieus VAWTs: a combined numerical and experimental assessment. *Energy Conversion and Management*, 136, 318–328.
- Bianchini, A., Ferrari, G. and Ferrari, L. (2015). Pitch optimization of small Darrieus wind turbine. *Energy Procedia*, 81, 122 – 132.
- Bidaoui, H., Abbassi, I., Bourdi, A. and Darcherif, A. (2019). Wind speed data analysis using Weibull and Rayleigh distributions functions, Case study: Five Cities Northern Morocco. *Procedia Manufacturing*, 32, 786-793.
- Bilir, L., Imir, M., Devrim, Y. and Albostan, A. (2015). Seasonal and yearly wind speed distribution and wind power density analysis based on Weibull distribution function. *International Journal of Hydrogen Energy*, xxx, 1-10.
- Biswas, A. and Gupta, R. (2014). Unsteady aerodynamics of a twist bladed H-Darrieus rotor in low Reynolds number flow. *Journal of Renewable and Sustainable Energy*, 6(033108), 1-12.
- Cai, X., Zhang, Y., Ding, W. and Bian, S. (2019). The aerodynamic performance of H-type Darrieus VAWT rotor with and without winglets: CFD simulations. *Energy Sources, Part A: Recovery, Utilization, and Environmental Effects*. doi: 10.1080/15567036.2019.1691286
- Caineng, Z., Qun, Z., Guosheng, Z. and Bo, X. (2016). Energy revolution: From a fossil energy era to a new energy era. *Natural Gas Industry*, B 3, 1-11.
- Carneiro, T.C., Melo, S.P., Carvalho, P.C.M. and Braga, A.P.S. (2016). Particle Swarm Optimization method for estimation of Weibull parameters: A case study for the Brazilian northeast region. *Renewable Energy*, 86, 751-759.
- Carrigan, T.J., Dennis, B.H., Han, Z.X. and Wang, B.P. (2012). Aerodynamic Shape Optimization of a Vertical- Axis Wind Turbine Using Differential Evolution. *ISRN Renewable Energy*, Article ID 528418, 16 pages. doi:10.5402/2012/528418

- Castelli, M.R., Englaro, A. and Benini, E. (2011). The Darrieus wind turbine: Proposal for a new performance prediction model based on CFD. *Energy*, 36, 4919-4934.
- Celik, A.N. (2003). A statistical analysis of wind power density based on the Weibull and Rayleigh models at the southern region of Turkey. *Renewable Energy*, 29, 593-604.
- Chang, T.P. (2011). Performance comparison of six numerical methods in estimating Weibull parameters for wind energy application. *Applied Energy*, 88, 272–282.
- Chen, W.H., Chen, C.-Y., Huang, C.-Y. and Hwang, C.-J. (2017). Power output analysis and optimization of two straight-bladed vertical-axis wind turbines. *Applied Energy*, 185, 223–232.
- Chen, J, Chen, L, Xu, H., Yang, H., Ye, C. and Liu, D. (2016). Performance improvement of a vertical axis wind turbine by comprehensive assessment of an airfoil family. *Energy*, 114, 318-331.
- Chen, Y. and Lian, Y. (2015). Numerical investigation of vortex dynamics in an H-rotor vertical axis wind turbine. *Engineering Applications of Computational Fluid Mechanics*. 9(1), 21-32, DOI: 10.1080/19942060.2015.1004790
- Chaurasiya, P.K., Ahmed, S. and Warudkar, V. (2017). Study of different parameters estimation methods of Weibull distribution to determine wind power density using ground based Doppler SODAR instrument. *Alexandria Engineering Journal*. <http://dx.doi.org/10.1016/j.aej.2017.08.008>
- Chowdhury, A.M., Akimoto, H. and Hara, Y. (2016). Comparative CFD analysis of Vertical Axis Wind Turbine in upright and tilted configurations. *Renewable Energy*, 85, 327-337.
- Colonbo, U. (1992). Development and the global environment". The energy–environment connection. *Washington: Island Press*, 3–14.
- Dabiri, J.O. (2011). Potential order-of-magnitude enhancement of wind farm power density via counter-rotating vertical-axis wind turbine arrays. *Journal of Renewable And Sustainable Energy*, 3: 043104.
- Daróczy, L., Janiga, G. and Thévenin, D. (2018). Computational fluid dynamics based shape optimization of airfoil geometry for an H-rotor using a genetic algorithm. *Engineering Optimization*, 50(9), 1483-1499. doi: 10.1080/0305215X.2017.1409350
- Daroczy, L., Jaaniga, G., Petrasch, K., Webner, M. and Thevenin, D. (2015). Comparative analysis of turbulence models for the aerodynamic simulation of H-Darrieus rotors. *Energy*, 90, 680-690.
- Dorvlo, A.S.S. (2002). Estimating wind speed distribution. *Energy Conversion and Management*, 43, 2311–2318.

- Durrani, N., Hameed, H., Rahman, H. and Chaudhry, S.R., (2011). A detailed Aerodynamic Design and analysis of a 2D vertical axis wind turbine using sliding mesh in CFD. *49th AIAA Aerospace Sciences Meeting including the New Horizons Forum and Aerospace Exposition 4 - 7 January 2011*, Orlando, Florida.
- Durak, M. and Sen, Z. (2002). Wind power potential in Turkey and Akhisar case study. *Renewable Energy*, 25, 463–472.
- Eboibi, O., Danao, L.A.M. and Howell, R.J., (2016), “Experimental investigation of the influence of solidity on the performance and flow field aerodynamics of vertical axis wind turbines at low Reynolds numbers”, *Renewable Energy*, 92, 474-483.
- Elkhoury, M., Kiwata, T. and Aoun, E. (2015). Experimental and numerical investigation of a three-dimensional vertical-axis wind turbine with variable-pitch. *J. Wind Eng.Ind.Aerodyn.*, 139, 111–123.
- Elnaggar, M., Edwan, E. and Ritter, M. (2017). Wind Energy Potential of Gaza Using Small Wind Turbines: A Feasibility Study. *Energies*, 10, 1229. doi:10.3390/en10081229
- Fagbenle, R.O., Katende, J., Ajayi, O.O. and Okeniyi, J.O. (2011). Assessment of wind energy potential of two sites in North-East, Nigeria. *Renewable Energy*, 36, 1277-1283.
- Faghani, G. R., Ashrafi, Z.N. and Sedaghat, A. (2018). Extrapolating wind data at high altitudes with high precision methods for accurate evaluation of wind power density, case study: Center of Iran. *Energy Conversion and Management*, 157, 317–38. doi:10.1016/j.enconman.2017.12.029
- Farrugia, R.N. (2003). The wind shear exponent in a Mediterranean island climate. *Renewable Energy*, 28, 647–653.
- Feretic, D., Tomsic, Z. and Cavlina, N. (1999). Feasibility analysis of wind-energy utilization in Croatia. *Energy*, 24, 239-246.
- Franchina, N., Persico, G. and Savini, M. (2019). 2D-3D Computations of a Vertical Axis Wind Turbine Flow Field: Modeling Issues and Physical Interpretations. *Renewable Energy*, 136, 1170-1189.
- Gaddada, S. and Kodicherla, S.P.K. (2016). Wind energy potential and cost estimation of wind energy conversion systems (WECSs) for electricity generation in the eight selected locations of Tigray region (Ethiopia). *Renewables: Wind, Water and Solar*, 3 (10), 13 pages.
- Garcia, A., Torres, J.L., Prieto, E. and de Francisco, A. (1998). Fitting Wind Speed Distributions: A Case Study. *Solar Energy*, 62 (2), 139–144.
- Genc, A., Erisoglu, M., Pekgor, A., Oturanc, G., Hepbasli, A. and Ulgen, K. (2015). Estimation of Wind Power Potential Using Weibull Distribution. *Energy Sources*, 27 (9), 809-822.

- Giorgetta, S., Pellegrinia, G. and Zanforlinb, S. (2015). CFD investigation on the aerodynamic interferences between medium-solidity Darrieus Vertical Axis Wind Turbines. *Energy Procedia*, 81, 227 – 239.
- Gualtieri, G. and Secci, S. (2012). Methods to extrapolate wind resource to the turbine hub height based on power law: A 1-h wind speed vs. Weibull distribution extrapolation comparison. *Renewable Energy*, 43, 183–200. doi:10.1016/j.renene.2011.12.022
- Gugliani, G.K. (2020). Comparison of different multi-parameters probability density models for wind resources assessment. *J. Renewable Sustainable Energy*, 12, 063303. doi: 10.1063/5.0024052
- Guo, Y., Li, X., Sun, L., Gao, Y., Gao, Zh. and Chen, L. (2019). Aerodynamic analysis of a step adjustment method for blade pitch of a VAWT. *Journal of Wind Engineering & Industrial Aerodynamics*, 188, 90-101.
- Gupta, R. and Biswas, A. (2010). Computational fluid dynamics analysis of a twisted three-bladed H-Darrieus rotor. *Journal of Renewable and Sustainable Energy*, 2, 043111, 15 pages.
- Hashem, I. and Mohamed, M.H. (2018). Aerodynamic performance enhancements of H-rotor Darrieus wind turbine. *Energy*, 142, 531-545.
- Hau, E. (2006). *Wind Turbines: Fundamentals, Technologies, Application, Economics*. Springer. Germany.
- He, G. and Kammen, D.M. (2014). Where, when and how much wind is available? A provincial-scale wind resource assessment for China. *Energy Policy*. <http://dx.doi.org/10.1016/j.enpol.2014.07.003>
- Hoogwijk, M. and Graus, W. (2008). *Global potential of Renewable energy Sources: a Literature Assessment*. ECOFYS.
- Howell, R., Qin, N., Edwards, J. and Durrani, N. (2010). Wind tunnel and numerical study of a small vertical axis wind turbine. *Renewable Energy*, 35, 412–422.
- ILO (2011): *Skills and Occupational Needs in Renewable Energy*. https://www.ilo.org/wcmsp5/groups/public/---ed_emp/---ifp_skills/documents/publication/wcms_166823.pdf
- IPCC (2014): <https://www.ipcc.ch/report/ar5/wg3/>
- IRENA (2020): *Renewable Energy and Jobs: Annual review 2020*. <https://www.irena.org/publications/2020/Sep/Renewable-Energy-and-Jobs-Annual-Review-2020>
- Ismail, F. and Vijayaraghavan, K. (2015). The effects of aerofoil profile modification on a vertical axis wind turbine performance. *Energy*, 80, 20-31.

- Jacobson, M.Z. and Deluchhi, M.A. (2011). Providing all global energy with wind, water and solar power Part1: Technologies, energy resources, quantities and areas of infrastructure and materials. *Energy Policy*, 39, 1154–1169.
- Jafaryar, M., Kamrani, R., Gorji-Bandpy, M., Hatami, M. and Ganji, D.D. (2016). Numerical optimization of the asymmetric blades mounted on a vertical axis cross-flow wind turbine. *International Communications in Heat and Mass Transfer*, 70, 93–104.
- Jiang, Y., He, Ch., Zhao, P. and Sun, P. (2020). Investigation of Blade Tip Shape for Improving VAWT Performance. *J. Mar. Sci. Eng.*, 8, 225. doi:10.3390/jmse8030225
- Jin, X., Zhao, G., Gao, K. and Ju, W. (2015). Darrieus vertical axis wind turbine: Basic research methods. *Renewable Energy and Sustainable Energy Reviews*, 42, 212-225.
- Joo, S., Choi, H. and Lee, J. (2015). Aerodynamic characteristics of two-bladed H-Darrieus at various solidities and rotating speeds. *Energy*, 90, 439-451.
- Jung, C. and Schindler, D. (2019). Wind speed distribution selection – A review of recent development and Progress. *Renewable and Sustainable Energy Reviews*, 114, 109290.
- Kaldellis, J.K. and Zafirakis, D. (2011). The wind energy (r)evolution: A short review of a long history. *Renewable Energy*, 36(7), 1887-1901.
- Kalogirou, S.A. (2004). Solar thermal collectors and applications. *Progress in Energy and Combustion Science*, 30, 231–295.
- Katinas, V., Gecevicus, G. and Marciukaitis, M. (2018). An investigation of wind power density distribution at the location with low and high wind speeds using statistical model. *Applied Energy*, 218(1), 442-451.
- Katinas, V., Marčiukaitis, M., Gecevičius, G. and Markevičius, A. (2017). Statistical analysis of wind characteristics based on Weibull methods for estimation of power generation in Lithuania. *Renewable energy*, 113, 190-201.
- Kavade, R.K. and Ghanegaonkar, P.M. (2018). Optimization and Performance Analysis of Vertical Axis Wind Turbine with Blade Pitching at Best Position Angle for Different Tip Speed Ratios. *International Journal of Ambient Energy*. doi:10.1080/01430750.2018.1492442
- Keyhani, A., Ghasemi-Varnamkhasti, M., Khanali, M. and Abbaszadeh, R. (2010). An assessment of wind energy potential as a power generation source in the capital of Iran, Tehran. *Energy*, 35, 188–201.
- Khalfa, D., Benretem, A., Herous, L. and Meghlaoui, I. (2014). Evaluation of the adequacy of the wind speed extrapolation laws for two different roughness meteorological sites. *American Journal of Applied Sciences*, 11 (4), 570–83. doi:10.3844/ajassp.2014.570.583
- Kose, R. (2004). An evaluation of wind energy potential as a power generation source in Kutahya, Turkey. *Energy Conversion and Management*, 45, 1631-1641.

- Kragic, I. M., Vucina, D. and Milas, Z. (2018). Numerical workflow for 3D shape optimization and synthesis of vertical-axis wind turbines for specified operating regimes. *Renewable Energy*, 115, 113-127.
- Lam, H.F. and Peng, H.Y. (2016). Study of wake characteristics of a vertical axis wind turbine by two- and three-dimensional computational fluid dynamics simulations. *Renewable Energy*, 90, 386-98.
- Lanzafame, R., Mauro, S. and Messina, M. (2014). 2D CFD Modeling of H-Darrieus Wind Turbines using a Transition Turbulence Model. *Energy Procedia*, 45, 131-140.
- Lawan, S.M., Abidin, W.A.W.Z., Chai, W.Y., Baharun, A. and Masri, T. (2013). The Status of Wind Resource Assessment (WRA) Techniques, Wind Energy Potential and Utilisation in Malaysia and Other Countries. *ARPJ Journal of Engineering and Applied Sciences*, 8(12), 10391053.
- Lee, Y.-T. and Lim, H.-C. (2015). Numerical study of the aerodynamic performance of a 500 W Darrieus type vertical-axis wind turbine. *Renewable Energy*, 83, 407-415.
- Li, C., Xiao, Y., Xu, Y., Peng, Y., Hu, G. and Zhu, S. (2018). Optimization of blade pitch in H-rotor vertical axis wind turbines through computational fluid dynamics simulations. *Applied Energy*, 212, 1107–1125.
- Li, Q., Maeda, T., Kamada, Y., Murata, J., Furukawa, K. and Yamamoto, M. (2015). Effect of number of blades on aerodynamic forces on a straight-bladed Vertical Axis Wind Turbine. *Energy*, 90, 784-795.
- Li, Q., Maeda, T., Kamada, Y., Murata, J., Yamamoto, M., Ogasawara, T., Shimizu, K. and Kogaki, T. (2016). Study on power performance for straight-bladed vertical axis wind turbine by field and wind tunnel test. *Renewable Energy*, 90, 291-300.
- Mahmoud, M.S. and Xia, Y. (2012). *Applied Control Systems Design*. Springer, eBook.
- Manwell, J.F., Rogers, A.L., McGowan, J.G. and Bailey, B.H. (2002). An offshore wind resource assessment study for New England. *Renewable Energy*, 27, 175–187.
- Mathew, S., Pandey, K.P. and Anil Kumar, V. (2002). Analysis of wind regimes for energy estimation. *Renewable Energy*, 25, 381-399.
- Mazarbhuiya, H.M.S.M., Biswas, A. and Sharma, K.K. (2018). Performance investigations of modified asymmetric blade H-Darrieus VAWT rotors. *Journal of Renewable and Sustainable Energy*, 10, 033302. doi: 10.1063/1.5026857
- MNRE report 2020-21. <https://mnre.gov.in/knowledge-center/publication>.
- Mohammadi, K., Alavi, O., Mostafaeipour, A., Goudarzi, N. and Jalilvand, M. (2016). Assessing different parameters estimation methods of Weibull distribution to compute wind power density. *Energy Conversion and Management*, 108, 322–335.

- Mohamed, M.H., Dessoky, A. and Alqurashi, F. (2019). Blade shape effect on the behavior of the H-rotor Darrieus wind turbine: Performance investigation and force analysis. *Energy*, Vol.179, pp. 1217-1234.
- Mohamed, M.H. Ali, A.M., Hafiz, A.A. (2015). CFD analysis for H-rotor Darrieus turbine as a low speed wind energy converter. *Engineering Science and Technology, an International Journal*, 18, 1-13.
- Mohamed, M.H. (2013). Impacts of solidity and hybrid system in small wind turbines performance. *Energy*, 57, 495-504.
- Mohamed, M.H. (2012). Performance investigation of H-rotor Darrieus turbine with new airfoil shapes. *Energy*, 47, 522-530.
- Murthy, K.S.R. and Rahi, O.P. (2016). Preliminary assessment of wind power potential over the coastal region of Bheemunipatnam in northern Andhra Pradesh, India. *Renewable Energy*, 99, 1137-1145.
- Ngala, G.M., Alkali, B. and Aji, M.A. (2007). Viability of wind energy as a power generation source in Maiduguri, Borno state, Nigeria. *Renewable Energy*, 32, 2242–2246.
- Al-Nhoud, O. and Al-Smairan, M. (2015). Assessment of Wind Energy Potential as a Power Generation Source in the Azraq South, Northeast Badia, Jordan. *Modern Mechanical Engineering*, 5, 87-96.
- Nobile, R., Vahdati, M., Barlow, J.F. and Mewburn-Crook, A. (2014). Unsteady flow simulation of a vertical axis augmented wind turbine: A two-dimensional study”. *Journal of Wind Engineering and Industrial Aerodynamics*, 125, 168-179.
- Nze-Esiaga, N. and Okogbue, E.C. (2014). Assessment of Wind Energy Potential as a Power Generation Source in Five Locations of South Western Nigeria. *Journal of Power and Energy Engineering*, 2, 1-13.
- Optis, M., Rybchuk, A., Bodini, N., Rossol, M. and Musial, W. (2020). 2020Offshore Wind Resource Assessment for the California Pacific Outer Continental Shelf’. *Golden, CO: National Renewable Energy Laboratory*. NREL/TP-5000-77642. <https://www.nrel.gov/docs/fy21osti/77642.pdf>
- Owusu, P.A. and Asumadu-Sarkodie, S. (2016). A review of renewable energy sources, sustainability issues and climate change mitigation. *Cogent Engineering*, 3, 14 pages.
- Ozay, C. and Celiktas, M.S. (2016). Statistical analysis of wind speed using two-parameter Weibull distribution in Alaçatı region. *Energy Conversion and Management*, 121, 49–54.
- Oztopal, A., Sahin, A.D., Akgun, N. and Sen, Z. (2000). On the regional wind energy potential of Turkey. *Energy*, 25, 189-200.

- Parakkal, J.U., El-Kadi, Kh., El-Sinawi, A., Elagroudy, S. and Janajreh, I. (2019). Numerical analysis of VAWT wind turbines: Joukowski vs classical NACA rotor's blades. *Energy Procedia*, 158, 194–1201.
- Patankar, S.V. (1980). *Numerical heat transfer and fluid flow*. S.I.: CRC press.
- Patel, V. (2017). Potential and Installed Capacity of Major Renewable Energy Sources in India. *International Journal of Engineering Technology Science and Research*, 4(5), 333-338.
- Pishgar-Komleh, S.H., Keyhani, A. and Sefeedpari, P. (2015). Wind speed and power density analysis based on Weibull and Rayleigh distributions (a case study: Firouzkooch county of Iran)". *Renewable and Sustainable Energy Reviews*, 42, 313–322.
- Qin, N., Howell, R., Durrani, N., Hamada, K. and Smith, T. (2011). Unsteady Flow Simulation and Dynamic Stall Behaviour of Vertical Axis Wind Turbine Blades. *Wind Engineering*, 35(4), 511-526.
- Rahman, S. M. and Chattopadhyay, H. (2019a). Statistical assessment of wind energy potential for power generation at Imphal, Manipur (India). *Energy Sources, Part A: Recovery, Utilization, and Environmental Effects*. doi: 10.1080/15567036.2019.1675814
- Rahman, S.M. and Chattopadhyay, H. (2019b). Performance evaluation of four widely accepted numerical methods to estimate Weibull parameters for wind speed data of Kolkata, India. International Conference on Recent Developments in Mechanical Engineering, (ICRDME 2019) March 21-22, 2019, S.A. Engineering College, Chennai, India.
- Rahman, S.M., Chattopadhyay, H. and Romesh, L. (2020). Feasibility of Wind Energy as Power Generation Source at Shillong (Meghalaya). *Advances in Mechanical Engineering, Lecture Notes in Mechanical Engineering*, 1303-1313. https://doi.org/10.1007/978-981-15-0124-1_115
- Rahman, S. M. and Chattopadhyay, H. (2020). A new approach to estimate the Weibull parameters for wind energy assessment: Case studies with four cities from the Northeast and East India. *International Transaction Electrical Energy System*. doi:10.1002/2050-7038.12574
- Rahman, M., Salyers, T.E., El-Shahat, A., Ilie, M., Ahmed, M. and Soloiu, V. (2018). Numerical and Experimental Investigation of Aerodynamic Performance of Vertical-Axis Wind Turbine Models with Various Blade Designs. *Journal of Power and Energy Engineering*, 6, 26-63.
- Rai, G.D. (1997). *Non-Conventional Source of Energy*. Khanna Publishers, pp. 16-42.

- Rehman, S., Halawani, T.O. and Mohandes, M.(2003). Wind power cost assessment at twenty locations in the kingdom of Saudi Arabia. *Renewable Energy*, 28, 573–583.
- Rehman, S. and Ahmad, A. (2004). Assessment of wind energy potential for coastal locations of the Kingdom of Saudi Arabia. *Energy*, 29, 1105–1115.
- Rehman, S. and Al-Abbadi, N.M. (2007). Wind shear coefficients and energy yield for Dhahran, Saudi Arabia. *Renewable Energy*, 32, 738–749.
- Rehman, S., Shoaib, M., Siddiqui, I., Ahmed, F., Tanveer, M.R. and Jilani, S. (2015). Effect of wind shear coefficient for the vertical extrapolation of wind speed data and its impact on the viability of wind energy project. *Journal of Basic & Applied Sciences*, 11, 90–100. doi:10.6000/1927-5129.2015.11.12
- Renewables 2021 Global Status Report “REN21”. <https://www.ren21.net/reports/global-status-report/>
- Rezaeiha, A., Montazeri, H and Blocken, B. (2019). On the accuracy of turbulence models for CFD simulations of vertical axis wind turbines. *Energy*, 180, 838-857.
- Rezaeiha, A., Kalkman, I. and Blocken, B. (2017). CFD simulation of a vertical axis wind turbine operating at a moderate tip speed ratio: Guidelines for minimum domain size and azimuthal increment. *Renewable Energy*, 107, 373-385.
- Rocha, P.A.C., Sousa, R.C., Andrade, C.F. and Silva, M.E.V. (2012). Comparison of seven numerical methods for determining Weibull parameters for wind energy generation in the northeast region of Brazil. *Applied Energy*, 89, 395–400.
- Rogowski, K., Hansen, M.O.L. and Lichota, P. (2018). 2-D CFD Computations of the Two-Bladed Darrieus-Type Wind Turbine. *Journal of Applied Fluid Mechanics*, 11(4), 835-845.
- Safari, B. and Gasore, J. (2010). A statistical investigation of wind characteristics and wind energy potential based on the Weibull and Rayleigh models in Rwanda. *Renewable Energy*, 35, 2874-2880.
- Sagharichi, A., Zamani, M. and Ghasemi, A. (2018). Effect of solidity on the performance of variable- pitch vertical axis wind turbine. *Energy*, 161, 753-775.
- Saleh, H., Aly, A.A.E. and Abdel-Hady, S. (2012). Assessment of different methods used to estimate Weibull distribution parameters for wind speed in Zafarana wind farm, Suez Gulf, Egypt. *Energy*, 44, 710-719.
- Saxena, B.K. and Rao, K.V.S. (2015). Comparison of Weibull parameters computation methods and analytical estimation of wind turbine capacity factor using polynomial power curve model: case study of a wind farm. *Renewables: Wind, Water, and Solar*, 2 (3), 1-11.

Seguro, J.V. and Lambert, T.W. (2000). Modern estimation of the parameters of the Weibull wind speed distribution for wind energy analysis. *Journal of Wind Engineering and Industrial Aerodynamics*, 85, 75-84.

Sengupta, A.R., Biswas, A. and Gupta, R. (2016a). An Analysis of Wind Energy Potential of Silchar (Assam, India) by Using Different Models. *International Journal of Engineering and Management Sciences*, 7 (2), 100-107.

Sengupta, A.R., Biswas, A. and Gupta, R. (2016b). Studies of some high solidity symmetrical and unsymmetrical blade H-Darrieus rotors with respect to starting characteristics, dynamic performances and flow physics in low wind streams. *Renewable Energy*, 93, 536-547.

Serban, A., Paraschiv, L.S. and Paraschiv, S. (2020). Assessment of wind energy potential based on Weibull and Rayleigh distribution models. *Energy Reports*, 6, 250–267.

Serdari, E., Berberi, P., Muda, V., Buzra, U., Mitrusi, D. and Halili, D. (2017). Wind Profile Characteristics and Energy Potential Assessment for Electricity Generation at the Karaburun Peninsula, Albania. *Journal of Clean Energy Technologies*, 5(4), 310-313.

Shata, A.S.A. and Hanitsch, R. (2006a). Evaluation of wind energy potential and electricity generation on the east coast of Mediterranean Sea in Egypt. *Renewable Energy*, 31, 1183–1202.

Shata, A.S.A. and Hanitsch, R. (2006b). The potential of electricity generation on the east coast of Red Sea in Egypt. *Renewable Energy*, 31, 1597–1615.

Shaban, A.H., Resen, A.K. and Bassil, N. (2020). Weibull parameters evaluation by different methods for windmills farms. *Energy Reports*, 6, 188–199.

Shu, Z.R., Li, Q.S. and Chan, P.W. (2015). Investigation of offshore wind energy potential in Hong Kong based on Weibull distribution function. *Applied Energy*, 156, 362–373.

Shukhla, D.L., Mehta, A.U., Modi, K.V. (2018). Dynamic overset 2D CFD numerical simulation of a small vertical axis wind turbine. *International Journal of Ambient Energy*, 41(12), 1415-1422.

Siddiqui, M.S., Durrani, N. and Akhtar, I. (2015). Quantification of the effects of geometric approximations on the performance of a vertical axis wind turbine. *Renewable Energy*, 74, 661-670.

Singh, R. (2018) Energy sufficiency aspirations of India and the role of renewable resources: Scenarios for future. *Renewable and Sustainable Energy Reviews*, 81, 2783–2795.

Sobhani, E., Ghaffari, M. and Maghrebi, M.J. (2017). Numerical investigation of dimple effects on darrieus vertical axis wind turbine. *Energy*, 133, 231-241.

- Strickland, J.H. (1975). *The Darrieus turbine: A performance prediction model using multiple streamtubes*. Technical report, Sandia National Laboratories.
- Soulouknga, M.H., Oyedepo, S.O., Doka, S.Y. and Kofane, T.C. (2017). Assessment of Wind Energy Potential in the Sudanese Zone in Chad. *Energy and Power Engineering*, 9, 386-402.
- Soulouknga, M.H., Doka, S.Y., Revanna, N., Djongyang, N. and Kofane, T.C. (2018). Analysis of wind speed data and the wind energy potential in Faya-Largeau, Chad, using Weibull distribution. *Renewable Energy*, 121(1), 1-8.
- Subramanian, A., Yogesh, S.A., Sivanandan, H., Giri, A., Vasudevan, M., Mugundhan, V. and Velamati, R.K. (2017). Effect of airfoil and solidity on performance of small scale vertical axis wind turbine using three dimensional CFD model. *Energy*, 133, 179-190.
- Sumair, M., Aized, A., Gardezi, S.A.R., Rehman, S.U. and Rehman, S.M.S. (2020). A novel method developed to estimate Weibull parameters. *Energy Reports*, 6, 1715–1733.
- Suzen, Y.B. and Huang, P.G. (2000). Modeling of flow transition using an intermittency transport equation. *J. Fluids Eng.* 122, 273–284.
- Tai, F.-Z., Yun, T.-H., Kang, K.-W. and Lee, J.-H. (2013). Analysis of small vertical wind turbine having H-Darrieus blades with stall delay model. *Journal of Renewable and Sustainable Energy*, 5 (052011), 1-11.
- Tank, V., Bhutka, J. and Harinarayana, T. (2016). Wind Energy Generation and Assessment of Resources in India. *Journal of Power and Energy Engineering*, 4, 25-38.
- Tizgui, I., Guezar, F.E., Bouzahir, H. and Benaïd, B. (2017). Comparison of methods in estimating Weibull parameters for wind energy applications. *International Journal of Energy Sector Management*. <https://doi.org/10.1108/IJESM-06-2017-0002>
- UNCTAD Note. (2010): The future energy matrix and renewable energy: implications for energy and food security, Note by the UNCTAD secretariat, 12 January, 2010. https://unctad.org/system/files/official-document/cimem2d8_en.pdf
- Ucar, A. and Balo, F. (2009). Evaluation of wind energy potential and electricity generation at six locations in Turkey. *Applied Energy*, 86, 1864–1872.
- Usta, I. (2016). An innovative estimation method regarding Weibull parameters for wind energy applications. *Energy*, 106, 301-314.
- Usta, I., Arik, I., Yenilmez, I. and Kantar, Y.M. (2018). A new estimation approach based on moments for estimating Weibull parameters in wind power applications. *Energy Conversion and Management*, 164, 570–578.

- Wais, P. (2017). Two and three-parameter Weibull distribution in available wind power analysis. *Renewable Energy*, 103, 15-29.
- Wang, J., Hu, J. and Ma, K. (2016). Wind speed probability distribution estimation and wind energy assessment. *Renewable and Sustainable Energy Reviews*, 60, 881-889.
- Weisser, D. (2003). A wind energy analysis of Grenada: an estimation using the ‘Weibull’ density function. *Renewable Energy*, 28, 1803–1812.
- Wekesa, D.W., Wang, C. and Wei, Y. (2016). Empirical and numerical analysis of small wind turbine aerodynamic performance at a plateau terrain in Kenya. *Renewable Energy*, 90, 377-385.
- Werapun, W., Tirawanichakul, Y. and Waewsak, J. (2015). Comparative Study of Five Methods to Estimate Weibull Parameters for Wind Speed on Phangan Island, Thailand. *Energy Procedia*, 79, 976 – 981.
- Werapun, W., Tirawanichakul, Y. and Waewsak, J. (2017). Wind Shear Coefficients and their Effect on Energy Production. *Energy Procedia*, 138, 1061-1066.
- Wilcox, D.C. (1993). Comparison of two-equation turbulence models for boundary layers with pressure gradient. *AIAA J.* 31, 1414–1421.
- Yilmaz, V. and Celik, H.E. (2008). A statistical approach to estimate the wind speed distribution: the case of Gelibolu region 2. *Dogus Universitesi Dergisi*, 9(1), 122-132.